DECADAL VARIABILITY IN THE ARCTIC OCEAN – GREENLAND-ICELAND-NORWEGIAN SEAS ICE-OCEAN-ATMOSPHERE CLIMATE SYSTEM

A

THESIS

Presented to the Faculty

of the University of Alaska Fairbanks

in Partial Fulfillment of the Requirements

for the Degree of

DOCTOR OF PHILOSOPHY

By

Dmitry Dukhovskoy, B.S., M.S., J.D.

Fairbanks, Alaska

December 2003

DECADAL VARIABILITY IN THE ARCTIC OCEAN –

GREENLAND-ICELAND-NORWEGIAN SEAS

ICE-OCEAN-ATMOSPHERE CLIMATE SYSTEM

By

Dmitry Dukhovskoy

RECOMMENDED:

L. Kovalik

Uma S Bhatt

Mark A Johnson

Advisory Committee Co-Chair

A. Proshutinsky

Advisory Committee Co-Chair

Head, Program in Marine Science and Limnology

APPROVED:

Dean, School of Fisheries and Ocean Sciences

Dean of the Graduate School

November 4, 2003

Date

ABSTRACT

This study investigates the decadal variability of the Arctic Ocean – Greenland, Iceland, Norwegian seas (GIN Sea) system and possible mechanisms driving variability. The theoretical foundation of this work is the theory of *Proshutinsky & Johnson* [1997] that two major climate states of the Arctic – Anticyclonic Circulation Regime (ACCR) and Cyclonic Circulation Regime (CCR) – are driven by variations in the freshwater contents of the Arctic Ocean and the GIN Sea.

It is hypothesized that the Arctic Ocean and the GIN Sea form an auto-oscillatory ice-ocean-atmosphere climate system with a quasi-decadal period of interannual variability. The system is characterized by two stages: (1) cold Arctic (ACCR) – warm GIN Sea with weak interaction between the basins; (2) warm Arctic (CCR) – cold GIN Sea with intense interaction between the basins. Surface air temperature and dynamic height gradients between the basins drive the auto-oscillations. This study investigates interactions between the Arctic Ocean and the GIN Sea.

To test the hypothesis, a simple model of the Arctic Ocean and Greenland Sea has been developed. The Arctic shelf processes have been parameterized in a box model coupled with an Arctic Ocean module. Both the Arctic Ocean and Greenland Sea modules are coupled with a thermodynamic ice model and atmospheric models. Several model experiments have been conducted to adjust the model and to reproduce the auto-oscillatory behavior of the climate system.

One of the major results of this work is the simulation of auto-oscillatory behavior of the Arctic Ocean – GIN Sea climate system. Periodical solutions

obtained with seasonally varying forcing for scenarios with high and low interaction between the regions reproduce major anomalies in the ocean thermohaline structure, sea ice volume, and fresh water fluxes attributed to ACCR and CCR regimes. According to the simulation results, the characteristic time scale of the Arctic Ocean – GIN Sea system variability reproduced in the model is about 10-15 years. This outcome is consistent with theory of *Proshutinsky and Johnson* [1997] and shows that the Arctic Ocean – GIN Sea can be viewed as a unique auto-oscillating system.

TABLE OF CONTENTS

LIST OF FIGURES

LIST OF TABLES

LIST OF ABBREVIATIONS

AO	Arctic Oscillation
ACCR	Anticyclonic circulation regime
AIW	Arctic Intermediate Water
ASW	Arctic Surface Water
AW	Atlantic Water
CB	Canadian Basin
CCR	Cyclonic circulation regime
EB	Eurasian Basin
EGC	East Greenland Current
FWC	freshwater content
GSDW	Greenland Sea Deep Water
HL	halocline layer, subscript denotes relevant to HL
lAIW	lower Arctic Intermediate Water
ML	mixed layer, subscript denotes relevant to ML
NAO	North Atlantic Oscillation
NSDW	Norwegian Sea Deep Water
PIW	Polar Intermediate Water
PW	Polar Water
SAT	surface air temperature
SLP	sea level pressure
SSH	sea surface height
SSS	sea surface salinity
uAIW	upper Arctic Intermediate Water
WSC	West Spitsbergen Current

LIST OF NOTATIONS

A_{AO}	area of the Arctic Ocean model domain
A_{GS}	area of the Greenland Sea model domain
a_0	air-ice velocity parameter
a^*	cloud attenuation
B_{fl}	buoyancy flux
C_{di}	ice-water drag coefficient
C_p	air specific heat
C_{wp}	water specific heat
cld	fractional cloudiness
D_z	coefficient of vertical eddy diffusivity
d_j	Julian day
F_{Dshw}	downwelling shortwave radiation
F_{LWo}	outgoing longwave radiation
F_{LWi}	incoming longwave radiation
F_{adv}	heat advection
F_{ins}	insolar radiation
F_{lat}	latent heat flux
F_{lw}	net longwave radiation
F_{mlt_GS}	energy required to melt advected ice Q_{mlt_GS}
F_{rfl}	reflected solar radiation
F_{sens}	sensible heat flux
F_{shw_inc}, F_{shw}	incoming shortwave radiation
F_{surf}	surface heat flux in the shelf box model
F_{tot}	surface heat flux

F_w	water heat flux to the ice bottom
g'	reduced gravity
H_{atm}	height of the atmospheric box
H_{ice}	ice thickness
h_{Ekm}	Ekman depth
h_{Ob}	Monin – Obukhov depth
k_{ice}	thermal conductivity in ice
h_{ml}	mixed layer depth
h_w	mixed layer thickness without ice draft
h_z	vertical space step
k_{snow}	thermal conductivity in snow
L_{ice}	latent heat of fusion of fresh ice
m_0	proportionality coefficient that parameterizes dissipation of forced convection in the entrainment formula
Pr_{i_ao}	ice production in the Arctic Ocean model
Pr_{i_sh}	ice production in the shelf model
Pr_{i_GS}	ice production in the Greenland Sea model
Q_{AtW}	Atlantic water inflow to the Greenland Sea
Q_{Ber}	Bering water inflow to the Arctic Ocean
Q_{GSDW}	GSDW inflow to the Greenland Sea
Q_{NSDW}	NSDW inflow to the Greenland Sea
$Q_{(P-E)}$	net precipitation flux
Q_{PW}	Polar Water inflow to the Greenland Sea
Q_{atl_sh}	Atlantic water inflow to the shelf
Q_f	river runoff
Q_{g_atl}	total Arctic Ocean outflow to the North Atlantic
Q_{gML_atl}	Arctic Ocean outflow to the North Atlantic from ML

Q_{ice}	ice export from the Arctic Ocean and shelf models
Q_{lAIW}	lAIW inflow to the Greenland Sea
Q_{mao}	inflow to the shelf box from the Arctic mixed layer
Q_{mlt_GS}	volume of ice melted in the Greenland Sea model
Q_{sh}	total shelf outflow to the interior Arctic Ocean
Q_{sh_ml}	shelf outflow to the interior Arctic Ocean mixed layer
Q_{uAIW}	uAIW inflow to the Greenland Sea
q_0	shelf outflow at salinity equal to shelf water salinity
$q_{sh}(z), (S)$	shelf outflow at a given depth z, salinity S
Ri_o	overall Richardson number
Ri_T	transition Richardson number
r_{cld}	cloud reflectivity
S_{PW}	Polar Water salinity
S_{atl}	salinity of the Atlantic layer in the Arctic Ocean model
S_{ml}	mixed layer salinity
S_{sh}	salinity in the shelf box model
S_{xx}	maximum salinity where shelf outflow function, q_{sh}, is zero
T_0	surface air temperature
T_{0_ao}	Arctic surface air temperature
T_{0_sh}	surface air temperature in the shelf region
T_{PW}	Polar Water temperature
T_{atl}	temperature of the Atlantic water
T_{atl}	temperature of the Atlantic layer in the Arctic Ocean model
$T_{fr}(S)$	freezing temperature for given salinity
T_{ml}	mixed layer temperature
T_{sh}	water temperature in the shelf box model
t_{stp}	time step

u_*	friction velocity
V_{ice}	ice speed
W_{10}	wind speed
w_a	vertical advection velocity
w_e	entrainment velocity
α	albedo
γ	adiabatic temperature gradient
γ_i	thermal conductance of the combined ice-snow slab
ε^*	effective emissivity
ε	ratio of sea water density to ice density
κ	proportionality coefficient that parameterizes dissipation of free convection in the entrainment formula
λ_{out}	number of outlets in the Arctic Ocean model for total Arctic Ocean outflow to the North Atlantic
μ_{Ber}	coefficient for Bering water inflow to the Arctic
ξ	fraction of the rejected salt consumed for the shelf water salinity increase
ρ_{air}	air density
ρ_{ice}	ice density
ρ_{ml}	ML density
$\rho_{ao}(z)$	Arctic Ocean density
$\rho_{sh\_out}(z)$	density of the shelf outflow
σ	Stefan-Boltzman constant
τ	wind stress
ϕ	total outflow of salt from the shelf box model
χ	coefficient of heat advection

DEDICATION

To my parents

Zoya and Stanislav Dukhovskoy

Acknowledgments

I wish to thank my two advisors, Dr. Mark Johnson and Dr. Andrey Proshutinsky, for support, friendship, and effective guidance throughout my work. Their readiness to help has been especially appreciated. I extend special thanks to Dr. Zygmunt Kowalik for his help and useful advice during this work. I also thank Dr. Uma Bhatt and Dr. David Newman for their critical reading of this manuscript and helpful suggestions. Finally I acknowledge my family and my friends from the School of Fisheries and Ocean Sciences (SFOS) the University of Alaska Fairbanks, whose support and friendship encouraged me throughout this study.

This work was funded by Alaska Sea Grant through the Center for Global Change, University of Alaska Fairbanks, and funding from the National Science Foundation and the National Science Foundation – International Arctic Research Center, in grants to Mark Johnson, SFOS, was also used to support me during these studies. An additional travel grant through the SFOS Graduate Student Travel Fund helped support recent travel.

Chapter 1 INTRODUCTION

Recent polar studies indicate that the Arctic climate has experienced significant changes during the last decades [e.g., *Jones et al.*, 1986; *Hurrell and van Loon*, 1997; *Jones et al.*, 1999; *Serreze et al.*, 2000; *Moritz et al.*, 2002; *Polyakov et al.*, 2002a]. One possible explanation of these observed changes in the Arctic environment is simply the natural variability of the Arctic. In other words, these changes are caused by positive-negative feedback mechanisms of the natural Arctic climate system and interaction with adjacent regions rather than by anthropogenic factors. Several dominant time scales of Arctic climate variability have been proposed [*Slonosky et al.*, 1997; *Mysak and Venegas*, 1998; *Polyakov and Johnson*, 2000; *Venegas and Mysak*, 2000; *Goosse et al.*, 2002; *Gudkovich and Kovalev*, 2002]. This study is focused on the decadal climate variability in the Arctic. The theoretical foundation for this research is the theory of *Proshutinsky and Johnson* [1997] for the existence of the anticyclonic – cyclonic regime cycle in the Arctic with a period of 8 – 15 years. *Proshutinsky and Johnson* [1997] and *Proshutinksy et al.* [2002] have shown that the regime shifts in the Arctic can affect the convection region in the central Greenland Sea by varying freshwater outflow through the Fram Strait.

The major hypothesis of this study is that the Arctic Ocean and Greenland, Iceland and Norwegian seas (GIN Sea) are an ice-ocean-atmosphere climate system that generates quasi-decadal climate oscillations in the Arctic. The amplitude and frequency of these oscillations are determined by characteristics of the system. Thus, the observed decadal variability in the Arctic can be a manifestation of auto-oscillatory behavior of the climate system.

Section 1.1. Arctic Ocean

In this study, the Arctic Ocean boundaries are considered according to those adopted at the NATO Research Workshop on the Freshwater Budget of the Arctic Ocean, 1998, [*Lewis*, 2000]: "the Arctic Ocean is defined as being bounded by: the Russian mainland, a line across Bering Strait, the north coast of Alaska and the northernmost limit of the islands in the Canadian Arctic Archipelago, then across Kennedy Channel to Peary Land, across from Svalbard, down to Nordkapp of Norway and so back to the Russian coast." The surface area is about $9.x10^6$ km^2 [*Rudels and Friedrich*, 2000] to $9.55x10^6$ km^2 [*Aagaard and Carmack*, 1989]. The Deep Arctic Basin or interior Arctic Ocean is deeper than the 200-m isobath.

1.1.1. Bathymetry and major basins

The Lomonosov Ridge divides the interior Arctic Basin into two major basins: the Eurasian and the Amerasian basins. The ridge crest is defined by the 2000-m isobath with two shallow sills (~1500 m) in the western and eastern Arctic. The Eurasian Basin (EB) is divided by the Gakkel Ridge (~2500-3000 m) into the Nansen and the Amundsen basins (Fig. 1.1). The Amerasian Basin consists of the Canadian and the Makarov basins divided by the Alpha (2000-1500 m) and the Mendeleev (2500-2000 m) ridges separated by the 3000 m deep Cooperation Gap. In most polar oceanography literature, the Amerasian basin is referred to as the Canadian Basin without discerning the Makarov Basin [*Carmack*, 1990]. The same terminology is used in this thesis: the Amerasian Basin is called the Canadian Basin (CB) unless the Makarov Basin features need to be distinguished.

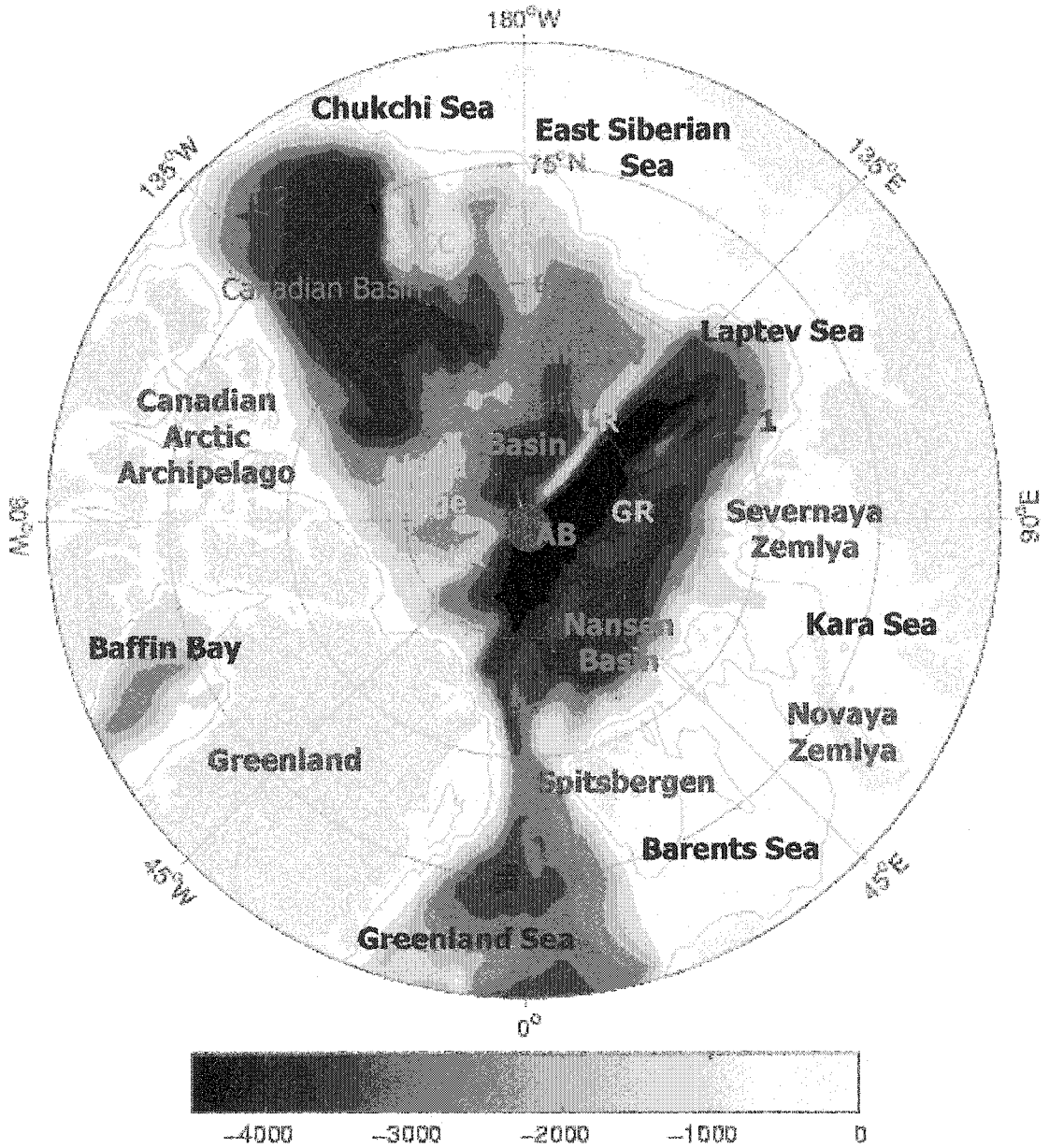

Fig. 1.1. Arctic Ocean bathymetry. *Abbreviations on the map denote: AB – Amundsen Basin; GR – Gakkel Ridge; LR – Lomonosov Ridge; MR – Mendeleev Ridge; CC – Chukchi Cap. Red stars numbered "1" and "2" mark locations of T/S profiles plotted in Fig. 1.2. The isobaths contour the 200 and 2000-m depths.*

All basins are about 4000 m deep. Amundsen Basin is the deepest, the largest part of which is occupied by the Pole Abyssal Plain delimited by the 4000-m isobath with the deepest part at 88°N, 30°E (>4400 m). Water volumes of the Canadian and Eurasian basins are 7.3×10^6 and 5.9×10^6 km^3, respectively [*Aagaard et al.*, 1985].

One of the specific features of the Arctic Ocean bathymetry is a wide shelf zone. A typical width of the Eurasian shelf is from 600 to 800 km [*Carmack*, 1990]. The surface area of the shelf is approximately 1/3 of the Arctic Ocean [*Rudels and Friedrich*, 2000].

Another morphological peculiarity of the Arctic Ocean is its confinement by land masses. Being surrounded by land, the Arctic Ocean has limited interaction with the World Ocean. The interaction with the Pacific Ocean occurs through a narrow (~82 km width) and very shallow (average depth is 40-50 m) Bering Strait [*Doronin*, 1986]. The most important strait through which the Arctic Ocean genuinely interacts with the World Ocean is the roughly 3000 m deep Fram Strait. That allows the Arctic Ocean to exchange both surface and deep waters with the North Atlantic. The width of the Fram Strait is about 550 km at 80° N.

1.1.2. Water masses and circulation

Water masses

The first classification of water masses of the Arctic Ocean likely was done by F. Nansen. He divided the water column into three layers: surface water, Atlantic layer, and deep water [*Nansen*, 1928]. According to recent studies [*Aagaard*,

1981; *Aagaard et al.*, 1985; *Carmack*, 1990; *Swift et al.*, 1997; *Rudels*, 1998; *Carmack*, 2000], the basic stratification of the Arctic Ocean can be described by four layers: Mixed (surface) Layer (Polar Mixed Layer), Halocline complex (Halocline Layer), intermediate depth Atlantic Layer (Polar Intermediate Water), and Deep Water (Polar Deep Water) which is divided into upper deep water (or transitional layer) (uDW) and lower deep water (lDW).

The average characteristics of the layers are presented in Table 1.1. Sometimes the Polar Mixed Layer and Halocline Layer are considered as one water mass termed Polar Water (PW) [*Carmack*, 1990]. Characteristics of the Polar Water are low temperature (<0° C) and salinity (<34.4 psu).

Table 1.1. Average characteristics of the Arctic Ocean water layers

Water layers		Depth interval, m	Potential temperature, °C	Salinity, psu
Mixed Layer		0 to ~50	θ near freezing	$30 < S < 33.5$
Halocline		~50 to 200	$-1.4 < \theta < 0$	$33 < S < 34.3$
Atlantic Layer		~200 to 750	$0 < \theta$	$34.5 < S < 34.9$
uDW		~750 to 1500	$\theta < 0$	$34.9 < S < 34.92$
lDW	CB	> 1500	$\theta \sim -0.5$	S ~34.95
	EB	> 1500	$\theta \sim -0.9$	S ~34.93

According to Swift et al. [1997] and Aagaard [1981].

(a) Mixed Layer

The mixed layer is the upper 30-60 m in winter and much shallower (up to 15-20 m) in summer [*Stigebrandt*, 1981; *Doronin*, 1986]. The mixed layer water in the

Arctic Ocean is characterized by low salinities near the freezing point (Figs. 1.2 and 1.3), with an average salinity of 32.7 psu [*Coachman and Aagaard*, 1974], which varies from above 34 psu north of Svalbard to below 32 psu in the Makarov Basin [*Rudels*, 1998].

Sources of fresh water in the surface mixed layer are sea ice meltwater, river runoff and precipitation, however, the melting-freezing cycle is the most important source for maintaining the mixed layer in the Arctic Ocean. *Aagaard et al.* [1981] suggested that even without any external freshwater sources, the seasonal ice melting-freezing would maintain a low-salinity mixed layer.

(b) Halocline Layer

The halocline layer consists of the upper Cold Halocline Layer (CHL) and Lower Halocline Water (LHW) [*Steele and Boyd*, 1998]. These parts can be seen on most Arctic T/S vertical profiles (Fig. 1.2). The CHL is characterized by isothermal, close-to-freezing-point water in the halocline [*Aagaard et al.*, 1981].

In 1944, P. Shirshov, a participant of the "North Pole" ice drifting camp, observed a cold halocline below a shallow (25 m to 50 m) mixed layer in the Eurasian Basin. He attributed this water to the lower surface layer [*Shirshov*, 1944]. Later, several different mechanisms of CHL formation were proposed [*Treshnikov and Baranov*, 1972; *Aagaard et al.*, 1981; *Rudels et al.*, 1996; *Steele and Boyd*, 1998; *Rudels and Friedrich*, 2000].

The thermohaline structure of the halocline layer varies within the Arctic Ocean. *McLaughlin et al.* [1996] compared the halocline structure within the Canadian

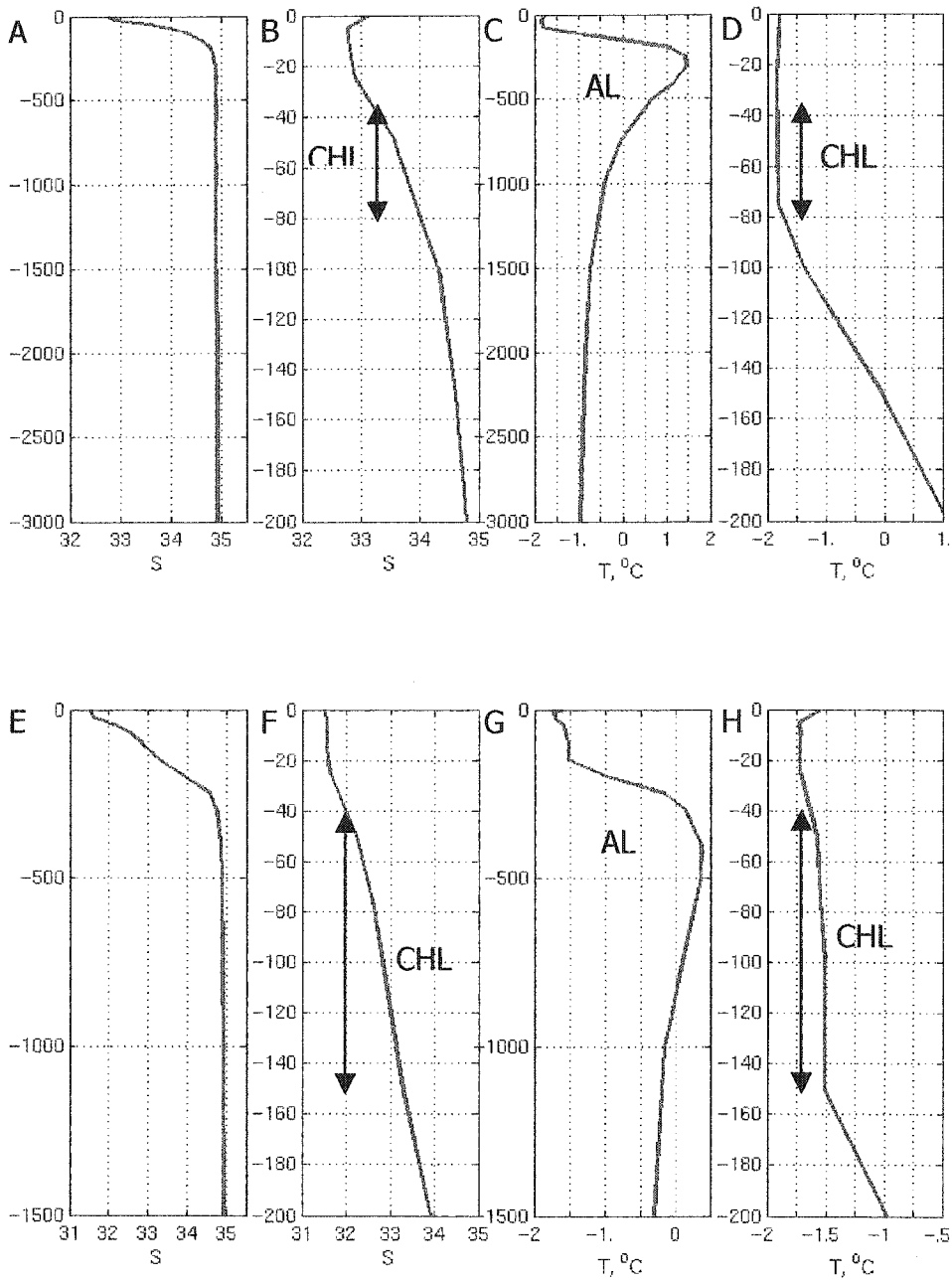

Fig. 1.2. Winter T/S profiles in the Arctic Ocean. *Upper panels show T/S profiles for the station in the Eurasian Basin marked "1" in Fig. 1.1, lower panels show profiles for the station in the Beaufort Gyre marked "2" in Fig. 1.1. Vertical axis is depth in m. (A) S profile. (B) Upper 200 m of (A). Red arrow denotes Cold Halocline Layer, CHL. (C) T profile: positive T values mark location of the Atlantic Layer (AL). (D) Upper 200 m of (C). (E) S profile. (F) Upper 200 m of (E). (G) T profile; note different scale compared to (C). (H) Upper 200 m of (G). Adopted from EWG Atlas of the Arctic Ocean [1998].*

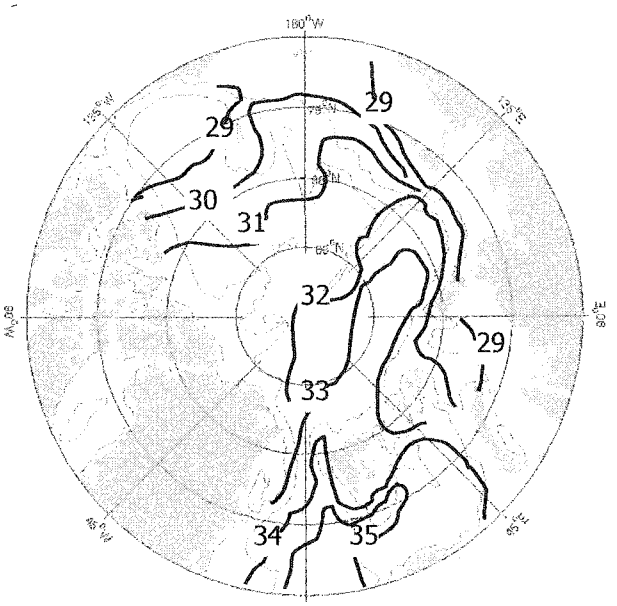

Fig. 1.3. Salinity distribution at 5 m depth in the Arctic Ocean. *Based on Carmack [1990].*

and Eurasian basins and found that Arctic halocline structures can be divided into eastern and western assemblies. The two assemblies are separated by the Atlantic/Pacific front that lies parallel to the Lomonosov or Mendeleyev ridges and shifts its position with interannual periodicity. *Aagaard et al.* [1981] supposed that the CHL feature was more pronounced in the Eurasian Basin. In the Canadian Basin, the CHL was not well pronounced or absent due to Bering water inflow. The thermal structure of the halocline in that region showed a temperature maximum near 75 to 100 m in depth representing the summer Bering water.

There are two prominent mechanisms of halocline formation in the Arctic Ocean mentioned by *Aagaard et al.* [1981]: upwelling on the Arctic shelves and cooling

of the Atlantic water; and salinization of surface shelf waters by brine expulsion during freezing with their consequent advection into the interior Arctic Ocean.

The first mechanism was discussed earlier by *Coachman and Barnes* [1962]. These authors hypothesized that, being forced upward in the submarine canyons of the Kara and Barents seas, the Atlantic water mixed with the surface shelf water. Consequent cooling to the freezing point made this mixture dense enough to sink into the arctic pycnocline. Evidence of Atlantic water upwelling on the Arctic Seas shelves has been presented in the scientific literature. For example, indications of upwelling were observed in Barrow Canyon in April – August, 1973 [*Mountain et al.*, 1976], on the northern Alaska shelf [*Aagaard et al.*, 1981], and on the Russian Arctic Sea shelf [*Gakkel*, 1957; *Nikiforov and Shpaikher*, 1980].

Viewing salinization of shelf water as the most reasonable mechanism of the Arctic halocline supply, *Aagaard et al.* [1981] mentioned several sources for the Arctic Ocean halocline. In the Eurasian Basin, the sources are located in the following regions: from Spitsbergen to Franz Josef Land, between Franz Josef Land and Novaya Zemlya (St. Anna Trough) and Voronin Trough, and the northern part of the Laptev Sea.

Primary sources for the Canadian Basin halocline are to the east of the New Siberian Islands: the Chukchi Sea and the Bering Sea. The Bering Sea inflow injects water more saline than 33.5 into the Arctic halocline at a rate of about $1x10^6$ $m^3 \cdot s^{-1}$. The Chukchi Sea is the most significant contributor of cold saline water to the interior Arctic Ocean. Based on the observed high salinities in the eastern Chukchi Sea in winter and satellite sea ice concentration images, *Aagaard et al.* [1981] hypothesized the existence of numerous areas of sea ice divergence in the region. Mechanical removal of ice would keep a high ice

production rate throughout the whole cold season, providing intense salinization of the Chukchi Sea water. Estimates of the amount of water more saline than 34 produced on the Chukchi Sea shelf in winter are of the order of 0.5×10^6 $m^3 \cdot s^{-1}$.

(c) Atlantic Layer

All temperature (T) profiles from the Arctic Ocean have a maximum within the 200-500 m depth interval (Figs. 1.2C and 1.2G). The maximum in Arctic Ocean temperature profiles was documented by F. Nansen during the Fram expedition [*Nansen*, 1902]. He first suggested that Atlantic Water entered through the Fram Strait and spread around the Arctic Ocean.

Since *Nansen* [1902], the Atlantic water is usually identified in the Arctic Ocean water column by positive temperatures ($\theta > 0°C$). The average depth interval for the Atlantic water is 200-700 m. The upper boundary of the Atlantic layer is at the 50 m depth in the Nansen Basin close to Spitsbergen; in the Canadian Basin the upper boundary of the Atlantic layer deepens to 300 m. The lower boundary of the layer is almost at the same depth over the Arctic Ocean (~800 – 1000 m), except for the Lomonosov Ridge, where it rises to 700 m [*Doronin*, 1986]. The temperature maximum is well pronounced in profiles from the Eurasian Basin. The temperature maximum deepens as the Atlantic Water spreads to the Canadian Basin. At the entrance to the Arctic Basin, Atlantic water has a maximum of about +3.5° C, but only +0.4° C in the Canadian Basin [*Doronin*, 1986].

The Atlantic layer is formed from the modified Atlantic water carried from the North Atlantic. Atlantic water enters the Arctic Mediterranean[1] at the southern part of the Norwegian Sea as one of the branches of the North Atlantic Current. This flow, called the Norwegian Atlantic Current, crosses the Norwegian Sea and bifurcates near the Barents Sea into two streams. One stream, the West Spitsbergen Current, flows northward and the other part flows westward into the Barents Sea. Large transformations of the Atlantic water occur in the Nansen Basin and the Barents Sea [*Rudels and Friedrich*, 2000].

(d) Deep Water

Deep water of the Arctic Ocean is defined as lying below the lower 0° C isotherm [*Aagaard*, 1981; *Carmack*, 1990]. *Aagaard* [1981] discerned two types of deep water: the upper Deep Water (uDW) (S < 34.92) and the lower Deep Water (lDW) (S > 34.92 to > 34.93). The interface between the deep waters is sharp, and its depth varies significantly by hundreds of meters both in space and time.

Distinct features of the deep hydrography of the Arctic Ocean include [*Aagaard*, 1981; *Aagaard et al.*, 1985; *Swift et al.*, 1997]:

(1) the Eurasian Basin is colder than the Canadian Basin by about 0.5°C;

(2) high, deep salinities ranging through the Arctic Ocean from 34.94 psu to 34.95 psu;

(3) the Canadian Basin is saltier than the Eurasian Basin, and the Canadian Basin contains the most saline water in the Arctic Mediterranean;

---

[1] The Arctic Mediterranean seas extend from the Greenland-Scotland Ridge into the polar basins. They comprise the Greenland, Iceland and Norwegian Seas as well as the Arctic Ocean with its shallow shelf seas: the Barents Sea, the Kara Sea, the Laptev Sea, the East Siberian Sea and the Chukchi Sea [*Rudels*, 1998].

(4) *in situ,* the deep water in the Eurasian Basin is denser than the Canadian Basin due to lower temperatures in the first basin and the nonlinearity of the equation of state for sea water [*Aagaard et al.*, 1985].

The origin of the deep waters is still being discussed. Before the 1980's, *Nansen's* [1902] idea that the Arctic Ocean deep water had its origin in the Greenland and Norwegian seas dominated [*Metcalf*, 1960; *Timofeyev*, 1960; *Treshnikov and Baranov*, 1972]. Later, the oceanographic observations revealed higher, deep water salinities in the Arctic Basin than that in the GIN Sea and forced polar oceanographers to look for additional salt sources in the region.

Aagaard [1981] and *Doronin* [1986] mentioned the Atlantic water and dense shelf winter water as the most likely sources of the deep waters. In a later paper, *Aagaard et al.* [1985] were more categorical in rejecting the Atlantic water as a possible salt source for the deep Canadian water and accepting the shelf water as the "... only one likely salt source, viz., the adjacent continental shelf seas, where brine expulsion during freezing produces cold and saline water" (p. 4836, [*Aagaard et al.*, 1985]).

Recently, Greenland Sea Deep Water and dense shelf water from the Barents and Kara seas were proposed as primary sources for the deep waters in the Eurasian Basin [*Aagaard et al.*, 1981; *Swift et al.*, 1983]. uDW is presumably fed by a relatively direct advective link with the deep Greenland Sea. Because lDW has higher salinities than the Greenland deep water, another salinity source is required. This probably occurs on the shelves. lDW is then formed by mixing of uDW with this more saline water. The source for the Canadian Basin deep water is very dense shelf waters [*Aagaard et al.*, 1985]. Observations in the Northern Bering Sea during winter 1980-1981 [*Schumacher et al.*, 1983] and Chukchi Sea

during winter 1982 [*Aagaard et al.*, 1985], revealed the occurrence of extremely dense shelf water where the observed salinity was greater than 36.5 psu within 20 km of the coast in the Chukchi Sea near Alaska. Thus, *Aagaard et al.* [1985] concluded that the deep Canadian Basin was fed by relatively small volumes of the shelf water.

Circulation

The circulation of the Arctic Ocean varies with depth. The principle large-scale surface circulation of the Arctic Ocean and of the sea ice is determined by two major flow fields: the Transpolar Drift and Anticyclonic flow around the Canadian Basin which forms the Beaufort Gyre (Fig. 1.4A) [*Carmack*, 2000]. The Transpolar Drift Current crosses the Arctic Ocean from the East Siberian Sea to the Fram Strait. The characteristic velocity of the current is 0.02 $m \cdot s^{-1}$ in the Canadian Basin and 0.05 $m \cdot s^{-1}$ near the Fram Strait. Water velocity in the Beaufort Gyre is about 0.02-0.03 $m \cdot s^{-1}$ [*Doronin*, 1986].

The general circulation of the Atlantic Water is believed to be cyclonic around the Arctic Ocean (Fig. 1.4 B). Based on the T/S structure of the Arctic Ocean, *Rudels and Friedrich* [2000] concluded that a large part of the Atlantic inflow recirculates in the Eurasian Basin and even within the Nansen Basin. A small fraction (0.5 Sv, ~20% of the Atlantic Water) crosses the Lomonosov Ridge and enters the Makarov Basin [*Rudels*, 1998]. After counterclockwise circulation in the Makarov and Canadian basins, significantly modified Atlantic Layer water re-enters the Eurasian Basin and flows toward the Fram Strait. Thus, general circulation of the Atlantic water in the Arctic Ocean is cyclonic.

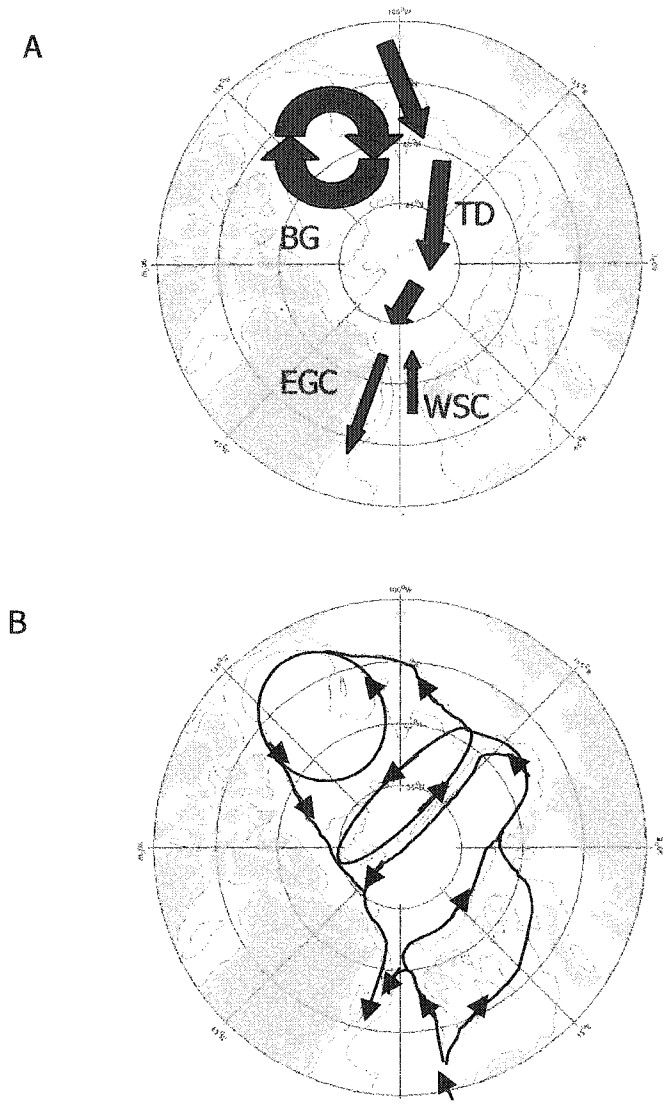

Fig. 1.4. Schematic diagram of the principal large-scale water circulation in the Arctic Ocean. *(A) Circulation of the surface layer (based on [Rigor et al., 2002]): BG – Beaufort Gyre, TD – Transpolar Drift Current, EGC – East Greenland Current, WSC – West Spitsbergen Current. (B) Atlantic water circulation in the Arctic Basin. Based on [Rudels et al., 1994].*

The large-scale circulation of the Arctic deep water is also cyclonic. The flow is slow, typically of order 0.01 $m \cdot s^{-1}$. Presumably, the Eurasian and Canadian basins do not exchange their deep water.

Inflows and outflows of the Arctic Ocean

The Arctic Ocean interacts with the North Atlantic and the Pacific Ocean through Fram Strait, the channels of the Canadian Arctic Archipelago, the Barents Sea, and Bering Strait.

(a) Fram Strait

There are two countercurrents in Fram Strait: the East Greenland Current (EGC) and the West Spitsbergen Current (WSC) (Fig. 1.4 A). Being the northern continuation of the Norwegian Atlantic Current, WSC is saline (~35 psu) and relatively warm (>0°C up to +4°C). As WSC approaches Spitsbergen, some fraction of the flow recirculates into the Greenland Sea with EGC, and the rest of the flow enters the Arctic Ocean. The major inflow occurs north of Spitsbergen and flows eastward along the continental slope. WSC varies seasonally with a maximum transport in late autumn and winter and minimum flow in summer. Reported estimates of the Atlantic inflow through the Fram Strait vary significantly in different papers from 1.3 Sv[2] [*Bourke et al.*, 1988] to 7.1 Sv [*Aagaard and Greisman*, 1975].

---

[2] 1 Sv = 1×10^6 $m^3 \cdot s^{-1}$.

Estimates of EGC are still not accurate. Most of the recent studies indicate a value about 3.0 Sv [e.g., *Bourke et al.*, 1988; *Foldvik et al.*, 1988]. The vertical structure of EGC differs with depth. In the upper (~150 m) layer, the PW is exported from the Arctic mixed layer and halocline. In the deeper levels, very saline and slightly warmer (θ = -0.85° C, S = 34.94) Eurasian Basin Deep Water (EBDW) is carried to the deep GIN Sea [*Aagaard et al.*, 1985]. The EBDW exits the Arctic Ocean along the Greenland slope with an estimated velocity in the order of 0.01 $m \cdot s^{-1}$. It is driven by thermohaline heterogeneity between the deep GIN Sea and Arctic Ocean.

The largest transport of freshwater with the EGC through Fram Strait is from ice flux. Estimates of the ice volume and area fluxes vary widely, and range from 1900 $km^3 \cdot yr^{-1}$ (0.06 Sv) [*Thomas et al.*, 1996] to 5000 $km^3 \cdot year^{-1}$ (0.16 Sv) [*Vinje and Finnekasa*, 1986]. *Kwok and Rothrock* [1999] analyzed ice motion in Fram Strait from satellite passive microwave data to obtain the ice area export through the strait during winter (October through May) of 1978-1996. Those authors obtained an average winter area flux of 6.7×10^5 km^2, which is approximately 7% of the area of the Arctic Ocean. The estimates for the whole year were 9.19×10^5 $km^2 \cdot yr^{-1}$ and 2366 $km^3 \cdot yr^{-1}$ (0.075 Sv) for the annual area flux and volume flux, respectively. Those authors noted high daily, monthly, and interannual variability of ice area fluxes.

(b) Barents Sea

Another route of the Atlantic water inflow into the Arctic Ocean is through the Barents Sea. *Rudels and Friedrich* [2000] assumed that this Atlantic flow was as large, or even larger, than through Fram Strait. The Barents Sea gains about

$75x10^{12}$ $m^3 \cdot yr^{-1}$ (~2.3 Sv), approximately 36% of the sea volume, of salty and warm water from the Norwegian Sea [*Doronin*, 1986]. A complex transformation of the Atlantic water occurs in the Barents Sea. The Atlantic water splits into several branches on the Barents Sea shelf. *Rudels* [1998] estimated inflow of Atlantic water into the Arctic Ocean through the Barents Sea was 1.2 Sv which entered the Arctic Ocean as a narrow ~1000 m thick wedge through the St. Anna Trough. There are also dense-water flows into the Arctic Ocean from the Barents Sea through the Victoria Channel [*Rudels*, 1984].

(c) Canadian Arctic Archipelago (CAA)

The Arctic Ocean also interacts with the North Atlantic through the CAA which is characterized by complex topography, narrow channels, relatively deep sills (300-400 m) in the western margin of the continental shelf, and shallow (less than 100 m) sills in the central and southern parts. Most channels are not significant in the Arctic Ocean – North Atlantic interaction due to their small cross-section area. However, *Melling* [2000] asserted that there were 4 channels through which a large fraction of flow passed: the Kennedy Channel (Nares Strait), Hell Gate and Cardigan Strait, Wellington Channel, and Barrow Strait. Estimates of the volume flux through the CAA are sparse. Net flow through the CAA is likely toward the North Atlantic. Estimates for net flux through Lancaster, Jones, and Smith Sounds varied from $2.2x10^4$ $km^3 \cdot yr^{-1}$ to $5.4x10^4$ $km^3 \cdot yr^{-1}$ (0.7 – 1.7 Sv) [*Collin*, 1962].

The CAA channels are covered with ice all year with an average thickness of 3 – 5 m [*McLaren et al.*, 1984; *Melling*, 2000]. The ice flux through the CAA has a seasonal cycle. From January to June stable ice arches are formed in all the CAA

channels, choking them, and immobilizing the ice. During the rest of the year, ice export to the North Atlantic occurs. The pack ice drifts at 5 to 25 $cm \cdot s^{-1}$ in the major channels [*Kozo*, 1991]. Using 10 $cm \cdot s^{-1}$ as a mean speed for the pack ice motion through the key straits within CAA during 6 months, *Melling* [2000] determined the ice flux to be ~500 $km^3 \cdot yr^{-1}$ (0.015 Sv). This is about 20% of the volume ice flux through the Fram Strait.

(d) Bering Strait

Pacific waters flowing through the Bering Strait mostly affect the Chukchi and East Siberian seas. A steric-level drop from the North Pacific to the Arctic Ocean of about 0.5 m drives a mean current northward through the Bering Strait. Most variation in flow is wind-forced [*Roach et al.*, 1995]. The northward transport of waters through the Bering Strait has both significant seasonal and interannual variability. A mean volume transport through Bering Strait is 0.83±0.66 Sv during a year [*Roach et al.*, 1995]. The higher values correspond to the warm period of the year (April – August). *Roach et al.* [1995] reported that interannual variability of the volume transport was 0.1 Sv but could reach 50% of the mean flow.

Thermohaline characteristics of the Bering flow reveal high seasonal and interannual variability. Average salinities in autumn are 32.0 psu in the eastern and 32.6 psu in the western part. Seasonal variability of the salinity is 2 psu, with a maximum salinity occurring in early April. In March and April 1991, the salinity reached 34.5- 34.8 in the western part.

Bering Sea water is created north of Bering Strait in the Chukchi Sea [*Coachman et al.*, 1975]. The T/S characteristics of the Bering flow undergo significant

transformations while crossing the Chukchi Sea shelf and transform into the Bering Sea water. In summer, salinity of the Bering Sea Water ranges from 32.2 to 33.0 psu, and temperatures from +0.8° to +5° C. In winter, the temperature of the Bering Sea Water core decreases northward from the Bering Strait at a rate of ~1 to 3 $x10^{-3}$° C·km^{-1}. The Bering Water (both summer and winter) is thought to supply the halocline in the Canadian Basin [*Swift et al.*, 1997; *Carmack*, 2000].

1.1.3. Freshwater balance as a characteristic climatic feature of the Arctic Ocean

An important feature of the Arctic Ocean is the large positive balance of freshwater, which has been estimated to be about 890 $km^3 \cdot yr^{-1}$ (Table 1.2). The Arctic Ocean stores large amounts of fresh water in liquid and solid (ice) forms. The mean storage of liquid fresh water in the Arctic Ocean is estimated to be $8.x10^4$ km^3 plus $1.73x10^4$ km^3 of fresh water stored in sea ice [*Aagaard and Carmack*, 1989]. The major components of the freshwater budget for the Arctic Ocean are: ice, river runoff, Bering water inflow, and precipitation – evaporation (P-E).

Components of the freshwater budget

(a) Sea Ice

The annual mean ice-covered area of the Arctic Ocean (including the Barents Sea) is about $6.5x10^{12}$ m^2 with seasonal variations of 3 to $4x10^{12}$ m^2 [*Carmack*,

2000]. The major uncertainty on the Arctic sea ice is the mean sea ice thickness. Most estimates are around 3 m [*Hibler*, 1979]. Arctic sea ice accounts for a significant store of freshwater. *Aagaard and Carmack* [1989] have estimated the mean freshwater volume stored in sea ice at 1.73×10^{13} m^3, which is over 20% of the liquid freshwater stored in the Arctic Ocean.

Table 1.2. Fresh water budget for the Arctic Ocean

Components of the budget	Transport, $km^3 \cdot yr^{-1}$
Precipitation – Evaporation	900
Water import through Bering Strait	1670
Import with Norwegian Coastal Current	250
Runoff	3300
Ice export through Fram Strait	-2790
Water export through Fram Strait	-820
Water export through Canadian Archipelago	-920
Saline water import through Barents Sea	-540
Saline water import with West Spitsbergen Current	-160
Net (gain)	**890**

From *Aagaard and Carmack* [1989], reference salinity 34.8 psu

Thorough investigations of the sea ice mass balance in the Arctic Ocean have been done by *Thomas et al.* [1996]. Those authors used a thermodynamic ice growth model, satellite concentration data, and observed buoy velocities to compute the time histories of the thickness distributions of the first-year and multi-year ice for seven regions of the Arctic Ocean for the period 1979-1985. *Thomas et al.* [1996] reported that the Arctic ice cover consisted primarily of

multi-year ice (60% by area and 82% by volume) and most of this ice was ridged. Another conclusion was that the average sea-ice thickness was 2.7 m with a seasonal variation of 30% and interannual variation of 10%. All regions except the Chukchi Sea had net ice growth, net export, and net salt input to the ocean surface.

The drift of sea ice on a seasonal time scale follows the wind pattern. A rule-of-thumb is that sea ice moves with a speed of about 2% of the surface wind and about 45° to the right of the wind. According to the mean sea level pressure field over the Arctic Basin (see, e.g.,[*Rigor et al.*, 2002]), the wind stress drags sea ice towards the Fram Strait. Some ice accumulates near the northern part of the CAA, where the highest mean thicknesses of 7-8 m occur [*Bourke and McLaren*, 1992; *Wadhams et al.*, 1992]. The average ice thickness distribution obtained from submarine sonar data shows very thick ice (4 – 6 m) off the Canadian Archipelago, with thinner ice (~2 m) off the Siberian coast [*Hibler*, 1979]. Mean ice thickness at the North Pole in April – May ranges from ~3 m to 4.8 m [*McLaren et al.*, 1994].

(b) River runoff

River runoff provides a substantial share of the positive freshwater balance of the Arctic Ocean. River runoff in the region has large seasonal and interannual variability. Most estimates of total annual streamflow into the Arctic ranges from 3230 $km^3 \cdot yr^{-1}$ [*Semiletov et al.*, 2000] to 3500 $km^3 \cdot yr^{-1}$ [*Macdonald*, 2000]. The Arctic Ocean gains 63-67%[3] of the annual Siberian river runoff during June to

[3] This is approximately 1573 – 1673 $km^3 \cdot yr^{-1}$, based on Table 2 in *Gordeev* [2002].

August. During winter to early spring, December to April, the Arctic Ocean receives a small fraction of the annual river runoff: 8-10% of the Asian and North American rivers[4] and 12-14% of the European rivers[5] [*Shiklomanov et al.*, 2000]. In Table 1.3 water discharge rates of some of the Arctic rivers are presented.

(c) Bering Strait inflow

The Bering water is a significant source of freshwater for the Canadian Basin. It makes the halocline fresher than that in the Eurasian Basin [*Carmack*, 2000]. The freshwater import from the Pacific is estimated to be 1670 $km^3 \cdot yr^{-1}$ (~0.05 Sv) referenced to $S = 34.8$ [*Carmack*, 2000].

Table 1.3. Arctic river runoff characteristics

Authors	Yenisei	Ob	Lena	Kotuy	Pechora	Indigirka	Kolyma	Mackenzie
Macdonald [2000]	1133		767		130	213		330
Carmack [1990]	603	530	520	105	130	57	102	340
Semiletov et al. [2001]	586	403	525	-	-	50	74	-
Prowse and Flegg [2000]	596	401	548	-	110	46	80	284
Gordeev [2000]	620	429	525	-	131	61	132.2	-

River runoff is in $km^3 \cdot yr^{-1}$.

[4] ~220 – 280 $km^3 \cdot yr^{-1}$, from Table 2 in *Gordeev* [2000] and Table 5 in *Grabs et al.* [2000].
[5] This is ~55.6 – 64.8 $km^3 \cdot yr^{-1}$, Table 2 in *Gordeev* [2000].

(d) Precipitation - Evaporation

Estimates of precipitation less evaporation (hereinafter, P-E) are uncertain. This flux usually is estimated via aerological methods, using vertical atmospheric profiles of humidity and winds [*Serreze et al.*, 1995]. The P-E flux has a strong seasonal variability with the minimum occurring from December through March and the maximum in September, which is more than double the minimum value [*Serreze and Barry*, 2000].

Freshwater storage and export

The largest fraction of the freshwater budget of the Arctic Ocean is stored in the sea ice and upper layers. *Rudels and Friedrich* [2000] estimated the freshwater content of different layers in the Arctic Ocean. According to their calculations, the volume of freshwater in the ice and mixed layer and halocline exceeds that in the lower layers.

The excess of freshwater flows in liquid and solid phases out of the Arctic Basin through Fram Strait and the Canadian Archipelago straits into the North Atlantic. *Rothrock et al.* [2000] used satellite data to obtain the following transport estimates. The freshwater equivalent of ice export through the Fram Strait relative to 34.8 psu is 2.8×10^3 $km^3 \cdot yr^{-1}$, of ocean export through the Fram Strait is 0.76×10^3 $km^3 \cdot yr^{-1}$, and of ocean export through the Canadian Archipelago is 1.13×10^3 $km^3 \cdot yr^{-1}$. Estimating the transport salinity at 33.7 psu, *Aagaard and Carmack* [1989] computed liquid freshwater fraction in the PW transport through Fram Strait to be 1110 $km^3 \cdot yr^{-1}$ (~0.035 Sv).

Rates of freshwater export vary among years, causing variation in surface salinity in the Greenland and Iceland seas. *Alekseev et al.* [1994] and *Häkkinen* [1995] suggested that positive anomalies in the freshwater export from the Arctic inhibit the deep convection in the Greenland Sea, thus reducing oceanic heat flux to the atmosphere. Anomalously high positive freshwater exports from the Arctic Basin, the largest known as the Great Salinity Anomaly (GSA) [*Dickson et al.*, 1988], can shut off convection in the GIN Sea completely. Thus, the freshwater flux is very important in controlling climate variability in the region.

1.1.4. Seasonal variability in the Arctic

Due to the large annual cycle of the incoming solar radiation, the Arctic atmosphere has significant seasonal variability. The difference between the monthly mean surface air temperature in January and in July is about 30°C. In summer, intense warming of the troposphere causes fading of the anticyclonic vorticity and settling of a cyclone over the central Arctic. In the upper ocean the seasonal signal weakens poleward and becomes small in the central Arctic Ocean.

Seasonal values for winter (January through April) and summer (July and August) of some meteorological and hydrological characteristics of the central Arctic and central Laptev Sea are presented in the Table 1.4 (based on *Gorshkov* [1980]).

Table 1.4. Some seasonal characteristics in the Arctic

Characteristics	Central Arctic		Central Laptev Sea	
	Winter	Summer	Winter	Summer
Surface air T, °C	<-35 to -32	-2 to +0.2	-30 to -20	+4 to +6
Sea level pressure, mb	1012 to 1018	<1010	1012 to 1018	1012
Mixed layer T, °C	<-1.7	~-1.7	<-1.7	+1
Mixed layer S, psu	31 to 31.5	30 to 30.5	~30 to 30.5	26 to 29

Section 1.2. Greenland, Iceland, Norwegian seas

Greenland, Iceland, and Norwegian seas (GIN Sea) are bounded by the eastern coast of Greenland, northern coast of Iceland, western coast of Norway, and Spitsbergen (Fig. 1.5). This region is a buffering zone between the Arctic Ocean and Atlantic Ocean. The surface area of the GIN Sea is 2.55×10^6 km^2 [*Aagaard and Carmack*, 1989]. Despite its small surface area, this region is highly significant both for the Arctic and Northern Atlantic. For the Arctic, the GIN Sea is the major source of heat advected through the ocean and atmosphere. For the North Atlantic, the GIN Sea, through Denmark Strait, provides the densest component of the Northwest Atlantic Bottom Water, a principle component of the North Atlantic Deep Water [*Swift et al.*, 1980].

1.2.1. Bathymetry

The GIN Sea consists of four major basins [*Perry*, 1986] (Fig. 1.5): the Norway (67°N, 2°W), Lofoten (70°N, 5°E), Greenland (75°N, 5°W), and Boreas (77°N, 1°E) Basins. The morphological basins do not correspond to the physical oceanographic subdivision of the region into Greenland, Norwegian and Iceland seas. The physical oceanographic classification has been done on the basis of circulation patterns and thermohaline structures of the GIN Sea regions. Because bathymetric ridges significantly affect water circulation and redistribution, they coincide with the boundaries of the Greenland, Iceland, and Norwegian seas. The most dominant ridge in the basin is the midocean ridge, which in the

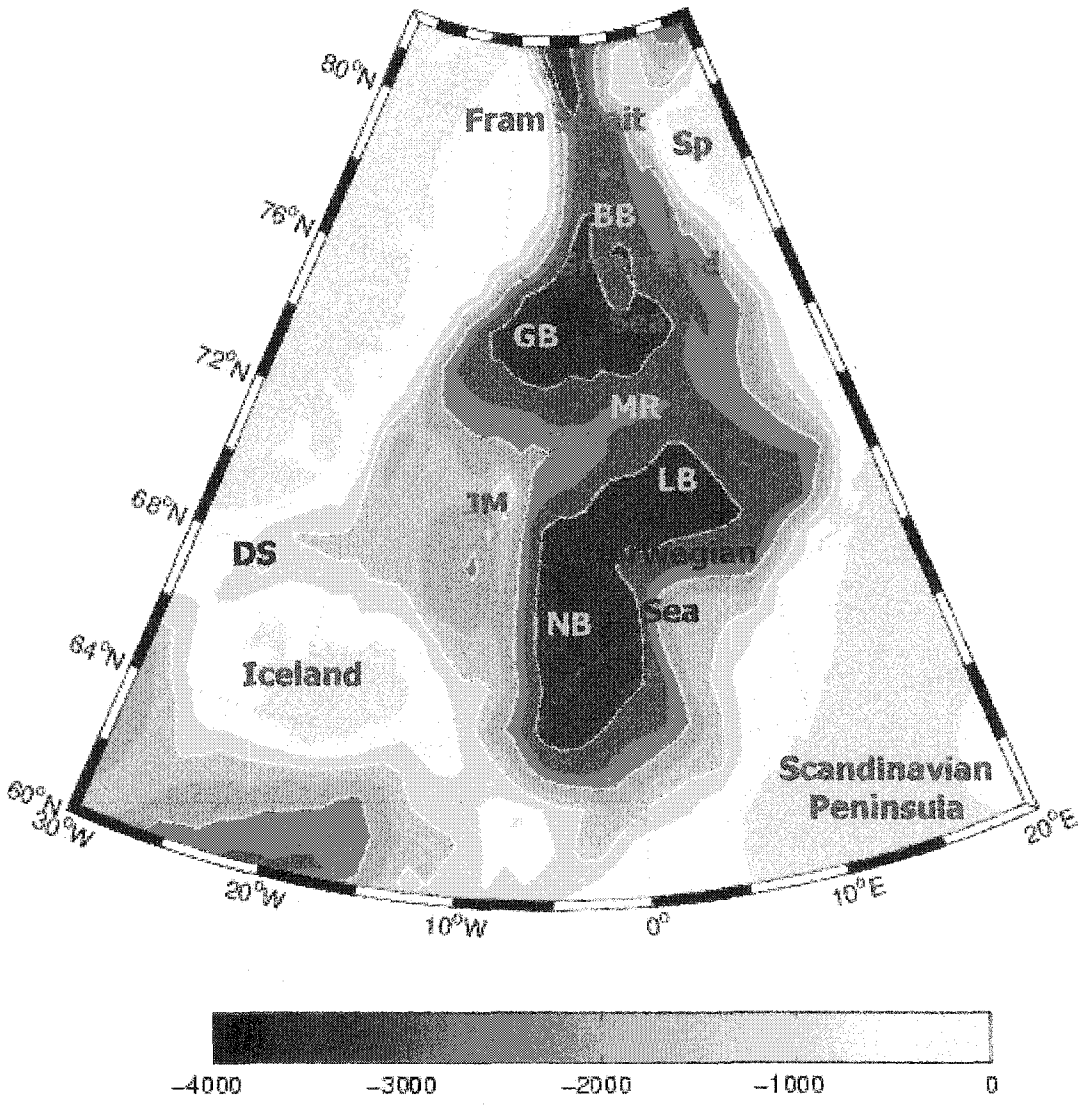

Fig. 1.5. Geogrpahic nomenclature and bathymetry of the GIN Sea. *Abbreviations on the map denote: DS – Denmark Strait; Sp – Spitsbergen; JM – Jan Mayen; BB – Boreas Basin; GB – Greenland Basin; LB – Lofoten Basin; NB – Norway Basin; MR – Mohns Ridge; KR – Kolbeinsey Ridge; IFR – Iceland-Faeroe Ridge; FST – Faeroe-Shetland Trough. The isobaths contour the 1000, 2000, and 3000-m depths.*

GIN Sea comprises the Kolbeinsey Ridge (sometimes called Iceland-Jan Mayen Ridge), the Mohns Ridge, and the Knipovich Ridge (Atka Ridge). The midocean ridge roughly delimits the Greenland Sea boundaries.

The GIN Sea is deep, with the floor of most of its basins below the 2000-m isobath. The exception is the Iceland Sea, which encompasses the area between Iceland, Greenland, and the island of Jan Mayen, and is located on the shallow Iceland Plateau, with most of its floor above the 2000-m isobath. The Norwegian Sea is the deepest of the GIN seas (depths are >3200 m) and occupies the western part of the GIN Sea.

Exchange between the GIN Sea and the North Atlantic occurs through several channels (troughs). The Faeroe-Shetland Trough is a deep (~1000 m) channel that separates the Faeroe Islands platform from the continental shelf of western Europe [*Perry*, 1986]. The Iceland-Faeroe path is shallow where it crosses the Iceland-Faeroe Ridge. The Denmark Strait is a shallow (300-500 m) strait between Iceland and Greenland with a maximum depth of 600 m.

1.2.2. Water masses, circulation, and oceanic fronts

Water masses

The GIN Sea includes several water masses from different sources. The following water masses have been discerned in the region [*Swift et al.*, 1980; *Johannessen*, 1986; *Swift*, 1986; *Carmack*, 1990].

(a) Atlantic Water (AW)

AW enters the GIN Sea with the Norwegian Atlantic Current through the Faeroe-Shetland Channel. At the entrance to the region, the AW has a salinity of ~35.3

psu and 8° C in winter and 10° C in summer. When the AW reaches Spitsbergen its salinity has been reduced to 35 psu and temperature has dropped by ~5° C. The AW is identified by a salinity >35 psu. The AW is mostly imported into the Arctic Ocean by the West Spitsbergen Current and North Cape Current. In the Fram Strait, a large fraction of the AW flow splits off westward from the West Spitsbergen Current and submerges under the south-flowing Polar Water [*Aagaard and Coachman*, 1968]. This branch of the Atlantic Water in the Greenland Sea is termed the Return Atlantic Current [*Muench*, 1990]. The estimates of this flow are 0.8 Sv south at 79° N and 0.4 Sv between 79° N and 81° N [*Bourke et al.*, 1988].

(b) Polar Water (PW)

PW is formed in the Arctic Ocean and is conveyed to the GIN Sea by the East Greenland Current. The PW includes waters from the Arctic Ocean mixed layer and halocline; its depth is ~150 m. PW is cold (<0° C) and fresh (<34.4). Its temperature varies from the freezing point at the surface (in winter) to 0° C at its bottom. Salinity changes from 30 to 34 – 34.4 psu over the same depth interval.

(c) Polar Intermediate Water (PIW)

PIW is found near the East Greenland Current and in the Denmark Strait with temperatures < 0° C and salinities <34.7 psu.

(d) Arctic Surface Water (ASW)

ASW is the surface water in the central gyres of the Greenland and Iceland seas. This water mass results mostly from mixing of the AW and PW. Hence, the ASW is fresher and cooler than the AW: it has temperatures from 0 to 3° C and salinities from 34.4 to 34.9 psu. However, the ASW is denser than either the PW or AW, and is not a simple mixture of the two water masses [*Carmack*, 1990]. Instead, PW and AW are modified by air-sea interactions to form ASW. The central Greenland Sea (Greenland Gyre region) is thought to receive very little PW from the East Greenland Current [*Johannessen*, 1986; *Swift*, 1986; *Alekseev et al.*, 1994; *Vinje et al.*, 2002]. *Aagaard and Carmack* [1989] argued that only a small fraction (~3%) of the freshwater conveyed by the East Greenland Current reached the convective region of the Greenland Gyre.

(e) Arctic Intermediate Water (AIW)

AIW has a temperature between 0° and 2° C and a salinity between 34.7 and 35 psu. The AIW is formed by winter cooling of the Atlantic Water and mixing with deep waters. *Swift and Aagaard* [1981] have subdivided the AIW into two water types in accordance with the T-S behavior in the AIW: lower AIW (lAIW) and upper AIW (uAIW). The uAIW lies in between the temperature minimum and the temperature maximum and has both temperature and salinity increasing with depth. *Swift et al.* [1980] assumed that some fraction of the uAIW is formed at the sea surface north of Iceland in winter. The lAIW overlays the deep water masses. It includes the temperature and salinity maxima at depths of about 250 to 400 m. The temperature and salinity in the lAIW range from 0 °C to 3 °C and from 34.9 to 35 psu and both are decreasing with depth.

(f) Norwegian Sea Deep Water (NSDW)

NSDW is the densest water mass in the Norwegian and Iceland seas. This water also occurs around the periphery of the Greenland Sea. Even though it is more saline (34.9 to 34.94 psu), because it is warmer (-0.4° to −1.1° C below 2000 m), it is less dense than Greenland Sea Deep Water.

(g) Greenland Sea Deep Water (GSDW)

GSDW is the coldest (-1.3 to -1.2° C) and freshest (34.88 to <34.9 psu) deep water among the deep water masses of the Arctic Mediterranean. GSDW is found only in the central gyre of the Greenland Sea. The origin of GSDW is still debated. Presumably, GSDW is formed by subsurface modification of AIW which involves double-diffusive process [*Carmack and Aagaard*, 1973; *Swift*, 1986]. Both NSDW and GSDW are the dominant water masses in the GIN Sea, accounting for about 70% of the total volume.

Circulation

The obvious characteristic of the region is cyclonic circulation in the Greenland Sea (Fig. 1.6), which is bounded by the West Spitsbergen Current, Return Atlantic Current, East Greenland Current north of Jan Mayen, and the Jan Mayen Polar Current. The largest part of the AW inflow to the GIN Sea is transported by the Norwegian Atlantic Current. Another, though much less pronounced, inflow of AW into the GIN Sea is the North Icelandic Irminger Current, the northward branch of the Irminger Current. The East Greenland Current originates in the

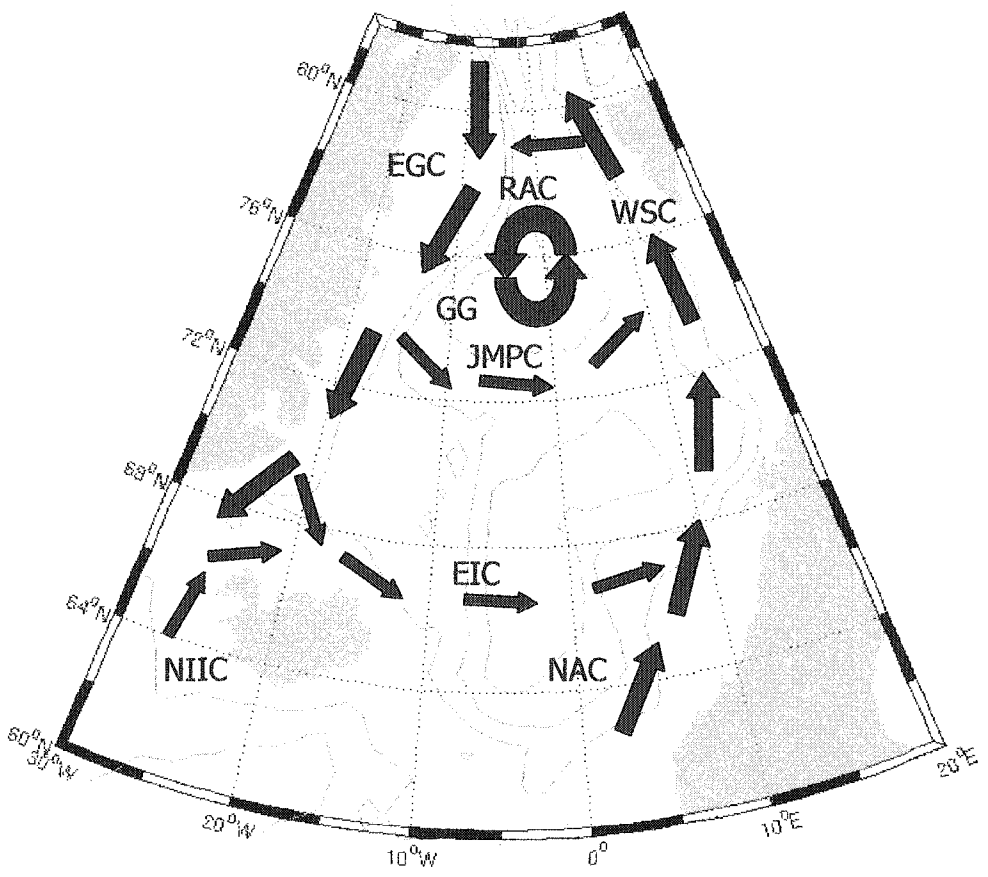

Fig. 1.6. Principle large-scale surface circulation in the GIN Sea. *Abbreviations denote: EGC – East Greenland Current; RAC – Return Atlantic Current; WSC – West Spitsbergen Current; GG – Greenland Gyre; JMPC – Jan Mayen Polar Current; EIC – East Icelandic Current; NIIC – North Icelandic Irminger Current; NAC – Norwegian Atlantic Current. Based on Swift [1986].*

Fram Strait, where Arctic Ocean waters mix with the Return Atlantic Water. The current flows southward along the Greenland continental margin. EGC splits near Jan Mayen Island into two branches. The larger branch, the Jan Mayen Polar Current, turns eastward and forms the southern boundary of the Greenland Gyre [*Carmack*, 1990]. The bulk of EGC exits the GIN Sea through Denmark Strait.

Malmberg et al. [1972] estimated that 1.6 Sv exited Denmark Strait above 300 m.

Both surface and subsurface outflows from the GIN Sea into the North Atlantic occur through the Denmark Strait and Faeroe-Shetland and Faeroe-Iceland straits. *Sukhovey* [1970] used *in situ* observations to obtain the transport estimates in the straits. He estimated water flow into the North Atlantic through the Faeroe-Shetland strait to be 2.75×10^5 $km^3 \cdot yr^{-1}$ (8.7 Sv), through the Faeroe-Iceland Strait to be 1.66×10^5 $km^3 \cdot yr^{-1}$ (5.3 Sv), and through the Denmark Strait 1.77×10^5 $km^3 \cdot yr^{-1}$ (5.6 Sv).

Most of the flow in Denmark Strait is the continuation of the East Greenland Current. The vertical stratification in Denmark Strait is significant. Salinity changes from <34.6 psu in the upper layers to >34.9 psu near the bottom (Fig. 9 in [*Swift et al.*, 1980]). The deep water formed in the GIN Sea overflows through Denmark Strait and across the ridges between Iceland and Scotland. Current measurements indicate that the deep overflow in Denmark Strait is intermittent [*Worthington*, 1969; *Swift et al.*, 1980]. *Swift et al.* [1980] concluded from the analysis of the observations in the Denmark Strait that the principle dense component of the overflow (~34.9 psu) was AIW.

Oceanic fronts

Surface currents in the GIN Sea with considerably different water characteristics cause significant horizontal T/S gradients over the area (Fig. 1.7). Regions of high and permanent gradients in these fields, which are the boundaries of

different water types, are oceanic fronts [*Johannessen*, 1986]. *Swift* [1986] has discerned three hydrographic regions in the GIN Sea. The Atlantic domain is the region dominated by Atlantic waters. The Polar domain is the region of direct polar influence. Between these two regions exists a transition region termed the arctic domain (Fig. 1.7). The ocean front between the polar and the arctic domains is the polar front, and the front between the Atlantic waters and the arctic domain is the arctic front.

The arctic domain is the region of specific interest in this study, because deep convection takes place there. According to *Swift* [1986], the most important features of this domain are 1) upper-layer waters are denser than that in the other two domains; 2) the vertical stability of the water column is lower than in the adjacent domains; 3) a small amount of PW reaches the arctic domain; 4) the formation of dense water masses in the arctic domain essentially consists of modification of Atlantic Water; and 5) Atlantic Water only penetrates the arctic front after it becomes dense enough to enter the domain, through cooling.

1.2.3. Sea ice in the GIN Sea

The Norwegian Sea is free of ice year round except for the northernmost part which may have some ice in cold years. The Iceland Sea has seasonal ice cover which spreads over the area from December through May and retreats westward during the rest of the year.

The largest part of the Greenland Sea is free of ice during most of the year, but posses a "permanent" ice region due to the East Greenland Current transporting

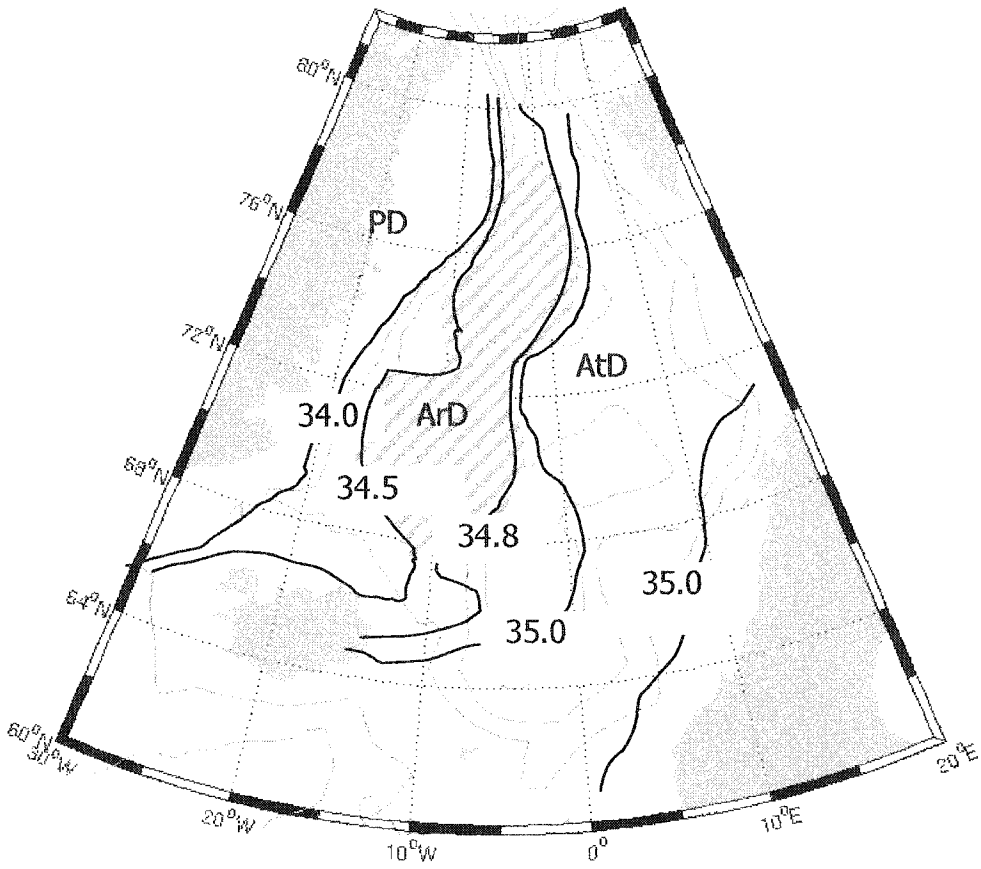

Fig. 1.7. Summer surface salinity and hydrographic regions in the GIN Sea. *The GIN Sea is characterized by large horizontal salinity gradients. According to the hydrographic characteristics, the following regions can be discerned: Polar domain (PD), Arctic domain (ArD), and Atlantic domain (AtD). The shaded area indicates the Arctic domain. Based on Swift [1986].*

ice from the Arctic Ocean year round. This region can be delimited by the east Greenland continental shelf. The south-eastern part of the Greenland Sea (eastward of ~5°E and southward of 77°N) stays free of ice during the year. There are large seasonal and interannual variations in the ice concentration of the rest of the Greenland Sea. Generally, ice concentration is very low in the center of the Greenland Cyclone Gyre (6°W - 0°W, 74°N - 76°N) and a large bay

forms in the winter ice pack known as "Nordbukta" ("North Bay" in Norwegian). To the south of the Greenland Gyre region, there is a so called "Odden" region ("the Icy Cape") (6°W – 0°W, 72°N - 74°N) covered by the ice tongue [*Carsey and Roach*, 1994; *Pawlowicz*, 1995]. The ice tongue in this region during a winter ("Odden event") is the surface manifestation of the Jan Mayen Current, where fresh surface water and cold Polar Water is exported from the Arctic Ocean. *Pawlowicz* [1995] noted the southern boundary of the Odden (when it existed) approximately coincided with the Polar Ocean Front, extending northeastward from Jan Mayen Island. The Odden/Nordbukta events are very inconsistent. Having analyzed Arctic ice concentrations from 1953 to 1988 acquired from the National Center for Atmospheric Research, *Pawlowicz* [1995] reported that in some years the Odden does not appear, and even when it does, the Nordbukta does not always appear. *Pawlowicz* [1995] concludes that the deepest winter convection in the Greenland Gyre coincides with extremely low (or zero) ice concentrations before mid-April and significant wind stress over the region.

1.2.4. Air-sea heat flux and deep convection in the GIN Sea

The GIN Sea is a region of large heat fluxes to the atmosphere. *Nikiforov and Shpaikher* [1980] assert that the GIN Sea – Barents Sea region has the largest turbulent heat flux to the atmosphere of any location. The annual mean turbulent sensible heat flux from the ocean into the atmosphere at the northern part of the GIN Sea is more than 95 $W \cdot m^{-2}$, with a February mean flux of about 170 $W \cdot m^{-2}$ [*Gorshkov*, 1980]. The estimates of the mean total heat flux to the atmosphere in the GIN Sea are around 100 $W \cdot m^{-2}$ [*Hakkinen and Cavalieri*, 1989;

Aukrust and Oberhuber, 1995] with maximum values of 400 $W \cdot m^{-2}$ in the Greenland Sea and Barents Sea during winter. Monthly means of the surface heat flux for the central Greenland Sea (74°N – 76°N, 5°W – 5°E) obtained from the NOAA-CIRES Climate Diagnostic Center [*CDC*] are given in Table 1.5. It should be noted that the heat flux in winter is a highly variable characteristic (second row in Table 1.5) and mostly determined by the ice concentration and convection depth.

Table 1.5. Monthly mean surface heat flux of the central Greenland Sea

	Jan	Fb	Mr	Ap	May	Jn	Jl	Ag	Sp	Oc	Nv	Dc
Mean flux[(a)]	-260	-237	-212	-89	80	170	164	82	-34	-149	-215	-255
STD[(b)]	105	93	124	64	33	21	14	16	29	57	87	92

(a) $W \cdot m^{-2}$, negative flux is to the atmosphere.
(b) Standard deviation, $W \cdot m^{-2}$.

The heat accumulated in the atmosphere over the GIN Sea is conveyed eastward by westerly flows and advected into the Arctic over the shelf seas. The most noticeable advection of heat into the Arctic is during the cold season. In some winters the advection may reach as far east as the Laptev Sea. Such deep heat penetration into the Arctic can be identified on the sea level pressure maps by the pressure trough spreading form the Icelandic Low over the Barents, Kara and Laptev seas. However, the routes of wind flows vary greatly from year to year.

Air-sea heat flux in the GIN Sea in winter strongly depends on the rate of convection in the central Greenland Sea which is an area for ocean deep convection and deep water formation, which has been intensively studied in

recent years [*Carmack and Aagaard*, 1973; *Rudels et al.*, 1989; *Clarke et al.*, 1990; *Johannessen et al.*, 1991; *Alekseev et al.*, 1994; *Aukrust and Oberhuber*, 1995; *Hakkinen*, 1995; *Pawlowicz*, 1995]. Another region of dense water formation by means of deep convection is the Iceland Sea. Nevertheless, thermohaline convection in the Iceland Sea is believed to be much shallower than that in the Greenland Sea [*Aagaard et al.*, 1985], although the convection in the Greenland Gyre is not always deep. In some years, the local convection in the Greenland Sea was limited to the upper hundred meters or even less [*Schlosser et al.*, 1991; *Alekseev et al.*, 1994; *Pawlowicz*, 1995]. Mechanisms of deep convection in the Greenland and Iceland seas have not been completely identified.

Helland-Hansen and Nansen [1909] assumed that there were two regions of deep convection and deep water formation: the Greenland Sea and to a lesser extent the Norwegian Sea. Cooling of the surface layers during winter was proposed as the driving force of the convection. Those authors hypothesized that as the surface layer cooled down to the freezing point, it became denser than the underlying water resulting in overturn. *Metcalf* [1960] used winter observations in the Greenland Sea but found no vertical homogeneity of a water column, which should happen if *Helland-Hansen and Nansen* [1909] were correct. Thus, *Metcalf* [1960] suggested that sinking of the dense water does not occur in the vertical plane but rather along isopycnal surfaces. *Killworth* [1979] suggested a localized chimney mechanism to describe deep convection. *Hakkinen* [1987] described a mechanism of upwelling near the ice edge, which after subsequent cooling might result in convection. *Rudels* [1998] proposed a simple mixed-layer box model which reproduced the convection in several steps: brine rejection during ice freezing causes haline convection and heat entrainment into the upper layer that melts some ice and restratification occurs. The process

repeated in the model until the whole ice slab melted by oceanic heat. After that the thermal convection developed in the Greenland Sea. According to the model estimates, the thermal convection in the Greenland Sea started by the end of winter – beginning of spring.

Two major stages in deep convection evolution should be noticed. During this first stage, the preconditioned thermohaline structure of the upper layer is achieved to allow the onset of thermohaline convection [*Alekseev et al.*, 1994]. Second, deep thermal convection occurs. *Aleskeev et al.* [1994] investigated the interannual variability of the thermohaline structure in the Greenland Gyre during convective and non-convective years. The authors distinguished three possible types of thermohaline structure in the Greenland Sea Gyre: non-convective (normal), convective, and pre-convective. To start deep convection, the pre-convective thermohaline conditions should be reached in the upper layer. The pre-convective surface salinity was estimated to be 34.819 psu. Additional salt injection is the necessary pre-condition to start overturning. *Alekseev et al.* [1994] hypothesized that the events of intense surface to bottom convection were the results of single, strong, salt water intrusions.

1.2.5. Seasonal variability in the GIN Sea

Seasonal variability of the atmospheric parameters in the GIN Sea (Table 1.6) is smaller than that in the Arctic (Table 1.4). In contrast, the upper ocean of the GIN Sea has a stronger seasonal signal in T and S fields, compared with the central Arctic Ocean. The seasonal changes of thermohaline structure are observed within almost the whole water column in the central Greenland Sea

(Fig. 5 in [*Pawlowicz*, 1995]). There are two reasons for such deep penetration of the seasonal signal. The first reason is seasonally varying cyclone vorticity of the water in the central Greenland Sea. Due to the strong cyclone vortex in winter, the upward vertical advection (Ekman pumping) brings deep water in the center of the Gyre up to the surface, causing "doming" GSDW. In summer, a weak cyclone vortex cannot support the GSDW dome and deep water retreats and is replaced by NSDW. The second reason is deep convection which spreads downward the characteristics of the upper layer in winter. Observations prove that the thermohaline structure in the Greenland Gyre during deep convection years differs from that during shallow convection years [*Alekseev et al.*, 1994].

Table 1.6. Some seasonal characteristics in the central Greenland Sea

Characteristics	Central Greenland Sea	
	Winter[a]	Summer[b]
Surface air[c] T, °C	-6 to -8	+2 to +4
Sea Surface T[d], °C	0 to -1.5	+3 to +5
300 m T[d], °C	~ -1	0 to -1
Sea Surface S[d], psu	34.5 to 35.	33 to 34.8
300 m S[d], psu	34.9 to 35.	34.9 to 35.

(a) January through March.
(b) June through August.
(c) [*CDC*].
(d) [*Gorshkov*, 1980].

Section 1.3. Interannual variability in the Arctic Ocean and GIN Sea

The first researchers who noticed the climate change in the Arctic were *Knipovich* [1921], *Vize* [1940], *Scherhag* [1931], and *Lysgaard* [1949] who discussed the observed warming in the Barents – Kara Seas region, Nordic Seas and northern Europe in 1900-1940. The real bloom of investigation of the climate change in the Arctic and adjacent regions was related to establishing the network of meteorological stations in the Arctic during 1950 [*Przybylak*, 2002]. Numerous expeditions conducted in the Arctic and GIN Sea after the middle of the last century contributed a significant share of observational data as well. Accumulated data records over several years provided evidence of interannual variability of the Arctic and GIN Sea regions. There are, however, still two major shortages in data bases of the Arctic and adjacent areas. First, due to severe climate conditions in high latitudes, the available observations are irregular in time and space: most of the data are obtained in the warm season in the Arctic and even those are scarce. Second, the duration of most of the records is not long enough to identify variability of decadal or longer time scales with sufficient confidence. Besides, it is questionable if the existing century-long or longer data sets [*Jones et al.*, 1986; *Hansen and Lebedeff*, 1987; *Gruza et al.*, 1988] can be representative samples from the population defined as the true northern hemisphere climate characteristic [e.g., *Elsner and Tsonis*, 1991; *Przybylak*, 2002].

1.3.1. Variability of the hydrologic characteristics

Arctic Ocean

Although the Arctic Ocean may have a very stable and unchangeable thermohaline structure, observations show that it exhibits substantial interannual variability, especially in the upper layers. Oceanographic observations have recently identified warming and salinificaiton of the upper Arctic Ocean in the late 1980's and 1990's. For example, *Carmack et al.* [1995] used results from the LARSEN-93 expedition to compare the potential temperature maximum representing the core of Atlantic water within the Arctic Ocean with that reported by *Treshnikov* [1977]. The LARSEN data show evident warming in the upper Arctic Ocean and particularly in the Makarov Basin. The cause of the warming observed in the Arctic Ocean is still obscure. The authors hypothesized that the warming was most likely associated with an increase in the transport and/or temperature of Atlantic Water into the Eurasian Basin.

Swift et al. [1997] compared the 1994 Arctic Ocean Section (AOS94) with other historical records and reported that the data from AOS94 expedition showed considerably warmer water in the Atlantic layer. The 1994 temperature in the Chukchi boundary region was warmer by at least 0.2° C. *Swift et al.* [1994] explained the observed warming of the Atlantic layer by a warming of the source waters in the Norwegian Sea. Those authors further hypothesized that such warming of the source waters was the result of lower heat fluxes during warmer winters in the Norwegian Sea region, which might be explained by the North Atlantic Oscillation (NAO).

The freshwater content of the Arctic Ocean varies from year to year. Evidence of significant interannual variability of the upper halocline in the Arctic Ocean during

the 1990s was presented by *Steele and Boyd* [1998], who reported salinization of the Eurasian Basin. *Steele and Boyd* [1998] hypothesized that the redistribution of the freshwater flux in the Arctic Ocean explained both events observed in 1990s. Similarly, *Dickson* [1999] asserted that the observed salinization of the upper Eurasian Basin was caused by a shift in discharge of the western Siberian river runoff, which had happened in the late 1980s.

The role of freshwater in the salinity changes in the Arctic Ocean has been investigated in *Johnson and Polyakov* [2001]. They reported that changes in the atmospheric circulation over the Laptev Sea caused eastward deflection of the freshwater flux and enhanced sea ice divergence in the region. Numerous ice-free areas led to intense brine rejection during cold seasons, which provided a substantial salinification of the upper Laptev Sea. Both eastward diversion of Siberian rivers and salinification of the upper Laptev Sea significantly reduced the freshwater flux from the sea to the upper Eurasian Basin and led to it developing a positive salinity anomaly.

Another indication of long-period variability in the Arctic Ocean is sea level change. Monthly mean sea level data obtained at tide-gauge stations in the Eurasian seas show a positive trend in sea level with an accelerated rate of sea surface height increase in 1970-1990s, which might be an indication of climate change in the Arctic [*Proshutinsky et al.*, 2001]. *Proshutinksy et al.* [2001] revealed that most of the observed sea level rise could be explained by atmospheric forcing and by changes in the thermohaline circulation due to changes in the temperature and salinity fields in the Arctic Ocean. The authors argued that such changes had been caused by global warming processes, which changed the atmospheric circulation over the region, ice distribution and its growth/melting rates, and thermohaline fields in the Arctic Ocean.

Changes in the thermohaline structure of the Arctic Basin should be necessarily related to low-frequency variability of the basin-wide ocean circulation. Model studies of the Atlantic inflow in the Arctic Ocean conducted by *Zhang et al.* [1998] demonstrated noticeable changes in the ocean circulation at the upper 500 m that had occurred in 1989-1996 compared with 1979-1988. According to model outputs, during 1989-1996 the velocity field in the Arctic Ocean was less anticyclonic especially in the Beaufort Sea as a result of a relatively weak Beaufort high. In the GIN Sea, the Atlantic Water flow was intensified by an expansion of the European subarctic low.

Central Greenland Sea

The largest interannual changes of the oceanographic characteristics in the Greenland Gyre take place in the upper layer. The interannual variability of salinity is higher than that of temperature. The highest interannual variability in surface salinity is in August and autumn, ±0.3 psu, varying from <34 to 34.3 psu in August and from <34.4 to ~34.91 psu in October (Fig. 4 in *Pawlowicz* [1995]). *Alekseev et al.* [1994] found that the thermohaline structure in the Greenland Gyre varied markedly in the years of deep convection compared with years without that structure. The thermohaline structure in the Gyre when deep convection was observed is characterized with almost uniform vertical distribution of water column properties (Fig. 3 in *Alekseev et al.* [1994]).

The East Greenland and Jan Mayen currents are sources of the negative salinity anomalies in the Greenland Gyre. Estimates of inflow rates of the Polar Water

are uncertain. *Swift* [1986] asserted that only a small fraction of the PW from the East Greenland and Jan Mayen Currents entered the central Greenland Gyre.

Thermohaline structure of the water column in the central Greenland Sea determines the development of deep convection. In some years, winter convection in the Greenland Sea is shallow and in other years it can be deeper than 1500 m. For example, *Budéus et al.* [1993] noted winter convection reached only 250 m depth in 1990. *Schlosser et al.* [1991] reported that the formation of Greenland Sea Deep Water by convection was damped by the GSA in the late 1970s and early 1980s. *Alekseev et al.* [1994] found four years in 1980s (1984, 1986, 1988, and 1989) when deep convection occurred.

1.3.2. Sea ice variability

Arctic Ocean

Some authors argue that too little is known about natural variability of Arctic sea-ice thickness to consider the observed ice changes as evidence for the response of the sea ice cover to global climate change [*McLaren*, 1989; *McLaren et al.*, 1990; *McLaren et al.*, 1994]. Others find the sea ice variations to be a very convincing fingerprint of global climate change [*Vinnikov et al.*, 1999]. Data on sea ice, however, indicate evidence of ice thinning in the North Pole region in the late 1980s relative to the late 1970s [*Wadhams*, 1994]. Passive microwave data show substantial regional changes in the sea ice extent [*Parkinson*, 1992]. *Rothrock et al.* [1999] reported significant thinning of the ice cover in the central Arctic Ocean during 1990s. The comparison of sea-ice draft data from submarine cruises between 1993 and 1997 with data acquired from 1958 through 1976

revealed that the mean ice draft had decreased by 1.3 m in most of the interior Arctic Ocean in the 1990s. In contrast, *McLaren et al.* [1994] argued that the large interannual variability of the sea ice thickness obscured any signals of ice cover thinning in the region. The linear least-squares fit to the observations is not statistically significant.

A recent attempt to explain changes in ice cover in the Arctic with only a change in thermodynamic forcing may be incomplete. *Zhang et al.* [2000] conducted a numerical study of changes in sea ice thickness using a coupled sea ice-ocean model. Those authors argued that almost 80% of the ice thinning could be explained by increased ice advection away from coast and enhanced cyclonic anomaly in ice motion both driven by the NAO. Such abnormalities in sea ice motion result in increased production of thin ice during winter.

Another possible reason, besides thermodynamics, for recent decreases in Arctic ice cover in summer was forwarded by *Maslanik et al.* [1996]. The authors attributed the ice thinning in 1990s with the increase in cyclone frequency since 1989. Cyclone intensification over the Siberian seas favors stronger southerly winds, which, apart from heat advection onto the shelf region, push ice northward. Also, increased cyclone activity causes ice divergence within the consolidated ice pack producing more leads and polynyas [*Serreze et al.*, 1990]. The role of atmospheric forcing in the sea ice thickness distribution in the Arctic Ocean was studied by *Rigor et al.* [2002]. They showed a significant correlation between sea ice motion anomalies and sea level pressure trends in the Arctic expressed via the Arctic Oscillation (AO) index.

Central Greenland Sea

Ice conditions in the central Greenland Sea vary from year to year. During some years, no ice was observed, whereas during other years ice concentraion was high, especially in the eastern part of the central Greenland Sea. The role of ice formation in the Greenland Gyre's deep convection remains uncertain. *Carsey and Roach* [1994] concluded, from the satellite data, that there was a strong relationship between ice cover features in the Nordbukta and Odden. *Pawlowicz* [1995] showed a relationship between the timing and concentration of ice coverage in the Greenland Gyre and deep convection. Conversely, *Vinje et al.* [2002] believed that sea ice formation might not be that important in development of the deep convection in the central Greenland Sea.

1.3.3. Variability of the meteorological characteristics

Meteorological characteristics, such as surface air temperature (SAT), precipitation, atmospheric pressure, and river runoff, have higher variability than the oceanographic parameters. Among all characteristics, SAT is a better-known element of the Arctic climate. Analysis of the observational SAT in the 20th century shows larger variability in data from the Arctic region than from the lower latitudes [*Kelley and Jones*, 1982; *Kelley et al.*, 1982]. Model studies predict amplified Arctic warming due to global warming. This so-called polar amplification, which is assumed to be an intrinsic feature of the Arctic [*Moritz et al.*, 2002], has been disputed recently [*Polyakov et al.*, 2002a; *Polyakov et al.*, 2002b; *Polyakov et al.*, 2002c; *Przybylak*, 2002].

Surface air temperature

The annual average SAT in the Arctic estimated for 1951-1990 varies within the range −14°C to −18°C ±10%. For the central Greenland Sea, the annual average SAT is −8°C +20% and −40% (Fig. 5.2 in *Przybylak* [2002]). SAT in the Greenland Sea is more variable than in the Arctic Ocean, and the distribution of the Greenland Sea SAT is skewed towards negative anomalies. From long-term data sets, it is generally accepted that the annual SAT in the Arctic had a positive trend in the 1920s to early 1940s, then decreased until the end of the 1960s, and again warmed after 1975 [*Dmitriev*, 1994; *Jones*, 1994]. The warming of the Arctic was faster during the 1990s than during earlier periods. The warmest decade in the Arctic was 1931 – 1940. The Arctic has been rapidly warming since 1990. During 1990-2000, the greatest warming occurred in the Canadian Arctic and Alaska and in the northern Greenland Sea. The weakest warming, for that same period, was in the Russian Arctic [*Przybylak*, 2002].

Precipitation

Precipitation is inconsistent in time and space. The annual values vary from 600-800 mm in the western Greenland Sea to <50 mm in the northern Canadian Arctic and East-Siberian Sea [*Gorshkov*, 1980; *Burova*, 1983]. The range of variability of annual precipitation is largest in the coolest areas of the Arctic. The variability over the Canadian Basin reaches ± 30% of the mean value. Over the rest of the Arctic, the coefficient of variability is ~ 20% [*Przybylak*, 2002]. Variability of precipitation in the Arctic does not follow the SAT. According to *Przybylak* [2002], negative anomalies of precipitation clearly dominated during the warmest decade in the Arctic in 1931-1940. Over 1951-1990, precipitation

decreased in an area slightly greater than the Arctic and adjacent regions: Greenland Sea, Eurasian shelf, and the southeastern part of the Canadian Arctic. During the recent warming, however, anomalies of precipitation are positive over most of the Arctic coinciding with the SAT trend in the same area. The positive trends in annual precipitation in 1990 – 2000 have been observed in the central and western Arctic. The Eurasian shelf has a negative trend over the same period.

River runoff

The overall, long-term mean river inflow into the Arctic Ocean for 1921-1996 is estimated at 2430 $km^3 \cdot yr^{-1}$. Interannual variability of the total river runoff is not large and lies within ± 10% of the mean value [*Shiklomanov et al.*, 2000]. The maximum inflow (4870 km^3) was observed in 1974, and the minimum inflow (3820 km^3) in 1953. Like precipitation, the interannual variability of the river runoff to the Arctic Ocean does not show a significant correlation with SAT. The recent warming in the Arctic is associated with a 3-5% increase of the river inflow to the ocean, which is well within natural variability [*Shiklomanov et al.*, 2000].

Atmospheric pressure

Another important index of climate variability in the Arctic is the atmospheric pressure and, in particular, sea level pressure (SLP). The mean pattern of SLP in the Arctic is characterized by anticyclonic vorticity over the largest part of the basin. On a multiyear time scale, the SLP oscillates, indicating either decreasing

or increasing anticyclonic vortex. Atmospheric pressure in the upper troposphere – lower stratosphere over the high latitudes characterizes the intensity of the Polar Vortex. There are a number of studies of high latitude atmospheric pressure change and its relation to other components of the climate system. For example, *Vangengeim* [1952] and later *Girs* [1974] studied daily 500-mb pressure field over the northern hemisphere. They reported that the general atmospheric circulation in the hemipshere with a several day time-scale was determined by the Rossby waves in the upper troposphere. In particular, *Girs* [1974] asserted that under the conditions of small Rossby waves, the general atmospheric circulation was westward (zonal) and no heat was advected into the Arctic. This promoted further Arctic cooling. According to *Girs* [1974], years with anomalously frequent occurrences of such atmospheric circulation would lead to cold Arctic.

Gudkovich [1961] explained two types of surface circulation patterns in the Arctic Ocean defined by the SLP distribution. The intensified polar high forced anticyclonic surface water circulation in the Canadian Basin. The dissipation of the polar high led to contraction of the anticyclonic circulation. This idea was supported by *Walsh et al.* [1996] who observed a decrease in sea level pressure since 1988 and enhancement of atmospheric cyclonic vorticity over the Arctic.

Thompson and Wallace [1998] analyzed the 850-mb geopotential heights. The first EOF mode indicated that the thickness of the lower atmosphere over the Arctic and surrounding areas behaves in the opposite manner. When the troposphere becomes thicker over the Arctic Basin, it is thinning over the adjacent regions, and vice versa. This spatial pattern is known as the Arctic Oscillation (AO).

A correlation between the SLP decrease in the central Arctic and increase in cyclone activity was reported in *Serreze et al.* [1997]. Similar to other studies, those authors showed that the cyclone activity over the North Atlantic was greater during the positive NAO mode and shifted poleward. The cyclone penetration into the Arctic led to intense ice melting. *Maslanik et al.* [1996] asserted that increased cyclone activity since 1989 had caused a reduction of the ice cover in the Arctic Ocean through a combination of dynamics and thermodynamics.

1.3.4. Timescales for climate variability in the Arctic

The observed variability in the polar region has been intensively studied in recent decades [*Budyko*, 1977; *Mysak and Power*, 1992; *Wadhams*, 1994; *Slonosky et al.*, 1997; *Mysak and Venegas*, 1998; *Rigor et al.*, 2002]. The central question in these studies was how regular were the observed climate variations. From observations and model studies, several dominant timescales of climate variability in the Arctic have been proposed.

Nikiforov and Shpaikher [1980] hypothesized that atmospheric and oceanic circulation in the Arctic was driven by the feedback mechanisms between atmospheric, terrestrial hydrological and oceanic processes. The hypothesized timescale of this variability was 5 – 6 years.

Ten-year period oscillations of the first Empirical Orthogonal Function (EOF) modes for winter sea ice concentration, sea level pressure, 500-hPa height and

850-hPa temperature since the 1960s were discerned by *Slonosky et al.* [1997]. A large portion of the variance lay within a decadal timescale.

Another mechanism for decadal climate variability in the Arctic was proposed by *Mysak et al.* [1998]. Based on the results of the EOF analysis of the sea ice concentration (SIC) and SLP time series in the Arctic, *Mysak et al.* [1998] suggested a feedback loop for the decadal Arctic climate cycle which relates SIC and SLP in the Greenland, Barents, Laptev, and Beaufort seas. The oscillation of the SLP anomalies was assumed to be linked to the two phases of the NAO. Recently, *Venegas and Mysak* [2000] surmised the existence of several timescales of natural climate variability in the Arctic with periods of 6-7, 9-10, 16-20 and 30-50 years.

A mechanism of a quasi-decadal (15-18 years) climate variability of the Arctic Ocean – Greenland Sea system was reported in *Goosse et al.* [2002]. A suggested feedback loop in the ice-ocean system was driven by different ice production rates in the Arctic which affect the salinity of the outflow to the Greenland Sea. *Goosse et al.* [2002] argued that salinity variations of the Arctic water outflow controlled the development of the deep convection in the Greenland Sea.

Proshutinsky and Johnson [1997] proposed a theory for the existence of an anticyclonic - cyclonic regime cycle in the Arctic with a period of 8-15 years which formed a basis for a major assumption of climate variability in the Arctic. Details of the anticyclonic - cyclonic regime shift and the role of freshwater in this mechanism are presented in the next chapter.

Section 1.4. Summary

- This chapter gave a general description of the Arctic Ocean and GIN Sea atmosphere-ice-ocean climate system. The prominent features of the two regions are the positive freshwater balance of the Arctic Ocean and intense heat flux to the atmosphere in the GIN Sea.

- The area of the most intense heat flux in the GIN Sea is the Greenland Sea. Interannual variability of the heat flux can be related to the deep convection in the central Greenland Sea.

- Arctic Ocean and GIN Sea exhibit interannual variability, most of which has a quasi-decadal time scale.

Chapter 2 ARCTIC OCEAN – GREENLAND SEA AS AN AUTO-OSCILLATORY CLIMATE SYSTEM

The long-period climate variability of the Arctic Ocean and Greenland, Iceland, Norwegian Seas (GIN Sea) have several dominant time scales. Most researchers believe that a quasi-decadal timescale is dominant for Arctic climate variability. This study is focused on the anticyclonic – cyclonic decadal regime shifts in the Arctic with a hypothesized timescale of 10-15 years [*Proshutinsky and Johnson*, 1997]. It is further hypothesized that there are two processes that determine low-frequency variability in the region. The first process is freshwater flux from the Arctic Ocean to the GIN Sea. The second is heat flux from the GIN Sea to the Arctic Ocean. It is believed that the observed anticyclonic – cyclonic regime shifts are a manifestation of an auto-oscillatory behavior of the system. Auto-oscillatory behavior is initiated and supported by the climate system itself. The period of these oscillations is determined by the properties of the system. Existence of energy sources within the system is a necessary condition for auto-oscillations [*Gudkovich and Kovalev*, 2002]. Another condition of an auto-oscillatory system requires feedback mechanisms that return the system to its initial state.

In the Arctic Ocean – GIN Sea system, there are two energy sources: (1) potential energy of the Arctic Ocean (specifically the Beaufort Gyre), which is accumulated during the anticyclonic and released during the cyclonic regime; (2) the internal energy of the GIN Sea atmosphere, which increases during the anticyclonic and decreases during the cyclonic regime. The auto-oscillatory behavior is realized through the positive-negative feedback mechanism discussed in this chapter.

In this study, the focus is on the central Greenland Sea because, first, this is a region where deep convection occurs and, through it, drives high surface heat fluxes to the winter atmosphere. Due to extremely high winter surface heat fluxes (see Table 1.5), this region is important in climate shaping. Second, the central Greenland Sea is sensitive to variability of the freshwater outflow from the Arctic Ocean [e.g., *Proshutinsky et al.*, 2002]: high freshwater export can shut off the convection. Hence, the convective behavior in the central Greenland Sea is modeled as a key example of GIN Sea variability induced by the Arctic Ocean freshwater outflow.

In this chapter a description of the anticyclonic – cyclonic regime shifts theory and the role of freshwater in this mechanism are presented. Then the hypothesized auto-oscillatory behavior is explained followed by the goals of the study.

Section 2.1. Anticyclonic – cyclonic regime shifts in the Arctic

Proshutinsky and Johnson [1997] (*P&J* hereafter) surmised the existence of two regimes of wind-forced circulation in the Arctic Ocean. Following the foregoing theoretical ideas [e.g., *Gudkovich*, 1961; *Gudkovich and Nikiforov*, 1965], *P&J* identified two dominant climate states in the Arctic characterized by anticyclonic and cyclonic oceanic circulations. In their model study, *P&J* used sea surface heights (SSH) in the center of the basin-wide circulation as an integral measurement (index) describing the transition of the Arctic Ocean circulation from anticyclonic (ACCR) to cyclonic (CCR) (see Fig. 9 in *P&J*). SSH reflect the intensity of the barotropic wind-driven basin-wide circulation in the Arctic Ocean. Positive values of the SSH in the center of the circulation indicated anticyclonic rotation of the surface water, negative values corresponded to the cyclonic circulation. The two wind-driven ice and water circulation regimes appeared to alternate at intervals of 5-7 years, resulting in a period of 10-15 years.

The analysis of the sea level pressure (SLP) fields in the Arctic during CCR and ACCR has identified a "seesaw" pattern in SLP, meaning that the increase of SLP over the Arctic Ocean corresponds to the SLP decrease over the Siberia, Alaska, and western Canada [*Johnson et al.*, 1999]. Similar behavior was found in other studies [*Mysak and Venegas*, 1998; *Thompson and Wallace*, 1998]. According to *Johnson et al.* [1999], the major feature of SLP fields during anticyclonic winter was that a high SLP ridge extended across the western Arctic. During cyclonic winter, the SLP high weakened over the central Arctic and withdrew toward Russia. Also the Icelandic Low was stronger, and extended farther into Baffin Bay, and the Barents, Kara, and Laptev Seas. Summer SLP patterns also differed for CCR and ACCR. During cyclonic summer, the low SLP region extended from

the GIN Sea to the central Arctic Ocean and provided cyclonic forcing. During anticyclonic summer, a high SLP cell stayed over the Beaufort Gyre.

It is noteworthy that seasonal cycles of Arctic climate are different in the two regimes. *Proshutinsky et al.* [1999] compared and described observed and simulated anomalies of environmental parameters in terms of the two regimes theory. *Polyakov et al.* [1999] compared the seasonal cycle in years attributed to CCR and ACCR. Based on these two and other studies related to the regime shifts in the Arctic [*Proshutinsky and Johnson*, 1997; *Johnson et al.*, 1999; *Polyakov and Johnson*, 2000; *Proshutinsky et al.*, 2001], the meteorological and hydrological characteristics in the Arctic Ocean – GIN Sea region for CCR and ACCR are summarized in Table 2.1.

Recently, *Proshutinsky et al.* [2002] proposed a mechanism of freshwater accumulation and release in the Beaufort Gyre as a primary regulator of the regime shifts in the Arctic and GIN Sea. *Proshutinsky et al.* [2002] hypothesized that during ACCR the Beaufort Gyre accumulated freshwater and potential energy through the convergence of sea ice and surface water maintained by the anticyclonic vorticity of the atmosphere over the Arctic. During CCR, a weakened anticyclonic vortex was not able to maintain the accumulated freshwater surplus within the Beaufort Gyre, and the Arctic Ocean released freshwater to the North Atlantic. From *Proshutinsky et al.* [2002], it follows that the interaction between the Arctic Ocean and the GIN Sea is determined by the dynamic height gradient between the Beaufort Gyre and the North Atlantic. When ACCR characterizes the Arctic, the dynamic height gradient is increasing due to freshwater accumulation in the Beaufort Gyre. The transition from ACCR to CCR is characterized by weakening of the anticyclone over the Arctic and freshwater release from the Beaufort Gyre to the GIN Sea. After several CCR years of increased freshwater

outflow to the North Atlantic, the gradient decreases, ceasing the interaction between the basins.

Table 2.1. Hydrological and meteorological characteristics of the studied region for different regimes

Characteristics	ACCR	CCR
Wind speed	Lower	Higher
Surface air temperature	Cooler mean winter SAT[a] (max difference is in March)	Warmer mean winter SAT
Cloudiness	Lower	Higher
Ice drift speeds (Central Arctic)	Lower	Higher
Ice drift speeds (Beaufort Gyre)	Higher	Lower
Ice transport by the Transpolar Drift Current	Intensified, export from the East-Siberian, Laptev and Kara seas	Export from the Canadian Basin
SLP in the central Arctic	Positive anomaly	Negative anomaly
Precipitation	Decreased over the ocean, increased over the land	Increased over the ocean, decreased over the land
River runoff	Increased	Decreased
Ice volume flux into the GIN Sea	Lower	Higher

Table 2.1. Continued

Characteristics	ACCR	CCR
Ice thickness	Much thicker (+0.2 to +0.4 m in the Beaufort Gyre, +1.1 to +1.6 m in the Central Arctic [*Polyakov et al.*, 1999])	Thinner
Freshwater transport through Fram Strait	Significantly lower due to anticyclonic vortex piling up the surface freshwater in the Beaufort Gyre	Significantly higher due to prevailing winds that cause more intense outflow from the arctic ocean and due to weakening of the anticyclone over the Arctic
Atlantic layer	Upper boundary is concave down with a camber in the Central Arctic and Beaufort Gyre, intense flow onto the shelf	Upper boundary is convex up, no or little flow onto the shelf
Sea level	Positive anomaly in the Central Arctic and Beaufort Gyre, negative anomaly on the periphery	Negative anomaly in the Central Arctic and Beaufort Gyre, rise on the periphery
Shelf – Arctic Basin exchange	Surface water from shelf, deep water on shelf	Surface water on shelf, deep water from shelf
Winds over the Eurasian Shelf Seas	Towards the Eurasian Basin pushing surface water and ice into the interior Arctic Ocean	Winds drive river water eastward, causing salinification of the upper Eurasian (Nansen) Basin

Table 2.1. Continued

Characteristics	ACCR	CCR
Salinity of the surface Arctic Ocean[b]	Higher due to increased ice freezing, redistribution of the river runoff	Lower due to increased ice melting. *Polyakov et al.* [1999] considered additional ice melting during the CCR as one of the major processes responsible for negative salinity anomaly. Additional ice melt causes freshening of the upper ocean in the Eurasian Basin and Canadian Basin

(a) Surface air temperature.
(b) Here the general tendency of S changes are mentioned. In reality, different regions of the Arctic Ocean can reveal different S variability. For example, due to redistribution of the increased river runoff during ACCR and surface water convergence, S in the Beaufort Gyre may even decrease [*Proshutinsky, personal communication*].

Section 2.2. Hypothesis: Mechanism of auto-oscillatory behavior of the Arctic Ocean – Greenland Sea climate system

The theoretical foundation for this study is the *P&J* theory of the anticyclonic – cyclonic regime shifts in the Arctic. It is assumed that both the heat flux from the GIN Sea to the Arctic and freshwater flux from the Arctic Ocean to the GIN Sea drive the ACCR/CCR shift. Intense heat flux causes the transition from ACCR to CCR. The response of the Arctic Ocean to the anomalously high heat advection is increased freshwater release to the GIN Sea, which, through negative feedback loops, shuts off the vigorous heat advection to the Arctic and resettles the ACCR. Thus, the hypothesized mechanism of the climate variability in the Arctic Ocean – GIN Sea region has two transition pathways with two opposite climate states.

To characterize different regimes in the investigated climate system, *P&J* terminology is used: "ACCR" and "CCR". However, note that *P&J* terminology is attributed to the Arctic only. ACCR assumes a strong anticyclone in the Arctic. At the same time, there is a strong cyclone over the GIN Sea. Conversely, CCR assumes weakening of the anticyclone over the Arctic, while simultaneously, the cyclone over the GIN Sea weakens. Thus, ACCR implies cold Arctic with strong anticyclone and warm Greenland Sea with intensified cyclonic activity. The opposite climate state, CCR, means warm Arctic with weak anticyclone and cold Greenland Sea with ceased cyclogenesis.

2.2.1. ACCR: Cold Arctic / Warm Greenland Sea

The initial ACCR state of the system (Fig. 2.1) is characterized by the cold Arctic and warm Greenland Sea. During this state, the interaction between the regions is weak: the heat advection to the Arctic Ocean is low, and the Polar Water (PW) and ice fluxes to the Greenland Sea are small.

The energy balance of the earth can be written as [Chapter 8, *Matveev*, 1984]:

$$R_E = I_0'(1 - \alpha_E) - F_\infty , \qquad (2.1)$$

where I_0' is insolar radiation at the top of the atmosphere, α_E is albedo of the earth, and F_∞ is the energy radiated to space. For the high latitudes, energy loss is much higher than gain through a year, i.e. $|F_\infty| >> |I_0'(1-\alpha_E)|$ and the annual energy balance is negative. This means that without an additional energy source such as heat advection, the Arctic atmosphere rapidly cools, the atmosphere over the Arctic becomes denser, sea level pressure increases and anticyclone becomes stronger, i.e. ACCR dominates in the Arctic. In accordance with *Proshutinsky et al.* [2002], during the ACCR the freshwater content (FWC) in the Arctic Ocean is increasing. Thus, the Arctic Ocean accumulates potential energy in the surface water of the Beaufort Gyre. In all, the upper Arctic Ocean contains more freshwater and the atmosphere is colder.

During the ACCR, the Polar Water (PW) outflow to the Greenland Sea is low. Because the central Greenland Sea receives only a small fraction of the PW outflow, and even less during intense cyclonic activity in the region due to positive surface water divergence in a cyclonic gyre, the surface salinity in the

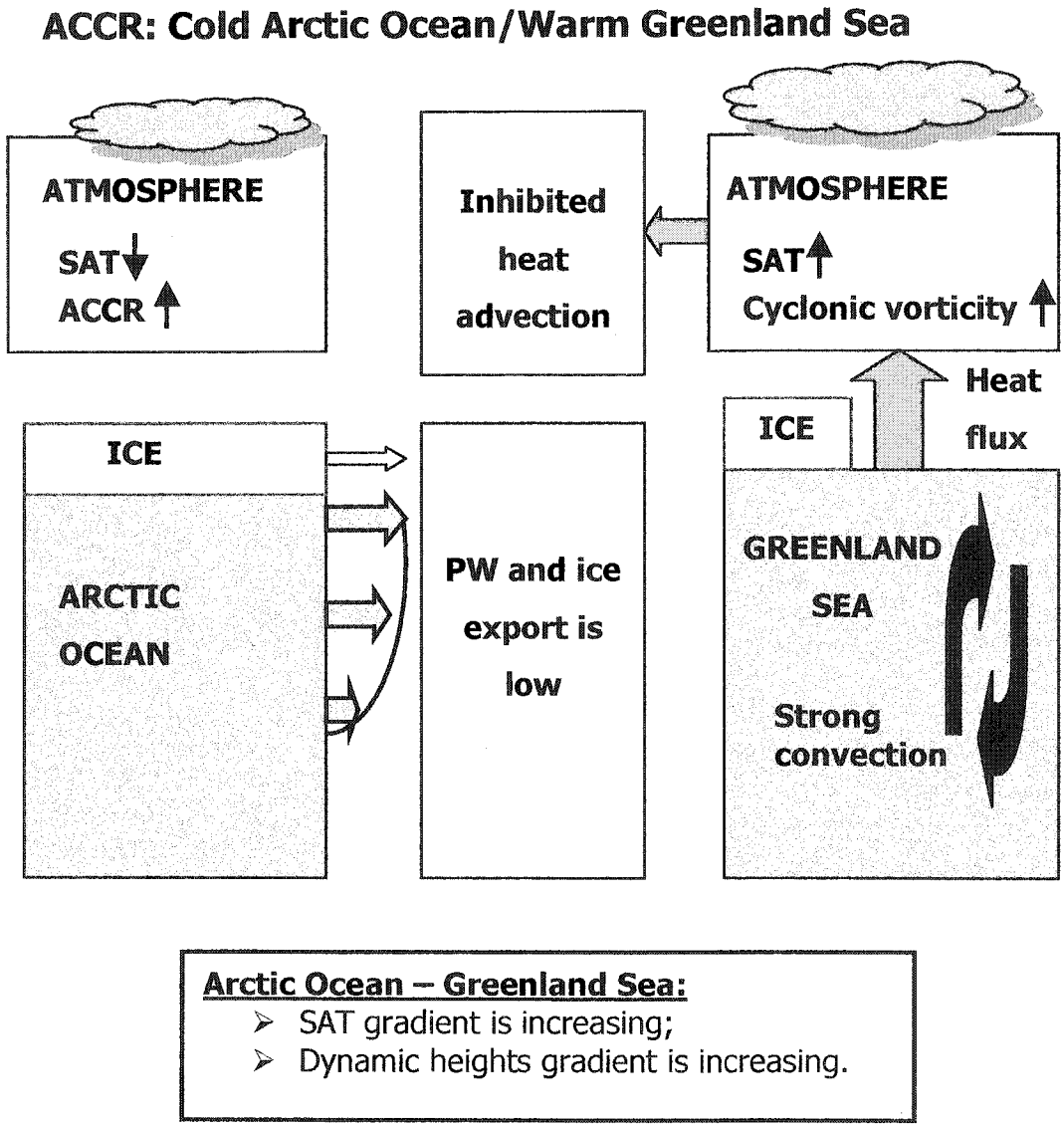

Fig. 2.1. ACCR state of the hypothesized behavior of the Arctic Ocean – Greenland Sea system. *The state is characterized by low interaction between the Arctic Ocean and Greenland Sea. Inhibited heat advection enhances cooling and anticyclonic vorticity in the Arctic. ACCR in the Arctic favors freshwater accumulation. The Greenland Sea is warm and saline. The low water column stability allows deep convection. Enhanced heat fluxes to the atmosphere cause warming of the Greenland Sea atmosphere. Both gradients – dynamic heights and SAT – are increasing. Large gradients initiate the interaction between the basins.*

central Greenland Sea is relatively high. The high surface salinity makes the water column stability close to neutral which favors deep convection in the central Greenland Sea in winter. Strong convection entrains heat from the underlying warm AIW and relatively warm NSDW. This heat is conveyed to the atmosphere, causing positive SAT anomalies in winter. During the warm season, when the heat flux is from the atmosphere to the sea, the atmosphere loses relatively little heat to the sea surface since the sea is warm with low sea ice concentration. This promotes atmospheric warming and intensification of the cyclonic vorticity over the Greenland Sea. In general, during ACCR, the Greenland Sea atmosphere is warming.

If one compared the Arctic Ocean and Greenland Sea regions, one would see that the SAT and dynamic height gradients between the regions were increasing during ACCR. These differences promote the interaction between the two areas and ACCR switches to CCR (Fig. 2.2).

2.2.2. CCR: Warm Arctic Ocean / Cold Greenland Sea

It is believed that the ACCR / CCR climate shift is initiated by the increased heat advection to the Arctic. Heat advection changes the energy balance in the Arctic, making it less negative and the atmosphere starts warming. A warm atmosphere affects the pressure field. The anticyclonic vorticity over the Arctic weakens and even may change to cyclonic in summer. Thus, ACCR shifts to CCR in the Arctic. From the weak anticyclonic vortex, the Arctic Ocean starts loosing its accumulated freshwater. The ice and PW outflow to the North Atlantic increases, and the central Greenland Sea receives more freshwater and the upper layer

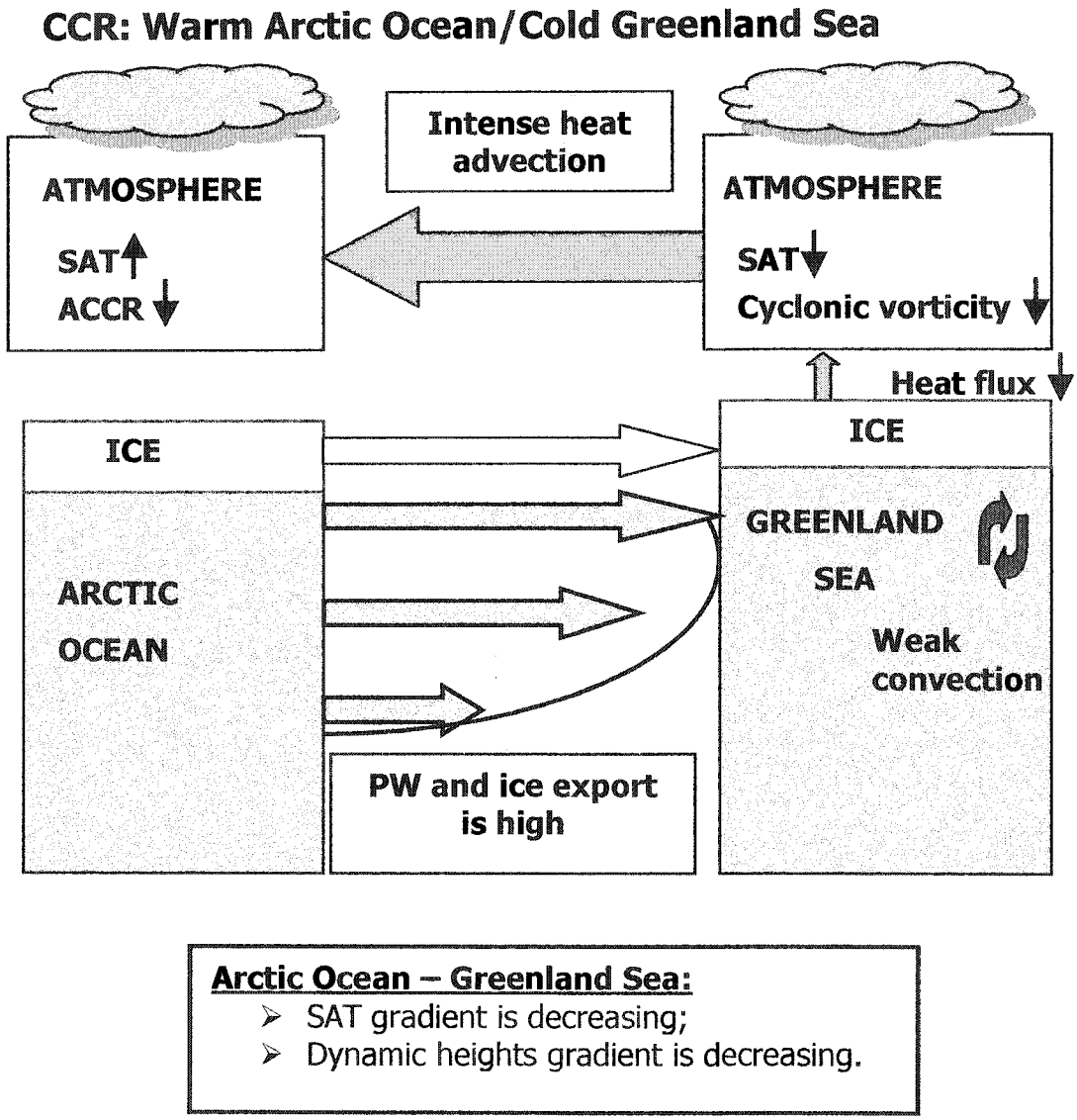

Fig. 2.2 CCR state of the hypothesized behavior of the Arctic Ocean – Greenland Sea system. *The state is characterized by intense interaction between the Arctic Ocean and Greenland Sea. Vigorous heat advection warms up Arctic atmosphere and damps the anticyclonic vorticity. ACCR shifts to CCR. The Arctic Ocean releases accumulated freshwater and ice to the Greenland Sea. The diluted surface layer inhibits convection in the Greenland Sea. Ice concentration increases and heat flux to the atmosphere weakens causing cooling of the Greenland Sea atmosphere. Both gradients – dynamic heights and SAT – are decreasing and after several years of CCR, the interaction stops.*

becomes fresher, increasing stability and suppressing deep convection. Without entrained heat from below, the upper mixed layer easily reaches the freezing point in winter and the ice cover appears. Both weak convection and ice cover reduce the heat flux to the atmosphere in winter. In summer, the heat flux from the atmosphere to the ocean supports ice melting and warming of the cold sea surface. In all, the atmosphere over the Greenland Sea is cooling and cyclonic vorticity is weakening.

After several years of the CCR state, the SAT and dynamic height gradients decrease. At some critical value the interaction between the two basins fades and the system rebuilds the ACCR.

2.2.3. Positive-negative feedback mechanisms in the auto-oscillatory climate system

In the Arctic Ocean, negative SAT anomalies strengthen the negative (anticyclonic) vorticity of the atmosphere which causes positive FWC anomalies. At the same time, the upper Greenland Sea becomes saltier. Hence the dynamic height gradient between the basins grows. A higher dynamic height gradient between the regions, due to the Arctic increased FWC, favors intense interaction between the Arctic and the Greenland Sea. Vigorous interaction leads to positive SAT anomalies in the Arctic, which tend to change the sign of vorticity, and so on. The diagram of these positive-negative feedback mechanisms in the two basins is shown in Fig. 2.3.

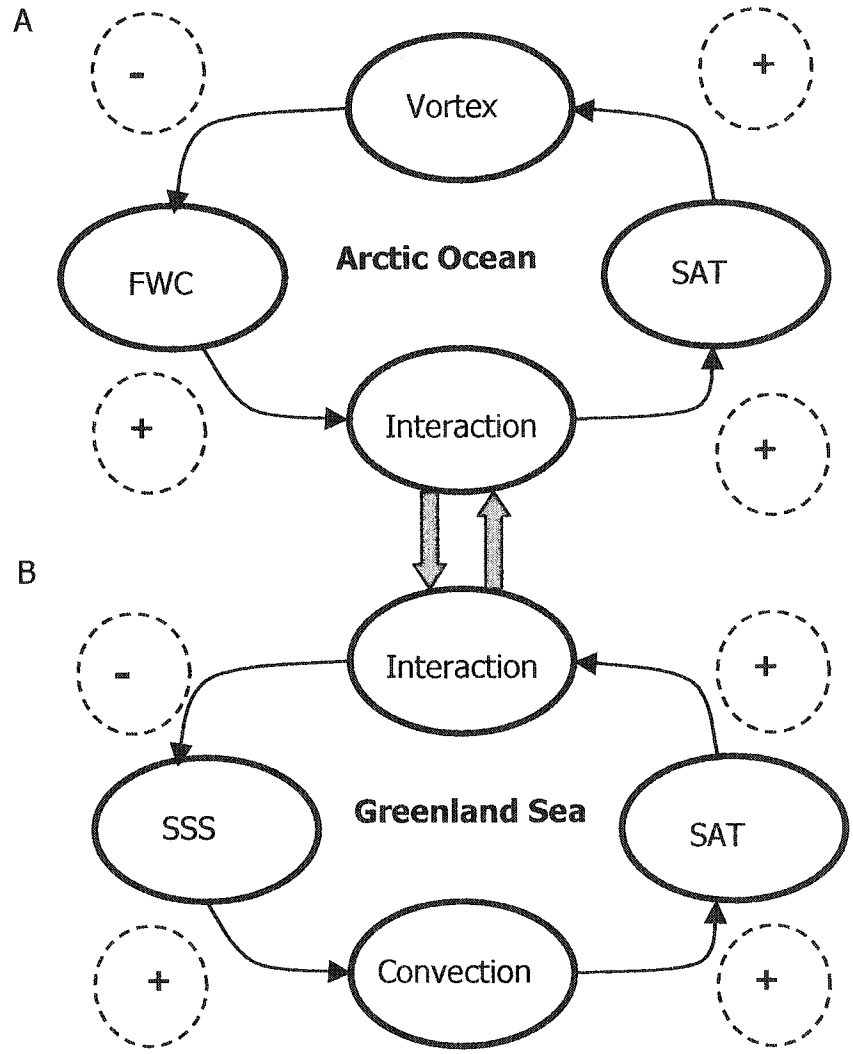

Fig. 2.3. Feedback loops in the real climate system. *(A) Arctic Ocean: negative SAT anomalies -> negative (anticyclonic) vorticity -> positive FWC -> intensified interaction -> positive SAT anomalies. (B) Greenland Sea: positive SSS -> intense convection -> positive SAT anomalies -> intensified interaction -> negative SSS.*

In the Greenland Sea, positive sea surface salinity (SSS) anomalies promote intense convection in the region which causes positive SAT anomalies. Large SAT gradients between the Arctic and Greenland Sea region favors intense interaction through heat advection to the Arctic followed by intense freshwater outflow to the Greenland Sea, which causes negative SSS anomalies in the central part, and the cycle continues.

It is important to note that if there were no interaction through the feedback loops, both regions would maintain ACCR: the Arctic would be cold with strong anticyclone, and the Greenland Sea region would be warm with intense deep convection in the Greenland Gyre. Two-way interaction between the basins provides the foundation of an auto-oscillatory behavior of the system, as the higher the disturbance signal sent to one basin, the stronger the response in the other basin.

What triggers this interaction? There are two possibilities: the freshwater flux or heat flux. Let us assume that the freshwater triggers the variability. The initial state is ACCR in the Arctic. It has been shown that without sufficiently large heat advection the Arctic Ocean will cool and maintain the ACCR. After several years of ACCR, the Arctic climate system reaches the steady state, i.e. SAT stops dropping, the anticyclone stops growing and FWC reaches its maximum. The dynamic height gradient between the two basins is large. Although the anticyclone is still strong and it keeps the freshwater in the Beaufort Gyre, large dynamic height gradients might provoke some intensification of the freshwater export to the North Atlantic. Very sensitive to the surplus of freshwater, the convection in the central Greenland Sea weakens. This leads to cooling of the Greenland Sea, decreasing of the SAT gradient between the Arctic and Greenland Sea, and further reduction of the heat advection to the Arctic. The

Arctic starts cooling, ACCR becomes stronger, and less freshwater is available for the outflow to the Greenland Sea. So, the freshwater outflow alone does not cause Arctic warming and ACCR/CCR shift. Moreover, the freshwater outflow damps the interaction between the basins and thus, strengthens ACCR of the system.

The following sequence of events is believed to take place. The increasing SAT gradient between the Arctic and adjacent Greenland Sea causes northward heat transport, changing the zonal heat fluxes to meridional. The Arctic starts receiving internal energy which, through the warming of the atmosphere, weakens or even changes the anticyclonic vorticity over the Arctic and releases freshwater to the Greenland Sea. Thus, heat flux triggers the interaction between the Arctic and Greenland Sea.

Section 2.3. Goals of the study

The purpose of this study is to investigate the low-frequency, natural climate variability in the Arctic and Greenland Sea regions. Particularly, the work is focused on a mechanism driving the ACCR/CCR shift in the Arctic discussed in *P&J*. To do that, the following hypothesis is given.

Hypothesis: The Arctic Ocean and Greenland Sea can be seen as a single ice-ocean-atmosphere climate system. There are two opposite climate states of the system: ACCR characterized by cold Arctic / warm Greenland Sea region, and CCR characterized by warm Arctic / cold Greenland Sea region. It is hypothesized that the decadal climate variability in the region is the manifestation of auto-oscillatory behavior of the Arctic Ocean – Greenland Sea climate system realized through the climate state shifts. ACCR/CCR regime shift is controlled by the two-way interaction between the regions realized through heat flux to the Arctic and freshwater flux to the Greenland Sea.

The major goal of the study is to verify the hypothesis and to simulate the auto-oscillatory behavior of the system. Other objectives of the study are:

- to investigate the role of freshwater flux in the climate variability in the Arctic Ocean and Greenland Sea;

- to explore the surface heat flux in the Greenland Sea under different climate states and its role in the interannual variability of SAT in the region;

- to study the thermohaline structure variability in the Greenland Sea and upper Arctic Ocean;

- to estimate the role of heat advection to the Arctic as a factor triggering the variability in the climate system.

To fulfill these objectives, an Arctic Ocean – Greenland Sea model has been developed and several model experiments have been designed and run. The description of the model and the experiments are given in the following chapters.

Section 2.4. Summary

- This chapter described the anticyclonic – cyclonic Arctic regime shifts theory by *Proshutinsky and Johnson* [1997], which is used as a theoretical background for this study.

- This study is focused on the central Greenland Sea as a key region of the GIN Sea.

- Evidence in support of the theory was reviewed demonstrating that the Arctic Ocean and Greenland Sea could form an auto-oscillatory climate system.

- The hypothesis and major goals of this research were discussed. The primary goal of the study is to test the hypothesis by simulating the auto-oscillatory behavior of the system.

Chapter 3 ARCTIC OCEAN AND GREENLAND SEA MODELS

There are a wide variety of different models of the polar regions [e.g., *Hakkinen*, 1987; *Smith et al.*, 1988; *Hakkinen and Geiger*, 2000]. In this chapter, models of the central Arctic Ocean, the Arctic shelf, and the central Greenland Sea are presented. It is believed that to verify the hypothesized auto-oscillatory behavior of the Arctic Ocean – GIN Sea system, it will be enough to parameterize the behavior of the most important components of the studied region, such as mixed layer dynamics, water export/import rates, ice production, and general shelf processes. As discussed in Chapter 2, this study is focused on the central Greenland Sea as a key region of the GIN Sea.

It is well known that the Arctic Ocean has a unique upper-layer thermohaline structure, which is almost independent of horizontal position [*Killworth and Smith*, 1984]. Thus a one-dimensional model might be sufficient to describe the general features of the upper layer. The *Kato-Phillips* model of the entrainment of the surface turbulent layer [*Kato and Phillips*, 1969], which has been further developed by *Stigebrandt* [1981; 1985] and *Bjork* [1989], has been chosen among several simple models of the polar regions. Some adjustments have been done to the model. A shelf box model has been added to the Arctic Ocean model to parameterize shelf processes affecting salinity redistribution in the water column of the Arctic Basin. A thermodynamic sea ice model [*Maykut and Untersteiner*, 1971; *Maykut*, 1986] has been coupled to all the models to describe the ice melting/freezing cycle. Two atmospheric models for the Greenland Sea and the Arctic Ocean are coupled to the sea-ice components.

In the next section, previous theoretical studies of the mixed layer dynamics and simulation of the upper layer and halocline are briefly discussed. Then the models of the Arctic Ocean, shelf and Greenland Sea regions, and the input parameters and data used in the simulations, are described.

Section 3.1. Previous theoretical and modeling studies of the upper layer dynamics

The Arctic Ocean is strongly stratified. The ice cover, upper (mixed) layer, and halocline are the most active layers in the Arctic Ocean water column, revealing both seasonal and interannual variability. All climate variability necessarily leads to thermohaline changes in the Arctic Ocean. Relatively small horizontal gradients of temperature and salinity within the real Arctic Ocean enable researchers to apply simple one-dimensional and box models to generate a realistic first-order description of the stratification and evolution of the upper Arctic Ocean. There is a wide variety of simple models describing seasonal and interannual pycnocline and mixed layer dynamics. Theoretical studies of upper layer dynamics have been performed by *Kitaigorodsky* [1960], *Kraus and Turner* [1967], *Turner and Kraus* [1967], *Kato and Phillips* [1969], *Turner* [1973], and *Pollard et al.* [1973] and others.

All the studies of the surface layer dynamics are based on the energy balance of the upper ocean. Generally two processes are responsible for possible mixing in the upper layer. First, the upper layer gains kinetic energy from the wind stress, mixing the upper with the underlying layer and increasing the potential energy of the water column. Thus, the kinetic energy transforms into potential. Second, the potential energy of the upper layer increases via cooling or salinification (e.g., during ice formation) until the system becomes unstable, and then convective mixing occurs.

Kitaigorodsky [1960] considered a steady-state model to compute energy balances in the vertical. *Kitaigorodsky* estimated the depth of the mixed layer

from a balance between the work of the wind stress and the work needed to mix heat downward from the surface. *Kraus and Turner* [1967] developed a time-dependent model of the mixed layer formation due to surface cooling and heating at depth, as well as the mechanical stirring due to wind stress. In their theoretical model, based on a laboratory experiment, *Turner and Kraus* [1967] found that the entrainment velocity depends on a friction velocity and on a stability parameter expressed in terms of an overall Richardson number (Ri_o):

$$Ri_o = \frac{gH\Delta\rho}{\rho u_*^2}, \qquad (3.1)$$

where g is gravitational acceleration, H is depth of a mixed layer, $\Delta\rho$ is density difference between the mixed layer and halocline, and u_* is friction velocity.

A similar conclusion was derived by *Kato and Phillips* [1969] based on a wind-driven entrainment experiment. *Kato and Phillips* found that the rate of increase of potential energy of the stratified fluid (i.e. the entrainment rate) is proportional to the rate of dissipation of kinetic energy per unit area in the turbulent layer. The observed entrainment velocity, w_e, was scaled using external parameters: the friction velocity $u_* = \left(\tau_s / \rho\right)^{1/2}$ of the imposed stress τ_s, the mixed layer depth, h_{ml}, and the mixed layer buoyancy or reduced gravity, $g' = g\,\delta\rho/\rho$, where $\delta\rho$ is the density jump across the lower boundary of the mixed layer. *Kato and Phillips* obtained a relation between the entrainment velocity and a Richardson number as a non-dimensional ratio:

$$\frac{w_e}{u_*} = 2m_0(Ri)^{-1} = 2.5\frac{\rho_0 u_*^2}{g\Delta\rho H}, \qquad (3.2)$$

where m_0 is an empirical proportionality coefficient obtained from a least-square fit to observational data.

Pollard et al. [1973] developed a dynamic instability model of the deepening of the mixed layer. It was hypothesized that the magnitude of the horizontal mean velocity difference (Δu) across the base of the mixed layer plays an important role in the mixing process. The overall (bulk) Richardson number

$$Ri_o = \frac{gh_{ml}\Delta\rho/\rho}{(\Delta u)^2} = 1 \qquad (3.3)$$

was used as a non-dimensional stability limit on the mixed layer depth.

Price et al. [1978] analyzed whether the relevant scale velocity in the parameterization of wind-driven deepening is a friction velocity (u_*) or the magnitude of the horizontal mean velocity difference (Δu^2) across the mixed layer interface. The modeling study showed that using Δu^2 (*Pollard et al.'s* [1973] approach) as a scale velocity gives better correspondence between the simulated and observed mixed layer deepening.

Several special cases of the mixed layer dynamics have been discussed in *Niiler and Kraus's* [1977] study. Their one-dimensional model describes mixed layer deepening or retreat as a function of wind stirring, velocity shear and buoyancy flux at the surface. *Niiler and Kraus* argue that the contribution of the velocity shear to the layer deepening becomes small when the mixed layer depth is

beyond some critical depth, h_f, which is a maximum limiting depth. The maximum limiting depth can be obtained from the equation for the mixed layer depth produced by the velocity shear when $t = \pi/f$ (f is Coriolis parameter):

$$h_{ml}\Big|_{t=\pi/f} = h_f = \left[Ri_* \frac{2u_*^4}{g' f^2}(1-\cos(ft)) \right]^{1/3}. \qquad (3.4)$$

After omission of the velocity shear term, *Niiler and Kraus* [1977] found an expression of the mixed layer deepening determined by the friction velocity, buoyancy flux at the surface and buoyancy of the mixed layer (B_f) :

$$\frac{dh_{ml}}{dt} = w_e = \frac{2m_0 u_*^3}{h_{ml} g'} + \frac{\kappa \cdot B_f}{g'}, \qquad (3.5)$$

where κ is another proportionality coefficient that is discussed later in the section.

Eq. (3.4) allows one to estimate the significance of the velocity shear in the Arctic Ocean and Greenland Sea. In their study, *Pollard et al.* [1973] assumed $Ri_*=1$. For the Arctic Ocean, friction velocity, u_*, is O(4.x10^{-3}), reduced gravity, g', is O(5.x10^{-3}), and the Coriolis parameter, f, is ~1.4x10^{-4} sec^{-1}. Thus $h_f \approx$ O(2 m). For the Greenland Sea (without ice cover): $u_* \sim$1.5x10^{-2} m·s^{-1}, g′ ~ O(1.x10^{-3} to 1x10^{-4}), which gives $h_f \approx$ O(15 to 45 m). The mixed layer depth is much deeper in the Arctic Ocean and Greenland Sea. This result shows that for simulation of mixed layer dynamics both in the Arctic Ocean and Greenland Sea, friction velocity is the relevant scale velocity in the parameterization of wind-driven deepening and the shear velocity can be neglected.

The above-mentioned studies are mostly concentrated on forced convection. However, in the Greenland Sea free convection plays a very significant role. It is proposed that "chimney" convection – a small space scale (less than 100 km) thermohaline convection – takes place in the Greenland Sea [*Killworth*, 1979]. A detailed study of small-scale convection has been conducted by *Chapman* [1997; 1998] who distinguished between shallow and deep convection. Shallow convection is characterized by very rapid deepening of the chimney when a homogeneous layer almost immediately spreads down to the bottom independent of the depth of the water column (that is why *Chapman* called such deepening "shallow convection"). In shallow convection, the effects of ambient stratification are negligible, so the fluid may be assumed initially homogeneous (neutral stability). In deep convection, however, the chimney never reaches the bottom because of strong stratification. The transition between the two types of convection occurs when $\Delta\rho_e \approx \delta\rho$, where the left hand side represents the density increase in the mixed layer due to the buoyancy flux, and the right hand side represents the density jump across the interface between the mixed and deep layers. *Chapman* [1997] introduced a scale factor to estimate if convection is shallow or deep under a given forcing. The scale factor is a transition Richardson number:

$$Ri_T = g\frac{\delta\rho}{\rho_0}h_0\left(B_0 r_0\right)^{-2/3} = 8, \qquad (3.6)$$

where h_0 is the mixed layer depth, B_0 is the buoyancy flux through the surface, and r_0 is the radius of a convective region. When $Ri_T < 8$ then convection should penetrate into the lower layer, if $Ri_T > 8$, then convection does not penetrate into the lower layer. This scale parameter will be used later to determine the

efficiency of free convection in the ocean models for the Greenland Sea and Arctic Ocean.

The theoretical studies of the mixed layer deepening have been successfully applied in one-dimensional simulations of the Arctic Ocean. *Stigebrandt* [1981] has used the *Kato and Phillips* [1969] formula for the mixed layer entrainment to develop a dynamical one-dimensional model for the salinity and thickness of the upper layer in the Arctic Ocean. There are two layers in the model: upper (mixed) layer and Atlantic layer. The entrainment velocity of the mixed layer boundary is parameterized by a combination of *Kato-Phillips* expression for the entrainment velocity and a term describing the modification of the entrainment velocity caused by the buoyancy flux from above (e.g. due to salt rejection during ice freezing):

$$w_e = \frac{2m_0 u_*^3}{g\beta(S_2 - S_1)H} - \varepsilon \frac{Q_f S_1}{A(S_2 - S_1)}, \qquad (3.7)$$

where β is the salinity expansion coefficient in the equation of state of sea water, m_0 is a constant proportionality coefficient, S_1 and S_2 are salinities of the mixed and Atlantic layer, respectively. The second term on the right hand side parameterizes the buoyancy flux from above. Q_f describes net freshwater flux, A is the surface area of the pycnocline, and ε is a parameter which is 1 if the buoyancy flux is greater than zero (freshwater supply is positive) and .05 otherwise. Eq. (3.7) parameterizes two types of convection: forced (the first term on the right hand side) and free (the second term) convection [*Kundu*, 1990]. The forced convection is driven by mechanically generated turbulence. The second term approximates an effect of free convection when the buoyancy flux is negative. Free convection alone could lead to entrainment of water from below.

In the Arctic, the efficiency of free convection is lower than that of the forced convection [*Stigebrandt*, 1981]. However, this might not be true for the Greenland Sea when deep thermohaline convection develops [*Chapman*, 1997].

Björk [1989] developed a one-dimensional time-dependant model to study seasonal variability of the upper Arctic Ocean. The mixed layer dynamics follow the pycnocline model developed by *Stigebrandt* [1985] for the Baltic Sea. The temperature and salinity change in the halocline layer are described by vertical advection-diffusion equations. The model reproduces a seasonal signal in the upper layer, although salinity values are slightly low for the interior Arctic Ocean: <29 at the end of summer and ~30.5 in May.

The *Huck et al.* [1999] model study is one of a few examples of a simple model used to analyze interannual variability in the ocean. Decadal variability of the thermohaline circulation in a square-geometry ocean was analyzed. *Huck et al.* proposed a box-model that captures the crucial phase shift between meridional overturning and north-south density gradient anomalies on the decadal timescales. It was shown that the mass exchange variability between the cold and warm boxes had been driven by a temperature gradient between the boxes.

Section 3.2. General description of the Arctic Ocean and Greenland Sea model

To verify the hypothesized behavior of the polar climate system, an Arctic Ocean – Greenland Sea model has been developed. The model domains are shown in Fig. 3.1. There are three parts of the model: the deep (interior) Arctic Ocean, the central Greenland Sea, and Arctic shelf region.

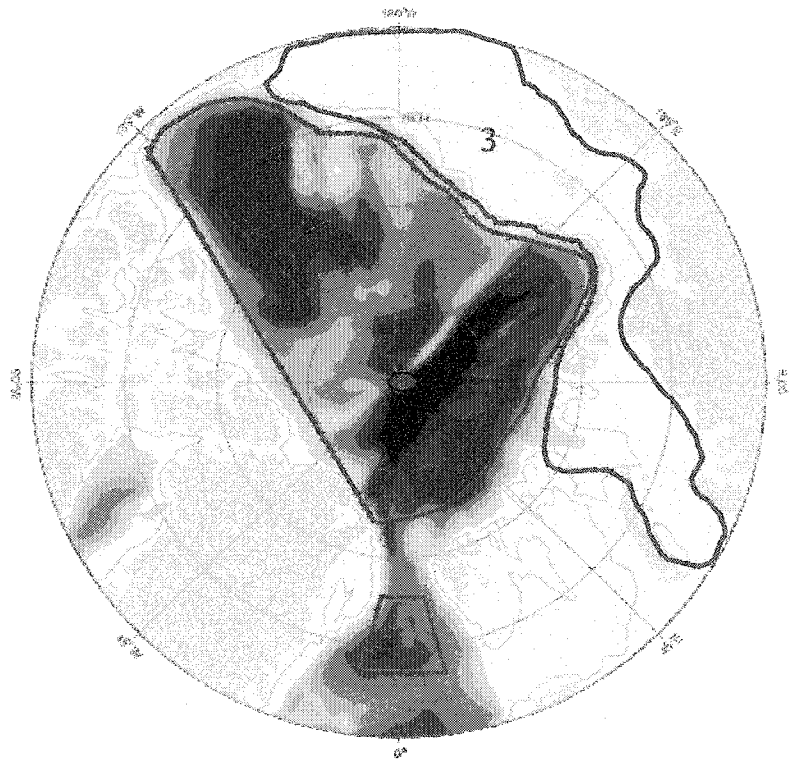

Fig. 3.1. Model domains. *(1) Central Greenland Sea. (2) Deep Arctic Ocean. (3) Arctic shelf region.*

- The interior Arctic Ocean part describes the variability in the upper ocean in the deep part of the basin, generally deeper than the 200-m isobaths.

- The central Greenland Sea part represents a convection region in the Greenland Gyre (5°W – 5°E longitude, 74°N – 76°N latitude) [*Johannessen*, 1986; *Swift*, 1986; *Pawlowicz*, 1995]. The center of the Greenland Gyre is approximately located at 2°E – 5°E and 74°N – 75°N (from Fig. 1, in *Carsey and Roach* [1994]). The model development assumes that the Greenland Sea module will always include the deep convection region.

- The shelf part describes the maintenance and formation of the Arctic Ocean halocline and the mixed layer. The shelf domain has not been designed to reproduce all features of the Arctic shelf. The shelf domain does not include the Barents Sea due to complexity of the Atlantic water transformation processes on the Barents Sea shelf.

A general diagram of the model is shown in Fig. 3.2. The model consists of two modules: the Arctic module and the Greenland Sea module. The Arctic module includes a shelf box model coupled with a thermodynamic sea ice model and an Arctic Ocean model coupled with the sea ice model and an atmospheric box model. The coupling between the shelf box model and the Arctic Ocean model is realized through the mixed layer (ML) outflow from the Arctic Ocean (Q_{mao}) and shelf outflow to the Arctic Ocean (Q_{sh}). The shelf box model performs two major tasks. First, it mixes the inflowing river runoff (Q_f), precipitation (in summer) and Q_{mao}. This gives more realistic seasonal variability to the upper Arctic Ocean. Without the shelf box, the fresh water inflows directly into the mixed layer as in *Björk's* [1989] model. The shelf box damps the seasonal signal in the interior basin. Second, the shelf model redistributes salt rejected during freezing season

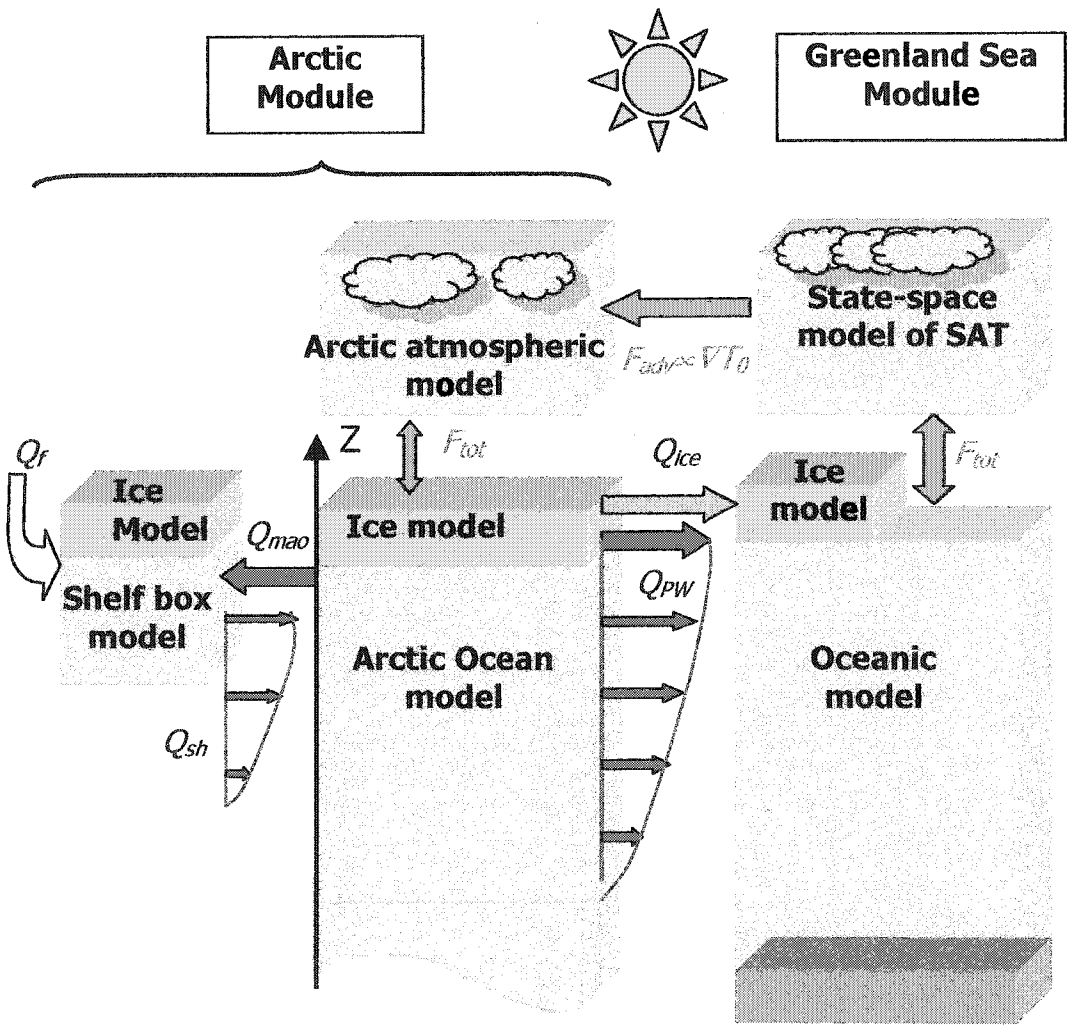

Fig. 3.2. Diagram of the Arctic Ocean – Greenland Sea model. *The model consists of two modules: the Arctic module and the Greenland Sea module. The Arctic module includes a shelf box model coupled with a thermodynamic sea ice model and an Arctic Ocean model coupled with the sea ice model and an atmospheric box model. The Greenland Sea module includes an oceanic model of the Greenland Sea region coupled with the sea ice model and a state-space model of SAT (T_0) in the Greenland Sea. Blue indices denote fluxes: Q_f – river runoff; Q_{sh} – shelf water inflow; Q_{mao} - Arctic Ocean inflow to the shelf; Q_{PW} – Polar Water inflow to the Greenland Sea; Q_{ice} – ice export to the Greenland Sea. Orange indices are heat fluxes: F_{tot} – surface heat flux; F_{adv} – advected heat to the Arctic. The interaction between the shelf model and the Arctic Ocean model is realized through Q_{mao} and Q_{sh}. The Greenland Sea module interacts with the Arctic module through Q_{PW}, Q_{ice}, and F_{adv}.*

within the water column of the Arctic Ocean. The details of the shelf box models are discussed in Section 3.3.2. Interaction between the Arctic Ocean and the Greenland Sea is realized through the ice (Q_{ice}) and polar water (Q_{PW}) import from the Arctic Ocean, and atmospheric heat advection (F_{adv}) from the Greenland Sea.

The Greenland Sea module includes an oceanic model of the Greenland Sea region coupled with the sea ice model and a state-space model of surface air temperature (SAT) in the Greenland Sea. Interaction between the Arctic Ocean and the Greenland Sea modules is realized through the ice, Q_{ice}, and polar water, Q_{PW}, import from the Arctic Ocean, and atmospheric heat advection from the Greenland Sea, F_{adv}.

Section 3.3. The Arctic module

The Arctic module includes the full-system Arctic model and shelf box model coupled with a sea ice model. The Arctic module describes seasonal and interannual variability in the Arctic ice-ocean-atmosphere climate system. The major goal of the Arctic module is to reproduce the anticyclonic/cyclonic circulation regime (ACCR/CCR) shifts under different heat advection scenarios from the Greenland Sea region.

3.3.1. Arctic Ocean model

The model describing the behavior of the upper interior Arctic Ocean is one-dimensional and time-dependent. This is the Arctic Ocean model of *Björk* [1989] with modifications in parameterization of the entrainment rate, shelf inflow/outflow and improved shelf – interior basin interaction. The area of the deep Arctic Ocean (A_{AO}) is ~0.61×10^{13} m^2. There are three layers in the model (Fig. 3.3): the mixed layer (ML), halocline layer (HL) and Atlantic Layer (AL). The depth of the ML is denoted as h_{ml}. The model describes deepening and shallowing of the ML, temperature and salinity changes in ML and HL. The characteristics of the Atlantic Layer, salinity (S_{atl} = 34.8 psu) and temperature (T_{atl} = 0.5°C) do not change. The model is coupled to a thermodynamic sea ice model, Greenland Sea model, and shelf box model. The oceanic model is coupled to the shelf box model via the prescribed outflow from the ML (Q_{mao}) and the import of shelf water (Q_{sh}) into the Arctic Ocean. The import of shelf water varies with depth. Q_{sh} is a function of the ice production rate on the shelf (the detailed

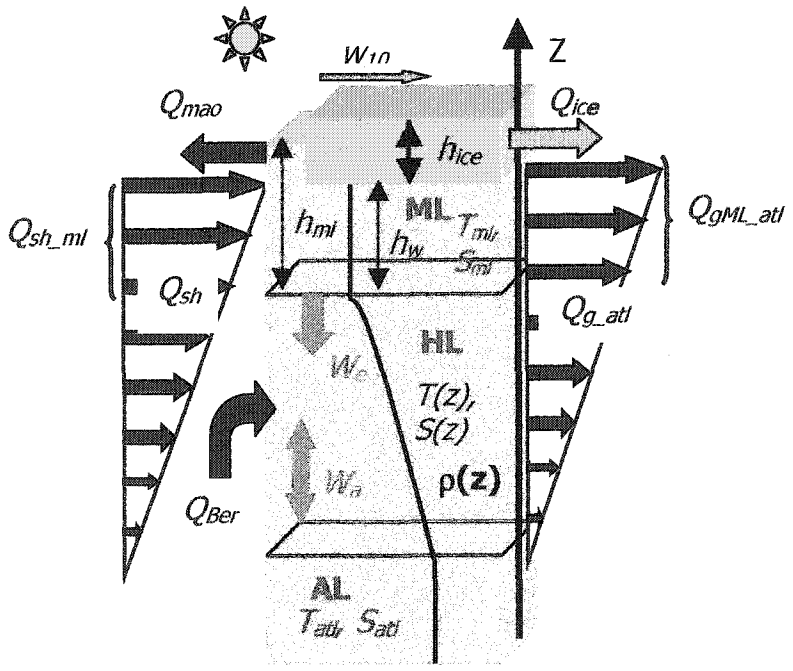

Fig. 3.3. Diagram of the Arctic Ocean model. *Three layers in the model: AL – Atlantic layer, HL – halocline layer, and ML – mixed layer. Characteristics of the layers: h_{ml} – ML thickness; h_w – ML thickness without ice draft; T_{ml} and S_{ml} – temperature and salinity of the ML; T(z) and S(z) – temperature and salinity of the HL; T_{atl} and S_{atl} – temperature and salinity of the AL. Volume fluxes: Q_{mao} – ML flow to the shelf; Q_{sh} – shelf water flow to the Arctic Ocean; Q_{sh_ml} – fraction of Q_{sh} flowing to the ML; Q_{Ber} – Bering water inflow; Q_{ice} – ice flux to the GIN Sea; Q_{g_atl} – geostrophic outflow to the North Atlantic; and Q_{gML_atl} – fraction of Q_{g_atl} from the ML. Other notations: W_{10} – wind; h_{ice} – ice thickness; W_e – entrainment velocity; W_a – vertical advection velocity; and ρ(z) – water density.*

description of Q_{sh} is presented in Section 3.3.2). Thus, the shelf model redistributes salt rejected from ice within the Arctic Ocean water column. The fraction of Q_{sh} inflowing into the ML is denoted as Q_{sh_ml}. There is also the Bering Water inflow (Q_{Ber}) with seasonally varying salinity, S_{Ber}, and temperature, T_{Ber}. The characteristics of the Bering Water are prescribed and kept constant. The Bering Water is isopycnally mixed with the Arctic Ocean water. The Arctic Ocean

exports ice (Q_{ice}) and water (Q_{g_atl}) to the North Atlantic. The fraction of the Arctic Ocean water outflow from ML is Q_{gML_atl}.

The ML is maintained by wind forcing (w_{10}), which generates forced convection, thermohaline processes which drive free convection, and vertical velocity resulting from the flow into and out of the layer. The effect of wind on the ML is parameterized using the friction velocity (u_*) which is the square root of stress caused by wind driven ice motion [e.g., *Kowalik*, 1984]. The ice production and melting cycle is calculated in the thermodynamic ice model. Free convection arises when salt is rejected from ice during freezing. Free convection ceases with the onset of melting. The deepening of the mixed layer is parameterized by the entrainment velocity (w_e), which defines the downward penetration of the ML.

HL properties are changed due to the vertical velocity, diffusion and injection of shelf and Bering water. The vertical velocity (w_a) is a function of depth and depends on the depth integrated inflow and outflow rates. If total outflow is larger than total inflow, w_a is positive meaning a movement of the isolines towards the sea surface.

Model equations

The mixed layer (ML) dynamics follow largely the Stigebrandt's pycnocline model [*Stigebrandt*, 1985] developed further and applied to the Arctic Ocean by *Björk* [1989]. According to *Stigebrandt* [1985], the ML thickness (h_{ml}) is determined by the following different dynamical regimes:

(1) If buoyancy flux (B_{fl}) at the sea surface is negative (i.e., the buoyancy of ML is reduced) and the entrainment velocity is downward, $B_{fl} \le 0$, $w_e \le 0$ (both forced and free convection take place), then:

$$\frac{dh_{ml}}{dt} = \frac{1}{A_{AO}}\left(Q_{sh\_ml} - Q_{mao} + Q_{gML\_atl} + \mu_{Ber} \cdot Q_{Ber} + \varepsilon \cdot Q_{ice}\right) - w_e, \qquad (3.8)$$

$$\text{where } \mu_{Ber} = \begin{cases} 1, & \rho_{Ber} \le \rho_{ml} \\ 0, & \rho_{Ber} > \rho_{ml}. \end{cases} \qquad (3.9)$$

(2) if $B_{fl} > 0$, $w_e \le 0$ (pure forced convection) then:

$$h_{ml} = \min\{h_{ml},\ h_{Ob},\ h_{Ekm}\}, \qquad (3.10)$$

where h_{Ob} is the Monin-Obukhov length $\left(h_{Ob} = {2m_0 (u_*)^3}/{B_{fl}}\right)$ and h_{Ekm} is the Ekman length $\left(h_{Ekm} = {\mathrm{K}_e \cdot u^*}/{f}\right)$, m_0 is an empirical proportionality factor (it is discussed in more detail in Subsection "The proportionality factors m_0 and κ"), the friction velocity is determined by $u_*^2 = C_{di} \cdot V_{ice}^2$, the ice-water drag coefficient C_{di} = 5.5x10^{-3}, the ice velocity is related to the wind velocity as $V_{ice} = a_0 \cdot W_{10}$, a_0 is the air-ice velocity parameter [*Thorndike and Colony*, 1982] which is taken 0.019 in June, July and August and 0.01 during the rest of the year, B_{fl} is the buoyancy flux, and $\varepsilon = \rho_w / \rho_{ice} \approx 0.9$.

Forced convection is possible at the beginning of the warm season at the onset of ice melt when the melting rate is too small to suppress the mechanical

turbulence over the deep (after winter convection) ML. However, without possible free convection, the ML cannot be deeper than either the Ekman Length (h_{Ekm}) scale or the Monin-Obukhov Length (h_{Ob}). Thus under such conditions, the depth of the pycnocline is defined as the shortest length scale among h_{ml}, h_{Ekm}, and h_{Ob}.

(3) $B_{fl} > 0$, $w_e > 0$ (retreat of the ML). The upward entrainment velocity makes no physical sense and under such conditions w_e is set to 0. The depth of the ML is defined by the minimum value between h_{Ekm} and h_{Ob}:

$$h_{ml} = \min\{h_{Ob}, \quad h_{Ekm}\}. \tag{3.11}$$

On the right hand side of Eq. (3.8) the prescribed terms (forcing) are Q_{Ber} and Q_{mao}. Both of the fluxes are kept constant. Q_{sh_ml} is calculated in the shelf box model and will be discussed later. The rest of the terms are calculated as follows. The ice export (Q_{ice}) from the Arctic Ocean is a function of net gain or loss of ice in the Arctic relative to the previous year.

The entrainment velocity is given by the formula:

$$w_e = -\frac{1}{g'}\left(\frac{2m_0\left(u^*\right)^3}{h_w} - \kappa \cdot B_{fl}\right) \tag{3.12}$$

where the reduced gravity is $g' = \frac{g(\rho(h_{ml+}) - \rho_{ml})}{\rho(h_{ml+})}$, $\rho(h_{ml+})$ is density just below the mixed layer, $h_w = h_{ml} - \varepsilon \cdot h_{ice}$, and

$$B_{fl} = g\beta\left\{\frac{1}{A_{AO}}\left[Q_{sh\_ml}(S_{ml} - S_{sh\_ml}) + \mu_{Ber}Q_{Ber}(S_{ml} - S_{Ber})\right]\right.$$
$$\left. - \varepsilon \Pr_{i\_ao}(S_{ml} - S_{ice})\right\}, \qquad (3.13)$$

where Pr_{i_ao} is ice production in the Arctic Ocean, and $\beta = \frac{1}{\rho}\frac{\partial \rho}{\partial S}$ is the coefficient of salt contraction. Given the air temperature, shortwave radiation flux, cloudiness, and relative humidity of the air, the ice production rate is obtained from the thermodynamic sea ice model [*Maykut and Untersteiner*, 1969; *Maykut*, 1986] coupled with the Arctic Ocean model.

Salinity changes in the ML are computed as follows:

$$\frac{dS_{ml}}{dt} = \frac{1}{h_w}\left\{\frac{1}{A_{AO}}Q_{sh\_ml}\left(\overline{S}_{sh\_ml} - S_{ml}\right) + \right.$$
$$\left. \varepsilon \Pr_{i\_ao}\left(S_{ml} - S_{ice}\right) - w_e\left(S(h_{ml+}) - S_{ml}\right)\right\}, \qquad (3.14)$$

where Q_{sh_ml} is the output (volume transport) from the shelf box model (see Eq. (3.41)), $\overline{S}_{sh\_ml}$ is the integrated salinity of the shelf outflow into the ML (Eq. (3.42)), and $S(h_{ml+})$ is salinity just below the ML.

Similar to *Björk* [1989] and *Stigebrandt* [1981], the outflow Q_{g_atl} is assumed to occur as geostrophically balanced coastal currents with the underlying Atlantic water at rest. The outflow is estimated by integrating the thermal wind equation across the flow. There are two major outlets for the Arctic Ocean water: the Fram Strait and channels of the Canadian Archipelago. *Stigebrandt* [1981] estimated the total number of "geostrophical outlets", λ_{out}, to be ~2.3. Model

experiments of *Björk* [1989] have revealed a good correspondence of the Arctic Ocean model behavior to the observations with λ_{out}=1.5.

According to *Björk* [1989], if the *Y*-axis is along the coast and the *X*-axis is across the flow with the coast located at $x = 0$ then the transport per unit depth across the outflow region is:

$$q_{atl}(z) = \int_0^{x_a} v_g dx = -\frac{g}{\rho_{atl} f} \int_z^{H_h} (\rho_{atl} - \rho(z)) dz, \tag{3.15}$$

where v_g is the coast-parallel velocity of the geostrophic flow, x_a is an offshore distance where $\rho(x,z) = \rho_{atl}$, and ρ_{atl} is the Atlantic water density.

Water volume flux from the ML to the North Atlantic is expressed:

$$Q_{gML\_atl} = \lambda_{outl} \int_0^{h_{ml}} q_{atl}(z) dz, \tag{3.16}$$

and the total outflow from the ML and halocline is:

$$Q_{g\_atl} = \lambda_{outl} \int_0^{H_h} q_{atl}(z) dz. \tag{3.17}$$

The sign convention is $Q_{g\_atl} < 0$, meaning water export from the Arctic basin.

Below the ML the local rate of change of S and T are:

$$\frac{\partial S}{\partial t} = w_a \frac{\partial S}{\partial z} + D_z \frac{\partial^2 S}{\partial z^2} + \frac{q_{sh}(S(sh))}{A_{AO}}(S(sh) - S),$$
$$\frac{\partial T}{\partial t} = w_a \frac{\partial T}{\partial z} + D_z \frac{\partial^2 T}{\partial z^2} + \frac{q_{sh}(T(sh))}{A_{AO}}(T(sh) - T), \qquad (3.18)$$

where w_a is the vertical velocity, D_z is the coefficient of eddy diffusivity, $S(sh)$ and $T(sh)$ are salinity and temperature of the shelf outflow at a given vertical grid point where densities of the shelf water and halocline layer are the same (see Section 3.3.2 for detail in computing $q_{sh}(S(sh))$). The vertical velocity is estimated as follows:

$$w_a(z) = \begin{cases} -\frac{1}{A_{AO}} \cdot \left\{ \lambda_{out} \int_0^z q_{atl}(z)dz + \int_{S_{sh}}^{S_{sh\_out}(z)} q_{sh}(S)dS - Q_{mao} + \varepsilon \cdot Q_{ice} \right\}, & z \le z_{Ber} \\ -\frac{1}{A_{AO}} \cdot \left\{ \lambda_{out} \int_0^z q_{atl}(z)dz + \int_{S_{sh}}^{S_{sh\_out}(z)} q_{sh}(S)dS - Q_{mao} + \varepsilon \cdot Q_{ice} + Q_{Ber} \right\}, & z > z_{Ber}, \end{cases} \qquad (3.19)$$

where $q_{sh}(S)$ is the shelf water outflow at a given depth z. This term is explained in Section 3.3.2. z_{Ber} is the depth level of the Bering water injection.

If the density of Bering Sea water is greater than the ML density, the change of S and T in the halocline layer at the depth where $\rho_{Ber} = \rho(z)$ is:

$$\frac{\partial S}{\partial t} = w_a \frac{\partial S}{\partial z} + D_z \frac{\partial^2 S}{\partial z^2} + \frac{q_{sh}(S(sh))}{A_{AO}}(S(sh) - S(z)) + \frac{Q_{Ber}}{A_{AO}}(S_{Ber} - S(z)),$$
$$\frac{\partial T}{\partial t} = w_a \frac{\partial T}{\partial z} + D_z \frac{\partial^2 T}{\partial z^2} + \frac{q_{sh}(T(sh))}{A_{AO}}(T(sh) - T(z)) + \frac{Q_{Ber}}{A_{AO}}(T_{Ber} - T(z)). \quad (3.20)$$

The semi-implicit Crank-Nicolson scheme with Thomas algorithm [*Fletcher*, 1988] has been applied to get a numerical solution of the Eq. (3.20). The values of the different constants used in the oceanic model are summarized in Table 3.1.

Table 3.1. Values of constants used in the Arctic Ocean model

Constant	Value	Units
Area of the deep Arctic Ocean (A_{ao})	0.61×10^{13}	m^2
Gravitational acceleration (g)	9.8	m/s^2
Coriolis parameter (f)	1.43×10^{-4}	s^{-1}
Ice-water drug coefficient (C_{di})	5.5×10^{-3}	
Empirical constant for the Ekman depth (K_e)	0.2	
Eddy diffusivity coefficient (D_z)	$1.x10^{-6}$	m^2/s
Depth of the HL	200	m
Salinity of the AL (S_{atl})	34.8	psu
Temperature of the AL (T_{atl})	0.5	°C
Bering jet thickness (H_{Ber})	10	m
Outflow from the ML to the shelf (Q_{mao})	0.4	Sv

The proportionality factors m_0 and κ

Most uncertainties in the parameterization of the ML deepening arise from the empirical coefficients, m_0 and κ. Mixed layer dynamics depend on the

entrainment rate given by Eq. (3.12). In this formula there are two empirical coefficients – proportionality factors – m_0 and κ that adjust the intensity of forced and free convection.

The first estimate of m_0 was obtained during *Kato and Phillips's* [1969] experiment. They suggested a value m_0 = 1.25. Other estimates of this proportionality factor are highly variable. For example, *Björk* [1989] estimates m_0 to be 0.7, *Stigebrandt* [1985] suggests m_0 = 0.6, *Phillips* [1977] gives m_0 = 6. Both *Björk* [1989] and *Stigebrandt* [1985] keep m_0 constant in their models. However a number of experiments (see e.g., [*Kantha*, 1975; *Phillips*, 1977]) show that m_0 is not constant and it is larger than originally estimated by *Kato and Phillips* [1969]. The model and experimental studies of the ML dynamics have shown that m_0 is a decreasing function of the bulk Richardson number [*Niiler and Kraus*, 1977]:

$$m_0 \propto \left(\frac{h_{ml} g'}{u_*^2} \right)^{-1} . \qquad (3.21)$$

According to *Niiler and Kraus* [1977], when the overall Richardson number is of order one hundred, m_0 is approximately 3.3. Rapid deepening of the mixed layer observed in the North Atlantic [*Stommel et al.*, 1969] made *Turner* [1969] suggest a higher value of m_0 = 8 which was later proved by observations in the Pacific Ocean [*Halpern*, 1974].

From several model experiments, the following ratio for m_0 is found to give a realistic behavior of the mixed layer (in case of wind forced deepening) both in the Arctic Ocean and Greenland Sea models used in the present research:

$$m_0 = \log\left[\left(\frac{100}{Ri_o}\right)^P\right] + 3.5, \tag{3.22}$$

$$m_0 = \begin{cases} 0, & if \quad m_o \le 0 \\ 8, & if \quad m_o \ge 8 \end{cases}, \tag{3.23}$$

where $Ri_o = \frac{h_{ml} \cdot g'}{u_*^2}$ is bulk Richardson number, and P ranges from 1.2 to 2.0 and is discussed more in Chapter 4. As one can see in the case of a shallow mixed layer in a weakly stratified water column, m_0 approaches large values and $m_0 >> \kappa$. Thus forced convection is a leading mechanism in the ML deepening (see Eq. (3.12)). The value of m_0 rapidly decreases as ML deepens (h_{ml} increases) and at some depth (depending on ambient stratification) m_0 becomes 0.

The ML deepening rate driven by thermohaline convection is determined by the proportionality factor κ. The κ coefficient describes dissipation of the convectively produced turbulence in Eq. (3.12). The higher the dissipation, the lower is κ. There are uncertainties about this coefficient. The value of κ may range from 1 to 0. For example, *Farmer* [1975] having analyzed observational data suggested that κ varied within the range from 0.003 to 0.113. Significantly higher values for κ were obtained by *Pollard et al.* [1973] who asserted that 25% of convective turbulence was spent for the mixed layer deepening.

It has been suggested that κ approaches zero as $h_{ml} \to \infty$ [*Niiler and Kraus*, 1977]. On the other hand, *Chapman* [1998] argued that in case of strong buoyancy flux and low water column stability, deep convection rapidly reaches the bottom and is not depth limited (opposite to the case of forced convection). In this case the energy dissipation is minimal and κ can approach 1. Thus, the

only factor – for given buoyancy flux - limiting thermohaline convection is the stratification (stability) of the water column. It is logical to assume that κ is a function of the water column stability: when stability is high the dissipation of the convection is high as well and κ turns to be small and vice versa.

The model runs require a reasonable proportionality factor κ for the Arctic Ocean and Greenland Sea models. First, a bulk Richardson number is compared with a transition Richardson number Eq. (3.6). According to *Chapman* [1997], if the bulk Richardson number (Ri_o) is greater than the transition Richardson number (Ri_T), the density gain in the upper layer (due to negative buoyancy flux) is not enough to overcome the density jump between the upper and lower layers. In this case convection should not penetrate into the lower layer and κ should be very small. Also it seems reasonable that κ approaches zero as $h_{ml}\to\infty$. If $Ri_o < Ri_T$ then, according to *Chapman* [1997], convection penetrates into the lower layer very fast and is not depth limited, assuming large κ. From the above theoretical discussions and model experiments, the following expressions for κ have been obtained:

$$\kappa = \begin{cases} 1, & if \quad B_{fl} > 0 \\ 0.9, & if \quad Ri_o < Ri_T \\ 0.01 \cdot \log\left(3000/h_{ml}\right), & if \quad Ri_o > Ri_T. \end{cases} \qquad (3.24)$$

Due to high stability of the water column in the Arctic Ocean ($Ri_o > Ri_T$) κ is always about 0.05, which corresponds to the value in *Björk's* [1989] model.

Time step and vertical resolution

The vertical resolution (h_z) in the model is 1 m. The time step (t_{stp}) is set depending on the entrainment velocity to fulfill the stability condition [*Kowalik and Murty*, 1993]:

$$-\frac{w_e \cdot t_{stp}}{h_z} \le 1. \tag{3.25}$$

In the model the time step is determined as follows:

$$t_{stp} = \begin{cases} \min\left\{ 0.5 * h_z / -w_e ; \quad 21600 \quad \text{sec} \right\}, & w_e < 0 \\ 21600 \quad \text{sec}, & w_e \ge 0. \end{cases} \tag{3.26}$$

Forcing in the Arctic Ocean model

The forcing parameters in the oceanic model of the Arctic Ocean region are: downwelling shortwave radiation, relative humidity, wind, water export from the ML to the shelf, and Bering Water inflow. The downwelling shortwave radiation has been calculated for 80°N using the Sun-Earth astronomical relationships [*Iqbal*, 1983]. All other forcings have been prescribed with monthly means, which have been linearly interpolated into daily data.

(a) Wind

Wind is highly variable, both in time and space. Scarce observations in the central Arctic cause biases in the mean estimates of surface wind, and different sources provide different mean estimates. In Table 3.2, several monthly estimates of the surface wind in the central Arctic are shown. From this table one can see that *Bjork's* [1989] wind estimates are too high and exceed maximum values of the wind data for the central Arctic obtained from the National Oceanic and Atmospheric Administration (NOAA) – Cooperative Institute for Research in Environmental Sciences (CIRES) Climate Diagnostic Center [*CDC*]. The other two sources agree with the NOAA-CIRES CDC data. In the present model, *Polyakov et al.'s* [1999] wind forcing parameters have been used.

(b) Water export from the ML to the shelf (Q_{mao})

Water from the Arctic Ocean to the shelf is mixed with the river runoff water, precipitation, and ice melt water during the warm season, or brine during ice formation (parameterization of the shelf processes is detailed in Section 3.3.2). The outflow from the shelf to the interior Arctic Ocean is determined by Q_{mao}. Therefore, the rate of water export from the Arctic Ocean ML to the shelf affects both the interior Arctic Ocean and shelf. The higher Q_{mao}, the lower the difference between the shelf and interior. Even rough estimates of Q_{mao} are difficult to find. Thus, several model runs have been performed with different Q_{mao} to get the best fit to observed Arctic Ocean characteristics. The results show that Q_{mao} = 0.8×10^6 to 1.2×10^6 $m^3 \cdot s^{-1}$ gives realistic T and S in the Arctic Ocean and on the shelf.

(c) Bering Water inflow

As mentioned in Chapter 1, the Bering Water inflow is accepted to be 1.0 Sv with no seasonal variation. Temperature and salinity of the inflow are given in Table 3.3.

Table 3.2. Surface wind estimates in the central Arctic

	Jan	Fb	Mr	Ap	May	Jn	Jl	Ag	Sp	Oc	Nv	Dc
NOAA-CIRES CDC[a] [*CDC*]												
min	4.5	4.64	4.4	4.1	3.9	3.9	4.4	4.7	4.6	4.6	4.54	4.9
max	8.2	8.21	8.1	7.7	6.3	6.5	6.98	6.8	7.18	7.4	7.82	7.9
[*Lindsay*, 1998]												
Mean	4.4	4.0	4.0	3.9	3.9	4.2	4.1	4.2	4.5	4.2	3.9	4.
STD	0.9	0.8	0.7	0.8	0.6	0.7	0.6	0.8	0.8	0.9	0.8	0.9
[*Bjork*, 1989][b]												
Mean	6.5	6.7	6.0	5.8	6.0	6.3	6.5	6.9	8.0	7.3	6.9	6.5
[*Polyakov et al.*, 1999][c]												
ACCR	7.0	5.9	6.0	5.4	4.5	4.5	4.7	4.4	5.3	5.9	6.2	6.6
CCR	7.0	7.0	6.5	6.0	5.0	5.2	5.2	6.1	5.8	6.4	6.2	6.5

(a) CDC derived NCEP reanalysis products pressure level; data range is obtained for the region 86°N – 90°N latitude and 0°E – 360°E longitude, averaged from January 1948 through December 2002.
(b) These are the values of "mixing wind" which is a function of the monthly wind and its standard deviation.
(c) Different monthly means for the central Arctic have been obtained by averaging wind over all years of the cyclonic regime in the Arctic (CCR) and the anticyclonic regime (ACCR).

Table 3.3. Bering Water characteristics

	Jan	Fb	Mr	Ap	May	Jn	Jl	Ag	Sp	Oc	Nv	Dc
T °C	-1.7	-1.7	-1.7	-1.7	-1.7	-0.5	0.5	1.0	0.5	-0.5	-1.0	-1.7
S, psu	32.4	32.6	32.7	32.6	32.5	32.2	32.	31.9	31.8	31.8	31.9	32.2

[*Gorshkov*, 1980; *Bjork*, 1989].

(d) Downwelling shortwave radiation and relative humidity

The downwelling shortwave radiation and relative humidity used in the model are presented in Table 3.4. Note that the downwelling shortwave radiation is the amount of radiation coming at the surface in the absence of clouds [*Maykut*, 1986]. The incoming radiation in the Arctic is much smaller due to high cloudiness (see Eqs. (3.73) and (3.74)). As an example, values of the incoming shortwave radiation for cloudiness 0.8 are given in Table 3.4.

Table 3.4. Shortwave radiation and relative humidity in the Arctic Ocean model

Jan	Fb	Mr	Ap	May	Jn	Jl	Ag	Sp	Oc	Nv	Dc
Downwelling shortwave radiation, $W \cdot m^{-2} \cdot sec^{-1}$											
0	0	40	189	379	468	425	259	79	3	0	0
Incoming shortwave radiation for $cld = 0.8$, $W \cdot m^{-2} \cdot sec^{-1}$											
0	0	27	100	257	317	288	175	54	2	0	0
Relative humidity [*Maykut*, 1986; *Lindsay*, 1998]											
0.78	0.78	0.78	0.78	0.86	0.92	0.92	0.92	0.9	0.82	0.8	0.8

3.3.2. Shelf box model

According to theoretical studies and observations, the Arctic shelves play an important role in development of the halocline layer (HL) structure [*Aagaard et al.*, 1981; *Schauer et al.*, 1997]. The purpose of the model is to reproduce an internal circulation within the system, drawing surface water from the interior Arctic Ocean on to the shelf and returning saline water into the HL. The shelf model describes seasonal variability of the salinity (S_{sh}) and water temperature (T_{sh}) on the shelf. In winter, when salt is rejected from ice, saline water flows into the HL. In summer, during intense ice melting and increased river runoff, relatively fresh water is conveyed to the ML. The area of the modeled region (A_{sh}), excluding the Barents Sea, is ~0.41×10^{13} m^2. The shelf region is presented as a homogeneous water mass in a box 50 m deep (h_{sh}). The time step is 6 hours. The shelf box model is coupled with the Arctic Ocean model through the inflow/outflow and with the thermodynamic sea ice model.

Model equations

(a) Outflows and inflows

A diagram of the shelf box model is shown in Fig. 3.4 A. The shelf is represented with a box, which exchanges water with the interior basin. There are four prescribed inflows: Q_{mao}, river runoff (Q_f), upwelled and transported from the Barents Sea Atlantic water (Q_{atl_sh}), and precipitation (P-E). Mixed layer water enters the box and is transformed by ice production or ice melting and freshwater inflow. The outflowing water is interleaved in the interior Arctic Ocean at the isopycnal levels.

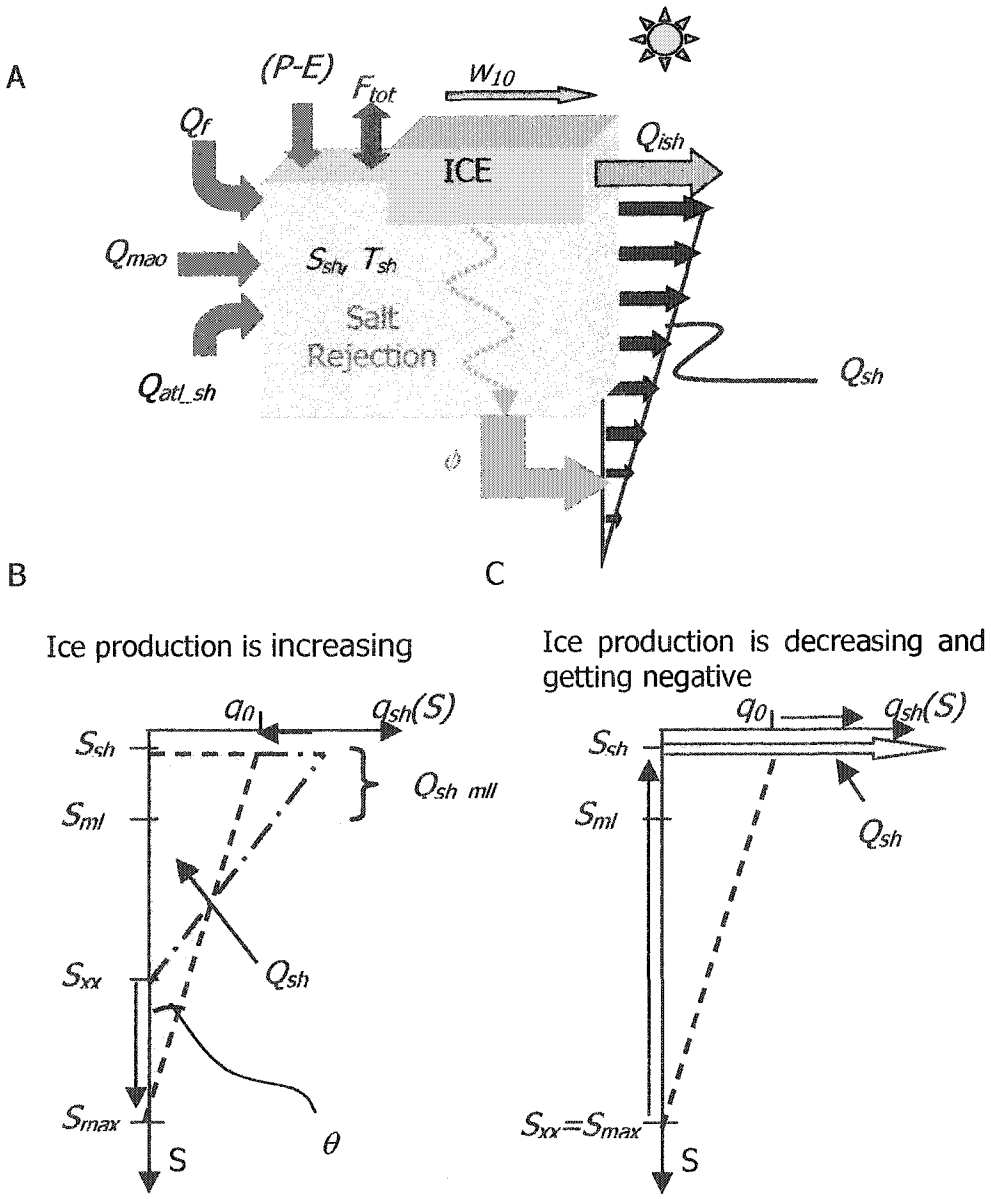

Fig. 3.4. Diagram of the shelf box model. *(A) Shelf box: S_{sh} – shelf water salinity; T_{sh} – shelf water temperature, under ice-free conditions it is a function of surface heat flux (F_{tot}); φ - salt flux to the interior Arctic Ocean; w_{10} – wind; Q_f – river runoff; Q_{mao} – inflow from the Arctic Ocean mixed layer; Q_{atl_sh} – Atlantic water inflow to the shelf; (P-E) – net precipitation; Q_{ish} – ice export from shelf; and Q_{sh} – shelf flux to the Arctic Ocean. (B) and (C) the outflow function $q_{sh}(S)$: $q_0=q_{sh}(S=S_{sh})$; $q_{sh}(S_{xx})=0$; S_{max} – limitting value for S_{xx}; and θ - angle between S-axis and $q_{sh}(S)$. When ice production is high and positive (B), S_{xx} increases approaching S_{max} and q_0 decreases. When ice production weakens (C), S_{xx} decreases and q_0 grows. When ice production becomes negative (ice melt), $q_0=Q_{sh}$.*

The total volume outflow from the shelf to the interior basin is $Q_{sh} = Q_{mao}$. Similar to *Bjork* [1989], Q_{sh} is parameterized by means of an outflow function (Figs. 3.4B and 3.4C), $q_{sh}(S)$, which is a function of salinity:

$$Q_{Sh} = \int_{Ssh}^{Sxx} q_{sh}(S)dS\,. \tag{3.27}$$

The outflow function is a simple distribution function of the volume outflow and its salinity. The largest outflow (q_0) corresponds to S_{sh} and then decreases towards higher salinities, becoming zero at salinity $S = S_{xx}$. The area under the $q_{sh}(S)$ line equals the total shelf outflow (Eq. (3.27)). It is obvious that S_{xx} depends on the ice production rate on the shelf. The less ice produced on the shelf, the less saline is the water flowing to the HL. Thus, S_{xx} is moving along the S axis (see Fig. 3.4C) reaching S_{sh}, when ice production is negative (ice is melting), and S_{max} under the highest ice production rate (Fig. 3.4B). To determine a relationship between the ice production, Q_{sh} (which equals the prescribed Q_{mao}) and S_{xx}, one proceeds as follows.

The total outflow of salt (ϕ) is:

$$\phi = \int_{Ssh}^{Sxx} q_{sh}(S)\cdot SdS\,. \tag{3.28}$$

On the other hand, when ice production is greater than zero, the total outflow of salt can be parameterized as:

$$\phi = (1-\xi)\cdot\varepsilon\cdot Q_{ice}(S_{sh} - S_{ice}) + Q_{sh}S_{sh}\,, \tag{3.29}$$

where ξ is a fraction of the rejected salt consumed for the shelf water salinity increase, viz. this amount of salt remains on the shelf:

$$\xi = \begin{cases} 0.2, & if \quad \mathrm{Pr}_{i\_sh} > 0 \\ 1, & if \quad \mathrm{Pr}_{i\_sh} \le 0, \end{cases} \tag{3.30}$$

Pr_{i_sh} is ice production on shelf:

$$\mathrm{Pr}_{i\_sh} = \frac{dH_{ice}}{dt}, \tag{3.31}$$

and Q_{ice} is the volume of newly formed ice ($m^3 \cdot sec^{-1}$):

$$Q_{ice} = \mathrm{Pr}_{i\_sh} \cdot A_{sh}. \tag{3.32}$$

When ice production (Pr_{i_sh}) is negative (ice melting) $\phi = Q_{sh} \cdot S_{sh}$, i.e. there is no salt flux into the HL and $S_{xx} = S_{sh}$, $q_0 = Q_{sh}$, which means that the interior basin and the shelf exchange waters within the surface layers. If ice production is positive, then S_{xx} is required to describe $q_{sh}(S)$ function.

Eq. (3.28) can be rewritten as (see Figs. 3.4B and 3.4C for details):

$$\begin{aligned} \phi &= \int_{S_{sh}}^{S_{xx}} \tan\theta \cdot (S_{xx} - S) \cdot S \cdot dS = \\ &\tan\theta \cdot \left[0.5 \cdot S_{xx} \cdot \left(S_{xx}^2 - S_{sh}^2\right) - \frac{1}{3} \cdot \left(S_{xx}^3 - S_{sh}^3\right) \right], \end{aligned} \tag{3.33}$$

where $\tan\theta = \dfrac{q_0}{(S_{xx} - S_{sh})}$.

From Eq. (3.33):

$$\tan\theta = \frac{\phi}{\left[0.5 \cdot S_{xx} \cdot \left(S_{xx}^2 - S_{sh}^2\right) - \frac{1}{3} \cdot \left(S_{xx}^3 - S_{sh}^3\right)\right]}. \tag{3.34}$$

From Fig. 3.4B one can see that $q_0 = q(S = S_{sh})$ can be obtained in two ways (Eqs. (3.35), (3.36)):

$$q_0 = \tan\theta \cdot (S_{xx} - S_{sh}) = \frac{\phi}{\left[0.5 \cdot S_{xx} \cdot \left(S_{xx}^2 - S_{sh}^2\right) - \frac{1}{3} \cdot \left(S_{xx}^3 - S_{sh}^3\right)\right]} \cdot (S_{xx} - S_{sh}), \tag{3.35}$$

or:

$$q_0 = \frac{2 \cdot Q_{sh}}{(S_{xx} - S_{sh})}. \tag{3.36}$$

Then, after equating (3.35) = (3.36), the final relation between the total salt flux, shelf outflow and S_{xx} is:

$$Q_{sh} = \frac{1}{2} \cdot \frac{\phi}{0.5 \cdot S_{xx}\left(S_{xx}^2 - S_{sh}^2\right) - \frac{1}{3}\left(S_{xx}^3 - S_{sh}^3\right)} \cdot (S_{xx} - S_{sh})^2. \tag{3.37}$$

In Eq. (3.37) there is one unknown, S_{xx}. Note that the total salt flux ϕ is estimated using Eq. (3.29). From Eq. (3.37) S_{xx} can be obtained by using one of the iteration methods. In the model, the Newton-Raphson iteration technique [*Kreyszig*, 1999] is applied.

During model experiments, it has been noticed that when ice production is very intense, it happens during the first few time steps at the onset of ice freezing, S_{xx} reaches too high values. Hence, a necessity arises to bound S_{xx}. There is evidence of highly saline water on the shelf bottom [e.g., *Aagaard et al.*, 1981]. *Rudels and Friedrich* [2000] argue that the salinities of the saline plumes produced on shelf must be above 35 psu when they pass 200 m, if they are to reach deeper than the temperature maximum in the Atlantic Layer. In the present model S_{max}=40. S_{xx} is not allowed to exceed S_{max}.

The last term that should be determined in the shelf model is the upwelled Atlantic water (Q_{atl_sh}). It is obtained from the salt balance of the shelf box and is explained in more detail below.

(b) T and S on the shelf

Temperature variability in the model is described by Eqs. (3.38) and (3.39). If $H_{ice} < 0$, then

$$\frac{dT_{sh}}{dt} = \frac{1}{h_{sh}} \cdot \left\{ \frac{F_{tot}}{\rho_{sh} \cdot C_{wp}} + \frac{1}{A_{sh}} \cdot \left[Q_{mao} \cdot (T_{ml} - T_{sh}) + Q_f \cdot (T_f - T_{sh}) + Q_{atl\_sh} \cdot (T_{atl} - T_{sh}) \right] \right\}, \tag{3.38}$$

where F_{tot} is the surface heat flux (positive to the ocean), ρ_{sh} is the shelf water density, C_{wp} is the water specific heat (4184.4 $J \cdot m^{-2} \cdot sec^{-1}$), and T_f is the river runoff temperature. During the fall season, the temperature of shelf water decreases. When T_{sh} reaches the freezing point, ice cover appears in the shelf box. The thermodynamic sea ice model [*Maykut and Untersteiner*, 1969; *Maykut*

and Untersteiner, 1971; *Maykut*, 1986] is used to describe seasonal variability in the sea ice cover. When $H_{ice} > 0$, temperature of the shelf water changes according to:

$$\frac{dT_{sh}}{dt} = \frac{1}{h_{sh}}\left\{\frac{-F_w}{\rho_{sh}\cdot C_{wp}} + \frac{1}{A_{sh}}\cdot \left[Q_{mao}\cdot(T_{ml}-T_{sh}) + Q_f\cdot(T_f - T_{sh}) + Q_{atl\_sh}\cdot(T_{atl}-T_{sh})\right]\right\} \tag{3.39}$$

where F_w is the water heat flux to the ice bottom. However, the model experiments show that during winter, shelf water temperature is insignificantly different from the freezing point.

Salinity changes in the shelf model are described by the equation:

$$\frac{dS_{sh}}{dt} = \frac{1}{h_{shw}}\cdot\left\{\frac{1}{A_{sh}}\left[Q_{mao}(S_{ml}-S_{sh}) - Q_f\cdot S_{sh} - Q_{(P-E)}\cdot S_{sh}\right] + \xi\cdot\varepsilon\cdot \mathrm{Pr}_{i\_sh}(S_{sh}-S_{ice})\right\} \tag{3.40}$$

(c) Shelf water outflow to the ML

The outflowing shelf water isopycnally mixes with the Arctic Ocean water. The upper flow gets into the ML (Q_{sh_ml}). Q_{sh_ml} is determined so the density of the shelf water flowing into the ML is less than or equal to ρ_{ml}. In summer, when no salt water is produced on the shelf and $S_{xx} < S_{ml}$, all shelf water flows into the ML and $Q_{sh\_ml} = Q_{sh}$. During the cold season, some fraction of Q_{sh} is denser than

ρ_{ml} and $Q_{sh\_ml} < Q_{sh}$. In winter, both $T_{ml} = T_{fr}(S_{ml})$ and $T_{sh} \approx T_{fr}(S_{sh})$ (T_{fr} is the freezing temperature), hence, Q_{sh_ml} is a function of the mixed layer salinity and from Eq. (3.27) and Fig. 3.4B:

$$Q_{sh\_ml} = \begin{cases} \int_{S_{sh}}^{S_{ml}} q_{sh}(S)dS = \int_{S_{sh}}^{S_{ml}} \tan\theta \cdot (S_{xx} - S)dS = \\ \dfrac{q_0}{S_{xx} - S_{sh}}\left\{S_{xx}(S_{ml} - S_{sh}) - 0.5\left(S_{xx}^2 - S_{sh}^2\right)\right\}, & S_{xx} > S_{ml} \\ Q_{sh}, & S_{xx} \le S_{ml}. \end{cases} \qquad (3.41)$$

The salinity of Q_{sh_ml} is calculated as a mean value for a given distribution function [*Rice*, 1995]:

$$\overline{S}_{sh\_ml} = \int_{S_{sh}}^{S_{ml}} \frac{q_{sh}(S) \cdot S}{Q_{sh\_ml}} dS = \frac{q_0}{Q_{sh\_ml} \cdot (S_{xx} - S_{sh})} \cdot \left[\frac{1}{2} S_{xx}\left(S_{ml}^2 - S_{sh}^2\right) - \frac{1}{3}\left(S_{ml}^3 - S_{sh}^3\right)\right]. \qquad (3.42)$$

When ice production is negative $\overline{S}_{sh\_ml} = S_{sh}$.

(d) Shelf water outflow to the halocline of the Arctic Ocean

When ice production on the shelf is high, saline plumes flow into the halocline of the Arctic Ocean. In this model, such events occur when $S_{xx} > S_{ml}$ (Fig. 3.4B). It

is assumed that saline shelf water isopycnally mixes with the halocline water. The outflow function $q_{sh}(S)$ is a function of salinity. Hence, in order to determine the shelf water outflow into the halocline of the Arctic Ocean at a given depth z, the corresponding salinity of the shelf outflow at this depth level $(S_{sh\_out}(z))$ has to be determined. To find $S_{sh\_out}(z)$ below ML, the initial condition is:

$$\rho_{ao}(z) = \rho_{sh\_out}\left(T_{fr}(S_{sh\_out}(z)), S_{sh\_out}(z)\right), \tag{3.43}$$

where ρ_{ao} is the Arctic Ocean density at a given depth level (z), ρ_{sh_out} is the density of the shelf outflow, $T_{fr}(S_{sh\_out}(z))$ is the freezing temperature for given salinity of the shelf outflow ($S_{sh\_out}(z)$) (the water temperature of plumes is at the freezing point). Given ρ_{ao}, $S_{sh\_out}(z)$ is obtained from Eq. (3.43) by an iteration method of false position. Finally, $q_{sh}\left(S = S_{sh\_out}(z)\right)$ is calculated (Fig. 3.4B):

$$q_{sh}(S) = \tan\theta \cdot (S_{xx} - S) = \frac{q_0}{S_{xx} - S_{sh}} \cdot (S_{xx} - S). \tag{3.44}$$

Constants and parameters used in the shelf box model are listed in Table 3.5.

Table 3.5. Values of constants used in the shelf box model

Constant	Value	Units
Area of the shelf region (A_{sh})	0.41×10^{13}	m^2
Inflow from the ML (Q_{mao})	1.1	Sv
Salinity of the river runoff (S_f)	0	psu
Oceanic heat flux (F_{water})	1.0	$W \cdot m^{-2}$

Forcing in the shelf box model

The forcing parameters in the shelf box model are: Atlantic water inflow, river runoff, meteorological characteristics (net precipitation, wind, and cloudiness), surface air temperature and shortwave radiation.

(a) Shortwave radiation

The downwelling shortwave radiation (F_0) daily values have been computed for 75° N latitude using equations of the Sun-Earth astronomical relationships [*Iqbal*, 1983] and empirical relationships between air mass, water vapor content and radiation depletion [*Shine*, 1984]. The incoming shortwave radiation is estimated using the empirical relation from [*Maykut*, 1986].

(b) Surface air temperature

It is believed that under ACCR, both the shelf and Arctic Ocean experience cooling [e.g., *Polyakov et al.*, 1999]. Thus the interannual variability of SAT is in-phase. Seasonal variability of SAT in the shelf region is different from that in the central Arctic Ocean: it is warmer in winter but almost the same in summer (see for example [*Gorshkov*, 1980])[1]. The shelf box model does not have an atmospheric component. The surface air temperature (SAT) in the shelf box is approximated through the relationship with the SAT in the Arctic Ocean atmospheric model:

[1] Here the reference is about average characteristics of the shelf regions in the Arctic, which might be not true for a particular shelf.

$$T_{0\_sh} = T_{0\_ao} + 4.5 - 2\sin\left(\frac{\pi}{365} d_j\right), \tag{3.45}$$

where T_{0_ao} is the Arctic SAT, d_j is Julian day.

(c) Atlantic water inflow

It has been generally accepted that the Atlantic water plays an important role in the shelf processes [*Gakkel*, 1957; *Mountain et al.*, 1976; *Aagaard et al.*, 1981; *Doronin and Proshutisnky*, 1991], yet estimates of the Atlantic water inflow are very uncertain in the oceanographic literature. In the model, Atlantic water is needed to maintain the salt balance on the shelf. The required rate of Q_{atl_sh} is obtained from the volume and salt balance constraints:

$$\overline{Q}_{atl\_sh} = -\frac{\overline{Q}_{mao}\left(\overline{S}_{ml} - \overline{S}_{sh}\right) - \overline{Q}_f \cdot \overline{S}_{sh} + \overline{Q}_{ice}\left(\overline{S}_{sh} - S_{ice}\right)}{S_{atl} - \overline{S}_{sh}}, \tag{3.46}$$

where bars denote the annual means, $S_{atl} = 34.8$, $T_{atl} = 0.5\,°C$. The annual mean salinity on the shelf is kept at 29.2 psu. The average value of the Q_{atl_sh} obtained from the model runs ranges from ~0.35 Sv to 0.75 Sv. For reference, *Doronin* [1986] estimated the rate of the Atlantic water upwelling on the Kara Sea shelf to be about 9×10^3 km^3·yr^{-1} (~0.28 Sv).

(d) River runoff and meteorological characteristics

In the shelf model monthly means of the river runoff (flux, T and S) and meteorological characteristics (precipitation, wind, and cloudiness) are used. During the computation the monthly values are linearly interpolated into daily data. In Table 3.6 the monthly means of these forcing parameters are shown.

Table 3.6. Monthly means of the river runoff and meteorological characteristics for the shelf model

Jan	Fb	Mr	Ap	May	Jn	Jl	Aug	Sp	Oc	Nv	Dc
River runoff, Q_f x 10^4, $m^3 \cdot sec^{-1}$, [*Bjork*, 1989]											
2.3	2.3	2.3	2.3	2.3	37.1	42.8	37.1	5.79	2.3	2.3	2.3
River runoff temperature, T_f, °C											
4.0	4.0	4.0	4.0	4.0	6.0	6.0	6.0	6.0	4.0	4.0	4.0
Net precipitation[(a)], *(P-E)x10^{-3}, m·day^{-1}*, [*Serreze and Barry*, 2000]											
-	-	-	-	-	0.4	0.45	0.58	-	-	-	-
Wind, w_{10}, $m \cdot s^{-1}$, [*CDC*]											
5.1	5.6	5.3	5.1	4.9	4.8	4.5	4.5	4.9	5.3	5.3	5.4
Cloudiness, *cld*, [*Gorshkov*, 1980]											
0.55	0.55	0.55	0.6	0.6	0.75	0.85	0.9	0.85	0.7	0.6	0.6

(a) Only summer values are considered for salinity changes of the shelf water.

3.3.3. Arctic atmospheric model

The interaction between the Greenland Sea and the Arctic is performed through the oceanic and atmospheric components. The close relation between the Arctic

climate state and heat advection from the North Atlantic region has been well documented. For example, *Mysak and Venegas* [1998] have proposed a decadal feedback loop for atmosphere-ice-ocean interactions in the Arctic and subarctic. In this loop one of the feedback components is an increased northward transport of warm air from the Greenland Sea associated with a positive NAO pattern. Thus in the present study, it is assumed that the Greenland Sea affects the Arctic Ocean climate state through the heat advection, which varies both seasonally and interannually.

A conceptual box model for the Arctic atmosphere is presented in Fig. 3.5. The model is forced by the insolar radiation (F_{ins}), cloudiness, heat advection (F_{adv}), and albedo of the ice surface. The surface air temperature ($T_{(0)}$) is estimated from a total energy balance (F_{tot_a}):

$$\frac{dT_{(0)}}{dt} = \frac{1}{H_{atm}} \frac{F_{tot\_a}}{\rho_{air} C_p}, \tag{3.47}$$

where H_{atm} = 8x10^3 m is the height of the atmospheric box, ρ_{air}=1.37 kg·m^{-3} is the air density, and C_p=1012 J·kg^{-1}·K^{-1} is the air specific heat. The total energy gain or loss in the box (F_{tot_a}) is estimated through the energy balance:

$$F_{tot\_a} = F_{tot(0)} + F_{tot(1)} + F_{adv}, \tag{3.48}$$

where $F_{tot(0)}$ is the energy balance on the bottom atmospheric box boundary (atmosphere – ice), $F_{tot(1)}$ is the energy balance on the upper atmospheric box boundary (atmosphere – space), and F_{adv} is heat advected from the Greenland Sea box. The energy balance on the bottom boundary ($F_{tot(0)}$) is calculated in the ice model of the Arctic Ocean. $F_{tot(0)}$ is slightly above zero during the cold season

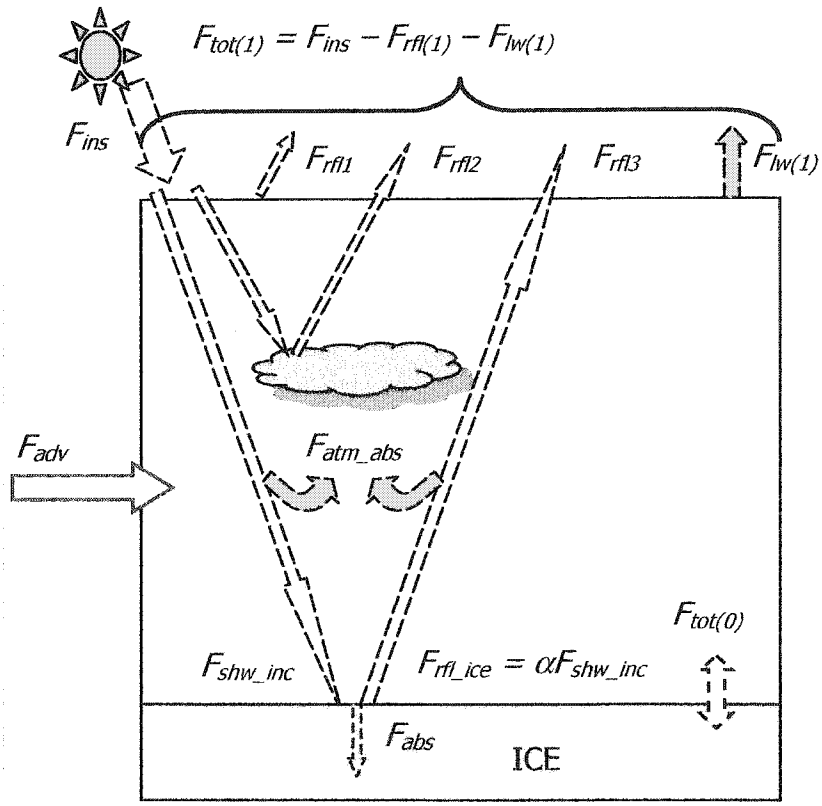

Fig. 3.5. Arctic atmospheric box model. *SAT is calculated from the total energy balance within the atmospheric box. The heat fluxes are: $F_{tot(1)}$ – heat flux at the upper boundary, $F_{tot(0)}$ – surface heat flux at the lower boundary, F_{adv} – heat advection, F_{ins} – insolar radiation, F_{rfl} – reflected shortwave radiation, $F_{lw(1)}$ – longwave flux at the top of the atmosphere, F_{atm_abs} – absorbed shortwave radiation by the atmosphere, F_{abs} – penetrated into ice shortwave radiation, F_{rfl_ice} – reflected by ice shortwave radiation, and F_{shw_inc} – incoming on the ice shortwave radiation.*

of the year due to heat loss of the ice surface (though no leads have been parameterized in the model). During the warm season, the atmosphere loses heat to the ice, which melts.

At the upper boundary the energy balance can be written as follows [*Wallace and Hobbs*, 1977]:

$$F_{tot(1)} = F_{ins} - F_{rfl(1)} - F_{lw(1)}, \tag{3.49}$$

where F_{ins} is the incoming solar radiation, $F_{rfl(1)}$ is the total reflected solar radiation off the upper boundary: $F_{rfl(1)} = F_{rfl1} + F_{rfl2} + F_{rfl3}$, and $F_{lw(1)}$ outgoing longwave radiation. The total energy balance of the top boundary of the atmospheric box is negative during winter and positive during summer.

The insolar radiation at the top of the atmosphere has been calculated using an equation of daily insolation [eq. (3.6), *Matveev*, 1984]. The total reflected solar radiation at the upper boundary has three components [*Wallace and Hobbs*, 1977]: back-scattered by air (F_{rfl1}), reflected by clouds (F_{rfl2}), and reflected by ice surface (F_{rfl3}). The back-scattered radiation is estimated at about 6% of the incoming solar radiation [*Wallace and Hobbs*, 1977]. The amount of solar radiation reflected by clouds is:

$$F_{rfl2} = r_{cld} \cdot cld \cdot F_{ins}, \tag{3.50}$$

where $r_{cld} \approx 0.44$ is cloud reflectivity [*Wallace and Hobbs*, 1977], and *cld* is the fractional cloudiness. The fraction of solar radiation reflected by ice surface and scattered back to space is obtained through the following steps. The amount of shortwave radiation incoming on the ice surface is calculated in the Arctic Ocean ice model. The fraction of the incoming solar radiation that reaches the bottom boundary is F_{shw_inc}/F_{ins}. The amount of ice reflected shortwave radiation is $\alpha \cdot F_{shw\_inc}$. On its way back to the top of the atmosphere, the ice reflected

shortwave radiation is also being absorbed and scattered by the atmosphere, and reflected from and absorbed by clouds. Thus it can be assumed that approximately the same fraction of the shortwave radiation reaches the upper boundary and passes away into space. Hence the amount of solar radiation reflected by ice surface is:

$$F_{rfl3} = \frac{F_{shw\_inc}}{F_{ins}} \cdot \left(\alpha \cdot F_{shw\_inc}\right) = \left(\frac{F_{shw\_inc}}{F_{ins}}\right)^2 \cdot \alpha \cdot F_{ins}\,. \tag{3.51}$$

The outgoing longwave radiation at the upper boundary is given by:

$$F_{LW(1)} = \varepsilon^* \cdot \sigma \cdot T_{air(1)}^4\,, \tag{3.52}$$

where the effective emissivity for the Arctic (ε^*) is computed using Eq. (3.86), and σ is the Stefan-Boltzman constant $5.67 \cdot 10^{-8}$ W·m^{-2} °K^{-4}. Air temperature at the upper boundary ($T_{air(1)}$) is estimated under the assumption of polytropic atmosphere (constant vertical temperature gradient):

$$T_{air(1)} = T_{air(0)} - \gamma \cdot H_{atm}\,, \tag{3.53}$$

where γ is the adiabatic temperature gradient. From *Matveev* [1984], the adiabatic temperature gradient for the Arctic can be approximated 0.6 – 0.7 °K·100 m^{-1}, with slightly lower values in summer (closer to 0.6°K·100 m^{-1}) and higher in winter (≥0.7°K·100 m^{-1}). In the model, the vertical temperature gradient (for SAT in degrees K) is calculated using the relation:

$$\gamma = 0.01 \cdot \left\{0.65 + 0.005 \cdot \left(243.15 - T_{air(0)}\right)\right\}, \tag{3.54}$$

where SAT, $T_{air(0)}$, is taken from the previous time step.

The heat advection to the Arctic depends on SAT gradient between the Greenland Sea and Arctic boxes. The idea is adopted from *Marotzke and Stone* [1995] and *Scott et al.* [1999] who investigated atmospheric meridional transports and ocean-atmosphere interactions. To describe the heat advection between "cold" and "warm" boxes in their model, *Marotzke and Stone* [1995] used a simplified parameterization assuming that the atmospheric heat transport is proportional to the meridional temperature gradient:

$$F_{adv} = \chi(T_2 - T_1), \qquad (3.55)$$

where $\chi \approx 1.3$ W· $m^{-2}.^{\circ}K^{-1}$, T_2 and T_1 are SAT in the warm and cold boxes respectively. *Henderson-Sellers and McGuffie* [1987] estimate this coefficient to be ~ 3 $W{\cdot}m^{-2}.^{\circ}C^{-1}$.

Section 3.4. Greenland Sea module

The primary goal of the Greenland Sea module is to describe the seasonal and interannual variability of the heat content of the GIN Sea region. To proceed, it is assumed that the heat content of the region is related to the air-sea surface heat flux. The air-sea heat flux, in turn, is determined by the intensity of deep convection in the Greenland Gyre. Thus, the central Greenland Sea is parameterized in the model. The ice-ocean model describes the seasonal and interannual variability of the thermohaline structure in the region. The state-space atmospheric model relates the surface heat flux and SAT anomalies. The area of the region of deep convection in the Greenland Sea (A_{GS}) is estimated to be ~0.135×10^{12} m^2 [*Aagaard and Carmack*, 1989].

3.4.1. Oceanic model of the central Greenland Sea region

The oceanic model describes the development of the thermohaline structure in the Greenland Gyre. It should be noted that the model describes basin-wide average thermohaline structure. Hence, it can not reproduce deep convection which is strongly believed to be a local event ("chimney" convection) forced by sudden, negative fluxes at the sea surface (e.g., local intrusion of the transformed Atlantic water which is salty and relatively cold as mentioned in *Alekseev et al.*, [1994]) with significantly smaller scales (less than 100 km) [e.g., *Killworth*, 1979; *Chapman*, 1998]. However, the model reproduces a pre-convective state of the Greenland Gyre with very low stability of the water column.

The structure of the model is outlined in Fig. 3.6. The model consists of several layers: the Mixed Layer (ML), the upper Arctic Intermediate Water (uAIW) layer, the lower Arctic Intermediate Water (lAIW) layer, the Norwegian Sea Deep Water (NSDW), and the Greenland Sea Deep Water (GSDW) layer. When ML deepens, some of the layers are eroded. On the top of the water column there is an ice sheet of thickness H_{ice}. The appearance and growth of the ice depends on the heat budget of the sea surface and characteristics of the Mixed Layer.

The ML behavior is mostly approximated with a pycnocline model developed by Stigebrandt [1985] and with Bjork's [1989] one-dimensional model for the vertical stratification of the upper Arctic Ocean. The ML characteristics (temperature (T_{ml}), salinity (S_{ml}) and depth (H_{ml})) depend on the Arctic water and North Atlantic water inflow, heat fluxes on the air-sea surface, ice growth/melt (if there is any) and wind. Temperature and salinity profiles in the HL at each time step are obtained through the numerical solution of temperature and salinity advection-diffusion equations.

The vertical space step (h_z) in the Greenland Sea model is 5 m. The time step, similar to the Arctic Ocean model, varies depending on the entrainment rate to fulfill Eq. (3.25). The time step is given by the formula:

$$t_{stp} = \begin{cases} \min\left\{ 0.5 * h_z / -w_e ; \quad 43200 \quad \text{sec} \right\}, & w_e < 0 \\ 43200 \quad \text{sec}, & w_e \geq 0. \end{cases} \qquad (3.56)$$

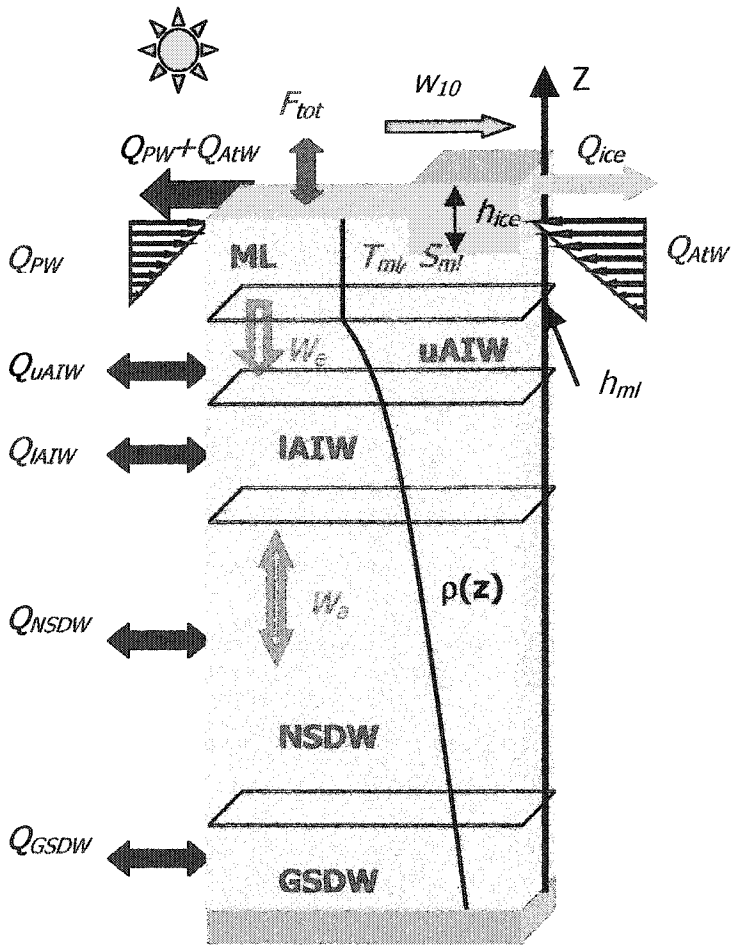

Fig. 3.6. Diagram of the Greenland Sea model. *Red indices denote layers in the model: ML – mixed layer; uAIW – upper Altlantic Intermediate Water; lAIW – lower Atlantic Intermediate Water; NSDW – Norwegian Sea Deep Water; and GSDW – Greenland Sea Deep Water. F_{tot} – surface heat flux; T_{ml} and S_{ml} – temperature and salinity of the ML; W_e – entrainment velocity; W_a – vertical velocity; $\rho(z)$ – water density; h_{ice} – ice thickness; w_{10} – wind; and h_{ml} – ML thickness. Volume fluxes: Q_{PW} – Polar Water inflow; Q_{AtW} – Atlantic Water inflow; Q_{ice} – ice export from the Greenland Sea; Q_{uAIW}, Q_{lAIW}, Q_{NSDW}, and Q_{GSDW} – inflow/outflow rates within the layers.*

Inflows and outflows in the Greenland Sea model

The inflows in the Greenland Sea model are the Polar Water (Q_{PW}), the transformed (cooled) Atlantic Water (Q_{AtW}), the uAIW (Q_{uAIW}), lAIW (Q_{lAIW}),

NSDW (Q_{NSDW}), and GSDW (Q_{GSDW}). In summer, the central Greenland Sea gains some ice advected from EGC (Q_{mlt_GS}) where it is presumably melted. To conserve the mass balance, the outflows from the layers equal the inflows. Q_{PW} is a fraction of the Arctic Ocean outflow Q_{g_atl} integrated from the surface to 100 m depth. The temperature (T_{PW}) and salinity (S_{PW}) of Q_{PW} are integrated values of Q_{g_atl} within the same depth range. In studies related to the central Greenland Sea, it has been noticed that the Greenland Gyre experiences a very small effect from the EGC receiving very little of the PW [*Swift*, 1986; *Alekseev et al.*, 1994]. *Swift* [1986] argues that the major source of salt in the region is the Atlantic water which penetrates the Arctic front. Also it is assumed that the inflow rates of the PW and AW have seasonal variability. In winter, when the cyclonic vortex in the Greenland gyre is intensified, the surface water is forced away from the Gyre and very little ambient water can penetrate the Arctic front. However in summer, when the cyclonic vorticity is significantly weakened, the ambient surface water and sea ice can easily penetrate the front and reach the center of the Gyre [*Johannessen*, 1986]. This idea is well corroborated by oceanographic observations [*Pawlowicz*, 1995] showing freshening of the central Greenland Sea in summer. The characteristics of the inflows used in the model are listed in the Tables 3.7 and 3.8.

Table 3.7. Monthly mean inflow characteristics of Q_{PW} and Q_{AtW} of the Greenland Sea model

	Jan	Fb	Mr	Ap	May	Jn	Jl	Aug	Sp	Oc	Nv	Dc
Q_{PW}/Q_{g_atl}	0.01	0.01	0.01	0.01	0.01	0.19	0.19	0.19	0.02	0.02	0.02	0.02
Q_{AtW}, *Sv*	0.03	0.03	0.03	0.03	0.03	2.1	2.1	2.1	.06	0.06	0.06	0.06
T_{AtW}, °C	0.2	0.2	0.2	0.2	0.5	2.0	2.0	2.0	1.0	0.5	0.2	0.2

Salinity of Q_{AtW} is constant 35.

In summer, the rate of ice melt is high in the EGC and can reach up to 0.72 m/month [*Vinje et al.*, 2002]. Ice melt freshens the PW carried by EGC [*Pawlowicz*, 1995]. In this model S_{PW} changes are parameterized as follows:

$$\frac{dS_{PW}}{dt} \cong \begin{cases} \frac{1}{100}\varepsilon \Pr_{i\_ao}(S_{PW} - S_{ice}), & \Pr_{i\_ao} < 0 \\ 0, & \Pr_{i\_ao} \geq 0. \end{cases} \qquad (3.57)$$

Table 3.8. Inflow characteristics of the Greenland Sea model

Inflow	Depth intervals, m		Volume flux, Sv	T, °C	S, psu
	Upper	Lower			
Q_{PW}	0	100	variable[a]	$\int_0^{100} Tdz$	$\int_0^{100} Sdz$
Q_{AtW}	0	200	variable[a]	variable[a]	35.00
Q_{uAIW}[b]	50	300	3.5[c]	-0.2	34.87
Q_{lAIW}[b]	300	500	3.5[c]	0.4	34.94
Q_{NSDW}[b]	500	2500	12.[c]	-0.7	34.92
Q_{GSDW}[b]	2500	bottom	6.[c]	-1.4	34.90
Q_{mlt_GS}	-	-	variable[d]		5

(a) See Table 3.7.
(b) [*Swift*, 1986].
(c) The volume fluxes have been estimated such that the T,S structure beneath the ML can restore during 3 non-convective summer months.
(d) Characteristics of Q_{mlt_GS} are discussed in Chapter 4.

The inflows of the PW and Atlantic water are approximated with linear functions q_{AtW} and q_{PW}, respectively:

$$q_{AtW}(z)=\begin{cases} q_{0,AtW}-\dfrac{q_{0,AtW}}{H_{AtW}}|z|, & |z|\le H_{AtW} \\ 0, & |z|>H_{AtW}, \end{cases} \tag{3.58}$$

$$q_{PW}(z)=\begin{cases} q_{0,PW}-\dfrac{q_{0,PW}}{H_{PW}}|z|, & |z|\le H_{PW} \\ 0, & |z|>H_{PW}, \end{cases} \tag{3.59}$$

where q_0 is the transport at the surface, H_{AtW} the thickness of the Atlantic water jet, and H_{PW} is the thickness of the PW jet. The value of q_0 can be easily found as:

$$q_{0,AtW}=\frac{2\cdot Q_{AtW}}{H_{AtW}}, \tag{3.60}$$

$$q_{0,PW}=\frac{2\cdot Q_{PW}}{H_{PW}}. \tag{3.61}$$

If the ML is shallower than the thickness of either of the jets, then the fraction of the inflows is calculated by integrating the Eqs. (3.58) and (3.59):

$$Q_{AtW}(z)=\int_0^z q_{AtW}(z)dz=q_{0,AtW}\cdot z\cdot\left(1-\frac{z}{2H_{AtW}}\right), \tag{3.62}$$

$$Q_{PW}(z)=\int_0^z q_{PW}(z)dz=q_{0,PW}\cdot z\cdot\left(1-\frac{z}{2H_{PW}}\right). \tag{3.63}$$

The rest of the inflows are injected beneath the ML.

Model equations

In general, the parameterization of ML dynamics in the Greenland Sea is similar to that in the Arctic Ocean described in Section 3.3.1. Here, a brief description of ML dynamics in the Greenland Sea is presented.

The ML thickness is also determined by three scale lengths: h_{ml}, h_{Ekm}, and h_{Ob} according to the dynamic regimes outlined in Eqs. (3.8) – (3.11). The length scale h_{ml} in the Greenland Sea is defined as:

$$\frac{dh_{ml}}{dt} = w_e + w_a. \tag{3.64}$$

The entrainment velocity is given by the Eq. (3.12). The vertical velocity is estimated through the Ekman pumping – wind stress curl relation [*Cushman-Roisin*, 1994]:

$$w_a = \frac{1}{\rho_0 f}\left(\frac{\partial \tau_y}{\partial x} - \frac{\partial \tau_x}{\partial y}\right) = \frac{1}{\rho_0 f} curl(\tau_{x,y}). \tag{3.65}$$

The wind stress curl over the Greenland Sea is adopted from [*Hellerman and Rosentstein*, 1983; *Jonsson*, 1991; *Maslowski*, 1994]:

Summer: $\tau(x,y) \approx 0$,

Fall: $\tau(x,y) = 3\text{x}10^{-7}$ Pa·m^{-1},

Winter: $\tau(x,y) = 6\text{x}10^{-7}$ Pa·m^{-1}.

For the strong cyclonic conditions the vertical velocity has been estimated to be in the order of $1x10^{-6}$ $m \cdot s^{-1}$. For weak cyclonicity the vertical pumping is in the order of $1x10^{-7}$ $m \cdot s^{-1}$ or even less.

The buoyancy flux at the sea surface is calculated using the following equation [*Turner*, 1973; *Stigebrandt*, 1985]:

$$B_{fl} = g * \left\{ \frac{\alpha}{\rho_{ml} \cdot C_{wp}} F_{tot} + \right.$$

$$\frac{\beta}{A_{GS}} \left[\int_0^{Hml} Q_{AtW} (S_{ml} - S_{AtW}) dz + \int_0^{Hml} Q_{PW} (S_{ml} - S_{PW}) dz \right] \qquad (3.66)$$

$$\left. - \varepsilon \cdot \beta \cdot \left[\Pr_{i\_GS} (S_{ml} - S_{ice}) + \frac{Q_{mlt\_GS} (S_{ml} - S_{ice})}{A_{GS}} \right] \right\},$$

where g is the gravitational acceleration, $\alpha = -\frac{1}{\rho} \frac{\partial \rho}{\partial T}$ is the coefficient of heat expansion and $\beta = \frac{1}{\rho} \frac{\partial \rho}{\partial S}$ is the coefficient of salt contraction, ρ_{ml} is the water (ML) density calculated through the equation of state [*Pond and Pickard*, 1989], C_{wp} = 4184.4 J $m^{-2} \cdot sec^{-1}$ is the water specific heat, F_{tot} is the air-sea heat flux (it is positive for the flux to the ocean), A_{GS} is the area of the central Greenland Sea, the proportionality coefficients are determined by the Eqs. (3.22) – (3.24), and Pr_{i_GS} is ice production in the region. Q_{mlt_GS} is the volume of ice advected from the EGC and melted in the central Greenland Sea during summer. This variable is discussed in Chapter 4.

The friction velocity is determined in different ways depending on presence of the ice cover in the region. If there is no ice cover the friction velocity is estimated according to the equation [*Hellerman and Rosentstein*, 1983; *Kowalik*, 1984]:

$$u_*^2 = C_{10} \cdot w_{10}^2 \cdot \frac{\rho_{air}}{\rho_w}, \tag{3.67}$$

where C_{10} is an empirical constant. Its value depends on the wind speed:

$$C_{10} = \begin{cases} 0.8 \cdot 10^{-3}, & w_{10} < 6 \quad m/s \\ 2.73 \cdot 10^{-3}, & w_{10} \geq 6 \quad m/s. \end{cases} \tag{3.68}$$

The salinity changes in the ML are described by the salt balance equation:

$$\frac{dS_{ml}}{dt} = \frac{1}{h_w} \cdot \left\{ \frac{1}{A_{GS}} \cdot \left[\int_0^{h_{ml}} Q_{AtW} \cdot (S_{AtW} - S_{ml}) dz + \int_0^{h_{ml}} Q_{PW} \cdot (S_{PW} - S_{ml}) dz \right] + \varepsilon \left[\frac{Q_{mlt\_GS}(S_{ice} - S_{ml})}{A_{GS}} + \Pr_{i\_GS} \cdot (S_{ml} - S_{ice}) \right] - w_e \cdot \frac{(S(h_{ml+}) - S_{ml})}{h_z} \right\}, \tag{3.69}$$

where Pr_{i_GS} is the ice production/melting rate (if there is any ice) and $S(h_{ml+})$ denotes the salinity just below the ML. The term under the integral sign describes the salt flux in the ML due to the fraction of the Atlantic water and PW inflows, which inject into the ML. The Eq. (3.69) is valid only for downward or

zero entrainment velocity, otherwise (during the ML retreat) there is no w_e term in the formula.

The variability of the ML temperature is significantly different depending on whether there is ice cover or not in the region. Under ice free conditions the temperature changes are given by

$$\frac{dT_{ml}}{dt} = \frac{1}{h_w} \cdot \left\{ \frac{F_{tot}}{\rho_w C_{wp}} + \right.$$

$$\left. \frac{1}{A_{GS}} \left[\int_0^{h_{ml}} Q_{AtW} \cdot (T_{AtW} - T_{ml}) dz + \int_0^{h_{ml}} Q_{PW} \cdot (T_{PW} - T_{ml}) dz \right] - \right. \tag{3.70}$$

$$\left. w_e \cdot \frac{(T(ml+1) - T_{ml}))}{h_z} \right\},$$

where F_{tot} is the surface heat flux:

$$F_{tot} = (1-\alpha) \cdot F_{shw} + F_{LWi} + F_{LWo} + F_{sens} + F_{lat} - F_{mlt}. \tag{3.71}$$

The fluxes F_{LWi}, F_{LWo}, F_{sens}, and F_{lat} are calculated using Eqs. (3.85), (3.87), (3.88), and (3.89) in Section 3.5. F_{mlt} is amount of energy needed to melt the advected ice Q_{mlt_GS} in summer:

$$F_{mlt} = \frac{Q_{mlt\_GS} \cdot \rho_{ice} \cdot L_{ice}}{A_{GS}}, \tag{3.72}$$

where L_{ice} is the latent heat of fusion of fresh ice. F_{shw}, in Eq. (3.71), is the incoming shortwave radiation at the sea surface. The value of F_{shw} depends on

cloudiness (*cld* in Eq. (3.74)) and is related to the shortwave downwelling radiation by the formula [*Maykut*, 1986]:

$$F_{shw} = a^* \cdot F_{Dshw}, \tag{3.73}$$

where F_{Dshw} is the downwelling shortwave radiation, and a^* is the cloud attenuation:

$$a^* = 1 - 0.63 * cld^3, \tag{3.74}$$

where *cld* is the fractional cloud cover.

The shortwave downwelling radiation daily values have been computed for 75° N latitude using equations of the Sun-Earth astronomical relationships [*Iqbal*, 1983]. Albedo of the sea surface (α_w) ranges between 0.02 to 0.16 depending on the sun zenith angle, sea roughness, cloudiness, and hour angle [*Doronin*, 2000]. According to *Matveev* [Chapter 6, 1984], the sea surface albedo in Polar regions varies within 0.15 to 0.20. In this study, $\alpha_w = 0.18$.

When the ML temperature drops below the freezing point for a given S_{ml}, the ice starts freezing. In this case, $F_{tot} = F_w$. F_w is heat flux from the water to the ice bottom parameterized by the relation [*Maykut and Untersteiner*, 1969]:

$$F_w = \rho_w C_{wp} D_z \frac{\partial T}{\partial z}, \tag{3.75}$$

where $D_z = 1 \times 10^{-5}$ m^2·sec^{-2} is the vertical eddy diffusivity.

Below the mixed layer the local rate of change of the salinity and the temperature are:

$$\begin{aligned}\frac{\partial S}{\partial t} &= w_a \frac{\partial S}{\partial z} + D_z \frac{\partial^2 S}{\partial z^2} + \frac{q_{in}(z)}{A_{GS}}(S_{in} - S(z)),\\ \frac{\partial T}{\partial t} &= w_a \frac{\partial T}{\partial z} + D_z \frac{\partial^2 T}{\partial z^2} + \frac{q_{in}(z)}{A_{GS}}(T_{in} - T(z)).\end{aligned} \tag{3.76}$$

The semi-implicit Crank-Nicolson scheme [*Fletcher*, 1988] has been applied to obtain the numerical solution of Eq. (3.76). q_{in} denotes an inflow of temperature T_{in} and salinity S_{in} at a given depth z. For example, for the NSDW inflow, q_{in} and Q_{NSDW} are related as follows:

$$Q_{NSDW} = \int_{z=500}^{2500} q_{in}\, dz\,, \tag{3.77}$$

$$q_{in} = \frac{Q_{NSDW}}{2000}\,. \tag{3.78}$$

When the upper homogeneous layer in the model is above the lower boundaries of the Atlantic and Polar water jets, the horizontal advection should be taken into account as well. The inflow rates at a given depth are given by the Eqs. (3.58) and (3.59). The salinity and temperature change at each grid point below the mixed layer can be calculated as follows:

$$\begin{aligned}\frac{\partial S(z)}{\partial t} &= \frac{1}{A_{GS}} \cdot [q_{AtW}(S_{AtW} - S(z)) + q_{PW}(S_{PW} - S(z))],\\ \frac{\partial T(z)}{\partial t} &= \frac{1}{A_{GS}} \cdot [q_{AtW}(T_{AtW} - T(z)) + q_{PW}(T_{PW} - T(z))].\end{aligned} \tag{3.79}$$

Forcing in the Greenland Sea model

The forcing parameters in the Greenland Sea are incoming shortwave downward radiation, wind, cloudiness, relative humidity and the freshwater flux from the Arctic Ocean. The freshwater import to the central Greenland Sea is described in Chapter 4. Monthly means of the other forcing parameters of the Greenland Sea model are presented in Table 3.9.

Table 3.9. Forcing in the Greenland Sea model

Jan	Fb	Mr	Ap	May	Jn	Jl	Aug	Sp	Oc	Nv	Dc
Downwelling shortwave radiation[a], $W \cdot m^{-2} \cdot sec^{-1}$											
0	10	73	213	376	458	418	273	113	23	0.9	0
Relative humidity [*Gorshkov*, 1980]											
0.7	0.7	0.7	0.7	0.85	0.95	0.95	0.95	0.9	0.7	0.7	0.7
Wind, $m \cdot sec^{-1}$ [*CDC*, 2003]											
10.1	9.8	9.6	8.8	6.9	5.5	5.5	5.8	7.3	8.6	9.3	9.8
Cloudiness [*Gorshkov*, 1980]											
0.65	0.65	0.65	0.7	0.8	0.87	0.91	0.91	0.75	0.75	0.7	0.65

(a) Calculated using the Sun-Earth astronomical relationships [*Iqbal*, 1983]

3.4.2. State-space model of the surface air temperature in the central Greenland Sea

The Greenland Sea is a region of anomalously high heat fluxes to the atmosphere during the cold season, reaching a value of 450 $W \cdot m^{-2}$. The total net flux in November through March is extremely variable. The low and high peak

values range from –10 and –20 $W \cdot m^{-2}$ to –410 and –500 $W \cdot m^{-2}$. It is assumed that the surface heat flux anomalies induce SAT anomalies in the region. To predict a next-day SAT anomaly given previous heat flux and SAT a state-space statistical model has been developed. Preliminary statistical analyses of the SAT and surface heat flux in the region have shown that simple linear, polynomial, or non-linear regression models do not give a good forecast. Conceptually the suggested model works in the following way: if there are several years in a row of increased heat flux to the atmosphere, mean SAT increases from year to year, and if the heat flux is low during several years, mean SAT drops form year to year.

To proceed, the SAT anomalies are viewed as a combination of signal and noise. The signal can be approximated with an autoregressive (AR) or moving average (MA) model. The noise is not a completely white noise process but some part of its variance is explained by the heat flux anomalies. Then the deviation (noise) can be regressed on the total flux from previous days. Such models belong to the state-space models [*Chatfield*, 1996].

The backward elimination method was applied to select the best model to fit the data. The original model was:

$$\begin{aligned} Y_t = {} & \alpha_1 Y_{t-1} + \alpha_2 Y_{t-2} + \alpha_3 Y_{t-3} + \alpha_4 Y_{t-4} + \alpha_5 Y_{t-5} \\ & + \beta_1 X_{t-1} + \beta_2 X_{t-2} + \beta_3 X_{t-1} Y_{t-1} + \beta_4 X_{t-2} Y_{t-2} + \varepsilon, \end{aligned} \tag{3.80}$$

where Y_{t-i} denotes SAT anomaly on the i^{th} previous day, X_{t-i} is the total net flux anomaly on the i^{th} pervious day, α's and β's are coefficients to be estimated, ε is an error which is, in the case of a good fit, an independent Gaussian random variable. After the backward elimination the final model is:

$$Y_t = \alpha_1 Y_{t-1} + \alpha_2 Y_{t-2} + \alpha_3 Y_{t-3} + \beta_1 X_{t-1} + \beta_2 X_{t-2} + \varepsilon. \quad (3.81)$$

Both model selection and finding the parameter estimates have been done using SAS – statistical program. The SAS output for the final model (Eq. (3.81)) are given in Tables 3.10 and 3.11. The over-all fit test (F - test) proves a good fit of the model. All t - tests reveal that the parameters are significantly different from zero at confidence level α = 0.05 (except for intercept which is zero). Fig. 3.7 shows fitted values of the SAT anomalies and NOAA-CIRES CDC reanalysis data [*CDC*] (subplot (A)). The model reproduces very well the SAT anomaly behavior. The histogram (Fig. 3.7B) and autocorrelation function (Fig. 3.7C) of the residual show that the error term (ε) is white noise with a standard normal distribution which also support the idea that the model (Eq. (3.81)) provides reliable 1-day forecasts of SAT in the region.

Table 3.10. Analysis of variance and *F*-test of the overall fit

Source	DF[a]	Sum of squares[b]	Mean Square[c]	*F* value[d]	*P* value[e]
Corrected total[f]	4011	3648.04			
Error[g]	4006	1441.97	0.35995		
Model[h]	5	2206.07	441.21	1225.76	<0.0001

(a) Degrees of freedom, which is (# of observations – (# of parameters + intercept)).
(b) Sum of squared errors; errors are the difference between the model and observations.
(c) Mean Square Error = Sum of Squares/DF.
(d) Test for the overall model fit, null hypothesis (H_0) is that all coefficients in the model are zero (except for the intercept); F=Mean Square Model / Mean Square Error.
(e) Probability that a random value from $F(5,4006)$ will exceed the observed F = 1225.76. If P value is less than the confidence level α, H_0 is rejected which proves that the model fits the data well.
(f) Restricted model with all coefficients zero except for the intercept.
(g) Complete (tested) model (Eq. (3.81)).
(h) (f) – (g).

Table 3.11. Parameter estimates and individual *t*-tests

	Parameter estimate[(a)]	Standard error[(b)]	*t* statistics[(c)]	*P* value[(d)]
Intercept	-1.65×10^{-4}	0.00947	-0.02	0.9861
α_1	0.80465	0.02256	35.67	<0.0001
α_2	-0.10905	0.02617	-4.17	<0.0001
α_3	0.10229	0.01574	6.50	<0.0001
β_1	0.08298	0.01988	4.17	<0.0001
β_2	-0.12	0.01976	-6.07	<0.0001

(a) Estimates for the intercept, α's and β's in Eq. (3.81).
(b) STD of the estimates.
(c) Individual *t*-tests for testing the hypothesis $\alpha_1 = 0$, $\alpha_2 = 0$, $\alpha_3 = 0$, $\beta_1 = 0$, and $\beta_2 = 0$.
(d) *P*-value, the probabilities that the absolute value of the corresponding *t*-statistic will exceed that of the *t*-value given, under the standard normality assumptions and assuming that the true parameter is zero. When *P*-value is less than the confidence level $\alpha = 0.05$, the null hypothesis is rejected, meaning that the true parameter is not zero and the model fits the data. Note that the *P*-value for the intercept (which is the mean value of all the data points estimated by SAS) is larger than 0.05, so the hypothesis that the intercept is zero is accepted, which is true as the data are SAT anomalies with mean zero.

The anomalies in Eq. (3.81) are standardized:

$$Y_{t-i} = \frac{T_{t-i} - \overline{T}_{t-i}}{std\left(\overline{T}_{t-i}\right)}, \tag{3.82}$$

$$X_{t-i} = \frac{F_{t-i} - \overline{F}_{t-i}}{std\left(\overline{F}_{t-i}\right)}, \tag{3.83}$$

where overbars denote a long-term daily mean. In the present model, the daily means are estimated from the previous 5 years. So, for example, after several warm years $\overline{T}_{t-i}$ will increase. All initial mean estimates used in the model have been derived from the daily CDC data for the period 1948-2001 [*CDC*].

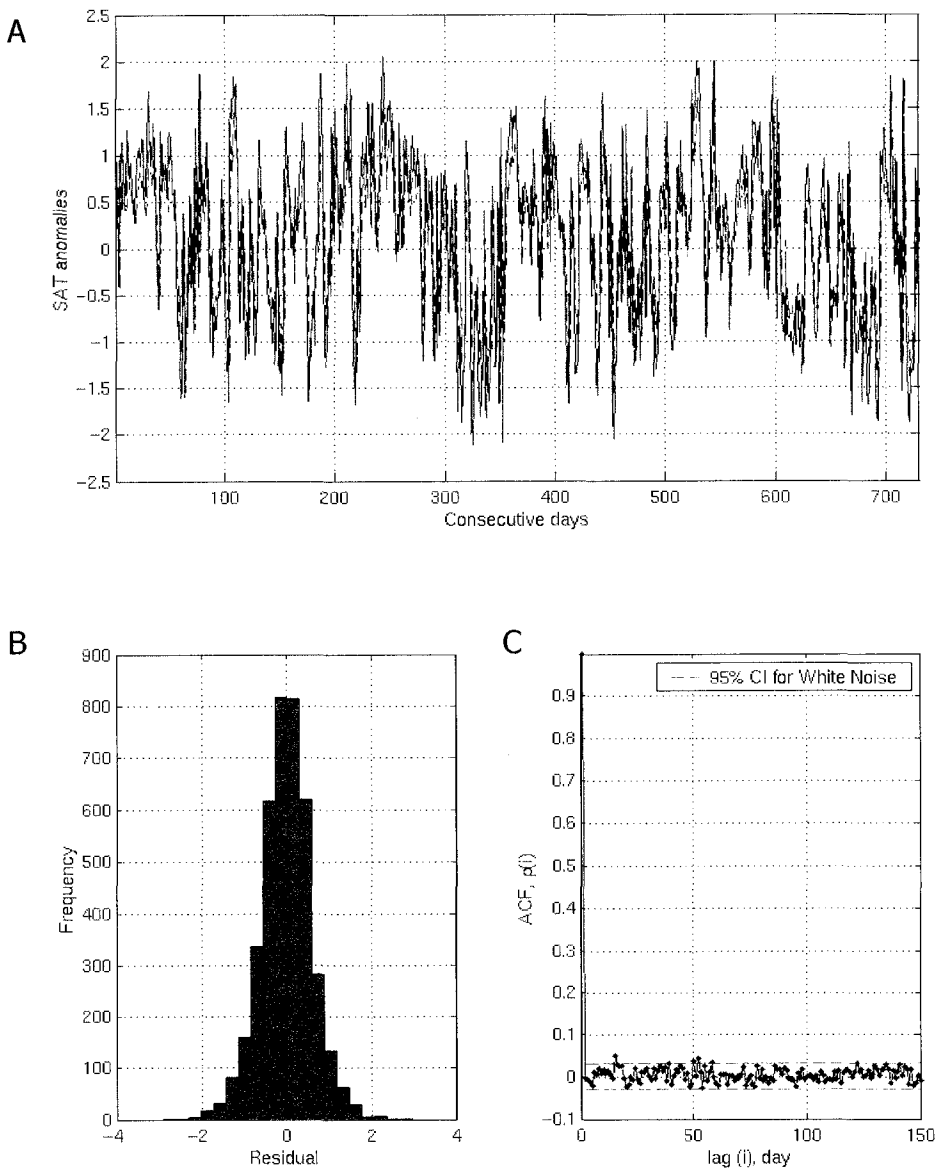

Fig. 3.7. State-space SAT model output for the central Greenland Sea. *(A) NOAA-CIRES CDC SAT data for 1990-1991 (blue solid line) and model predicted SAT (red dashed line). The model gives very accurate prediction. (B) and (C) Analysis of the residual (predicted SAT minus observed). The histogram (B) and auto-correlation function (C) of the residual unambiguously prove that it is white noise. This also shows a good fit of the model to the CDC data.*

The model (Eq. 3.81) is explicit as it allows one to calculate the SAT anomaly in the Greenland Sea region for a given day using the information from previous time steps. In order to get real values of SAT, Eq. (3.82) is solved for T_{t-i}. Model predicted SAT anomalies using CDC daily heat fluxes show a very good fit to the CDC SAT (Fig. 3.7A). Analysis of the residual (predictions minus observations) proves that this is white noise (Fig. 3.7B and 3.7C) which shows that the signal has been described by the model (Eq. (3.81)).

Section 3.5. Thermodynamic sea ice model

A thermodynamic linear sea ice model [*Maykut*, 1986] is applied for computing sea ice growth and melting rates. The heat fluxes at the upper ice surface are obtained as follows:

1) The net input of shortwave radiation equals $(1-i_0)(1-\alpha)F_{shw}$. The albedo of the ice surface equals:

$$\alpha_{ice} = 0.44 \cdot H^{0.28} + 0.08, \quad 0 < H_{ice} < 0.8m. \tag{3.84}$$

For perennial ice the albedo varies during a year. According to *Marshunova* [1961] and *Maykut and Untersteiner* [1969] the albedo changes from 0.85 in March to 0.57 in July or even down to 0.49 when the effects of summer melt ponds are taken into account. The penetration of the shortwave radiation is i_0=0.3 [*Maykut*, 1986].

2) The incoming longwave radiation is given by:

$$F_{LWi} = \varepsilon^* \cdot \sigma \cdot T_{air}^4, \tag{3.85}$$

where σ = 5.67·10^{-8} W·m^{-2}·°K^{-4} is the Stefan-Boltzman constant, and ε^* is the effective emissivity for the Arctic atmosphere given by:

$$\varepsilon^* = 0.7855 \cdot \left(1 + 0.2232 \cdot cld^{2.75}\right). \tag{3.86}$$

3) The outgoing longwave radiation is:

$$F_{LWo} = \varepsilon_L \cdot \sigma \cdot T_0^4, \tag{3.87}$$

where ε_L is the longwave emissivity of the ice (snow). It is equal to 0.99 when there is a snow cover and 0.97 when there are melt ponds. T_0 is the upper ice/snow surface temperature which has been obtained through the Newton-Raphson iteration [*Kreyszig*, 1999].

4) The turbulent sensible heat flux is formed by:

$$F_{sens} = \rho_{air} C_p C_S w_{10} (T_{air} - T_0), \tag{3.88}$$

where ρ_{air} is the air density (1.37 kg·m^{-3}), C_P is the specific heat of the air (1012 J·kg^{-1}·K^{-1}), C_S is the bulk transfer coefficient for sensible heat ($1.2 \cdot 10^{-3}$) [*Makshtas*, 1991], T_{air} is the air temperature at some reference height, and w_{10} is the wind speed.

5) The latent heat flux is:

$$F_{lat} = \rho_{air} L_{vp} C_e w_{10} (q_a - q_0), \tag{3.89}$$

where L_{vp} is the latent heat of vaporization (2.55×10^6 J·kg^{-1}) [*Makshtas*, 1991], C_e is the bulk transfer coefficient for latent heat (0.55×10^{-3}) [*Makshtas*, 1991]. The specific humidity at the surface (q_0) and the reference level (q_a) are calculated using the Magnus' formula (Eq. (3.90)), which relates the partial pressure (mb) of water vapor ($e_p(T)$) and the specific humidity (q):

$$q = \frac{0.622}{P} e_p(T), \tag{3.90}$$

where P is the surface atmospheric pressure (Pa), and $e_p(T)$ is the partial vapor pressure:

$$e_p(T) = f_r \cdot e(T). \tag{3.91}$$

In Eq. (3.91), f_r is relative humidity, which equals 1 for the surface as air at the ice surface is assumed to be saturated.

The saturation vapor pressure is parameterized by ([Chapter 13, *Matveev*, 1984; *Makshtas*, 1991]):

$$e(T) = e_0 \cdot 10^{\left[\frac{a_1(T_0-273.15)}{b_1+(T_0-273.15)}\right]}, \tag{3.92}$$

where e_0 is 611 Pa, a_1 = 7.63 for water and a_1 = 9.5 for ice, b_1 = 241.9 for water and b_1 = 265.5 for ice [*Matveev*, 1984], T_0 is surface temperature (°K).

6) Heat transfers from the ice bottom to the ice surface and vice versa (depending on the temperature gradient in the ice-snow slab) according to the relation:

$$F_{cond} = \frac{k_{ice} \cdot k_{snow}}{k_{snow} H_{ice} + k_{ice} H_{snow}} (T_b - T_0) = \gamma_i (T_b - T_0), \tag{3.93}$$

where k_{ice}=2.09 W $m^{-1}\cdot°K^{-1}$ and k_{snow} (k_{snow}=0.31 W $m^{-1}\cdot°K^{-1}$) are the thermal conductivity in ice and snow respectively, $H_{ice(snow)}$ is ice (snow) thickness, T_b is ice bottom temperature (it is kept at the freezing point for the given salinity of the top most grid point in water column), T_0 is ice (snow) surface temperature, and γ_i is thermal conductance of the combined ice-snow slab. The conductivity of ice depends on ice salinity and temperature [*Maykut*, 1986]:

$$k_{ice} = k_0 + \frac{\beta \cdot S_{ice}}{T_{ice}}, \tag{3.94}$$

where k_0 (W/m·°K) is the conductivity in pure ice, approximated by the formula [*Maykut*, 1986]:

$$k_0 = 9.828 \cdot e^{-0.0057 T_{ice}}, \tag{3.95}$$

where T_{ice} is in °K. In the model a typical value for k_0 (2.03 W $m^{-1}\cdot°K^{-1}$) [*Maykut and Untersteiner*, 1969] is used.

Having very small heat conductivity, snow on the ice surface damps the ice growth rate. According to *Doronin* [1997], there is an empirical relation between ice and snow thickness:

$$h_{snow} = \begin{cases} 0, & h_{ice} \le 0.05 \\ 0.05 \cdot h_{ice}, & 0.05 < h_{ice} \le 0.2 \\ 0.1 \cdot h_{ice}, & h_{ice} > 0.2. \end{cases} \tag{3.96}$$

In the Arctic, on flat and even ice fields the average maximum snow thickness ranges from 0.25 to 0.4 m by the onset of melting [*Bryazgin*, 1997]. The highest

rate of snow accumulation, 0.06 - 0.07 m/month, is during the beginning of the cold season (September – November), slowing down to 0.03 m/month afterwards. According to *Bryazgin* [1997], in the Arctic marginal seas the average snow thickness on ice fields is 1.5 times lower due to the shorter time period of snow accumulation than in the central Arctic. In early November, snow thickness on young ice is about 0.07 m, 0.16 m in January and 0.23 m in May.

In the model, accumulation of snow on the ice surface is parameterized by a linear time-dependent function of given ice thickness. So, the thicker the ice is, the higher the rate of snow accumulation. The maximum snow thickness in the Arctic Ocean model is limited to 0.4 m, and to 0.3 m in the shelf and Greenland Sea models.

Ice melting may occur at the bottom and the surface of the ice. When T_0 is below the freezing point, which is slightly less than 0° C for sea ice and depends on the ice salinity, then ice ablation starts. If the oceanic heat flux is larger than the conductive heat flux, ice accretion at the ice bottom is observed. When the surface temperature of the ice-snow slab rises higher than the freezing point, melting occurs. For simplicity, the melting rate of snow is the same as for the ice.

Finally, having computed all the components of the heat budget for the ice – snow slab, the heat balance for the upper boundary can be written:

$$F_{tot} + F_{mlt} = 0 . \qquad (3.97)$$

F_{mlt} is the heat loss due to ice/snow melting. When the surface temperature is below ice/snow freezing, this term is zero. If T_0 is at the melting point, any surplus of energy flux will be balanced by this term, giving the ice/snow melting:

$$F_{mlt} = \rho_{ice} L_{ice} \frac{d(H_{ice} + H_{snow})}{dt}, \tag{3.98}$$

where L_{ice}=3.34x10^5 J·kg^{-1} is the latent heat of fusion of fresh ice.

At the ice bottom boundary the ablation/accretion is determined by the F_{cond} and F_w. When $|F_{cond}| > F_w$ and $F_{cond} < 0$ (directed from the ice bottom to the ice surface) ice accretion takes place. Ice thickness change at the ice bottom is parameterized by the relation:

$$-\rho_{ice} L_{ice} \left(\frac{dH_{ice}}{dt} \right)_{bottom} = -F_{cond} + F_w . \tag{3.99}$$

Constants used in the ice model are given in Table 3.12.

Table 3.12. Values of constants used in the ice model

Constant	Value	Units
Penetration of the shortwave radiation in the ice (i_0)	0.3	
Longwave emissivity of the ice (ε_L)	0.97-0.99	
Stefan-Boltzman constant (σ)	5.67×10^{-8}	W m^{-2} $°K^{-4}$
Air specific heat (C_p)	1012	J kg^{-1} $°K^{-1}$
Air density (ρ_{air})	1.37	kg m^{-3}
Bulk transfer coefficient for sensible heat (C_s)	1.5×10^{-3}	
Latent heat of vaporization (L_{vp})	2.55×10^{6}	J·kg^{-1}
Bulk transfer coefficient for latent heat (C_e)	0.55×10^{-3}	
e_0	611	Pa
a_1	9.5	
b_1	265.5	
Thermal conductivity in snow (k_{snow})	0.31	W m^{-1}·$°K^{-1}$
Thermal conductivity in ice (k_{ice})	2.05	W m^{-1}·$°K^{-1}$
Thermal conductivity in pure ice (k_0)	2.03	W m^{-1}·$°K^{-1}$

Section 3.6. Summary

- This chapter described the Arctic Ocean – Greenland Sea model which was used in the study.

- The model has two modules: the Arctic module and the Greenland Sea module.

- The Arctic Ocean module includes the shelf box model coupled with a thermodynamic sea ice model and the Arctic Ocean model coupled with the sea ice model and atmospheric box model.

- The Greenland Sea module consists of the Greenland Sea model, sea ice model, and state-space atmospheric model.

- New parameterization of m_0 and κ was suggested, relative to that of *Stigebrandt* [1985] and *Bjork* [1989].

Chapter 4 MODEL STUDY OF THE ARCTIC OCEAN – GREENLAND SEA CLIMATE SYSTEM

Model experiments were performed to study the Arctic Ocean – Greenland Sea climate system with two major goals in mind. One was to obtain valid estimates for the model's free parameters and the second was to estimate their role in the Arctic Ocean – Greenland Sea climate system. The first group of experiments has been conducted as a sensitivity study. The second set of experiments has been designed to reproduce the auto-oscillatory behavior of the studied climate system discussed in Chapter 2.

In the first section, the first set of experiments and results are described. The second section presents the details of the auto-oscillatory model experiment, its output, and discussion of results of the study.

Section 4.1. Experiment 1: Sensitivity study of the Arctic Ocean – Greenland Sea model

The purpose of this experiment is to determine the appropriate values for the following free parameters: the coefficient of heat advection, χ, the outflow from the ML to the shelf, Q_{mao}, and the proportionality factors, m_0 and κ.

4.1.1. Coefficient of heat advection, χ

Design of the experiment

The model was run for 5 different values of the coefficient of heat advection: $\chi = \{0.5,\ 1.,\ 2.,\ 3.,\ 4.\}$. All other parameters were constant. Each run was for 5 years, which was enough to reach a steady solution for the atmosphere. After 5 years, the initial conditions were reset in the model.

Results

In the present model, the Arctic responds to different rates of heat advection from the Greenland Sea through an increase or decrease of the mean SAT. The changes in SAT drive further changes in the system such as the ice production rate and thermohaline structure of the upper ocean. Panel A in Fig. 4.1 shows simulated (blue lines) and observed (green asterisks and red solid line) SAT in the central Arctic during a single year. Five blue curves represent the last year for each model run for different values of the coefficient of heat advection:

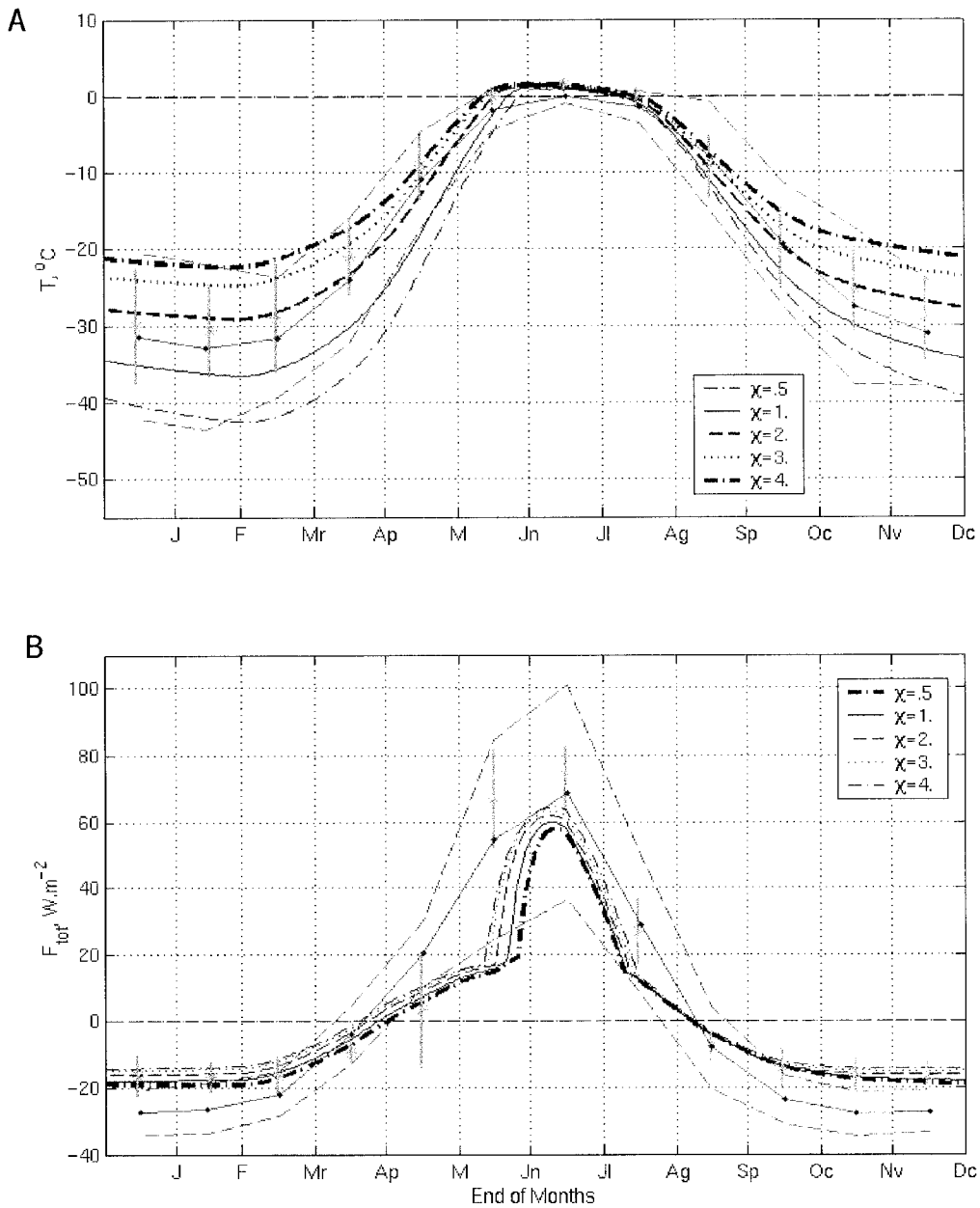

Fig. 4.1. Sensitivity study: Effect of χ on SAT and surface heat flux in the Arctic. *Blue curves are the model output for different χ, green vertical bars show 98% confidence interval for the monthly means denoted by green asterisks (NOAA-CIRES CDC data [CDC]), red dotted line and dashed red lines are mean SAT and 98% CI from Lindsay [1998]. (A) SAT: for χ = 1 to 3 $W \cdot m^{-2} \cdot {}^{\circ}K^{-1}$, the model simulates SAT close to observations. (B) Surface heat flux: the model does not match well with the CDC data, however it corresponds better with Lindsay [1998].*

$\chi = \{0.5,\ 1.,\ 2.,\ 3.,\ 4.\}$. The green asterisks mark the monthly mean SAT. The green vertical bars denote the 98% confidence intervals (CI) for the monthly means. The monthly means and their standard deviations have been estimated from the SAT daily data for the central Arctic (86°N poleward) for the period 1948 to 2001 from NOAA-CIRES CDC [*CDC*] (CDC data). The red dotted line is the mean SAT and the red dashed lines show the 98% CI from *Lindsay* [1998].

Fig. 4.1A shows clearly that the lower values of χ lead to a colder Arctic as expected. The variability of SAT is larger in the cold season, however, the summer amplitude of SAT is small because the Arctic gains substantial solar radiation and heat advection is not a primary source of energy. The case χ = 0.5 $W \cdot m^{-2} \cdot °K^{-1}$ results in an unrealistically cold Arctic. The opposite case χ = 4.0 $W \cdot m^{-2} \cdot °K^{-1}$ leads to a very warm Arctic. When χ = 2. $W \cdot m^{-2} \cdot °K^{-1}$ the model reproduces SAT close to the CDC data. The model tends to reproduce lower SAT in April and May than the CDC values.

In panel B of Fig. 4.1 the surface heat flux during a year is presented. The model output corresponds well with *Lindsay* [1998] data but does not match well the CDC data. In early June, the model underestimates heat flux from the atmosphere. This might be due to too simple a parameterization of cloudiness or albedo. Another possibility is slightly underestimated SAT in May as explained below.

The effect of χ on the surface heat flux is not noticeable in winter and has no effect in August and September. In general, lower χ causes slightly more intense heat flux from the ice-ocean system to the atmosphere in winter and dampened heat flux from the atmosphere to the ice-ocean system in the warm season. In winter when χ is low, the higher heat flux to the atmosphere is explained by

decreased SAT which leads to higher rates of the longwave and latent fluxes from the ice surface to the atmosphere. In spring, solar radiation starts warming the ice surface and its temperature becomes slightly warmer than SAT. The sensible heat becomes directed to the atmosphere, reducing the positive surface heat flux to the ice surface. The lower the SAT, the larger the sensible heat flux to the atmosphere, and the lower the surface heat flux to the ice surface. Lower heat flux reduces ice warming and delays the onset of ice melt. Rapid increase of the surface heat flux in early June (Fig. 4.1B) is related to the moment when the sensible heat flux changes sign and significantly more flux goes to the ice surface. The sign switches when the SAT finally exceeds the ice surface temperature, which is, in general, a few days later than the onset of ice melt. The rapid increase of F_{tot} continues unitl the middle of July when the incoming shortwave radiation starts rapidly decreasing. The rate of increase of F_{tot} ($\partial F_{tot}/\partial T$) does not depend on χ (Fig. 4.1B). Instead, the onset of the increase is shifted towards the end of June for the lower χ. Thus, for the lower χ, F_{tot} has shorter period of rapid increase and its maximum is less than for higher χ.

4.1.2. Mixed layer outflow to the shelf, Q_{mao}

Design of the experiment

To estimate the effect of the exchange between the interior Arctic Ocean and the shelf, the model was run under different rates of the Arctic Ocean outflow to the shelf: $Q_{mao} = \{0.1,\ 0.5,\ 1.,\ 2.\}$ (Sv). All other parameters were kept constant. The coefficient of heat advection (χ) was set to 2.0 $W \cdot m^{-2} \cdot s^{-1}$ which yields Arctic SAT close to the observed, long-term mean values. The model ran for seven

years for each Q_{mao} value. After that, the initial conditions were reset in the model. Although seven years were not enough for the model to reach steady state, the Arctic Ocean tendencies could be seen well enough to choose Q_{mao}. The goal of this experiment was to obtain a value of Q_{mao} that provided realistic seasonal behavior of the upper Arctic Ocean.

Results

In the model, $Q_{sh} = Q_{mao}$. Hence, with higher Q_{mao}, more freshwater is imported to the interior Arctic Ocean from the shelf. The ML salinity determines water column stability and, through it, the entrainment velocity and ML depth. Thus, to choose an appropriate value of Q_{mao}, h_{ml} and S_{ml} from the Arctic Ocean model have to be examined.

Fig. 4.2 presents simulated mixed layer depth h_{ml} and salinity S_{ml}. Panel A shows the evolution of the h_{ml} during the last year for different Q_{mao}. As mentioned in Chapter 1, h_{ml} in the central Arctic Ocean is generally less than 60 m. Simulated h_{ml} reached almost 80 m by April for $Q_{mao} = 0.1$ Sv, and 70 m for $Q_{mao} = 0.5$ Sv. The other two cases $Q_{mao} = 1.0$ and 2.0 Sv give realistic behavior of the h_{ml}. Thus, low exchange between the interior Arctic Ocean and the shelf leads to unrealistically deep ML stemming from too high S_{ml} (Fig. 4.2 B).

Mean mixed layer salinity in the central Arctic Ocean varies annually from 30.0 to 31.5 during a year (Table 1.4). For the cases $Q_{mao} = 0.1$ Sv, and $Q_{mao} = 0.5$ Sv, S_{ml} approaches 33 psu at the end of the winter. Too intense water exchange between the interior Arctic Ocean and the shelf ($Q_{mao} = 2.0$ Sv) causes strong

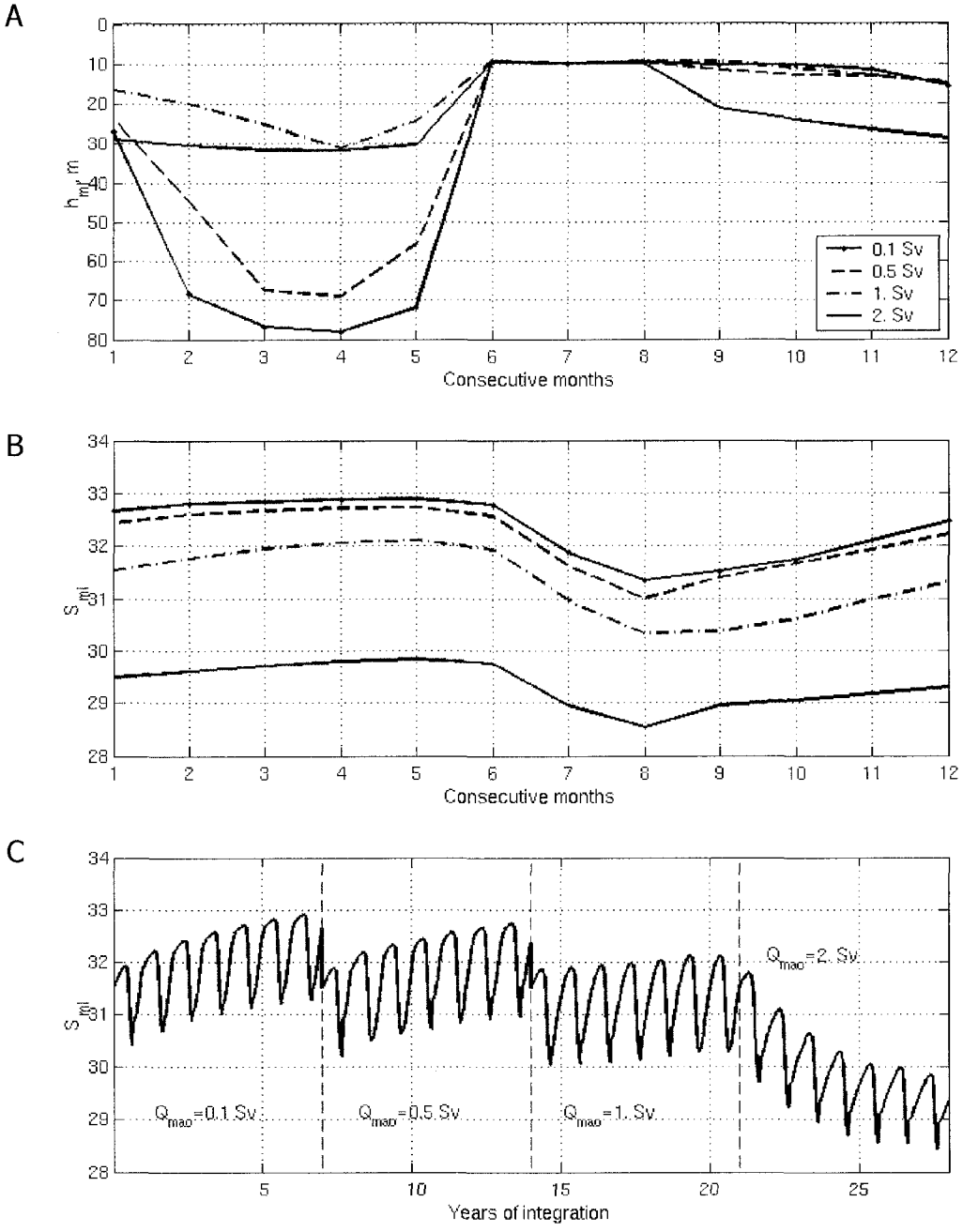

Fig. 4.2. Sensitivity study: Effect of Q_{mao} on the Arctic mixed layer. *(A) Simulated h_{ml}. Abscissa is months (January through December). The final years of the scenarios Q_{mao} = .1, .5, 1.0, and 2.0 Sv are plotted. Low exchange with the shelf leads to unrealistically deep mixed layer. (B) Similar to (A) but for S_{ml}. Extreme Q_{mao} yields too low or too high S_{ml}. (C) Time series for S_{ml} for the whole period of the model run. Vertical red dashed lines denote time intervals of the scenarios: 5, 10, and 15 years. For Q_{mao} = 1 Sv, the system is almost at a steady state.*

freshening of the upper layer. Examining daily output for S_{ml} for the full model run (28 years) (Fig. 4.2C) it is evident that for the case $Q_{mao} = 1.0$ Sv, S_{ml} changes within 30.2 to 32.1 which is in agreement with the observational estimates of the S_{ml} (Table 1.4). Hence from the model experiment, the case $Q_{mao} = 1.0$ Sv reproduces the average h_{ml} and S_{ml} for the interior Arctic Ocean.

4.1.3. Proportionality coefficient m_0 for the Arctic Ocean

Mixed layer deepening is governed by Eq. (3.12). The proportionality coefficients m_0 and κ control the entrainment velocity for a given water column density and surface buoyancy flux, B_{fl}. *Björk's* [1989] model with $m_0 = 0.7$ and $\kappa = 0.05$ (for negative B_{fl}), simulated a mixed layer salininty, S_{ml}, less than 29 in summer and ~30.5 at the end of the winter (Fig. 8 in *Björk* [1989]). From the observations (Tables 1.4 and 4.1), the characteristic summer S_{ml} ranges from 29.2 to 30.2 and h_{ml} is about 5 to 10 m. In winter, S_{ml} is from 31.08 to ~32.95. *Björk's* model has apparently underestimated S_{ml}. The mixed layer depth, however, was reasonable: about 10 m in summer and 30 m in winter. As soon as *Björk's* winter S_{ml} became less than the average summer salinity in the interior Arctic Ocean when the mixed layer was very shallow (~10 m), the proportionality coefficients might have made the entrainment velocity too high for such a fresh mixed layer. Also, during model experiments, constant m_0 yields entrainment hardly sensitive to changes of the water column stability. Instead, m_0 has been parameterized using Eqs. (3.22) and (3.23). By doing so, m_0 is no longer constant but at every time step is adjusted to the ambient conditions (stratification, friction velocity, buoyancy flux, and mixed layer depth). The following model experiment was

conceived to check if *Björk's* parameters are reliable and to choose a valid P in Eg. (3.22).

Table 4.1. Mean salinity and depth of the Arctic Ocean mixed layer[a]

Season and location	S, psu	Depth, m
Summer		
CB[b]	30.14 - 30.17	5
EB[b]	29.2 – 29.55	5
CB[c]	30.05 - 30.11	15
Beaufort Sea[c]	29.2 – 29.3	10
EB[c]	29.72 – 29.85	10
Beaufort Sea[c]	27.93	5
EB[d]	33.43 - 33.44	15
Winter		
CB[b]	30.96 – 30.99	25
CB[b]	31.43 – 31.68	40
Beaufort Sea[c]	31.2 – 31.6	25
CB[c]	30.89 – 30.97	25
EB[c]	32.68 – 32.95	25
CB[d]	~31.08	30

(a) [*EWG*, 1998].
(b) 1960s.
(c) 1970s.
(d) 1980s.

Design of the experiment

The model was run for 40 years. Every 10th year, m_0 was changed according to Table 4.2. For each m_0, the Arctic Ocean behavior was tested under "cold" ($\chi = 1.0\ \mathrm{W \cdot m^{-2} \cdot {}^{\circ}K^{-1}}$) and "warm" ($\chi = 3.0\ \mathrm{W \cdot m^{-2} \cdot {}^{\circ}K^{-1}}$) conditions meaning low and high values for the heat advection coefficient χ (Eq. (3.55)) listed in Table 4.2. Under the "warm" conditions, the mixed layer salinity S_{ml} decreases, the water column stability increases, and the convective penetration of the mixed layer is damped, leading to mixed layer shallowing. The situation is opposite under the "cold" Arctic conditions. Hence, different Arctic conditions allow one to compare the mixed layer dynamics simulated in the model under high and low water column stability. Every time either m_0 or χ was changed the initial conditions were reset in the model.

Table 4.2. Sensitivity study: Values of m_0 and χ in the Arctic Ocean

Years of integration	m_0	χ, $\mathrm{W \cdot m^{-2} \cdot {}^{\circ}K^{-1}}$
1-5	0.7[(a)]	1.0
6-10		3.0
11-15	$\log\left[\left(\frac{100}{Ri_o}\right)^{1.}\right]+3.5$	1.0
16-20		3.0
21-25	$\log\left[\left(\frac{100}{Ri_o}\right)^{1.5}\right]+3.5$	1.0
26-30		3.0
31-35	$\log\left[\left(\frac{100}{Ri_o}\right)^{2.}\right]+3.5$	1.0
36-40		3.0

(a) [*Bjork*, 1989].

Results

The model output is shown in Fig. 4.3. The abscissa on all the subplots is years of integration. Vertical dash-dotted lines separate model output for different m_0. The upper two panels show daily values of S_{ml} and h_{ml}. Blue segments of the curves in the upper two panels denote the "cold Arctic" ($\chi = 1.0\,\mathrm{W{\cdot}m^{-2}{\cdot}{^\circ}K^{-1}}$) and red segments correspond to the "warm Arctic" ($\chi = 2.0\,\mathrm{W{\cdot}m^{-2}{\cdot}{^\circ}K^{-1}}$). The lower panel shows annual mean S_{ml} and h_{ml}.

From Fig. 4.3 it follows that the case of constant m_0 = 0.7 (first 10 years of integration) tends to deepen the ML. Output from the longer model runs (not presented) revealed that under this condition, the steady state is reached after 15 years with winter h_{ml} about 80 m and S_{ml} slightly higher than 32.2. This is an obvious failure of this parameterization of m_0.

Another weakness of keeping m_0 constant is the low sensitivity of h_{ml} to drastic changes of water column stability caused by S_{ml} variability during "cold" and "warm" states (Fig. 4.3B). In Fig. 4.3C, means of h_{ml} and S_{ml} for all Aprils over the 40-year run, when the ML reaches its maximum depths, are shown. From this figure it follows that even when the ML becomes fresh (31 in April), the model keeps simulating relatively deep ML (~38 m). However, from Table 4.1 average winter ML depth is about 25 – 30 m for such salinity. Thus, the necessity for better parameterization of the entrainment velocity to reproduce more realistic ML dynamics is obvious.

More realistic behavior of the ML is achieved for m_0 parameterized by Eqs. (3.22) and (3.23). The reason is that Eq. (3.22) sets m_0 sensitivity to changes in the water column stability. As discussed earlier in Chapter 3, m_0 parameterizes the

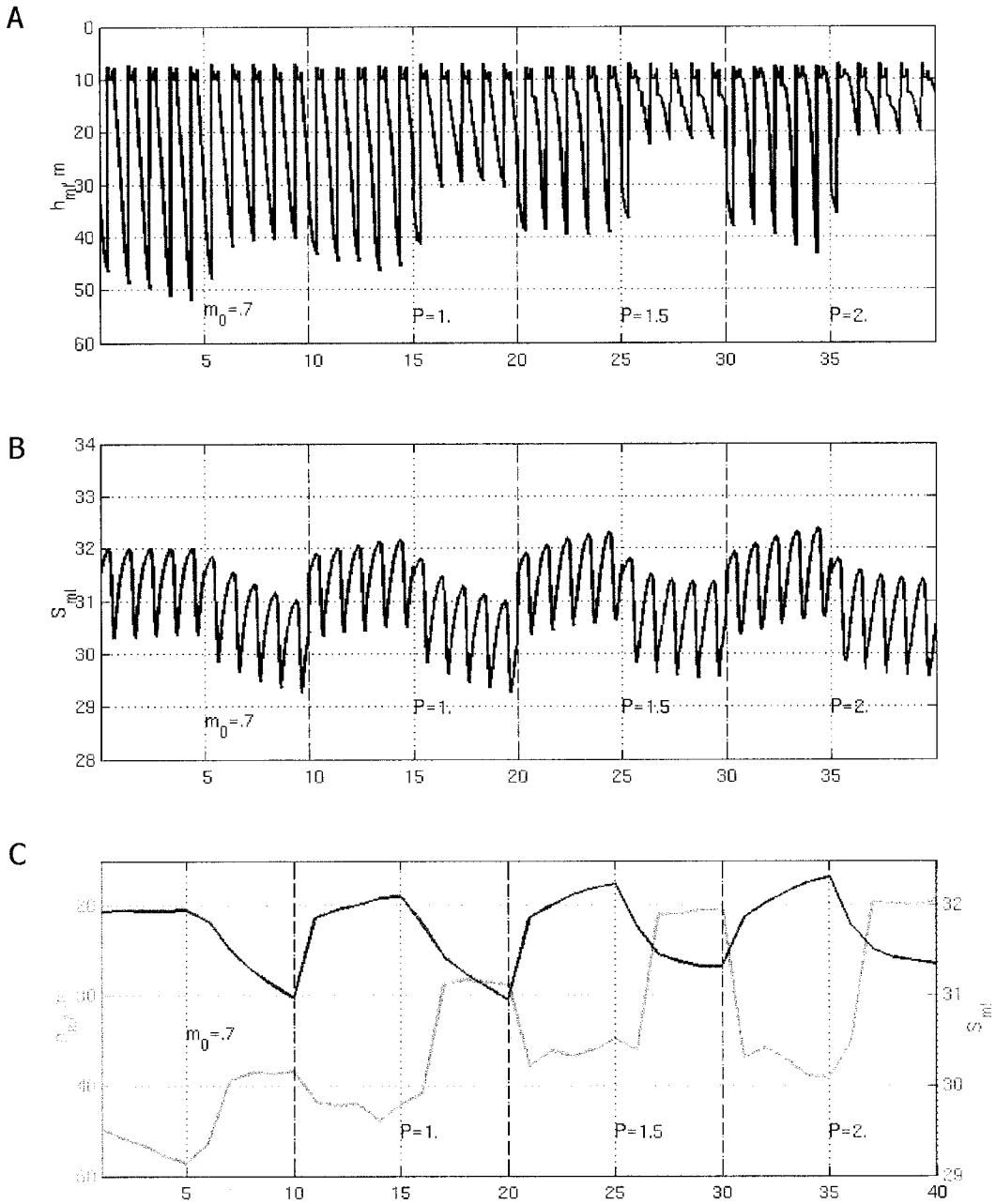

Fig. 4.3. Sensitivity study: Effect of m_0 on the Arctic Ocean mixed layer. *Time series for h_{ml} (A) and S_{ml} (B). Blue segments correspond to χ = 1.0, red to χ = 3.0 $W \cdot m^{-2} \cdot {}^{o}K^{-1}$. Abscissa is years of integration. On panel (C) h_{ml} and S_{ml} for all Aprils over the 40-year run are plotted. Vertical black dashed lines separate different ten year scenarios for m_0. Note that m_0 depends on P (Eq. (3.22)). Different P values are marked on the plots.*

dissipation of the turbulent energy in Eq. (3.12). In the suggested approach, when stability increases (meaning S_{ml} decreases), m_0 vanishes fast as ML deepens, meaning that the turbulent energy dissipates rapidly to overcome the increased water column stability. For $P = 1.5$ and $P = 2.0$, the model simulates deep ML for high S_{ml} and shallow ML for freshened upper layer, which matches expectations.

4.1.4. Proportionality coefficient κ for the Arctic Ocean

Design of the experiment

Another free parameter that determines the upper layer dynamics is κ (Eq. (3.12)). As discussed earlier, this coefficient parameterizes dissipation of the convectively produced turbulence. The model has been tested for two values of the coefficient: $\kappa = \{0.05, 0.99\}$. The first value is acquired from *Björk* [1989] and *Stigebrandt* [1981]. Scenario $\kappa = 0.99$ mimics a case of neglecting the dissipation of convection.

Table 4.3. Sensitivity study: Values of κ and χ in the Arctic Ocean

Years of integration	κ	χ, $W \cdot m^{-2} \cdot {}^{o}K^{-1}$
1-5	0.05	1.0
6-10		3.0
11-15	0.99	1.0
16-20		3.0

To test the effect of κ on the mixed layer deepening under different values of water column stability, each value of κ was tested under both "warm" ($\chi = 3.0\,\mathrm{W{\cdot}m^{-2}{\cdot}^{o}K^{-1}}$) and "cold" ($\chi = 1.0\,\mathrm{W{\cdot}m^{-2}{\cdot}^{o}K^{-1}}$) Arctic conditions (Table 4.3) and run for 5 years. After every 5 years, the model was returned to the initial conditions. Again, the "warm" and "cold" Arctic conditions lead to less and more water column stability, respectively.

Results

The mixed layer depth, h_{ml}, changes significantly for different κ (Fig. 4.4A). For $\kappa = 0.99$, h_{ml} is unrealistically deep in winter for the "cold" Arctic. After 5 years of integration, h_{ml} is ~88 m and the model has not yet reached the steady state. Due to larger entrainment velocity w_e (Fig. 4.4C), S_{ml} rapidly increases (Eq. (3.14)) which favors further deepening of the mixed layer. For the "warm" Arctic, $\kappa = 0.99$ leads to overestimation of the w_e (Fig. 4.4 C) and too deep h_{ml} (4.4 A) for such low S_{ml}. Hence, $\kappa = 0.05$ gives realistic behavior of the Arctic Ocean mixed layer.

4.1.5. Proportionality coefficient κ for the Greenland Sea

The goal of the sensitivity study for the Greenland Sea model was to obtain a good resemblance between the simulated and general features of the observed mixed layer dynamics. As stated in Chapter 1, deepening of the mixed layer in the central Greenland Sea has two stages. During the first stage, the upper layer

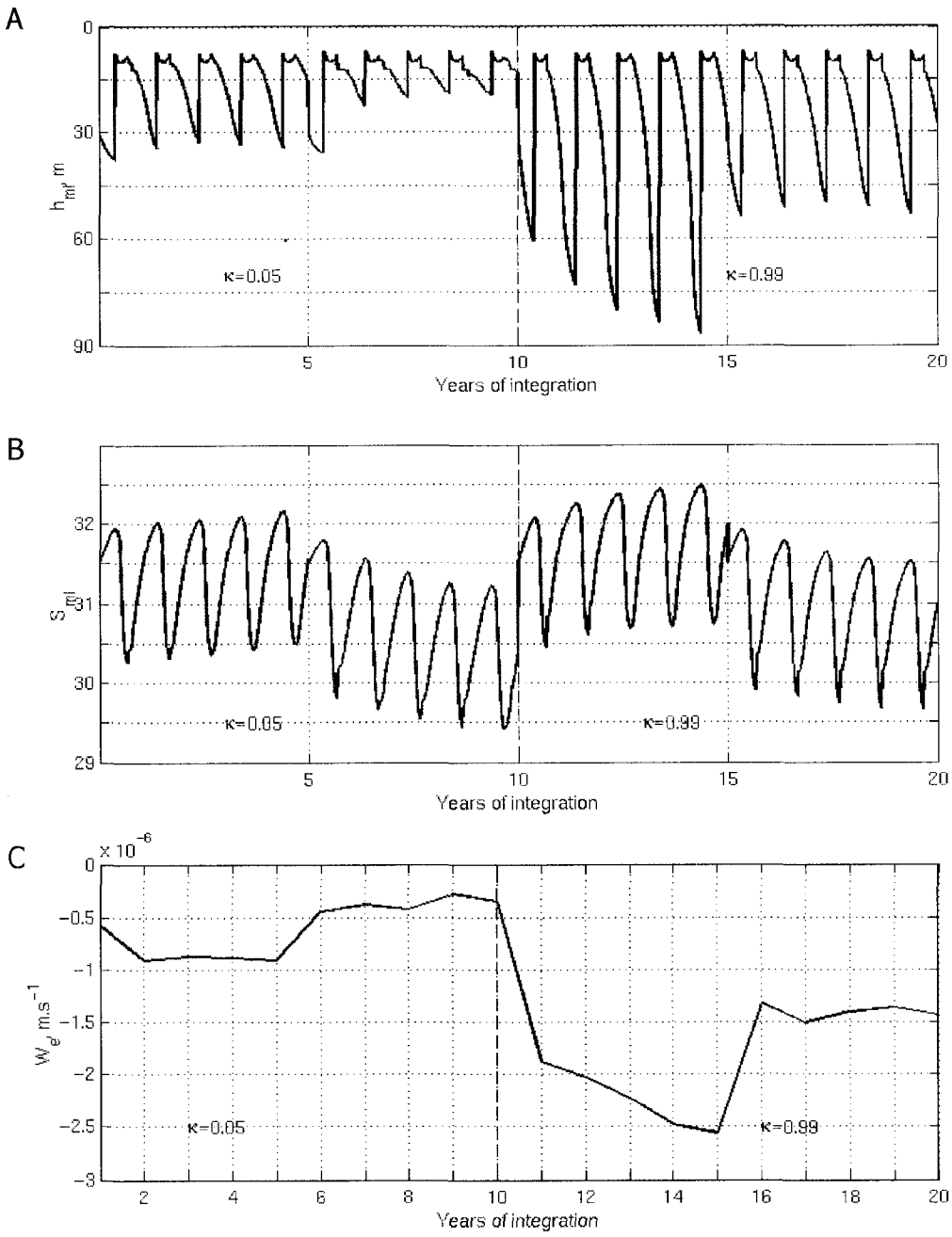

Fig. 4.4. Sensitivity study: Effect of κ on the Arctic Ocean mixed layer. *Time series of h_{ml} (A) and S_{ml} (B). Blue and red segments correspond to χ = 1.0 and 3.0 $W{\cdot}m^{-2}{\cdot}{}^{o}K^{-1}$ respectively. Black vertical dashed lines separate different ten year scenarios for κ = 0.05 and 0.99. (C) Annual means for the entrainment.*

density increases due to water cooling and salt advection until a pre-convective state is reached. During this stage, the mixed layer deepens slowly and stays relatively shallow as turbulent mixing can not penetrate too deep and convective mixing is not yet taking place. If the initial (after summer) mixed layer salinity S_{ml} is high, the mixed layer reaches quickly the pre-convective state and deep convection begins. If summer mixed layer freshening is intense and S_{ml} is low, the first stage will be protracted. In this case, intense cooling of a shallow mixed layer, without significant heat supply entrained from the lower warm layers, may lead to ice formation. Such behavior is expected to be reproduced by the model.

Design of the experiment

Three experiments have been conducted within this study. In the first experiment, *Björk's* [1989] values have been applied (Table 4.4). Two other experiments involve different parameterization of κ and w_e as a function of the water column stability. As outlined in Chapter 3, κ is determined by means of bulk Richardson number (Ri_o) and transition Richardson number (Ri_T), both discussed in *Chapman* [1997; 1998]. When the water column is stable and the buoyancy flux is not large enough to provide a significant gain of density for the mixed layer, i.e. $Ri_0 > Ri_T$, convection is suppressed [*Chapman*, 1997]. In this case, κ has been parameterized as:

$$\kappa = 0.01 \cdot \log\left(3000/h_{ml}\right), \quad if \quad Ri_o > Ri_T \,. \tag{4.1}$$

Table 4.4. Sensitivity study: Values of κ and χ in the Greenland Sea

Years of integration	κ, w_e	μ_{PW}	Line # in Fig. 4.5
1-5	κ = 0.05	0.7	"1"
6-10		2.0	"2"
11-15	κ = 0.99	0.7	"3"
16-20		2.0	"4"
21-25	$w_e = -\frac{h_z}{t_{stp}}$	0.7	"5"
26-30		2.0	"6"

If the water is almost neutrally stable and the buoyancy flux is large, $Ri_0 \le Ri_T$, then deep convection develops. The dynamics of the mixed layer have been parameterized in two different ways depending on when this condition is fulfilled. One way is to assume that the efficiency of the convective mixing is high, meaning that the dissipation is small, i.e. κ approaches 1:

$$\kappa = 0.99, \quad if \quad Ri_o \le Ri_T . \tag{4.2}$$

Alternatively, in another experiment, following *Chapman* [1997], it is assumed that the mixed layer deepens instantly by the next time step:

$$w_e = -\frac{h_z}{t_{stp}}, \tag{4.3}$$

where h_z is the depth interval step and t_{stp} is time step.

To test the effect of different parameterization of the convective entrainment, all the experiments were conducted for increased and suppressed Polar Water (PW) inflow to the Greenland Sea: $Q_{PW} = \mu_{PW} \cdot Q_{PW}$ (Table 4.4). Increased PW inflow leads to negative S_{ml} anomalies. Suppressed PW inflow reduces water column stability in the Greenland Sea. Each set of conditions has been kept for 5 years, and after that the initial conditions are reset in the model.

Results

Fig. 4.5A demonstrates significantly different mixed layer dynamics for different parameterization of the entrainment. Constant κ (lines "1" and "2") drives mixed layer deepening at a constant rate. A sharp deepening of the mixed layer that can be seen on the dashed blue line at the end of February is associated with the onset of ice freezing in the region which leads to higher negative buoyancy flux at the surface and, through it, to higher entrainment (Eq. 3.12). Such parameterization fails to describe the development of the "pre-convective" mixed layer: fast deepening starts as soon as the buoyancy flux changes sign at the end of August. Making κ a function of water column stability (lines "3" to "6") allows one to reproduce the first stage of the mixed layer deepening in the Greenland Sea. The entrainment rate is low in September. Then, as density of the mixed layer increases due to water cooling, the entrainment rapidly increases. Note that when κ = 0.99 (lines "3" and "4"), the mixed layer stays shallow longer (through middle October).

Different entrainment rates lead to different seasonal salinity changes in the mixed layer (Fig. 4.5C). As one can see from Eq. (3.69), salinity flux to the mixed layer from below, driven by entrainment, is proportional to the salinity gradient

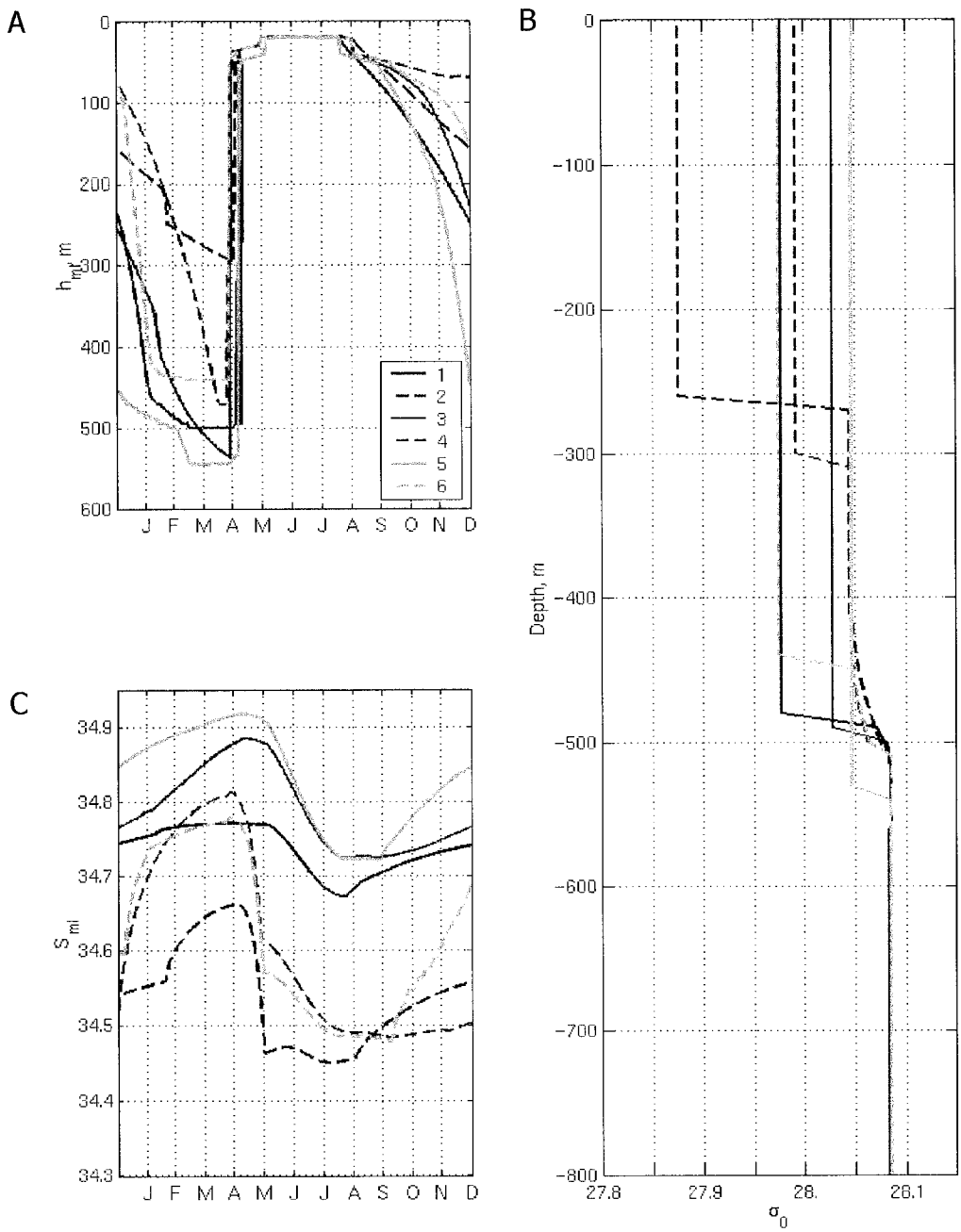

Fig. 4.5. Sensitivity study: Effect of κ on the Greenland Sea upper layer. *Output for h_{ml} (A) and S_{ml} (C) from the last years of different scenarios. Solid lines correspond to χ = 1.0 $W{\cdot}m^{-2}{\cdot}{}^{o}K^{-1}$, dashed line correspond to χ = 3.0 $W{\cdot}m^{-2}{\cdot}{}^{o}K^{-1}$. See Table 4.4 for line specifications. Abscissa is time, end of the months. (B) Density profiles for the upper 800 m for March for the last years of different scenarios.*

between the upper and lower layer and entrainment rate. For the low PW inflow (lines "1","3", and "5" in Fig. 4.5C) when no ice is formed in the Greenland Sea, salinity increase is proportional to the entrainment rate, or increase of the h_{ml} (Eq. (3.69)).

When PW inflow is increased, S_{ml} decreases and mixed layer deepening weakens. This may lead to ice forming in the Greenland Sea. For this case (dashed lines in Fig. 4.5C), an additional source of salt appears in the system: brine formation from ice production. During fall, salinity changes in the mixed layer are driven by the entrainment. In January – February, a rapid S_{ml} increase is caused by the onset of ice freezing in addition to entrainment.

Although the mixed layer thicknesses for different parameterizations of the entrainment do not differ much (compare three solid lines in Fig. 4.5B), the density distribution in the upper water column does differ. Fig. 4.5B shows significantly different water column density profiles in March for similar forcing parameters (one should compare separately solid and dashed lines for cases of suppressed and increased PW inflow).

The question is which of the profiles are more realistic? Or, for a given wind stress and buoyancy flux, can the mixed layer reach such depths? As mentioned above, forced convection (driven by wind) does not penetrate too deep, hence, by the end of winter and early spring the mixed layer deepening in the Greenland Sea is mostly driven by free convection. Let us use *Chapman's* [1997; 1998] scales to determine if the convection is possible for given conditions. Again, the Richardson transition number Ri_T is calculated (Eq. 3.6). If $Ri_T < 8$, convection penetrates into the lower layer. Calculated Ri_T for 6 density profiles are presented in Table 4.5.

Table 4.5. Sensitivity situdy: Ri_T for density profiles in Fig. 4.5

	$\rho_{1,}$ [(a)] kg·m^{-3}	$\rho_{2,}$ [(b)] kg·m^{-3}	g'x10^{-4}, m·s^{-2}	$h_{ml,}$ m	$\lvert B_f \rvert$, x10^{-8}, m^2·s^{-3}	Ri_T[(c)]
Line "1"	1027.98	1028.08	9.5	483.8	1.92	18.7
Line "2"	1027.88	1028.04	15.9	265.1	2.94	31.2
Line "3"	1028.03	1028.08	5.4	499.	2.13	21.
Line "4"	1027.99	1028.05	5.0	307.8	1.8	4.0
Line "5"	1028.05	1028.08	3.6	542.8	2.35	2.9
Line "6"	1027.98	1028.05	7.1	440.4	1.75	13.1

(a) $\rho_1 = \rho_{ml}$.

(b) $\rho_2 = \rho(h_{ml+})$.

(c) Radius of the Greenland Gyre is estimated to be $\left(0.135 \cdot 10^{12}/\pi\right)^{0.5} \approx 2.07x10^5 m$, u*≅0.017 m·s^{-1}.

From Table 4.5 it follows that deepening of the mixed layer was possible only for lines "4" and "5". All other lines should be at about the same depth for the rest of the cold season. As one can see from Fig. 4.5A, there is no deepening for lines "3" and "6" in March and April. However, lines "1" and "2" continue to deepen until the beginning of warm season and shallowing of the mixed layer. Such behavior contradicts physics and is caused by inadequate parameterization of the entrainment for the Greenland Sea. The other two ways of parameterization w_e (Eqs. (4.2) and (4.3)) seem to be appropriate.

Section 4.2. Experiment 2: Auto-oscillatory behavior of the climate system

4.2.1. Design of numerical experiment

The Arctic Ocean – Greenland Sea model has been designed to reproduce the cyclic ACCR/CCR regime shift in the Arctic Ocean as an auto-oscillatory behavior of the studied region. The energy sources necessary for auto-oscillations are the potential energy in the Arctic Ocean and internal energy of the Greenland Sea region. The anticyclonic regime in the Arctic is characterized by increasing the potential energy by accumulation of freshened surface water in the center of the basin-wide anticyclonic circulation and downward vertical velocities in the upper ocean [*Proshutinsky and Johnson*, 1997; *Proshutinsky et al.*, 2002]. Thus, deepening of the mixed layer is expected during ACCR. The accumulation of the freshened surface water in the Arctic Ocean leads to the reduction of its export to the North Atlantic. The one-dimensional Arctic Ocean model is not intended to reproduce the basin-wide circulation. Instead, the Arctic Ocean outflow to the North Atlantic (Q_{g_atl}) is changed for different regimes.

Heat advection to the Arctic is another tool to regulate an auto-oscillatory behavior in the system. A higher rate of heat advection raises the surface air temperature (SAT) in the Arctic, which can trigger all the changes in the region related to CCR, as discussed earlier.

The auto-oscillatory behavior of the system is achieved through a series of feedbacks. Fig. 4.6 shows the feedback mechanisms between different components in the model. The interaction between the Greenland Sea and the Arctic is realized through the Polar Water flow, Q_{PW}, and heat advection to the

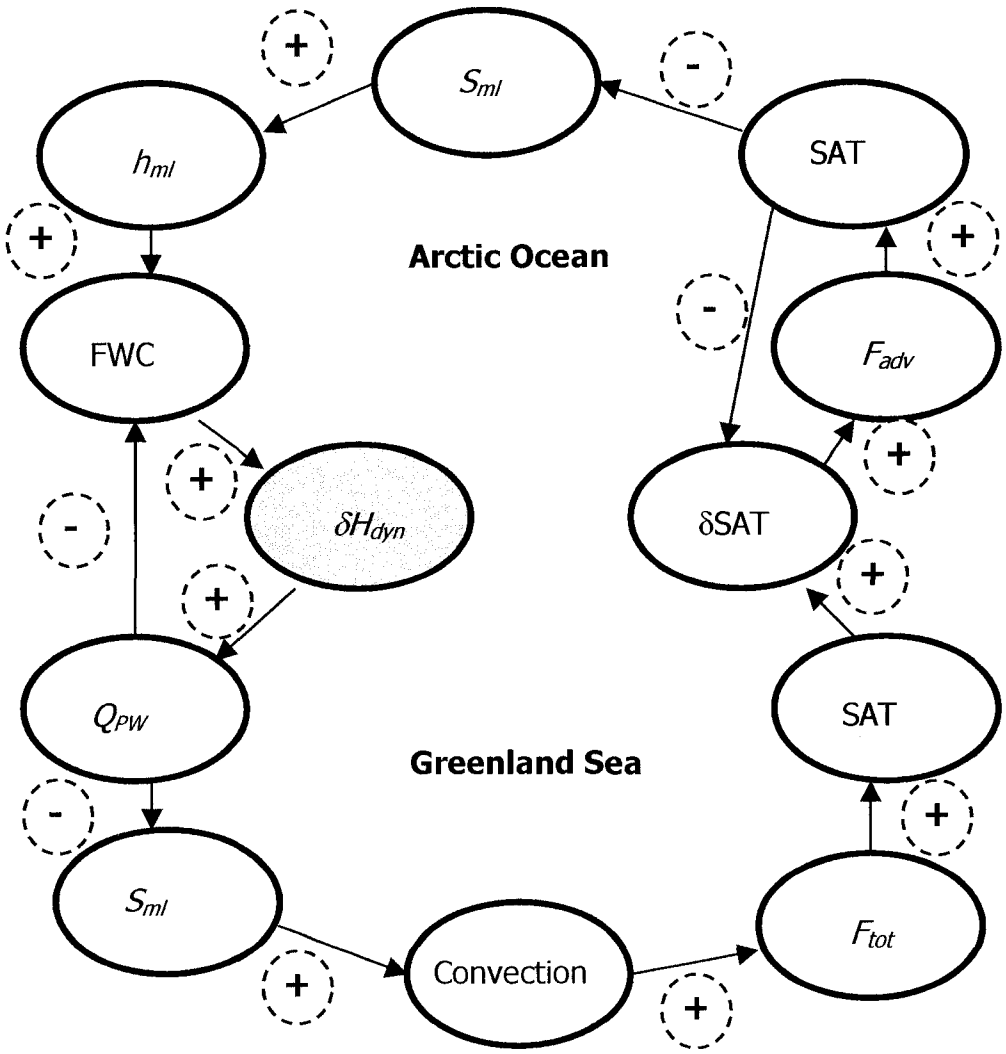

Fig. 4.6. Feedback loop in the simulated climate system. *The oscillatory behavior in the model is reproduced through a feedback loop. Arctic Ocean: positive SAT anomalies -> δSAT decrease -> F_{adv} decrease -> negative SAT anomalies -> positive S_{ml} anomalies -> deepening of h_{ml} -> FWC increase -> δH_{dyn} increase -> Q_{PW} increase -> FWC decrease; Greenland Sea: Q_{PW} increase -> S_{ml} decrease -> ceased convection -> reduced F_{tot} -> negative SAT anomalies -> δSAT decrease. The interaction between the basins is realized through Q_{PW} and F_{adv} (yellow ovals). The regime shift is controlled by δH_{dyn} (green oval).*

Arctic, F_{adv}. To proceed let us assume that the ACCR state of the system (cold Arctic / warm Greenland Sea) is reproduced. Under those conditions, F_{adv} is below the long-term mean, i.e. heat advection to the Arctic is suppressed. This causes negative SAT anomalies in the Arctic. Low temperatures increase ice production in winter and thus, the mixed layer salinity (S_{ml}). High S_{ml}, making the water column less stable, favors the higher rate of entrainment and deeper mixed layer (h_{ml}). A deeper mixed layer means deeper penetration of the low-salinity water and increased FWS. Thus, the upper part of the Arctic Ocean becomes less dense which leads to increased dynamic height gradient (δH_{dyn}). There is another mechanism which favors the increase of δH_{dyn} during simulated ACCR in the Arctic – Q_{PW}. Because Q_{PW} is decreased, the vertical advection in the Arctic water column is decreased as well, and the vertical temperature and salinity propagation from the salty and warm Atlantic layer is ceased. Thus, the upper halocline density decreases and δH_{dyn} increases during the ACCR reproduced in the model.

In the Greenland Sea during the ACCR, low Q_{PW} causes positive S_{ml} anomalies which favors deep convection. Deep convection initiates intense surface heat flux to the winter atmosphere (F_{tot}) and warming of the atmosphere. Positive SAT anomalies increase the SAT gradient (δSAT). Another factor that increases δSAT is cooling of the Arctic atmosphere. High δSAT tends to initiate the interaction between the regions.

The central question in the experiment is: when do the Arctic and Greenland Sea regions start to interact? It is assumed that differences in the two region's characteristics are the basis for developing oscillatory behavior through some pivoting mechanism.

Pivoting mechanism

To make the climate regimes in the Arctic Ocean and Greenland Sea oscillate, a pivoting mechanism that switches one regime to another needs to be identified and parameterized. In this study, the principle difference between the two climate states in the Arctic is the intensity of interaction between the Arctic and the Greenland Sea region. During CCR, when the interaction is high, the gradients in meteorologic and oceanographic characteristics between the two regions are decreasing. The opposite situation occurs during the ACCR: without heat advection from the Greenland Sea, the Arctic Ocean becomes fresher and colder, while the Greenland Sea warms and becomes more saline. Hence, the gradients between the two regions of SAT (δSAT) and dynamic height (δH_{dyn}) (see Fig. 4.6) can be used as indicators of "readiness" of the system to start or to stop the interaction. When the gradients reach some high critical value, the interaction starts and will continue until a minimum critical value is reached. It should be noticed that the system has different states depending on whether the gradients are increasing (ACCR state) or decreasing (CCR state). Thus for the same gradient between the regions there are two opposite states of the system characteriszed by low and high interaction. So, the system oscillates between the two states and cyclic transitions from one state to another occur within a hysteresis loop [*Serway*, 1996].

A surmised behavior of the studied system is outlined in Fig. 4.7. The regime shift in the model is controlled by δH_{dyn} (green oval in Fig. 4.6). The abscissa denotes the dynamic height gradient between the two basins. Two critical values are marked as δH_{max} and δH_{min}. The interaction, which can be expressed through the heat advection to the Arctic F_{adv} (Eq. (3.55)), between the Arctic Ocean and

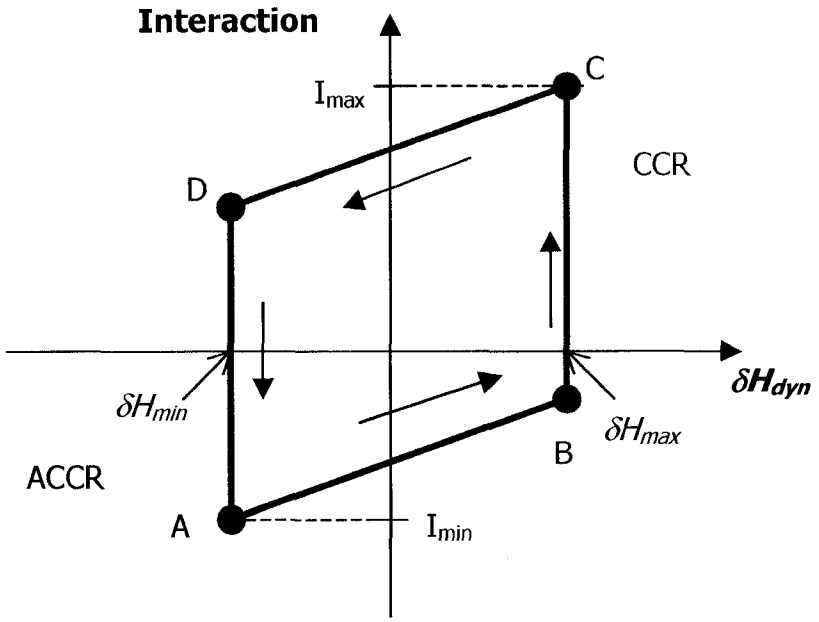

Fig. 4.7. Hysteresis curve for interaction between the Arctic Ocean and Greenland Sea. *At the beginning of ACCR the system is characterized by low interaction (I_{min}) and low gradient (δH_{dyn}) between the regions (point A). In the model, the interaction is realized through the heat advection (F_{adv}) and Polar Water outflow (Q_{PW}). During ACCR, δH_{dyn} is increasing which slightly stimulates the interaction. When the gradient between the basins reaches δH_{max} (point B) the system starts to interact strongly (I_{max}) and shifts to point C, and CCR settles over the Arctic. Intense interaction between the regions leads to decrease of the gradient which slightly suppress the interaction. After several years of CCR, the dynamic height gradient between the basins reaches its minimum (δH_{min}, point D) and the system switches to ACCR.*

the Greenland Sea varies from F_{min} to F_{max}. Let us assume that the system is at the state A, which is characterized by minimum interaction. At this point, the Arctic is under ACCR. The differences between the basins gradually increases leading to a slight intensification of heat advection to the Arctic. However this interaction is not enough to overcome the positive feedback mechanisms that continue to deepen the differences between the two basins, and δH_{dyn}

approaches δH_{max}. When the system reaches point B, i.e. $\delta H_{dyn} = \delta H_{max}$, the interaction between the basins begins and intense heat advection into the Arctic occurs (point C on the plot). The regime shifts to CCR. Under the conditions of strong heat advection to the Arctic and high polar water inflow to the central Greenland Sea, the gradients between the regions start decreasing and the interaction weakens. Finally, when the system reaches the state marked by point D, $\delta H_{dyn} = \delta H_{min}$, it is transferred into the original state with low interaction and ACCR regime in the Arctic.

In the model experiment, the following values have been set: δH_{min} = 0.164 m, δH_{max} = 0.173 m, the coefficient of heat advection χ=1.5 $W \cdot m^{-2} \cdot °K^{-1}$ during ACCR and χ=2.4 $W \cdot m^{-2} \cdot °K^{-1}$ during CCR.

Outflow function, Q_{g_atl}

The outflow function to the North Atlantic, Q_{g_atl}, is a geostrophic flow and no wind effect on the outflow is taken into account (Eqs. (3.15) – (3.17)). Being a function of the density difference between the upper Arctic Ocean and Atlantic water, Q_{g_atl} might be higher during ACCR, when the salinity difference between the upper Arctic Ocean and Greenland Sea is the largest. Q_{g_atl} is lower during CCR. However, this is opposite to the assumed behavior of the Polar Water flux to the Greenland Sea. From other studies [e.g., *Vinje and Finnekasa*, 1986; *Kwok and Rothrock*, 1999], it is believed that atmospheric forcing determines the freshwater flux to the Greenland Sea in hypothesized behavior of the climate system. A possible way this effect can be taken into account in the model is by prescribing lower outflow rate during ACCR and higher outflow rate during CCR. *Proshutinsky and Johnson* [1997] and *Proshutinsky et al.* [2002] argue that the

differences in the outflow rates of the Arctic Ocean water to the Greenland Sea are substantial under different regimes. *Polyakov et al.'s* [1999] model study indicates a twofold increase of the Arctic Ocean export to the North Atlantic in the upper 200 m during CCR compared to ACCR.

In the presented experiment, the following outflow rates are set for different regimes:

$$Q^*_{g\_atl} = \begin{cases} 0.7 \cdot Q_{g\_atl}, & ACCR \\ 1.5 \cdot Q_{g\_atl}, & CCR \end{cases} . \qquad \text{(eq_4_1)}$$

Further, it has been assumed that freshwater released from the Beaufort Gyre reaches the Greenland Sea with some delay. The estimates of time required for surface water from the Beaufort Sea to reach the Fram Strait are taken from *Rigor et al.* [2002] who argue that it takes about 1 to 2 years for ice at the North Pole to drift to Fram Strait. Thus, Q_{g_atl} is gradually increasing/decreasing during 2 years until it reaches $Q^*_{g\_atl}$.

Lower Q_{g_atl} favors the deepening of the ML in the Arctic Ocean (Eq. (3.8)), and higher values are conducive for ML shallowing. Hence, during ACCR the lower outflow rates contribute to the deepening of ML and through this, to the accumulation of freshwater, and potential energy, in the Arctic basin. A high outflow rate provides faster discharge of freshwater from the Arctic Ocean, ML shallowing, and reduction of the freshwater content of the basin. That is in agreement with the hypothesized freshening and salinization of the upper Arctic Ocean under different regimes.

Cloudiness

Cloudiness is another parameter in the model that slightly changes under different climate regimes. Based on observed 3 hr cloud measurements and surface air temperature measured on the Russian ice drifting station NP-4, *Makshtas et al.* [1999] established a strong positive cross-correlation between the surface air temperature and cloudiness. Thus, in warm years the frequency of overcast skies increases. During cold years, the number of days with clear skies increases. This corresponds to *Polyakov et al.'s* [1999] assumption that during CCR the Arctic sky is, in general, more cloudy. Similarly, it has been assumed that intense heat flux to the atmosphere in the Greenland Sea and a general warming of this region will cause increased cloudiness. On the contrary, cooling of the atmosphere increases the number of clear sky days. Under such assumptions, the cloudiness parameterization is presented in Table 4.6.

Ice volume flux to the Greenland Sea, Q_{mlt_GS}

It is assumed that ice from the EGC or Jan Mayen Current is advected into the central Greenland Sea [*Swift*, 1986; *Aagaard and Carmack*, 1989; *Vinje et al.*, 2002]. The rate of supply of ice is very uncertain. *Swift* [1986], having analyzed tritium data from the Greenland and Iceland seas, argued that even if ice from the EGC or Jan Mayen is incorporated into the Greenland Gyre, the supply rate must be low. The most probable season of ice advection into the central Greenland Sea is summer when the cyclonic vortex is weak. In the cold season, surface water and ice are forced away from the Greenland Sea.

Table 4.6. Cloudiness parameterization in the Arctic Ocean – Greenland Sea model for different regimes

	Jan	Fb	Mr	Ap	May	Jn	Jl	Aug	Sp	Oc	Nv	Dc
Arctic Ocean [(a)]												
ACCR	0.47	0.47	0.47	0.53	0.75	0.84	0.87	0.91	0.84	0.72	0.52	0.49
CCR	0.49	0.49	0.49	0.55	0.78	0.87	0.91	0.95	0.88	0.75	0.54	0.51
obs.[(b)]	0.47	0.49	0.50	0.53	0.76	0.85	0.89	0.91	0.88	0.75	0.54	0.51
Greenland Sea												
ACCR	0.65	0.65	0.65	0.7	0.8	0.87	0.91	0.91	0.75	0.75	0.7	0.65
ACCR	0.55	0.55	0.55	0.6	0.68	0.74	0.77	0.77	0.64	0.64	0.6	0.55
obs.[(c)]	0.5-0.8	0.5-0.8	0.5-0.8	0.6-0.8	0.6->0.9	0.7->0.9	0.7->0.9	0.7->0.8	0.7->0.8	0.7->0.8	0.6-0.8	0.5->0.8

(a)Shelf cloudiness is the same.
(b) [*Lindsay*, 1998].
(c) [*Gorshkov*, 1980].

The necessity of including ice volume flux was caused by a surplus of energy reflected in slightly warmer sea surface temperatures in the Greenland Sea model than was observed. Q_{mlt_GS} is estimated as a small fraction (5%) of ice volume flux through Fram Strait. The fraction of ice advected into the central Greenland Sea is speculative and mostly based on *Aagaard and Carmack* [1989] who estimated that about 3% to 6% of the annual freshwater load entering through Fram Strait penetrates into the Greenland Sea. The estimated ice volume flux through Fram Strait ranges from 0.06 to 0.16 Sv [*Kwok and Rothrock*, 1999]. Attributing lower ice advection to the Greenland Sea with ACCR, the following values for Q_{mlt_GS} have been used in the experiment:

$$Q_{mlt\_GS} = \begin{cases} 0.05 \cdot V_{flx} \cdot \sin\left(\pi(d_j - 145)/108\right), & if \quad 140 \le d_j \le 270, \\ 0, & otherwise, \end{cases} \qquad (4.4)$$

where V_{flx} is ice volume flux (0.16 Sv for CCR and 0.06 Sv for ACCR) and d_j is Julian day.

Polar Water and Atlantic Water inflows to the Greenland Sea

As mentioned earlier, there are no available observations on the amount of the Polar Water (PW) and Atlantic Water (AtW) inflowing into the central Greenland Sea. Although there are speculative, mostly qualitative, estimates saying that the amount of AtW entering the Greenland Gyre is much higher than the amount of PW (see, for instance [*Johannessen*, 1986; *Swift*, 1986; *Alekseev et al.*, 1994; *Pawlowicz et al.*, 1995]). The only quantitative estimate of the PW inflowing into the central Greenland Sea (Q_{PW}) has been found in *Aagaard and Carmack* [1989] (3 to 6% of the freshwater load of the EGC).

As determined in Chapter 3, Q_{PW} is a fraction of Q_{g_atl}. Several model experiments have been conducted to estimate Q_{PW}. In this model, the ratio, Q_{PW}/Q_{AtW}, determines the salinity in the upper Greenland Sea. The approximate ratio can be obtained from the salt balance:

$$\frac{Q_{PW}}{Q_{AtW}} = \frac{\bar{S}_{AtW} - \bar{S}_{ml}}{\bar{S}_{PW} - \bar{S}_{ml}}, \qquad (4.5)$$

where overbars denote annual means. For the prescribed values and from the model outputs: $\overline{S}_{AtW} = 35.0$, $\overline{S}_{ml} = 34.8$, $\overline{S}_{PW} = 32.0$. After substituting these values into Eq. (4.5), the ratio is $Q_{PW}/Q_{AtW} \approx 0.07$. This ratio is obtained under the assumption that the water masses (Q_{PW} and Q_{AtW}) completely flow into the mixed layer and, thus, the ratio gives only an intuitive estimate of what Q_{PW} could be for given values of Q_{AtW} and Q_{g_atl} (Table 3.7). A difficulty arises from the depth dependence of Q_{PW} and Q_{AtW} (Eqs. (3.58) and (3.59)). Thus, for a shallow mixed layer, when only the fraction of both fluxes inflow into the ML (Eqs. (3.62) and (3.63)), this ratio will significantly differ from 0.07.

In order to determine the appropriate values for Q_{PW}, several model experiments have been performed. The results (not presented) reveal that the annual mean ratio $Q_{PW}/Q_{AtW} \approx 3.7x10^{-2}$ leads to low water column stability in the Greenland Sea, with highly possible deep convection. For $Q_{PW}/Q_{AtW} \approx 8.0x10^{-2}$, there is strong freshening of the upper Greenland Sea and deep convection ceases. Monthly mean inflow characteristics of Q_{PW} and Q_{AtW} of the Greenland Sea model are presented in Table 3.7, Chapter 3.

In the model, an actual value of Q_{PW} is calculated as follows. For example, let us assume that the Arctic Ocean module simulated Q_{g_atl} = 0.8x10^6 m^3·s^{-1}. From Table 3.7, Q_{PW} = .8x10^4 m^3·s^{-1} in January – May, 1.52x10^5 m^3·s^{-1} in June through August, and 1.6x10^4 m^3·s^{-1} rest of the year. The annual ratio Q_{PW}/Q_{AtW} would be 8.0x10^{-2}, indicating that the Greenland Sea mixed layer would freshen for such Q_{g_atl}.

Spin-up years

The first 10 years of the model run are spin-up. During the first 2 years ACCR is kept in the Arctic followed by CCR during the next 5 years. Then ACCR is kept for 3 more years.

The values of parameters discussed in Chapter 3 and in this chapter that were used for experiment 2, where the auto-oscillatory behavior is explored, are summarized in Table 4.7.

4.2.2. Results and discussion

The simulated Arctic Ocean – Greenland Sea climate system reproduces the hypothesized auto-oscillatory behavior. In the simulation, the regimes shift in the system with a period ranging from 10 to 15 years (Fig. 4.8A). The simulated period of ACCR/CCR shifts corresponds to the hypothesized periodicity of *Proshutinsky and Johnson* [1997]. However, the simulated periodicity is not rigidly cyclic. The number of ACCR years slightly exceeds CCR years: 58 ACCR vs 52 CCR for 110 years of the model run. Annual mean dynamic height gradient, δH_{dyn}, is shown in Fig. 4.8B. It oscillates between the upper and lower limits δH_{max} and δH_{min} (magenta dashed lines). The system reveals some instability: during one cycle (e.g., year 29) δH_{dyn} changes its tendency and starts increasing as soon as it has reached δH_{min} and the regime shifts to the opposite. During another cycle (e.g. year 89), δH_{dyn} keeps decreasing one more year after the regimes has shifted. Preliminary analysis of the model output shows that the reason for such behavior of the system is the Arctic halocline. Any changes in the

Table 4.7. Values of parameters used in the oscillatory study

Parameters	ACCR forcing	CCR forcing
Arctic Ocean		
Q_{mao}, Sv	1.1	1.1
$Q^{*}_{g\_atl}$	$0.7 \cdot Q_{g\_atl}$	$1.5 \cdot Q_{g\_atl}$
V_{flx}, *Sv*	0.06	0.16
χ, $W \cdot m^{-2} \cdot {}^{o}K^{-1}$	1.5	2.4
m_0	$\log\left[\left(100/Ri_o\right)^{1.2}\right]+3.5$	
κ	$\begin{cases} 0.05, \text{if } B_{fl} < 0 \\ 1.0, \text{otherwise} \end{cases}$	
Greenland Sea		
m_0	$\log\left[\left(100/Ri_o\right)^{1.8}\right]+3.5$	
κ	$\begin{cases} 1, & if \quad B_{fl} > 0 \\ 0.99, & if \quad Ri_T < 8 \\ 0.01 \cdot \log\left(3000/h_{ml}\right), & if \quad Ri_T > 8. \end{cases}$	

halocline density affect the dynamic height gradient. The results have revealed that the halocline slowly adjusts to rapidly changing forcing parameters (heat advection, SAT, shelf inflow). Having a different response frequency than the forcing parameters, the halocline causes low-frequency instability in the system. However this assumption is speculative and needs further investigation and

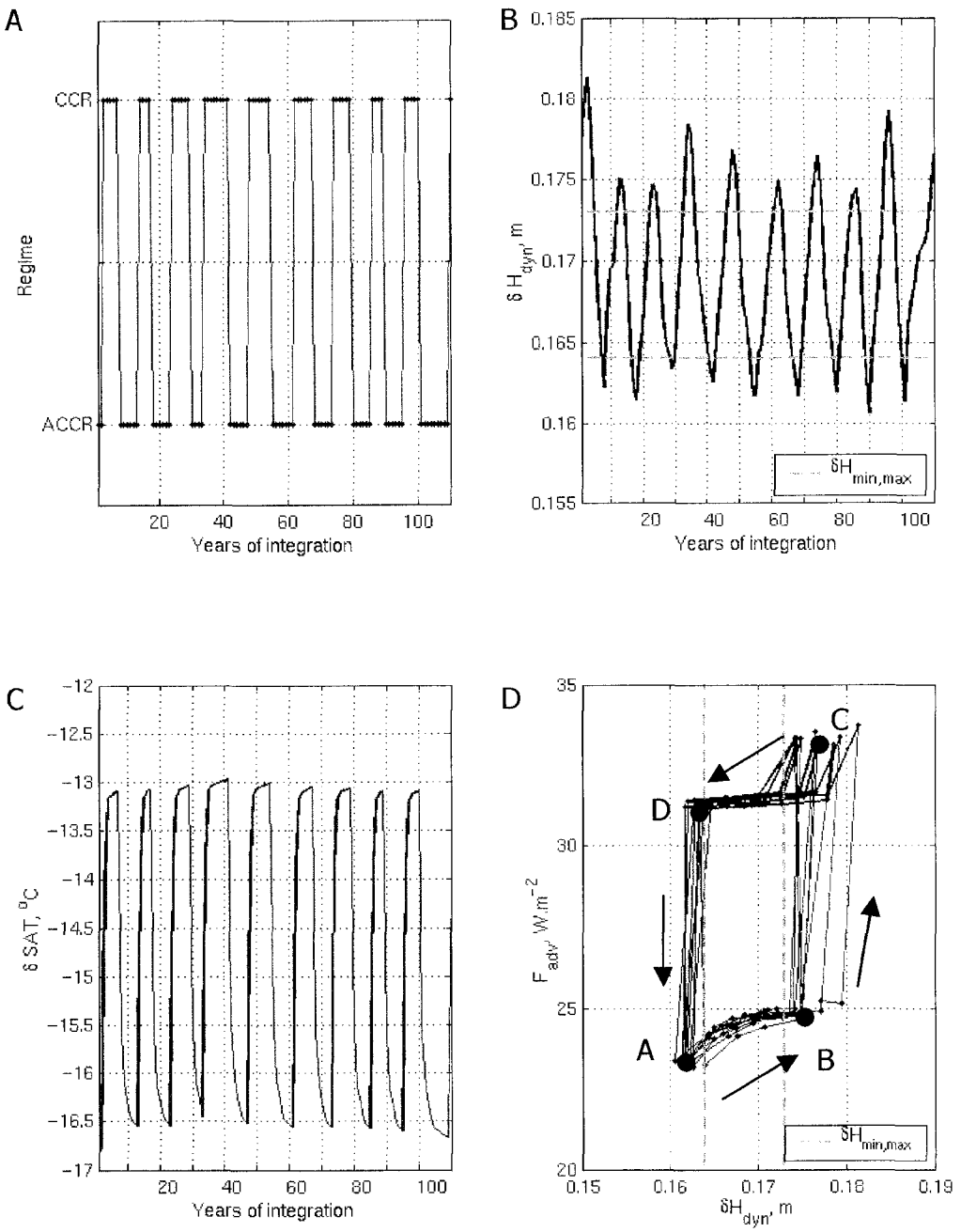

Fig. 4.8. Oscillatory study: Behavior of the system. *Red segments denote CCR, blue – ACCR. (A) Regime shifts. The model reproduces auto-oscillatory behavior of the climate system with a period 10-15 years. (B) Annual mean dynamic height gradient, δH_{dyn}. Magenta dashed lines are minimum and maximum δH_{dyn}. (C) Same as (B) but for the annual mean SAT gradient, δSAT. (D) Simulated behavior of the system in terms of interaction (heat advection, F_{adv}) vs δH_{dyn}. The model reproduces the hypothesized behavior shown in Fig. 4.7. Refer to Fig. 4.7 and text for detailed explanation.*

model experiments. Analysis of density distribution in the Arctic Ocean model under different climate states will be given later in the section.

Time series of surface air temperature (SAT) gradient, δSAT, between the two regions is shown in Fig. 4.8C. δSAT rapidly changes as soon as the coefficient of heat advection χ switches from one to another value. Slow changes during regimes are attributed to gradual warming or cooling of the Greenland Sea atmosphere responding to the surface heat flux changes (Eq. (3.81)).

Fig. 4.8D demonstrates that the model reproduces the behavior described earlier in Fig. 4.7. In figure 4.8D, the interaction characterized by heat advection F_{adv} to the Arctic is plotted versus δH_{dyn}. Similar to Fig. 4.7, at point A the system is at the low interaction stage in the beginning of ACCR. During ACCR, the system state changes to B when $\delta H_{dyn} = \delta H_{max}$ and the interaction proceeds (point C). During the first year of CCR, F_{adv} is maximal due to still warm Greenland Sea atmosphere and then it slightly drifts to lower values. When the system reaches D, the interaction decreases and ACCR resettles in the Arctic. The system returns to A.

SAT and surface heat flux

Selected output from the atmospheric models are presented in Fig. 4.9. The upper panels show daily average SAT for ACCR and CCR in the Greenland Sea model (panel A) and the Arctic model (B). The simulated SAT in the Greenland Sea lies within the 98% confidence interval (green vertical bars) of the means (green asterisks) obtained from NOAA – CIRES CDC SAT for the period 1948-2001 [*CDC*, 2003]. As one can see, the state-space model for the Greenland Sea

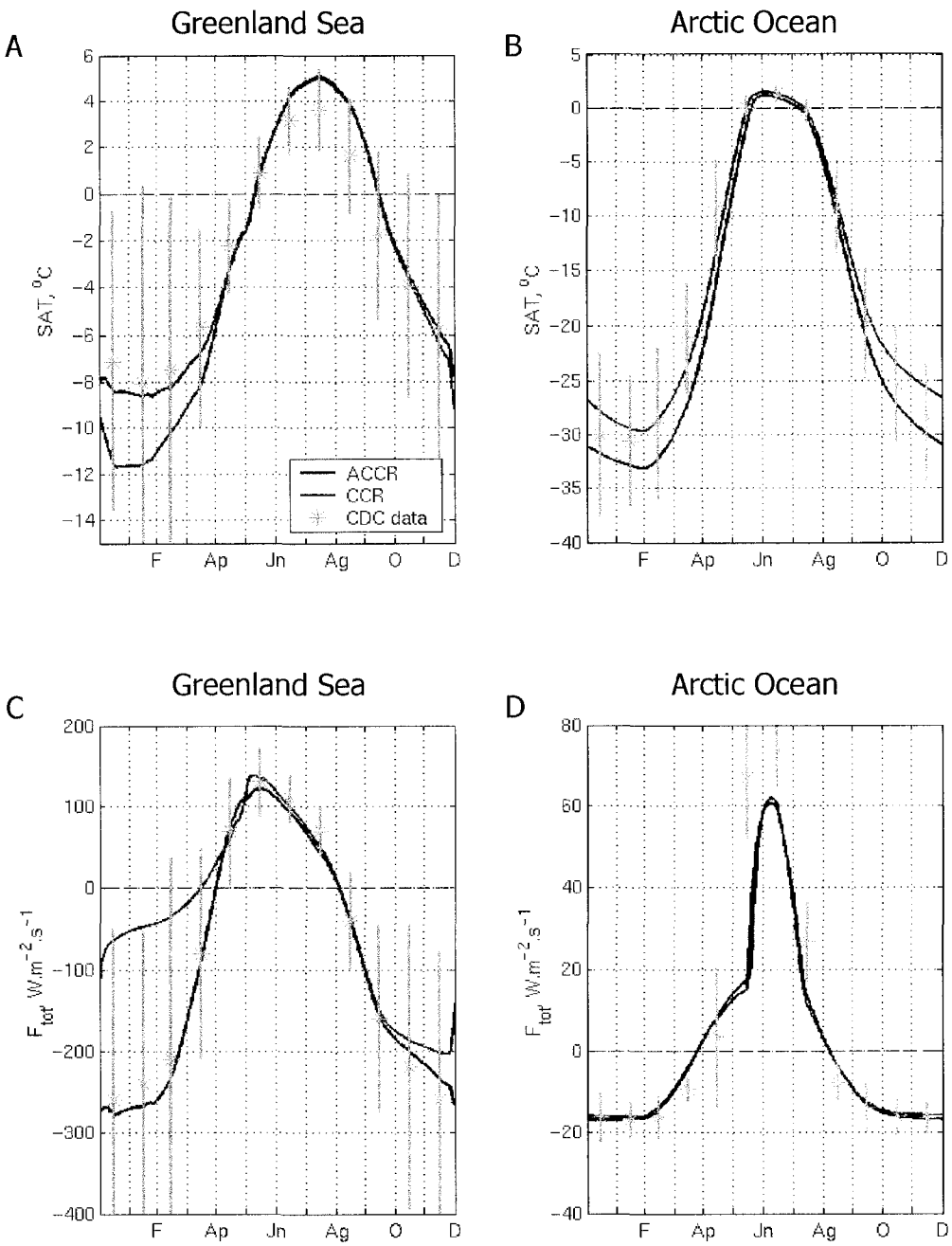

Fig. 4.9. Oscillatory study: Mean ACCR and CCR SAT and surface heat flux in the Arctic Ocean and Greenland Sea. *Time series of simulated daily SAT in the Greenland Sea (A) and the Arctic Ocean (B) averaged over the last years of ACCR (blue lines) and CCR (red lines) forcing. Green asterisks denote monthly mean values obtained from NOAA-CIRES CDC data over the period 1948-2001. Vertical green bars are the 98% confidence intervals for the CDC means. Abscissa is time, end of months. (C) Same as (A) but for the Greenland Sea surface heat flux. (D) Same as (B) but for the Arctic Ocean surface heat flux.*

SAT simulates warmer winter and early spring during ACCR (blue curve) compared to CCR (red curve). This is due to the difference in the surface heat fluxes F_{tot} during ACCR and CCR (Fig. 4.9C). Significant reduction of the heat flux in late December till middle April (red line) is due to the ice cover which appears in the Greenland Sea model under CCR forcing. Lower heat flux to the atmosphere cause negative SAT anomalies (Eq. (3.81) and Table (3.10)). During ACCR, the situation is opposite. Rapid deepening of the mixed layer entrains heat from below and gives it to the atmosphere resulting in a larger winter surface heat flux (Fig. 4.9C, blue line). Large F_{tot} induce winter SAT warming (Fig. 4.9A, blue line).

The SAT differences between simulated ACCR and CCR SAT is larger in the Arctic than the Greenland Sea (Fig. 4.9B). The difference between the SAT's may be unrealistic as some values lie beyond the 98% confidence interval, which shows that the model can reproduce extreme states of the Arctic climate. In the Arctic, due to colder SAT during ACCR, there are higher fluxes to the atmosphere in winter and lower fluxes to the ocean in summer, compared to CCR (Fig. 4.9D).

Arctic Ocean and shelf

The results from the Arctic Ocean and shelf models are plotted in Figs. 4.10 – 4.12. The diagram of the annual mean h_{ml} (Fig. 4.10A) reveals relatively fast shallowing of the mixed layer during CCR (red segments) and gradual deepening during ACCR (blue segments). Such behavior is due to lower entrainment velocities, w_e, during CCR and higher w_e during ACCR (Fig. 4.10D). The entrainment, in its turn, depends (Eq. 3.12) on the buoyancy flux B_f (Fig. 4.10C) and mixed layer salinity S_{ml} (Fig. 4.10B). Since the latter determines the water

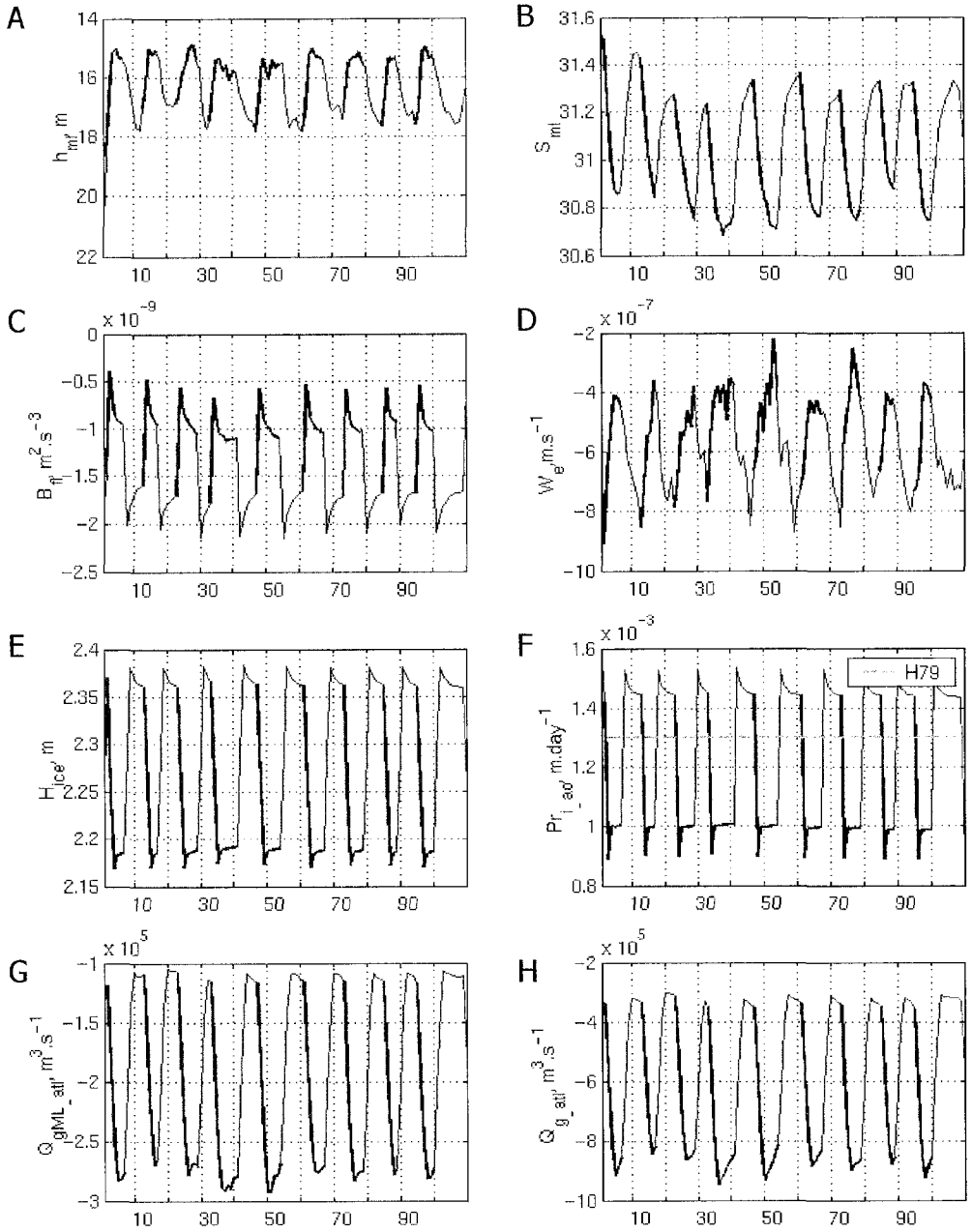

Fig. 4.10. Oscillatory study: Time series of annual output from the Arctic Ocean model. *Blue segments denote period of ACCR forcing, red segments – CCR forcing. Abscissa is time, years of integration. (A) Mixed layer depth. (B) Mixed layer salinity. (C) Buoyancy flux. (D) Entrainment velocity. (E) Ice thickness. (F) Ice production. Magenta dashed line shows annual ice production estimated by Hibler [1979]. (G) Outflow from the Arctic Ocean mixed layer to the Greenland Sea. (H) Total outflow from the Arctic Ocean to the Greenland Sea.*

column stability and reduced gravity g', higher S_{ml} promotes deepening of the mixed layer. The model reproduces well the expected variability of both B_{fl} and S_{ml} as can be seen from Figs. 4.10B and 4.10C. For ACCR, both B_{fl} and S_{ml} are higher than for CCR. The buoyancy flux depends on the ice production, Pr_{i_ao}, and shelf water inflow Q_{sh_ml} (Eq. (3.13)). From the lower SAT (Fig. 4.9B), Pr_{i_ao} is higher (Fig. 4.10F) and, accordingly, ice is thicker (Fig. 4.10E) during ACCR. Also shown with a magenta dashed line in Fig. 4.10F is the annual mean ice production obtained from *Hibler* [1979]. Thus, during ACCR the model simulates higher ice production than Hibler's estimate and lower production during CCR. In the model, outflow from the Arctic Ocean mixed layer Q_{qML_atl} (Fig. 4.10G) and total outflow Q_{g_atl} (Fig. 4.10H) are higher during CCR.

To see seasonal variability, time series of the Arctic Ocean model output are shown for 85th (ACCR) and 79th (CCR) years of the model run (Fig. 4.11). These years were randomly selected from the last ACCR and CCR years. The output shows that the model realistically simulates seasonality. The mixed layer (Fig. 4.11A) deepens during the cold season and shallows in summer when the entrainment velocity is zero (Fig. 4.11B). During summer when B_{fl} is large and positive (Fig. 4.11D) and entrainment is suppressed, the mixed layer depth is determined according to Eq. (3.11). It should be noted that when it is not zero, w_e is higher during ACCR (blue curve) due to higher mixed layer salinity (Fig. 4.11C). Simulated ice production (Fig. 4.11F) is reasonably close to *Hibler* [1979] results, although the model gives slightly lower ice growth in January through May and slightly lower ice melt in July through middle September. The onset of melting is in the beginning (CCR) – middle (ACCR) of May. Freezing starts by the middle of September.

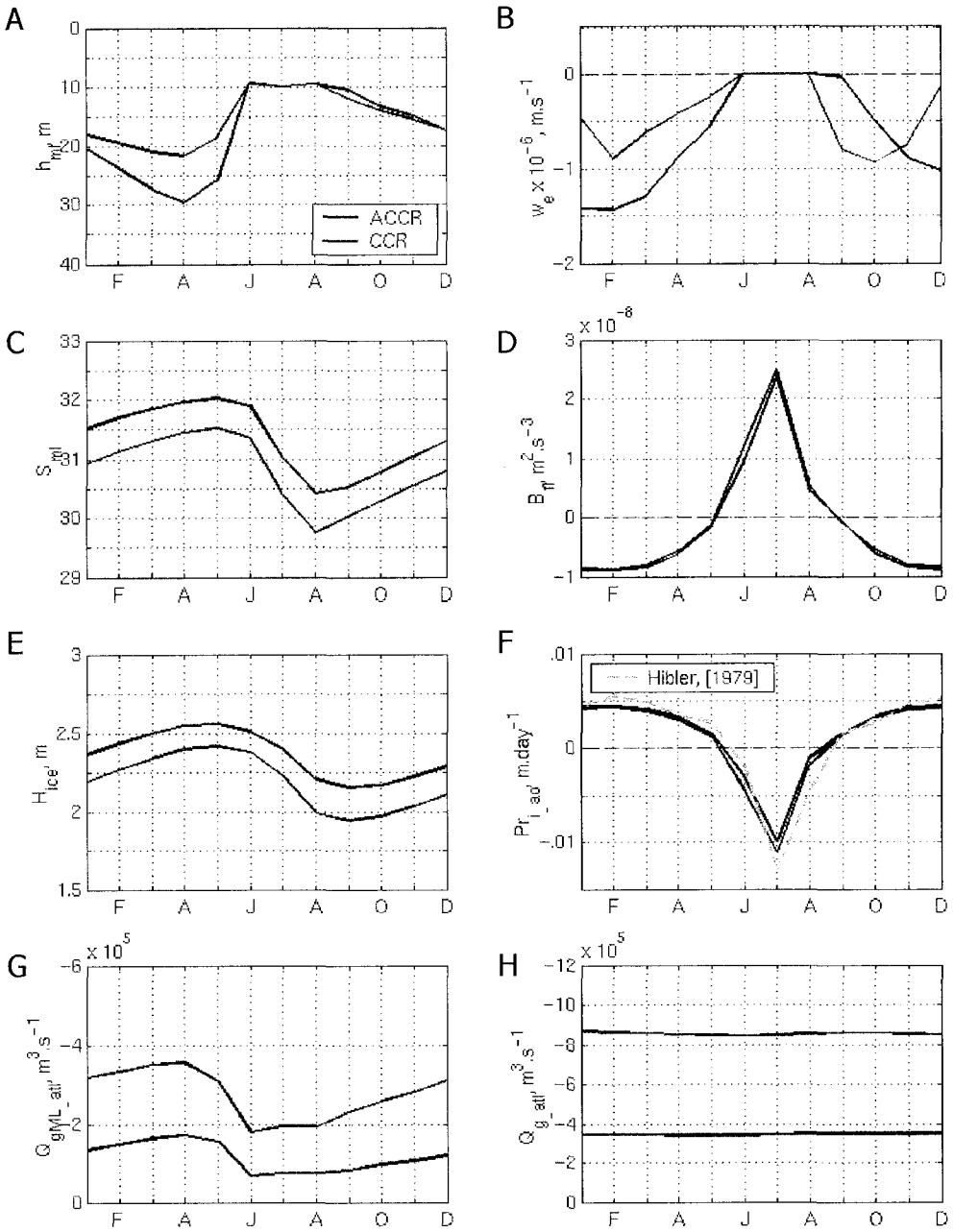

Fig. 4.11. Oscillatory study: Arctic Ocean model output for ACCR and CCR years. *Time series of monthly means for 85th (ACCR, blue curve) and 79th (CCR, red curve) years of integration. Abscissa is time, months. (A) Mixed layer depth. (B) Entrainment velocity. (C) Mixed layer salinity. (D) Buoyancy flux. (E) Ice thickness. (F) Ice production. (G) Outflow from the Arctic Ocean mixed layer to the Greenland Sea. (H) Total outflow from the Arctic Ocean to the Greenland Sea.*

Shown in Fig. 4.11G is the outflow from the Arctic Ocean mixed layer Q_{gML_atl}. Unlike the total outflow Q_{g_atl} (Fig. 4.11H), it has a strong seasonal signal, and oscillates in phase with the h_{ml}.

Fig. 4.12 presents the shelf model output for the same years as in Fig. 4.11. Shelf water salinity S_{sh} (Fig. 4.12A) changes with the ice freezing/melting cycle (Fig. 4.12D). The difference between ACCR and CCR shelf salinity is not significant. Fig. 4.12B shows salinity of the shelf inflow to the Arctic Ocean mixed layer S_{sh_ml}. It is an integrated characteristic and depends on the Arctic S_{ml} (Eq. 3.42). In winter, during ACCR S_{ml} is larger than during CCR (Fig. 4.10B), so ACCR S_{sh_ml} in winter is higher. When ice production is low or negative, $S_{sh\_ml} = S_{sh}$. Different S_{ml} during ACCR and CCR years also cause different amounts of shelf water outflow to the Arctic Ocean mixed layer Q_{sh_ml} (Fig. 4.12E) in accordance with Eq. (3.41). In the warm season, $Q_{sh\_ml} = Q_{sh}$ (magenta dashed line). From Fig. 4.12E it follows that in ACCR winter, the shelf contributes more water to the interior Arctic Ocean mixed layer. This inflow is more saline than during CCR (Fig. 4.12B). This is another reason, in addition to increased ice production, for higher S_{ml} in the Arctic Ocean during ACCR (Figs. 4.10B and 4.11C).

As soon as Q_{sh} is constant all years of the model run ($Q_{sh} = Q_{mao}$), more intense outflow to the Arctic Ocean mixed layer during ACCR means lower outflow to the Arctic Ocean halocline. However, lower halocline inflow does not necessarily mean lower salt flux. In Fig. 4.12C, the total outflow of salt from the shelf ϕ is plotted (blue and red solid curves). According to Eq. 3.28, ϕ is a function of S_{xx} and is mostly determined by ice production. When ice production is small or negative (ice melting) and $S_{xx} \le S_{ml}$, $\phi = Q_{sh} \cdot S_{sh}$ (dashed lines) meaning that no salt is advected from the shelf below the Arctic Ocean mixed layer. The

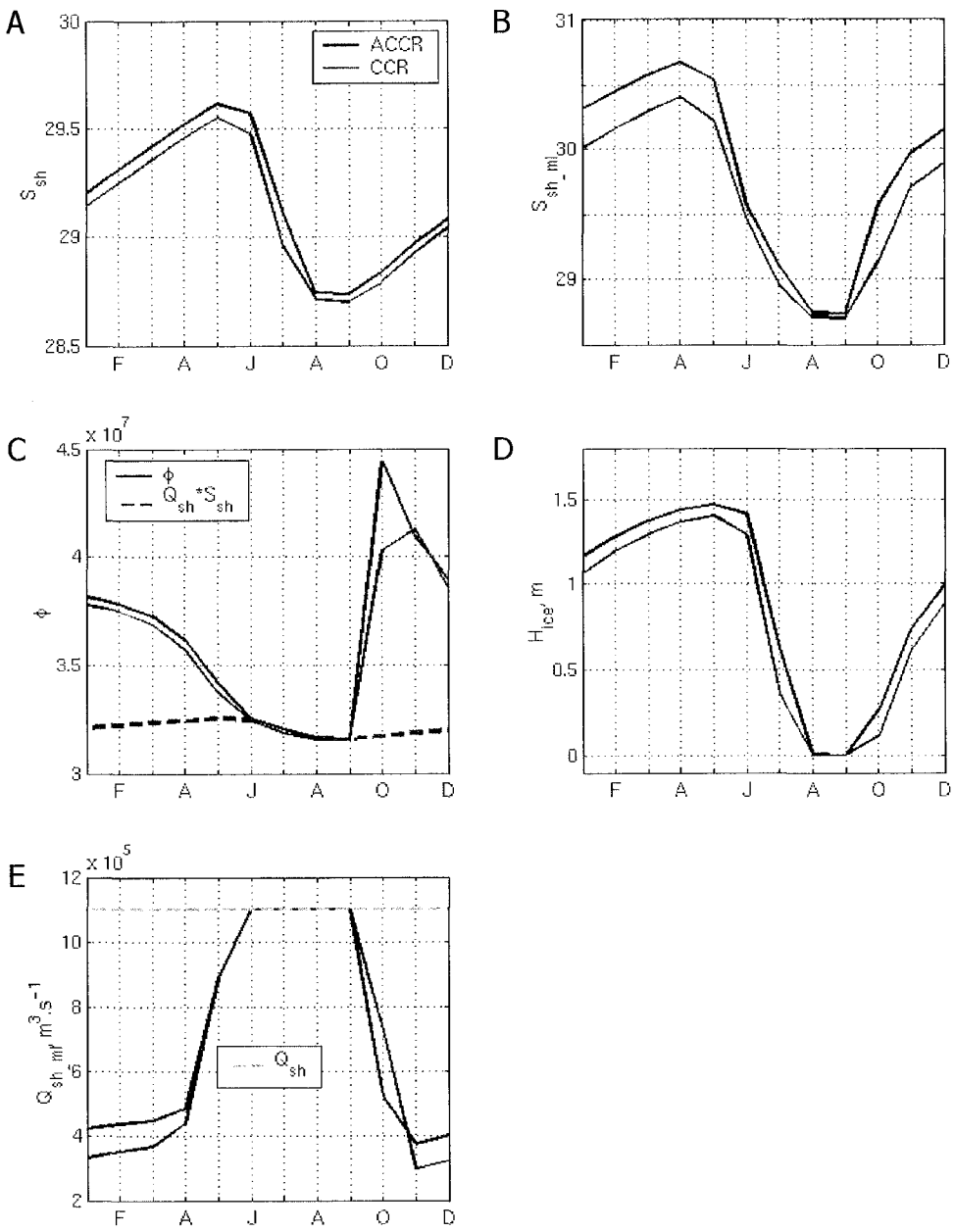

Fig. 4.12. Oscillatory study: Shelf model output for ACCR and CCR years. *Same as Fig. 4.11 but for the shelf model. (A) Shelf water salinity. (B) Salinity of Q_{sh_ml}. (C) Total outflow of salt from the shelf. Solid lines are real output, dashed line shows salt outflow without ice production on the shelf. (D) Ice thickness. (E) Outflow from the shelf to the Arctic Ocean mixed layer. Magenta dashed line is the total shelf outflow.*

difference $\phi - Q_{sh} \cdot S_{sh}$ shows the amount of surplus salt conveyed from the shelf to the interior Arctic Ocean (derived from Eqs. (3.27) and (3.28)):

$$\phi - Q_{sh} S_{sh} = \int_{S_{sh}}^{S_{xx}} q(S) \cdot S \cdot dS - S_{sh} \cdot \int_{S_{sh}}^{Sxx} q(S) dS = \int_{S_{sh}}^{S_{xx}} q(S) \cdot (S - S_{sh}) \cdot dS. \quad (4.6)$$

From Eq. (4.6) it is obvious that the larger S_{xx}, the bigger the difference between ϕ and $Q_{sh} \cdot S_{sh}$. Fig. 4.12C shows higher salt flux from the shelf to the Arctic Ocean mixed layer and halocline under ACCR forcing. The difference between ϕ and $Q_{sh} \cdot S_{sh}$ (dashed curves) is largest in October when intense ice formation occurs in the shelf model.

Central Greenland Sea

The output from the Greenland Sea model is presented in Figs. 4.13 and 4.14. In Fig. 4.13 the annual means of several characteristics are plotted. One-year long time series showing simulated seasonal variability of the Greenland Sea characteristics during ACCR and CCR years are shown in Fig. 4.14.

Increased freshwater inflow Q_{PW} (Figs. 4.13G and 4.14H) to the Greenland Sea damps convection. Figs. 4.13A and 4.14A show that after several years of CCR forcing the Greenland Sea mixed layer becomes shallower (red curve) and at the end of CCR convection is shut off – the maximum annual mixed layer does not

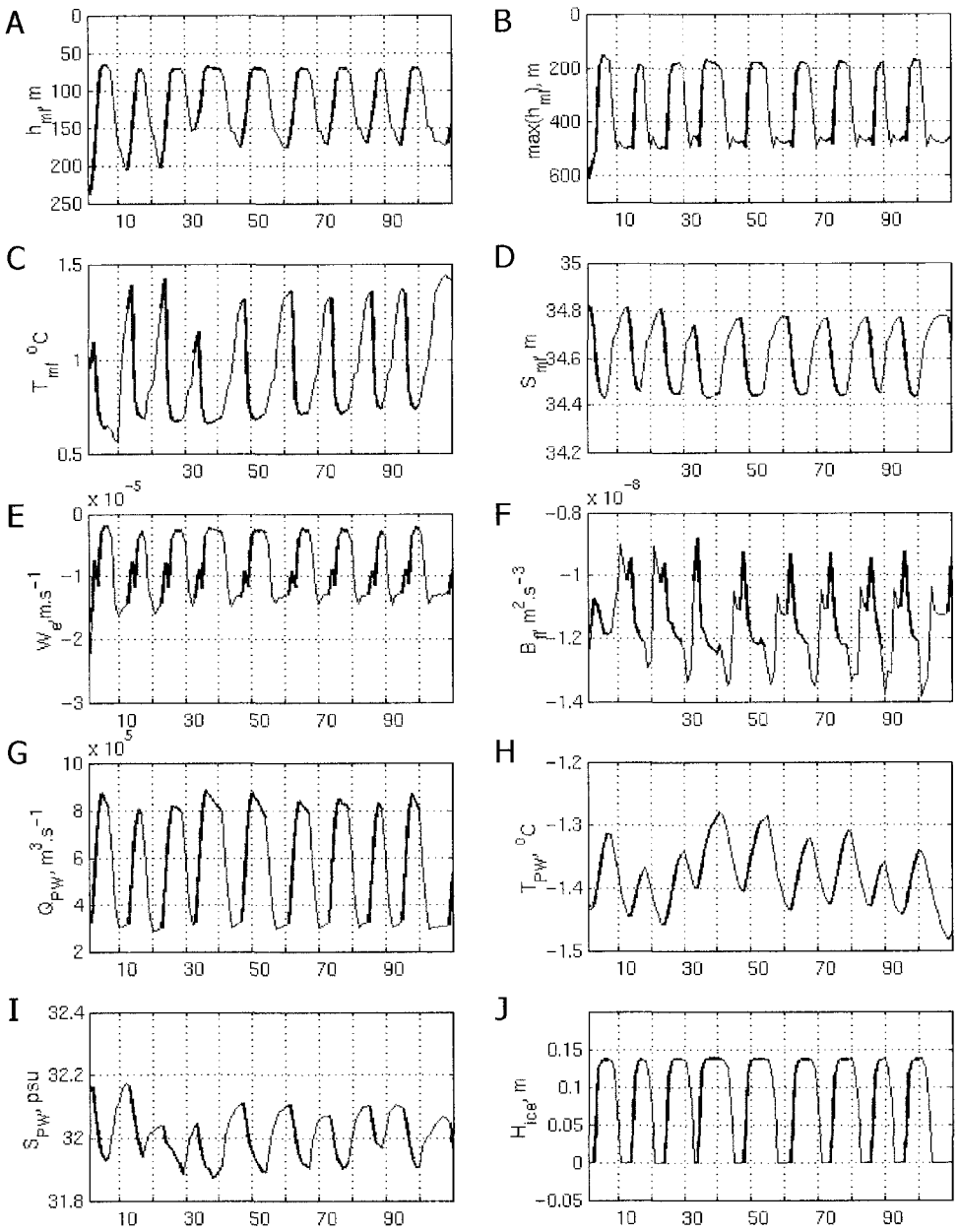

Fig. 4.13. Oscillatory study: Time series of annual output from the Greenland Sea model. *Blue segments denote period of ACCR forcing, red segments CCR forcing. Abscissa is years of integration. (A) Mean mixed layer depth. (B) Maximum annual mixed layer depth. (C) Mixed layer temperature. (D) Mixed layer salinity. (E) Entrainment velocity. (F) Buoyancy flux. (G) Polar water inflow. (H) Polar water temperature. (I) Polar Water salinity. (J) Ice thickness.*

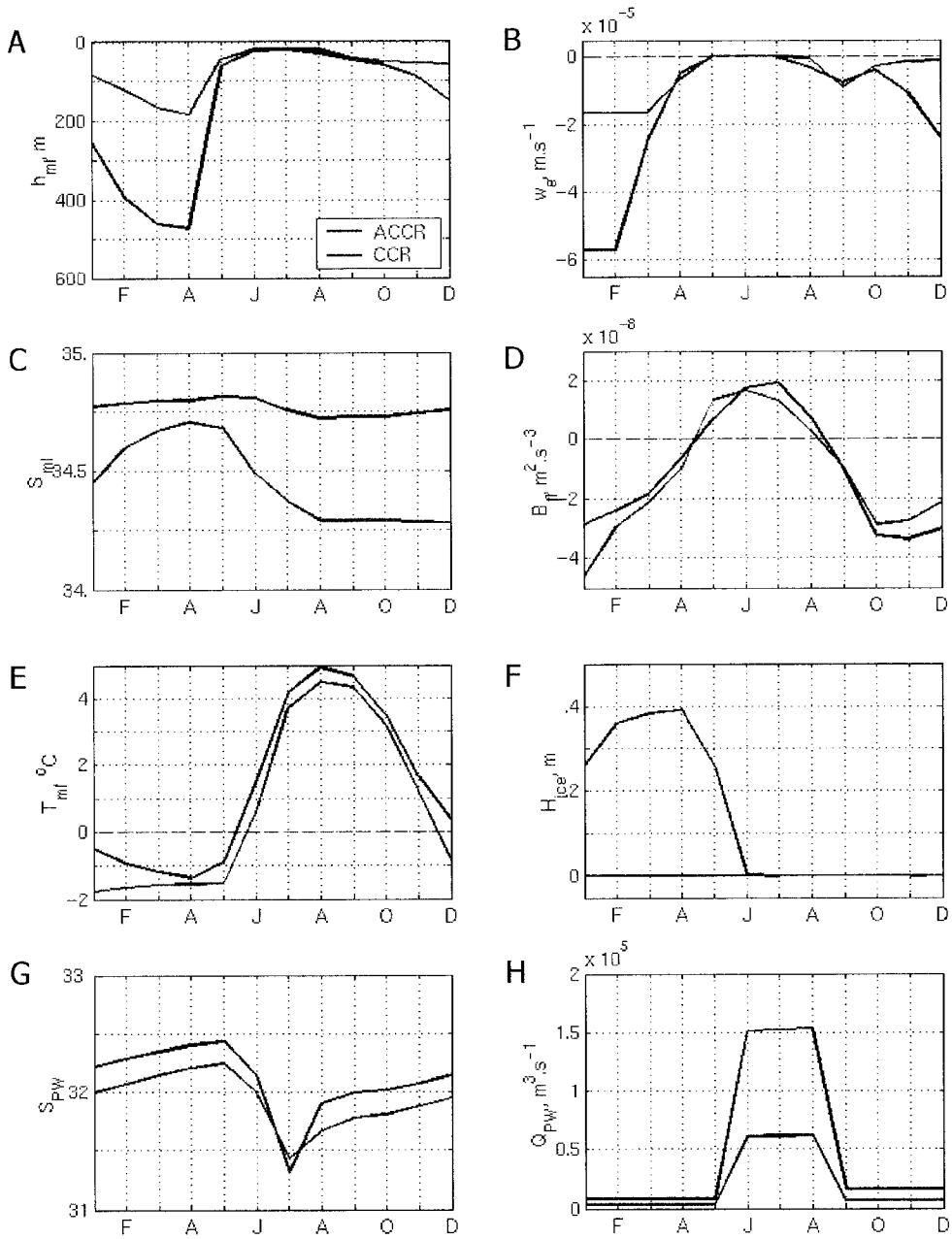

Fig. 4.14. Oscillatory study: Greenland Sea model output for ACCR and CCR years. *Time series of monthly means for 85th (ACCR, blue curve) and 79th (CCR, red curve) years of integration. Abscissa is time (months). (A) Mixed layer depth. (B) Entrainment velocity. (C) Mixed layer salinity. (D) Buoyancy flux. (E) Mixed layer temperature. (F) Ice. (G) Polar water salinity. (H) Polar water inflow.*

penetrate deeper than 200 m (Fig. 4.13B) and the entrainment velocity is lower than during ACCR (Figs. 4.13E and 4.14B). The mixed layer deepening is determined by the water column stability and buoyancy flux B_{fl} (Eq. 3.12). The stability is characterized by the density jump at the mixed layer lower boundary, i.e. by the mixed layer temperature T_{ml} and salinity S_{ml}. The model reproduces well the expected T_{ml} and S_{ml} variability observed in the Greenland Sea [*Pawlowicz et al.*, 1995; *Pawlowicz*, 1995]. As the mixed layer freshens and shallows, it rapidly cools. Notice in Fig. 4.14E that T_{ml} during CCR (red curve) drops fast to the freezing point, while T_{ml} during ACCR (blue curve) never reaches the freezing point. In terms of the density variability, T_{ml} and S_{ml} act in opposite ways – a drop in S_{ml} reduces mixed layer density, and cooling increases it, though not enough to overcome the effect of freshening.

Variability of the buoyancy flux is shown in Fig. 4.13F. It seems to signal a regime shift 1-3 years later. Note that after the regime shifts Bfl changes the tendency 1 – 3 years later. Such behavior is explained by inertia of the oceanic component in the system. Gradual changes in the Greenland Sea upper layer temperature and salinity cause delay in the response of the system to rapid changes of the forcing parameters. From Eq. (3.66), B_{fl} describes the net change of the potential energy in the mixed layer caused by temperature and salinity changes. Actually, Eq. (3.66) is a balance between the forcing parameters that alter the upper layer density. For example, at the beginning of the ACCR state, the Greenland Sea S_{ml} is low (Figs. 4.13D and 4.14C). This makes the second term, $\int_0^{Hml} Q_{AtW}(S_{ml} - S_{AtW})dz$, in Eq. (3.66) large and forces B_{fl} to become more negative. On the other hand, the differences ($S_{ml} - S_{PW}$) and ($S_{ml} - S_{ice}$) are low which makes the third and fifth terms in Eq. (3.66) less significant, and Q_{mlt_GS} and Q_{PW} are reduced during ACCR (Table 4.7 and Eq. (4.1)). Also, during the first

one to two years of ACCR, ice still appears in the model (Fig. 4.13J) due to low S_{ml}. All this makes B_{fl} more negative, meaning a rapid increase of the upper layer density in the beginning of ACCR. After several years of ACCR forcing, S_{ml} approaches S_{AtW} (Fig. 4.13D) and the term $\int_0^{Hml} Q_{AtW}(S_{ml} - S_{AtW})dz$ decreases, causing B_{fl} to vanish.

It is noteworthy that simulated interannual variability of polar water temperature T_{PW}, and salinity S_{PW}, advected into the Greenland Sea (Figs. 4.13H and 4.13I) promote the expected dynamics of the mixed layer. In ACCR years, S_{PW} is higher and T_{PW} is colder, i.e. denser, than during CCR.

Seasonal variability in the Greenland Sea upper layer is similar to the Arctic Ocean. Forced by seasonal freshening in summer (Fig. 4.14C) and by zero entrainment (Fig. 4.14B), the mixed layer becomes shallow (Fig. 4.14A) and warm (Fig. 4.14E). Due to the prescribed lower Q_{PW} (Fig. 4.14H), S_{ml} has lower seasonal amplitude during ACCR. During ACCR, S_{ml} starts increasing in early fall with the onset of the mixed layer deepening. Intense entrainment provides large salt flux from the lower layer into the mixed layer. During CCR S_{ml} does not change until late December or January when ice starts freezing (Fig. 4.14F).

Vertical distribution of water density in the Arctic Ocean and Greenland Sea models

The oscillatory study was designed under the assumption that T/S characteristics of the Arctic Ocean and Greenland Sea water column undergo significant changes under different climate regimes. Characteristics of the vertical structure

of the upper layer for both basins are presented in Fig. 4.15. Seasonal changes in the simulated Arctic Ocean take place in the upper 30-35 m (compare dashed and solid curves of the same color in the upper panels of Fig. 4.15). The interannual variability spreads deeper to approximately 150 m (compare curves of different colors in the same figures). The amplitude of the interannual variability fades with depth. In Fig. 4.15D, time series of annual density for three depth levels (50, 75 and 100 m) are presented. The amplitude of oscillations in the upper curve (100 m) is less than that of the lower curve (50 m).

Interannual variability of density in the Arctic Ocean halocline is caused by three factors (Eqs. (3.18) – (3.21)): vertical advection w_a, Bering water inflow Q_{Ber}, and shelf outflow q_{sh}. ACCR forcing promotes more intense (upward) vertical advection since the outflow to the Greenland Sea Q_{g_atl} is set high (Table 4.7). Higher rates of vertical advection cause positive anomalies in T and S in the upper halocline compared to CCR profiles (Figs. 4.15A and 4.15B).

The shelf inflow to the halocline does not change the density because shelf water is isopycnally mixed with halocline water. Nevertheless, it affects vertical T and S in the halocline. For a given density, shelf water is slightly less saline but colder than in the halocline. Thus, shelf inflow dampens the effect of vertical advection tending to decrease water temperature and salinity at a given depth level.

Bering water inflow affects the upper halocline. One can notice a bulge on the T profiles in Fig. 4.15B caused by relatively warm Bering water inflow. The temperature maximum is almost absent at the T profile for April ACCR (blue solid line) because the density of the mixed layer is high and the Bering water inflows directly into the mixed layer.

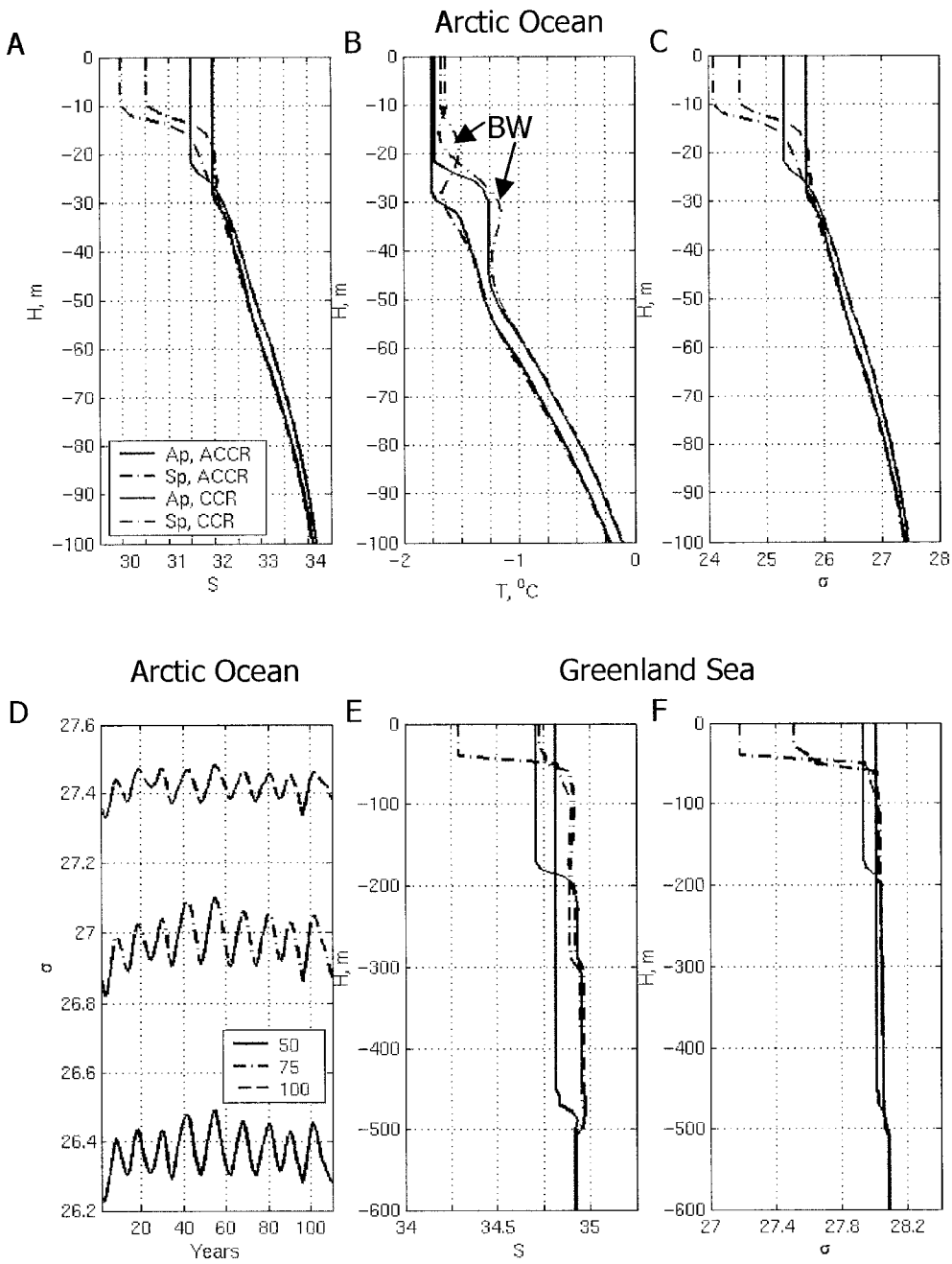

Fig. 4.15. Oscillatory study: Vertical structure of the upper layer of the simulated Arctic Ocean and Greenland Sea. *Blue lines correspond to ACCR forcing, red lines to CCR. Except for D: solid lines are April profiles, dashed-dotted lines are September profiles, and ordinate is depth. Arctic Ocean model: (A) Salinity. (B) Temperature. Arrows indicate "bulges" due to Bering Water (BW) inflow. (C) σ_0. (D) Time series of the annual σ_0 at the 50, 75, and 100-meter depth levels. Ordinate is σ_0, abscissa is time (years). Greenland Sea model: (E) Salinity. (F) Temperature.*

Seasonal variability of the Greenland Sea modeled convection is significant (Figs. 4.15E and 4.15F). For CCR forcing, the seasonal signal reaches only 200 m depth; for ACCR, it penetrates to the 500 m depth. Interannual variability reproduced in the model is related to this 200 – 500 m convection depth range. Deepening during ACCR is limited by the upper boundary of the Norwegian Sea Deep Water (NSDW). It should be noted that for ACCR, the density difference between the mixed layer and underlying water in April profile is extremely small ($g' = 5.7 \times 10^{-3}$ $m^2 \cdot s^{-1}$), i.e. the Greenland Sea is at the pre-convective state. This allows one to assume that under higher values of B_{fl}, which may occur at smaller space scales (for example, intrusion of salt water), chimney convection develops and easily penetrates into the NSDW.

Section 4.3. Summary

- Two groups of model experiments and their results were presented in this chapter: the sensitivity study and the oscillatory study.

- The sensitivity study was conducted to obtain valid estimates for the model's free parameters.

- The oscillatory study was designed to reproduce the auto-oscillatory behavior of the Arctic Ocean – Greenland Sea climate system.

- The major result of the model study was simulated auto-oscillatory ACCR/CCR shifts with a 10-15 year period.

Chapter 5 SUMMARY

Section 5.1. Major results

A simple model of the Arctic Ocean and Greenland Sea, coupled to a thermodynamic sea ice model and atmospheric component has been used to study decadal variability in the ice-ocean-atmosphere climate system. The central hypothesis that motivated the current investigation is that the behavior of the Arctic Ocean and GIN Sea is auto-oscillatory between two climate states with quasi-decadal periodicity. In this study, the central Greenland Sea is seen to be a focal place of the GIN Sea. The system is characterized by two opposite states: (1) cold Arctic and warm Greenland Sea region; (2) warm Arctic and cold Greenland Sea region. During the first state, ACCR dominates the Arctic, the interaction between the two basins is damped, and deep convection in the central Greenland Sea favors intense heat flux to the atmosphere over the Greenland Sea region. These conditions increase the dynamic height gradient between the two regions which ultimately force the interaction between them to start. The second state is characterized by intense interaction between the basins: the Arctic gains heat advected from the Greenland Sea region while shifting from ACCR to CCR, and the Greenland Sea receives freshwater released from the Arctic Ocean. By setting limiting values for the dynamic height gradient, the decadal variability of the observed system can be reproduced by the auto-oscillatory model.

The major result of this work is the simulation of auto-oscillatory behavior of the Arctic Ocean – Greenland Sea climate system. Periodical solutions obtained from simulations with seasonally varying forcing, for scenarios with high and low

interaction between the regions, reproduce major anomalies in the ocean thermohaline structure, sea ice volume, and fresh water fluxes attributed to ACCR and CCR regimes. According to the simulation results, the characteristic time scale of the Arctic Ocean – Greenland Sea system variability is about 10 to 15 years. This result is consistent with *Proshutinsky and Johnson's* [1997] theory and shows that the Arctic Ocean – Greenland Sea can be seen as a unique, auto-oscillating system.

In the course of this work, two groups of model experiments have been performed. The first group, the sensitivity study, determined appropriate range of values of parameters used in the model. The second group, the oscillatory study, was designed to reproduce auto-oscillations in the Arctic Ocean – GIN Sea climate system.

The sensitivity study showed that both the Arctic Ocean and shelf models are highly sensitive to the coefficient of heat advection, χ. For $1.9 \le \chi \le 2$ $W \cdot m^{-2} \cdot {}^{\circ}K^{-1}$, the mean Arctic conditions are reproduced by the model. For $\chi > 2$ $W \cdot m^{-2} \cdot {}^{\circ}K^{-1}$, the Arctic and the shelf warm, causing intense ice melting and water freshening. For $\chi < 1.9$ $W \cdot m^{-2} \cdot {}^{\circ}K^{-1}$, the Arctic and shelf box become cold, leading to higher ice production in winter and intense salinification of the upper Arctic Ocean.

The analysis of parameterization of the Arctic mixed layer deepening revealed that setting the proportionality coefficient m_0 as a function of the water column stability (Eqs. (3.22) and (3.23)) reproduces the mixed layer dynamics better than keeping it constant.

In the Greenland Sea model, free convection plays a leading role during the second half of the cold season when the water column stability in the region is

low. It has turned out that parameterization of the upper layer deepening is crucial in simulating different regimes in the region. Constant m_0 and κ lead to physically unrealistic deepening of the mixed layer (Fig. 4.5). Instead, setting both m_0 and κ to be functions of the water column stability (Eqs. (3.22) – (3.24)) reproduces two stages of the upper layer deepening described in other studies (see, for example [*Pawlowicz et al.*, 1995; *Pawlowicz*, 1995]): slow deepening with intense cooling of the mixed layer, and fast deepening driven by either saline or thermal convection after the mixed layer density has approached that of the underlying water. Such parameterization allows ice to appear in the model in case of intense freshening of the upper layer during CCR summer. Another important conclusion is that under the ACCR forcing (low freshwater inflow to the central Greenland Sea), the suggested parameterization of the entrainment leads to a "pre-convective" state of the central Greenland Sea, i.e. the water column stability is low enough to make the deep convection possible for a given buoyancy flux (see Table 4.5).

The second study, using the prescribed parameters (Table 4.7), reproduced the auto-oscillations of the Arctic Ocean – Greenland Sea climate system. In the simulation, the regimes shift with a period ranging from 10 to 15 years (Fig. 4.7A). However, the simulated periodicity is not rigidly cyclic. It has been assumed that the Arctic halocline, having a longer response to periodically changing forcing, can generate low-frequency oscillations in the system. This is the likely cause of the observed instability in the model behavior. The simulations agree well with the observed behavior.

Section 5.2. Major conclusions

The model experiments have shown:

- The Arctic Ocean and Greenland Sea can be viewed as an ice-ocean-atmosphere climate system with quasi-decadal, auto-oscillatory behavior in climate variability.

- There are two energy sources in the system that drive the auto-oscillations: potential energy which is accumulated in the Arctic Ocean (the Beaufort Sea) through converging flows of the surface freshwater and ice under ACCR; and internal energy which is accumulated in the GIN Sea region by means of intense heat flux to the atmosphere during years of deep convection in the Greenland Gyre (ACCR).

- The interaction between the regions is related to the surface air temperature and dynamic height gradients. Large gradients force the interaction to start. Small gradients do not promote the interaction.

- Heat advection to the Arctic is the first step in the interaction. Surplus heat ceases the anticyclonic vorticity in the atmosphere and shifts ACCR to CCR.

- Intense freshwater release from the Arctic Ocean to the GIN Sea shuts off the convection in the Greenland Gyre and reduces heat flux to the Arctic. Thus the freshwater flux tends to be the final stage of interaction between the basins. The Arctic then resettles into the ACCR regime.

- The mixed layer deepening in the central Greenland Sea is different under different climate states. It is highly sensitive to the amount of Polar Water that inflows into the basin. The annual mean amount of Polar Water that reaches the central Greenland Sea is estimated to be about 5-6% of that carried by the East Greenland Current. The twofold increase of this amount causes significant freshening of the upper Greenland Sea and shuts off the convection.

- Convection in the central Greenland Sea is controlled by Polar Water and Atlantic water inflow rates. The estimated ratio of the Polar Water inflow to the Atlantic water inflow is $Q_{PW}/Q_{AtW} \approx 3.7\text{x}10^{-2}$ for deep convection to be possible and $\approx 8.0\text{x}10^{-2}$ for no deep convection. The deepest mixed layer is simulated under the ACCR conditions.

- Freshwater inflow rates into the central Greenland Sea significantly change the surface heat flux. During the years of increased freshwater inflow, ice appears in the central Greenland Sea and surface heat flux is significantly reduced. This leads to a colder atmosphere in the GIN Sea.

- Thermohaline structure of the Arctic Ocean model exhibits significant variability under different climate regimes. During ACCR, the mixed layer becomes saltier and deeper, and the upper halocline becomes colder and fresher. In all, density of the upper Arctic Ocean decreases. During CCR, the mixed layer freshens and shallows, and the upper halocline warms and becomes saltier. In all, density of the upper Arctic Ocean increases.

- The mixed layer salinity in the Greenland Sea shows significant interannual variability due to different Polar Water inflow rates. Ice production alone is not able to significantly reduce the water column stability. The major salt source in the Greenland Sea is Atlantic water.

Section 5.3. Prospective studies

Future investigations can be conducted in several directions: a further sensitivity study of the model; parameterization of the deep convection in the Greenland Sea; testing alternative hypotheses of the causes of auto-oscillations; and mechanisms of heat advection to the Arctic.

Further investigation is required to determine how sensitive the auto-oscillatory behavior is to the prescribed parameters. As a result, a parameter space providing auto-oscillations in the system can be obtained.

One of the failures of the Greenland Sea model is its inability to reproduce instant deep convection. *Chapman's* [1997; 1998] theory can be applied as a possible approach to improve the Greenland Sea model.

In this research the major assumption was that there are two factors that determine the climate variability in the Arctic Ocean and GIN Sea, namely: heat advection and freshwater flux. However, no alternatives have been tested. For example, interannual variability in the Greenland Sea Gyre convection can be driven by the Atlantic water inflow. Also different rates of the Atlantic water inflow to the Arctic Ocean can significantly change the heat balance of the Arctic, although longer time scales than for atmospheric advection must then be considered.

Another possible direction for further research is the physical mechanism of heat advection to the Arctic Ocean. Planetary (Rossby) waves in the troposphere drive the near-surface atmospheric circulation. When the planetary waves develop into

stationary waves, meridional advection of heat is observed into the high latitudes. According to *Girs* [1974], in the years of anomalously warm Arctic the meridional atmospheric circulation dominated in the northern hemisphere. Further study is needed to find if these events are related to the ACCR/CCR regimes shift.

REFERENCES

1. Aagaard, K., and E.C. Carmack, The role of sea ice and other freshwater in the Arctic circulation, *J. Geophys. Res.*, *94*, 14485 - 14498, 1989.

2. Aagaard, K., and L.K. Coachman, The East Greenland Current north of Denmark Strait, I., *Arctic*, *21*, 181 - 200, 1968.

3. Aagaard, K., L.K. Coachman, and E.C. Carmack, On the halocline of the Arctic Ocean, *Deep-Sea Research*, *28*, 529-545, 1981.

4. Aagaard, K., and P. Greisman, Toward new mass and heat budgets for the Arctic Ocean, *J. Geophys. Res.*, *90*, 4833-4836, 1975.

5. Aagaard, K., J.H. Swift, and E.C. Carmack, Thermohaline circulation in the Arctic Mediterranean Seas, *J. Geophys. Res.*, *90*, 4833-4846, 1985.

6. Alekseev, G.V., V.V. Ivanov, and A.A. Korablev, Interannual variability of the thermohaline structure in the convective gyre of the Greenland Sea, in *Polar Oceans and Their Role in Shaping the Global Environment*, edited by O.M. Johannessen, R.D. Muench, and J.E. Overland, pp. 485-496, Geophysical Monograph Series, AGU, Washington D.C., 1994.

7. Aukrust, T., and J.M. Oberhuber, Modeling of the Greenland, Iceland, and Norwegian Seas with a coupled sea ice - mixed layer isopycnal ocean model, *J. Geophys. Res.*, *100*, 4771-4790, 1995.

8. Bjork, G., A one-dimensional time-dependent model for the vertical stratification of the upper Arctic Ocean, *J. Phys. Oceanogr.*, *19*, 52 - 67, 1989.

9. Bourke, R.H., and A.S. McLaren, Contour mapping of Arctic Basin ice draft and roughness parameter, *J. Geophys. Res.*, *97*, 17715-17728, 1992.

10. Bourke, R.H., A.M. Weigel, and R.G. Paquette, The westward turning branch of the West Spitsbergen Current, *J. Geophys. Res.*, *93*, 14065-14077, 1988.

11. Bryazgin, N.N., Snow on sea ice, in *Sea Ice (in Russian)*, edited by N.P. Muravieva, pp. 177-186, Gidrometeoizdat, St. Petersburg, 1997.

12. Budeus, G., A. Maul, and G. Krause, Variability in the Greenland Sea as revealed by a repeated high spatial resolution conductivity-temperature-depth survey, *J. Geophys. Res.*, *98*, 9985-10000, 1993.

13. Budyko, M.I., *Climate changes*, 261 pp., Waverly Press Inc., Baltimore, 1977.

14. Burova, L.P., *The moisture cycle in the atmosphere of the Arctic (in Russian)*, 128 pp., Gidrometeoizdat, Leningrad, 1983.

15. Carmack, E., and K. Aagaard, On the deep water of the Greenland Sea, *Deep Sea Res., 20*, 687-715, 1973.

16. Carmack, E., R.W. Macdonald, R.G. Perkin, F.A. McLaughlin, and R.J. Pearson, Evidence for warming of Atlantic water in the Southern Canadian Basin of the Arctic Ocean: Results from the LARSEN-93 expedition, *Geophys. Res. Lett., 22*, 1061-1064, 1995.

17. Carmack, E.C., Chapter 4: Large-scale physical oceanography of polar oceans, in *Polar Oceanography, Part A: Physical Science*, edited by W.O. Smith, pp. 171-222, Academic Press., San Diego, 1990.

18. Carmack, E.C., The Arctic ocean's freshwater budget: Sources, storage and export, in *The Freshwater Budget of the Arctic Ocean*, edited by E.L. Lewis et al., pp. 91-126, Kluwer Academic Publishers, the Netherlands, 2000.

19. Carsey, F.D., and A.T. Roach, Oceanic convection in the Greenland Sea Odden Region as interpreted in satellite data, in *Polar Oceans and Their Role in Shaping the Global Environment*, edited by O.M. Johannessen, R.D. Muench, and J.E. Overland, pp. 211-222, Geophysical Monograph Series, AGU, Washington D.C., 1994.

20. CDC, NOAA - CIRES Climate Diagnostic Center (CDC), NOAA, Boulder, Colorado (http://www.cdc.noaa.gov).

21. Chapman, D.C., A note on isolated convection in a rotating two-layer fluid, *J. Fluid Mech., 348*, 319-325, 1997.

22. Chapman, D.C., Setting the scales of the ocean response to isolated convection, *J. Phys. Ocean., 28*, 606-620, 1998.

23. Chatfield, C., *The Analysis of Time Series: An Introduction*, 283 pp., Chapman & Hall, Glasgow, 1996.

24. Clarke, R.A., J.H. Swift, J.L. Reid, and K.P. Koltermann, The formation of Greenland Sea Deep Water: double diffusion or deep convection, *Deep Sea Res., Part A, 37*, 1385-1424, 1990.

25. Coachman, L.K., and K. Aagaard, Physical oceanography of the arctic and sub-arctic seas, in *Marine Geology and Oceanography of the Arctic Ocean*, edited by Y. Herman, pp. 1-72, Springer, New York, 1974.

26. Coachman, L.K., K. Aagaard, and R.B. Tripp, Water masses, in *Bering Strait: The Regional Physical Oceanography*, pp. 11-73, University of Washington Press, Seattle, 1975.

27. Coachman, L.K., and C.A. Barnes, Surface waters in the Eurasian Basin of the Arctic Ocean, *Arctic*, *15*, 251-277, 1962.

28. Collin, A.E., Oceanographic observations in the Canadian Arctic and adjacent Arctic Ocean, *Arctic*, *15*, 194-201, 1962.

29. Cushman-Roisin, B., *Introduction to Geophysical Fluid Dynamics*, 290 pp., Prentice Hall, New Jersey, 1994.

30. Dickson, R., All change in the Arctic, *Nature*, *397*, 389-391, 1999.

31. Dickson, R.R., J. Meincke, S.-A. Malmberg, and A.J. Lee, The "Great Salinity Anomaly" in the Northern North Atlantic 1968-1982, *Prog. Oceanogr.*, *20*, 103-151, 1988.

32. Dmitriev, A.A., *Variability of atmospheric processes in the Arctic and their application in long-term forecasts (in Russian)*, 227 pp., Gidrometeoizdat, St. Petersburg, 1994.

33. Doronin, N.Y., and A.Y. Proshutisnky, Mathematical modeling in studies of Arctic Ocean circulation, in *Proceedings of the International Conference on the Role of the Polar Regions in Global Change*, edited by O.M. Johannessen et al., pp. 310-316, Geophysical Inst., Univ. of Alaska Press., Fairbanks, 1991.

34. Doronin, Y.P., *Regional oceanography (in Russian)*, 173 pp., Gidrometeoizdat, Leningrad, 1986.

35. Doronin, Y.P., Sea ice freezing and melting, in *Sea Ice (in Russian)*, edited by N.P. Muravieva, pp. 68-106, Gidrometeoizdat, St. Petersburg, 1997.

36. Doronin, Y.P., *Physics of the ocean (in Russian)*, 339 pp., State Hydrometeorological University, St. Petersburg, 2000.

37. Elsner, J.B., and A.A. Tsonis, Comparison of observed Northern Hemisphere surface air temperature records, *Geophys. Res. Lett.*, *18*, 1229-1232, 1991.

38. EWG, Environmental Working Group (EWG), Joint U.S. Russian Atlas of the Arctic Ocean for the Winter/Summer Period, [CD-ROM], Natl. Snow and Ice Data Cent., Boulder, Colorado, 1998.

39. Farmer, D.M., Penetrative convection in the absence of mean shear, *Quart. J. Roy. Meteor. Soc.*, *101*, 869-891, 1975.

40. Fletcher, C.A.J., *Computational techniques for fluid dynamics 1: Fundamental and general techniques*, 457 pp., Springer-Verlag, New York, 1988.

41. Foldvik, A., K. Aagaard, and T. Torresen, On the velocity field of the East Greenland Current, *Deep-Sea Res., Part A, 35*, 1335-1354, 1988.

42. Gakkel, Y.Y., Continental slope as a geographical region of the Arctic Ocean, *Izv. Vseross. Geogr. Obsch. (in Russian), 89* (6), 493-507, 1957.

43. Girs, A.A., *Method of macro-circulation for long-range weather forecasting (in Russian)*, Gidrometeoizdat, Leningrad, 1974.

44. Goosse, H., F.M. Selten, R.J. Haarsma, and J.D. Opsteegh, A mechanism of decadal variability of the sea-ice volume in the Northern Hemisphere, *Climate Dynamics, 19*, 61-83, 2002.

45. Gordeev, V.V., River inputof water, sediment, major ions, nutrients and trace metals from Russian territory to the Arctic Ocean, in *The Freshwater Budget of the Arctic Ocean*, edited by E.L. Lewis, E.P. Jones, P. Lemke, T.D. Prowse, and P. Wadhams, pp. 297-322, Kluwer Academic Publishers, The Netherlands, 2000.

46. Gorshkov, S.G., Atlas of Oceans: the Arctic Ocean, Ministry of Defense of the USSR, Moscow, 1980.

47. Grabs, W.E., F. Portmann, and T. De Couet, Discharge observation networks in Arctic regions: Computation of the river runoff into the Arctic Ocean, its seasonality and variability, in *The Freshwater Budget of the Arctic Ocean*, edited by E.L. Lewis et al., pp. 249-267, Kluwer Academic Publishers, the Netherland, 2000.

48. Gruza, G.V., E.Y. Rankova, and E.V. Rocheva, Analysis of global data variations in surface air temperature during instrument observation period (in Russian), *Meteor. Gidr., 25*, 16-24, 1988.

49. Gudkovich, Z.M., Relation of the ice drift in the Arctic basin to ice conditions in the Soviet Arctic seas (in Russian), *Tr. Okeanogr. Kom. Akad. Nauk SSSR, 11*, 14-21, 1961.

50. Gudkovich, Z.M., and E.G. Kovalev, On some mechanisms of cyclic climate changes in the Arctic and Antarctic (in Russian), *Oceanology, 42* (6), 815-821, 2002.

51. Gudkovich, Z.M., and E.G. Nikiforov, Investigation of water circulation in the Arctic Basin using a model (in Russian), *Okeanologiya, 5* (1), 75-83, 1965.

52. Hakkinen, S., A coupled dynamic-thermodynamic model of an ice-ocean system in the marginal ice zone, *J. Geophys. Res.*, *92*, 9469-9478, 1987.

53. Hakkinen, S., Simulated interannual variability of the Greenland Sea deep water formation and its connection to surface forcing, *J. Geophys. Res.*, *100*, 4761-4770, 1995.

54. Hakkinen, S., and D.J. Cavalieri, A study of oceanic surface heat fluxes in the Greenland, Norwegian, and Barents Seas, *J. Geophys. Res.*, *96*, 22009-22023, 1989.

55. Hakkinen, S., and C.A. Geiger, Simulated low-frequency modes of circulation in the Arctic Ocean, *J. Geophys. Res.*, *105*, 6549-6564, 2000.

56. Halpern, D., Observations of deepening of the wind-mixed layer in the northeast Pacific Ocean, *J. Phys. Oceanogr.*, *4*, 454-466, 1974.

57. Hansen, J., and S. Lebedeff, Global trends of measured surface air temperature, *J. Geophys. Res.*, *92*, 13345-13372, 1987.

58. Helland-Hansen, B., and F. Nansen, The Norwegian Sea, Its physical oceanography based upon the Norwegian researches 1900-1904, in *Report on Norwegian Fishery and Marine Investigations, 2, part1*, Malingske, Christiana (Oslo), 1909.

59. Hellerman, S., and M. Rosentstein, Normal monthly wind stress over world ocean with error estimates, *J. Phys. Oceanogr.*, *13*, 1093-1104, 1983.

60. Henderson-Sellers, A., and K. McGuffie, *A climate modelling primer*, 217 pp., J. Wiley & Sons, New York, 1987.

61. Hibler, W.D., III, A dynamic thermodynamic sea ice model, *J. Phys. Ocean.*, *9*, 815-846, 1979.

62. Huck, T., A. Colin de Verdiere, and A.J. Weaver, Interdecadal variability of the thermohaline circulation in box-ocean models forced by fixed surface fluxes, *J. Phys. Ocean.*, *29*, 893-910, 1999.

63. Hurrell, J.W., and H. van Loon, Decadal variations in climate associated with the North Atlantic oscillation, *Climatic Change*, *36*, 301-326, 1997.

64. Iqbal, M., *An introduction to solar radiation*, 390 pp., Academic Press, New York, 1983.

65. Johannessen, O.M., Brief overview of the physical oceanography, in *The Nordic Seas*, edited by B.G. Hurdle, pp. 103-127, Springer-Verlag, New York, 1986.

66. Johannessen, O.M., S. Sandven, and J.A. Johannessen, Eddy-related winter convection in the Boreas Basin, in *Deep Convection and Deep Water Formation in the Oceans*, edited by P.C. Chu, and J.C. Gascard, pp. 87-105, Elsiver Science, New York, 1991.

67. Johnson, M.A., and I.V. Polyakov, The Laptev Sea as a source for recent Arctic Ocean salinity changes, *Geophys. Res. Lett.*, *28*, 102017 - 102020, 2001.

68. Johnson, M.A., A.Y. Proshutinsky, and I.V. Polyakov, Atmospheric patterns forcing two regimes of Arctic circulation: a return to anticyclonic conditions?, *Geophys. Res. Lett.*, *26*, 1621-1624, 1999.

69. Jones, P.D., Hemispheric surface air temperature variations: A reanalysis and an update to 1993, *J. Climate*, *7*, 1794-1802, 1994.

70. Jones, P.D., M. New, D.E. Parker, S. Martin, and I.G. Rigor, Surface air temperature and its changes over the past 150 years, *Review of Geophysics*, *37* (2), 173-199, 1999.

71. Jones, P.D., T.M.L. Wigley, and P.B. Wright, Global temperature variations between 1861 and 1984, *Nature*, *322*, 430-434, 1986.

72. Jonsson, S., Seasonal and interannual variability of wind stress curl over the Nordic Seas, *J. Geophys. Res.*, *96*, 2649-2659, 1991.

73. Kantha, L., Turbulent entrainment at the density interface of a two-layer stably stratified fluid system, Geophysical Fluid Dynamics Lab. Tech. Rept. 75-1, John Hopkins Univ., 1975.

74. Kato, H., and O.M. Phillips, On the penetration of a turbulent layer into a stratified fluid, *J. Fluid Mech.*, *37*, 643-655, 1969.

75. Kelley, P.M., and P.D. Jones, Annual temperatures in the Arctic, 1881-1981, *Clim. Monit.*, *10*, 122-124, 1982.

76. Kelley, P.M., P.D. Jones, C.B. Sear, B.S.G. Cherry, and R.K. Tavakol, Variations in surface air temperatures: Pt. 2, Arctic regions, 1881-1990, *Mon. Wea. Rev.*, *110*, 71-83, 1982.

77. Killworth, P.D., On "chimney" formation in the ocean, *J. Phys. Oceanogr.*, *9*, 531-554, 1979.

78. Killworth, P.D., and J.M. Smith, A one-and-half dimensional model for the Arctic halocline, *Deep-Sea Res.*, *31*, 271-293, 1984.

79. Kitaigorodsky, S.A., On the computation of the thickness of the wind-mixing layer in the ocean, *Bull. Acad. Sci. USSR, Geophys. Ser.*, *3*, 284-287, 1960.

80. Knipovich, I.M., Thermic conditions in the Barents Sea at the end of May, 1921, *Byull. Rossiisk. Gidrolog. Instituta (in Russian)*, *9*, 10-12, 1921.

81. Kowalik, Z., Storm surges in the Beaufort and Chukchi Seas, *J. Geophys. Res.*, *89*, 10570 - 10578, 1984.

82. Kowalik, Z., and J.B. Matthews, Numerical study of the water movement driven by brine rejection from nearshore Arctic ice, *J. Geophys. Res.*, *88*, 2953-2958, 1983.

83. Kowalik, Z., and T.S. Murty, *Numerical modeling of ocean dynamics*, 481 pp., World Scientific Publishing, Singapore, 1993.

84. Kozo, T.L., The hybrid polynya at the Northern end of Nares Strait, *Geophys. Res. Lett.*, *18*, 2059-2062, 1991.

85. Kraus, E.B., and J.S. Turner, A one-dimensional model of the seasonal thermocline. II. The general theory and its consequences, *Tellus*, *19*, 98-106, 1967.

86. Kreyszig, E., *Advanced Engineering Mathematics*, 1156 pp., John Willey & Sons, New York, 1999.

87. Kundu, P.K., *Fluid mechanics*, 638 pp., Academic Press, San Diego, 1990.

88. Kwok, R., and D. Rothrock, Variability of Fram Strait ice flux and North Atlantic Oscillation, *J. Geophys. Res.*, *104*, 5177-5189, 1999.

89. Lewis, E.L., Introduction, in *The Freshwater Budget of the Arctic Ocean*, edited by E.L. Lewis, E.P. Jones, P. Lemke, T.D. Prowse, and P. Wadhams, pp. xv-xxi, Kluwer Academic Publishers, The Netherlands, 2000.

90. Lindsay, R.W., Temporal variability of the energy balance of thick Arctic pack ice, *J. Climate*, *11*, 313-333, 1998.

91. Lysgaard, L., Recent climatic fluctuations, *Fol. Geogr. Dan.*, *V*, 1-86, 1949.

92. Macdonald, R.W., Arctic estuaries and ice: a positive-negative estuarine couple, in *The Freshwater Budget of the Arctic Ocean*, edited by E.L. Lewis et al., pp. 383-408, Kluwer Academic Publishers, the Netherland, 2000.

93. Makshtas, A.P., *The heat budget of Arctic ice in the winter*, 77 pp., International Glaciological Society, Cambridge, 1991.

94. Makshtas, A.P., E.L. Andreas, P.N. Svyashchennikov, and V.F. Timachev, Accounting for clouds in sea ice models, *Atmos. Res.*, *52*, 77-113, 1999.

95. Malmberg, S.-A., H.G. Gade, and H.E. Sweers, Current velocities and volume transports in the East Greenland Current off Cape Nordenskjold in August-September 1965, in *Sea Ice*, pp. 130-139, National Research Council, Reykjavik, 1972.

96. Marotzke, J., and P.H. Stone, Atmospheric transports, the thermohaline circulation, and flux adjustments in a simple coupled model, *J. Phys. Oceanogr.*, *25*, 1350-1364, 1995.

97. Marshunova, M.S., Principal characteristics of the radiation balance of the underlying surface and of the atmosphere in the Arctic, *Trudy Arkt. Antarkt. Nauch. Issled. Inst.*, *229*, 1961.

98. Maslanik, J., M.C. Serreze, and R.G. Barry, Recent decrease in Arctic summer ice cover and linkages to atmospheric anomalies, *Geophys. Res. Lett.*, *23*, 1677-1680, 1996.

99. Maslowski, W., Numerical modeling study of the circulation of the Greenland Sea, Ph.D. thesis, Univ. Alaska Fairbanks, Fairbanks, 1994.

100. Matveev, L.T., *The Course of General Meteorology: Physics of Atmosphere (in Russian)*, 751 pp., Gidrometeoizdat, Leningrad, 1984.

101. Maykut, G.A., The surface heat and mass balance, in *The Geophysics of Sea Ice*, edited by N. Untersteiner, pp. 395-463, Plenum Press, 1986.

102. Maykut, G.A., and N. Untersteiner, *Numerical prediction of the thermodynamic response of Arctic sea ice to environmental changes*, 173 pp., The Rand Corporation, Santa Monica, 1969.

103. Maykut, G.A., and N. Untersteiner, Some results from a time-dependent thermodynamic model of sea ice, *J. Geophys. Res.*, *76*, 1550-1575, 1971.

104. McLaren, A.S., The under-ice thickness distribution of the Arctic basin as recorded in 1958 and 1970, *J. Geophys. Res.*, *94*, 4971-4983, 1989.

105. McLaren, A.S., R.G. Barry, and R.H. Bourke, Could Arctic ice be thinning?, *Nature*, *345*, 762, 1990.

106. McLaren, A.S., R.H. Bourke, J.E. Walsh, and R.L. Weaver, Variability in sea-ice thickness over the North Pole from 1958 to 1992, in *Polar Oceans and Their Role in Shaping the Global Environment*, edited by O.M. Johannessen, R.D. Muench, and J.E. Overland, pp. 363-371, Geophysical Monograph Series, AGU, Washington D.C., 1994.

107. McLaren, A.S., P. Wadhams, and R. Weintraub, The sea ice topography of M'Clure Strait in winter and summer of 1960 from submarine profiles, *Arctic*, *37*, 110-120, 1984.

108. McLaughlin, F.A., E.C. Carmack, R.W. Macdonald, and J. Bishop, Physical and geochemical properties across the Atlantic/Pacific water mass front in the southern Canadian Basin, *J. Geophys. Res.*, *101*, 1183-1197, 1996.

109. Melling, H., Exchanges of freshwater through the shallow straits of the North American Arctic, in *The Freshwater Budget of the Arctic Ocean*, edited by E.L. Lewis et al., pp. 479-502, Kluwer Academic Publishers, The Netherlands, 2000.

110. Metcalf, W.G., A note on water movement in the Greenland-Norwegian Sea, *Deep-Sea Res.*, *7*, 190-200, 1960.

111. Moritz, R.E., C.M. Bitz, and E.J. Steig, Dynamics of recent climate change, *Science*, *297*, 1497-1502, 2002.

112. Mountain, D.G., L.K. Coachman, and K. Aagaard, On the flow through Barrow Canyon, *J. Phys. Oceanogr.*, *6*, 461-470, 1976.

113. Muench, R.D., Chapter 5: Mesoscale phenomena in the polar oceans, in *Polar Oceanography, Part A: Physical Science*, edited by W.O. Smith, pp. 223-286, Academic Press., San Diego, USA, 1990.

114. Mysak, L.A., and S.B. Power, Sea-ice anomalies in the western Arctic and Greenland-Icelandic Sea and their relation to an interdecadal climate cycle, *Clim. Bull.*, *26*, 147-176, 1992.

115. Mysak, L.A., and S.A. Venegas, Decadal climate oscillations in the Arctic: A new feedback loop for atmospheric-ice-ocean interactions, *Geophys. Res. Lett.*, *25* (19), 3607-3610, 1998.

116. Nansen, F., Oceanography of the North Polar Basin, *The Norwegian North Polar Expedition 1893-96; Scientific Results*, *3* (9), 1-427, 1902.

117. Nansen, F., The oceanographic problems of still unknown Arctic regions; Problems of polar research, *Amer. Goegr. Soc. Spec. Publ.*, *7*, 1928.

118. Niiler, P.P., and E.B. Kraus, Chapter 10: One-dimensional models of the upper ocean, in *Modelling and Prediction of the Upper Layers of the Ocean*, edited by E.B. Kraus, pp. 143-172, Pergamon Press, London, 1977.

119. Nikiforov, Y.G., and A.O. Shpaikher, *Features of the formation of hydrological regime large-scale variations in the Arctic Ocean (in Russian)*, 269 pp., Gidrometeoizdat, Leningrad, 1980.

120. Parkinson, C.L., Spatial patterns of increase and decrease in the length of the sea ice season in the north polar region, 1979-1986, *J. Geophys. Res.*, *97*, 14377-14388, 1992.

121. Pawlowicz, A., J.F. Lynch, W.B. Owens, P.F. Worcester, W.M.L. Morawitz, and P.J. Sutton, Thermal evolution of the Greenland Sea Gyre in 1988-1989, *J. Geophys. Res.*, *100*, 4724-4750, 1995.

122. Pawlowicz, R., A note on seasonal cycles of temperature and salinity in the upper waters of the Greenland Sea Gyre from historical data, *J. Geophys. Res.*, *100*, 4715-4726, 1995.

123. Perry, R.K., Bathymetry, in *The Nordic Seas*, edited by B.G. Hurdle, pp. 211-236, Springer-Verlag, New York, 1986.

124. Phillips, O.M., Chapter 7: Entrainment, in *Modelling and Prediction of the Upper Layers of the Ocean*, edited by E.B. Kraus, pp. 92-101, Pergamon Press, UK, 1977.

125. Pollard, R.T., P.B. Rhines, and R.O.R.Y. Thompson, The deepening of the wind-mixed layer, *Geophys. Fluid Dyn.*, *4*, 381-404, 1973.

126. Polyakov, I.V., S.-I. Akasofu, U. Bhatt, R. Colony, C. Swingley, D. Walsh, and J. Walsh, Trends and variations in Arctic climate system, *EOS, AGU*, *83*, 547-548, 2002a.

127. Polyakov, I.V., G.V. Alekseev, R.V. Bekryaev, U. Bhatt, R. Colony, M.A. Johnson, V.P. Karklin, A.P. Makshtas, D. Walsh, and V. Yulin, Observationally based assessment of polar amplification of global warming, *Geophys. Res. Lett.*, *29*, 1878, 2002b.

128. Polyakov, I.V., R.V. Bekryaev, G.V. Alekseev, U. Bhatt, R. Colony, M.A. Johnson, A.P. Makshtas, and D. Walsh, Variability and trends of air temperature and pressure in the maritime Arctic, *J. Climate*, *in press*, 2002c.

129. Polyakov, I.V., and M.A. Johnson, Arctic decadal and inter-decadal variability, *Geophys. Res. Lett.*, *27*, 4097-4100, 2000.

130. Polyakov, I.V., A.Y. Proshutinsky, and M.A. Johnson, Seasonal cycles in two regimes of Arctic climate, *J. Geophys. Res.*, *104*, 25761-25788, 1999.

131. Pond, S., and G.L. Pickard, *Introductory Dynamical Oceanography*, 330 pp., Butterworth-Heinemann, Exeter, UK, 1989.

132. Price, J.F., C.N.K. Mooers, and J.C. Van Leer, Observation and simulation of storm-induced mixed-layer deepening, *J. Phys. Ocean.*, *8*, 582-599, 1978.

133. Proshutinsky, A., R.H. Bourke, and F.A. McLaughlin, The role of the Beaufort Gyre in Arctic climate variability: Seasonal to decadal climate scales, *Geophys. Res. Lett.*, *29* (23), 2100, doi:10.1029/2002GL015847, 2002.

134. Proshutinsky, A.Y., and M.A. Johnson, Two circulation regimes of the wind-driven Arctic Ocean, *J. Geophys. Res.*, *102*, 12493 - 12514, 1997.

135. Proshutinsky, A.Y., V. Pavlov, and R.H. Bourke, Sea level rise in the Arctic Ocean, *Geophys. Res. Lett.*, *28* (11), 2237-2240, 2001.

136. Proshutinsky, A.Y., I.V. Polyakov, and M.A. Johnson, Climate states and variability of Arctic ice and water dynamics during 1946-1997, *Polar Res.*, *18*, 135-142, 1999.

137. Prowse, T.D., and P.O. Flegg, Arctic river flow: A review of contributing areas, in *The Freshwater Budget of the Arctic Ocean*, edited by E.L. Lewis et al., pp. 269-280, Kluwer Academic Publishers, the Netherlands, 2000.

138. Przybylak, R., *Variability of air temperature and atmospheric precipitation in the Arctic*, 330 pp., Kluwer Academic Publishers, the Netherlands, 2002.

139. Rice, J.A., *Mathematical Statistics and Data Analysis*, 602 pp., Duxbury Press, Belmont, 1995.

140. Rigor, I.G., J.M. Wallace, and R. Colony, Response of sea ice to the Arctic Oscillation, *J. Climate*, *15*, 2648-2663, 2002.

141. Roach, A., K. Aagaard, C. Pease, S. Salo, T. Weingartner, V. Pavlov, and M. Kulakov, Direct measurements of transport of water and properties through Bering Strait, *J. Geophys. Res.*, *100*, 18443-18457, 1995.

142. Rothrock, D.A., R. Kwok, and D. Groves, Satellite views of the Arctic Ocean freshwater balance, in *The Freshwater Budget of the Arctic Ocean*, edited by E.L. Lewis et al., pp. 409-452, Kluwer Academic Publishers, the Netherlands, 2000.

143. Rothrock, D.A., Y. Yu, and G.A. Maykut, Thinning of the Arctic sea-ice cover, *Geophys. Res. Lett.*, *26*, 3469-3472, 1999.

144. Rudels, B., The Θ-T relations in the northern seas: Implications for the deep circulation, *Polar Res.*, *4*, 133-1359, 1984.

145. Rudels, B., Aspects of Arctic oceanography, in *Physics of Ice-Covered Seas: Lecture notes from a summer school in Savonlinna, Finland 6-17 June 1994*, edited by M. Lepparanta, pp. 517-569, Helsinki University Printing House, Helsinki, 1998.

146. Rudels, B., L.G. Anderson, and E.P. Jones, Formation and evolution of the surface mixed layer and halocline of the Arctic Ocean, *J. Geophys. Res.*, *101*, 8807-8821, 1996.

147. Rudels, B., and H.J. Friedrich, The transformations of Atlantic water in the Arctic Ocean and their significance for the freshwater budget, in *The freshwater budget of the Arctic Ocean*, edited by E.L. Lewis et al., pp. 503-532, Kluwer Academic Publishers, the Netherlands, 2000.

148. Rudels, B., E.P. Jones, L.G. Anderson, and G. Kattner, On the intermediate depth waters of the Arctic Ocean, in *Polar Oceans and Their Role in Shaping the Global Environment*, edited by O.M. Johannessen, R.D. Muench, and J.E. Overland, pp. 33-46, Geophysical Monograph Series, AGU, Washington D.C., 1994.

149. Rudels, B., D. Quadfasel, H. Friedrich, and M.-N. Houssais, Greenland sea convection in the winter of 1987-1988, *J. Geophys. Res.*, *94*, 3223-3227, 1989.

150. Schauer, U., R.D. Muench, B. Rudels, and L. Timokhov, Impact of eastern Arctic shelf water on the Nansen Basin intermediate layers, *J. Geophys. Res.*, *102*, 3371-3382, 1997.

151. Scherhag, R., Eine bemerkungswerte klimaanderung uber Nord-Europa, *Ann. Hydr. Mar. Met.*, 57-67, 1931.

152. Schlosser, P., G. Bohnisch, M. Rhein, and R. Bayer, Reduction of deep water formation in the Greenland Sea during 1980s: Evidence from tracer data, *Science*, *251*, 1054-1056, 1991.

153. Schumacher, J.D., K. Aagaard, C.H. Pease, and R.B. Tripp, Effects of a shelf polynya on flow and water properties in the Northern Bering Sea, *J. Geophys. Res.*, *88*, 2723-2732, 1983.

154. Scott, J.R., J. Marotzke, and P.H. Stone, Interhemispheric thermohaline circulation in a coupled box model, *J. Phys. Oceanogr.*, *29*, 351-365, 1999.

155. Semiletov, I.P., N.I. Savelieva, and G.E. Weller, Cause and effect linkages between atmosphere, the Siberian rivers and conditions in the Russian shelf seas, in *Changes in the Atmosphere-Land-Sea System in the Amerasian Arctic*, edited by I.P. Semiletov, pp. 63-96, Dalnauka, Vladivostok, RF, 2001.

156. Semiletov, I.P., N.I. Savelieva, G.E. Weller, I.I. Pipko, S.P. Pugach, A.Y. Gukov, and L.N. Vasilevskaya, The dispersion of Siberian river flows into coastal waters: Meteorological, hydrological and hydrochemical apsects, in *The Freshwater Budget of the Arctic Ocean*, edited by E.L. Lewis, E.P. Jones, P. Lemke, T.D. Prowse, and P. Wadhams, pp. 323-366, Kluwer Academic Publishers, the Netherlands, 2000.

157. Serreze, M.C., and R.G. Barry, Atmospheric components of the Arctic Ocean hydrologic budget assessed from rawinsonde data, in *The Freshwater Budget of the Arctic Ocean*, edited by E.L. Lewis et al., pp. 141-161, Kluwer Academic Publishers, the Netherlands, 2000.

158. Serreze, M.C., R.G. Barry, and J.E. Walsh, Atmospheric water vapor characteristics at 70 N, *J. Climate*, *8*, 719-731, 1995.

159. Serreze, M.C., F. Carse, and R.G. Barry, Icelandic Low cyclone activity: climatological features, linkages with the NAO, and relationships with recent changes in the Northern Hemisphere circulation, *J. Climate*, *10*, 453-464, 1997.

160. Serreze, M.C., J.A. Maslanik, R.H. Preller, and R.G. Barry, Sea ice concentrations in the Canada Basin during 1988: comparisons with other years and evidence of multiple forcing mechanisms, *J. Geophys. Res.*, *95*, 22253-23267, 1990.

161. Serway, R.A., *Physics for scientists and engineers*, 1442 pp., Saunders College Publishing, USA, 1996.

162. Shiklomanov, I.A., A.I. Shiklomanov, R.B. Lammers, B.J. Peterson, and C.J. Vorosmarty, The dynamics of river water inflow to the Arctic Ocean, in *The Freshwater Budget of the Arctic Ocean*, edited by E.L. Lewis et al., pp. 281-296, Kluwer Academic Publishers, the Netherlands, 2000.

163. Shine, K.P., Parameterization of shortwave flux over high albedo surfaces as a function of cloud thickness and surface albedo, *Q. J. R. Meteorol. Soc.*, *110*, 747-760, 1984.

164. Shirshov, P.P., *Scientifc results of the drifting station "North Pole". Report on the meeting at the Academy of Sciences of the USSR, February 14-17, 1944*, 157 pp., Academy of Sciences of the USSR Press., Moscow, USSR (RF), 1944.

165. Slonosky, V.C., L.A. Mysak, and J. Derome, Linking Arctic sea-ice and atmospheric circulation anomalies on interannual and decadal timescales, *Atmos. Ocean*, *35*, 333-366, 1997.

166. Smith, D.C.I., A.A. Bird, and W.P. Budgel, A numerical study of mesoscale ocean eddy interaction with a marginal ice zone, *J. Geophys. Res.*, *93*, 12461-12473, 1988.

167. Steele, M., and T. Boyd, Retreat of the cold halocline layer in the Arctic Ocean, *J. Geophys. Res.*, *103*, 10419 - 10435, 1998.

168. Stigebrandt, A., A model for the thickenss and salinity of the upper layer in the Arctic Ocean and the relationship between ice thickness and some external parameters, *J. Phys. Ocean.* (11), 1407 - 1422, 1981.

169. Stigebrandt, A., A model for the seasonal pycnocline in rotating systems with application to the Baltic proper, *J. Phys. Ocean.* (15), 1392 - 1404, 1985.

170. Stommel, H., K. Saunders, W. Simmons, and J. Cooper, Observations of the diurnal thermocline, *Deep-Sea Res.*, *16, Suppl.*, 269-284, 1969.

171. Sukhovey, V.F., Investigation of the water exchange between the Atlantic Ocean and Arctic Mediterranean based on observations, in *Marine Hydrophysical Observations (in Russian)*, pp. 125-147, Naukova Dumka, Kiev, 1970.

172. Swift, J.H., The Arctic waters, in *The Nordic Seas*, edited by B.G. Hurdle, pp. 129-153, Springer-Verlag, New York, 1986.

173. Swift, J.H., and K. Aagaard, Seasonal transition and water mass formation in the Iceland and Greenland seas, *Deep-Sea Res., Part A*, *28*, 1107-1129, 1981.

174. Swift, J.H., K. Aagaard, and S.-A. Malmberg, The contribution of the Denmark Strait overflow to the North Atlantic, *Deep-Sea Res., Part A*, *27*, 29-42, 1980.

175. Swift, J.H., E.P. Jones, K. Aagaard, E.C. Carmack, M. Hingston, R.W. Macdonald, F.A. McLaughlin, and R.G. Perkin, Waters of the Makarov and Canada basins, *Deep-Sea Res.*, *44*, 1503-1529, 1997.

176. Swift, J.H., T. Takahashi, and H.D. Livingston, The contribution of the Greenland and Barents seas to the deep water of the Arctic Ocean, *J. Geophys. Res.*, *88*, 5981-5986, 1983.

177. Thomas, D., S. Martin, D. Rothrock, and M. Steele, Assimilating satellite concentration data into an Arctic sea ice mass balance model, 1979 - 1985, *J. Geophys. Res.*, *101*, 20849-20868, 1996.

178. Thompson, D.W.J., and J.M. Wallace, The Arctic Oscillation signature in the wintertime geopotential height and temperature fields, *Geophys. Res. Lett.*, *25*, 1297-1300, 1998.

179. Thorndike, A.S., and R. Colony, Sea ice motion in response to geostrophic winds, *J. Geophys. Res.*, *87*, 5845-5852, 1982.

180. Timofeyev, V.T., *Water masses of the Arctic Basin (in Russian)*, 190 pp., Gidrometeoizdat, Leningrad, 1960.

181. Timofeyev, V.T., The movement of Atlantic water and heat into the Arctic Sea basin, *Deep-Sea Res.*, *9*, 358-361, 1962.

182. Treshnikov, A.F., Water masses of the Arctic Basin, in *Polar Oceans: proceedings of the Polar Oceans Conference held at McGill University, Montreal, May, 1974*, edited by M.J. Dunbar, pp. 17-31, Arctic Institute of North America, Calgary, 1977.

183. Treshnikov, A.F., and G.I. Baranov, *Structure of the water circulation in the Arctic Basin (in Russian)*, 157 pp., Gidrometeoizdat, Leningrad, 1972.

184. Turner, J.S., The influence of molecular diffusivity on turbulent entrainment across a density interface, *J. Fluid Mech.*, *33*, 639-656, 1968.

185. Turner, J.S., A note on wind-mixing at the seasonal thermocline, *Deep-Sea Res.*, *16, Suppl.*, 297-300, 1969.

186. Turner, J.S., *Buoyancy effects in fluids*, 367 pp., Cambridge University Press, 1973.

187. Turner, J.S., and E.B. Kraus, A one-dimensional model of the seasonal thermocline. I. A laboratory experiment and its interpretation, *Tellus*, *19*, 88-97, 1967.

188. Vangengeim, G.Y., Bases of the macrocirculation method for long-term weather forecasting for the Arctic, *Trudy Arkt. Antarkt. Nauch. Issled. Inst. (in Russian)*, *34*, 1-314, 1952.

189. Venegas, S.A., and L.A. Mysak, Is there a dominant timescale of natural climate variability in the Arctic?, *J. Climate*, *13*, 3412-3434, 2000.

190. Vinje, T., and O. Finnekasa, The ice transport through the Fram Strait, *Skrift. Norg. Polarinst.*, *186*, 1-39, 1986.

191. Vinje, T., T.B. Loyning, and I. Polyakov, Effects of melting and freezing in the Greenland Sea, *Geophys. Res. Lett.*, *29* (23), 2002.

192. Vinnikov, K.Y., A. Robock, R.J. Stouffer, J.E. Walsh, C.L. Parkinson, D.J. Cavalieri, J.F.B. Mitchell, D. Garrett, and V.F. Zakharov, Global warming and Northern Hemisphere sea ice extent, *J. Climate*, *286*, 1934-1937, 1999.

193. Vize, V.Y., *The sea climate in the Russian Arctic (in Russian)*, 124 pp., Izdat. Glavsevmorputi, Leningrad-Moscow, 1940.

194. Wadhams, P., Sea ice thickness changes and their relation to climate, in *Polar Oceans and Their Role in Shaping the Global Environment*, edited by O.M. Johannessen, R.D. Muench, and J.E. Overland, pp. 337-361, Geophysical Monograph Series, AGU, Washington D.C., 1994.

195. Wadhams, P., W.B. Tucker III, W.B. Krabil, J.H. Swift, J.C. Comiso, and N.R. Davis, Relationship between sea ice freeboard and draft in the Arctic Basin, and implications for ice thickness monitoring, *J. Geophys. Res.*, *97*, 20325-20334, 1992.

196. Wallace, J.M., and P.V. Hobbs, The global energy balance, in *Atmospheric Science: An Introductory Survey*, pp. 316-358, Academic Press, San Diego, 1977.

197. Walsh, J.E., W.L. Chapman, and T.L. Shy, Recent decrease of sea level pressure in the central Arctic, *J. Climate*, *9*, 480-486, 1996.

198. Worthington, L.V., An attempt to measure the volume transport of Norwegian Sea overflow water through the Denmark Strait, *Deep-Sea Res.*, *16 (Suppl.)*, 421-432, 1969.

199. Worthington, L.V., The Norwegian Sea as a mediterranean basin, *Deep-Sea Res.*, *17*, 77-84, 1970.

200. Zhang, J., D. Rothrock, and M. Steele, Recent changes in the Arctic sea ice: The interplay between ice dynamics and thermodynamics, *J. Climate*, *13*, 3099-3114, 2000.

201. Zhang, J., D.A. Rothrock, and M. Steele, Warming of the Arctic Ocean by a strengthened Atlantic inflow: Model results, *Geophys. Res. Lett.*, *25*, 1745-1748, 1998.